Analysis of Distributive Mixing During Polymer Blending in Twin Screw Extruders Using Reactive Polymer Tracers

By

Gifford Shearer

A Thesis
presented to the University of Waterloo
in fulfilment of the
thesis requirement for the degree of
Doctor of Philosophy
in
Chemical Engineering

Waterloo, Ontario, Canada, 2000

The University of Waterloo requires the signatures of all persons using or photocopying this thesis. Please sign below, and give address and date.

ABSTRACT

A novel quantitative method for analyzing distributive mixing during polymer blending in a co-rotating twin screw extruder was developed. This method employed a mixing limited interfacial reaction between two reactive polymer tracers to gain direct evidence of the generation of interfacial area during polymer blending. The tracers were based on a low molecular weight amorphous polyolefin wax containing a high concentration of terminal double bonds, which were targeted for functionalization with anhydride and primary amine functional groups. These functional groups were selected because their coupling reaction is extremely fast under the conditions employed during polymer processing in extruders. A melt-phase Alder Ene reaction between the terminal double bond of the polyolefin and the double bond of maleic anhydride was used to introduce a terminal succinic anhydride functional group. Hydroboration followed by amination was completed in solution with THF to introduce terminal primary amine functional groups. For the mixing experiments, the reactive polymers were blended into polypropylene (PP) resins at a concentration of 5wt%, which was adequate for quantitative analysis of the anhydride functional group conversion using a FT-IR spectrometer.

Distributive mixing, or the generation of interfacial area, was investigated during melt-melt blending of two segregated PP streams in a co-rotating twin screw extruder. Each PP stream contained one of the reactive polymers, which come into contact and react at the growing interface. A tandem single / twin screw extruder apparatus was used to perform the melt-melt blending experiments. One stream was metered to the beginning of the twin screw extruder, and the second was melt fed at a desired downstream position using the single

screw extruder. As verified using model interfacial reactions, the coupling of anhydride and primary amine functional groups was mixing limited, and the anhydride conversion was linearly related to the interfacial area available for the reaction. A slit die at the end of the twin screw extruder was used to prepare a film for FT-IR analysis of the anhydride conversion, which was a direct measurement of the overall distributive mixing performance of the melt-melt blending section of the twin screw extruder. Experiments were completed to investigate the effects of operating conditions, screw configuration, and polymer viscosity on the overall distributive mixing. In addition, a washout of the anhydride polymer tracer was used to measure the cumulative RTD in the melt-melt blending section. Distributive mixing increased with the average residence time, but it was not related to the macromixing. With respect to the kneading block geometry, the overall distributive mixing performance followed the trend of: forward > reverse > neutral at 50 g/min and reverse > neutral > forward at 100 g/min. Distributive mixing with neutral and reverse kneading block was controlled by the average residence time, the shear rate, and the fully filled volume. Conversely, the screw configuration containing the forward kneading block exhibited different trends with respect to the operating conditions, and its superior mixing at the low flow rate was attributed to possible regions of flow stagnation. In addition to the effects of operating conditions and screw design, the melt-melt blending of lower viscosity PP resins resulted in significantly greater distributive mixing.

Specially designed sampling devices were used to investigate the distributive mixing profile along the length of the twin screw extruder during melt-melt blending. The mixing profiles for screw configurations containing neutral and reverse kneading block were similar. In particular, 60 to 85% of the overall distributive mixing was completed in the conveying

section prior to each kneading block. In contrast, the best local distributive mixing was completed in the forward kneading block, especially at lower flow rates. Mixing in conveying sections predominately occurred in the fully filled region due to the higher shear rates applied to the polymer melt. The fully filled fraction was the controlling variable for distributive mixing in the conveying section because it incorporated the effects of both the operating conditions and the pressure at the end of the conveying section. Local residence time measurements were completed in the conveying section and kneading block using a carbon black tracer and an IR temperature probe. This method was valid for the determination of the local average residence time in the extruder, but the distribution of residence times was affected by the local flow field at the probe position. The combination of a longer local average residence time and a polymer backup in the conveying elements prior to the partially filled forward kneading block suggested the existence of stagnant flow regions. These stagnant flow regions were also manifested by a significantly larger melt temperature rise across the forward kneading block. Flow through the high shear rate gaps in the forward kneading block caused its superior local distributive mixing as well as the higher melt temperature rise.

ACKNOWLEDGMENTS

I would like to thank my supervisor, Professor Costas Tzoganakis, for all his support and advice in this research. Thank you for suggesting a challenging and rewarding research topic.

All the fellow students of the polymer processing group have helped to make the last four years truly enjoyable. In particular, I wish to single out Mike Thompson and Minhee Lee for all the advice they have given me as well as their friendship.

I have had the pleasure to present my research at many technical conferences, and the questions and comments I received greatly benefited this research. In particular, I would like to thank Dr. Chi-Kai Shih of DuPont and Professor Ica Manas-Zloczower of Case Western Reserve University for their helpful questions and comments.

I would like to thank the following companies for material donations for this research: Crowley Chemicals, Montell, Equistar, and Standard Products. I would like to graciously acknowledge the Natural Sciences and Engineering Research Council (NSERC) of Canada for their financial support.

I would like to thank all my family for their love and prayers; Bill and Heidi Shearer, Carol and Rod Fox, Bob and Marylyn McRoberts, Glenda Shearer, Phil and Libby McRoberts, Steve McRoberts.

Finally, I would like to dedicate this thesis to my wife, Rebecca, and our family. I cannot thank you, Rebecca, enough for your love and guidance in my life. The Lord has blessed us with so much in these last few years. Jared, you are a gift from God that brightens our lives everyday. So many wonderful changes and so many more to come...

This righteousness from God comes through faith in Jesus Christ to all who believe.

There is no difference, for all have sinned and fall short of the glory of God,

and are justified freely by his grace through the redemption that came by Christ Jesus.

Romans 3:22-24

To my family

TABLE OF CONTENTS

LIST OF TABLES

LIST OF FIGURES

NOMENCLATURE

Abbreviations

BEM	Boundary Element Method
^{13}C NMR	Carbon Nuclear Magnetic Resonance
DSC	Differential Scanning Calorimetry
EPDM	Ethylene Propylene Terpolymer Rubber
EPR	Ethylene Propylene Rubber
EPR-g-mAh	Maleic Anhydride Grafted Ethylene Propylene Rubber
EVA	Ethylene Vinyl Acetate
FAN	Flow Analysis Network
FEM	Finite Element Method
FT-IR	Fourier Transform Infrared
^{1}H NMR	Proton Nuclear Magnetic Resonance
H_2O_2	Hydrogen Peroxide
HDPE	High Density Polyethylene
IR	Infrared
LDPE	Low Density Polyethylene
LLDPE	Linear Low Density Polyethylene
mAh	Maleic Anhydride
MFI	Melt Flow Index
N_2	Nitrogen
NaCl	Sodium Chloride
NaOH	Sodium Hydroxide
Net SEC	Net Specific Energy Consumption (kW hr/kg)
PA6	Polyamide-6 or nylon-6
PBT	Poly(Butylene Terephthalate)
PC	Polycarbonate
PDI	Polydispersity Index
PDMS	Polydimethylsiloxane
PE	Polyethylene
PP	Polypropylene
PP-g-mAh	Maleic Anhydride Grafted Polypropylene
PPO	Poly(Phenylene Oxide)
PS	Polystyrene
RTD	Residence Time Distribution
SEM	Scanning Electron Microscopy
SMA	Styrene Maleic Anhydride Copolymer
TCB	Trichlorobenzene
TEM	Transition Electron Microscopy
THF	Tetrahydrofuran
TiO_2	Titanium Oxide
wt%	Weight Percent

Symbols

β	Temperature Coefficient in Power-law Viscosity Model (1/°C)
β_i	Coefficient in Linear Regression Model
ε	Energy Dissipation Rate (W/kg)
$\dot{\gamma}$	Apparent Shear Rate (s^{-1})
η	Apparent Shear Viscosity (Pa.s)
λ_k	Kolmogoroff Size Scale (μm)
ν	Kinematic Viscosity (m^2/s)
σ^2	Variance of a RTD (s^2)
C_{HCl}	HCl Concentration in Titration Standard (M)
C_{sAh}	Concentration of Succinic Anhydride Functional Groups in PP (mole/g PP)
D	Screw Diameter (m)
f(t)	Residence Time Density Function
H	Channel Depth of Single Screw Extruder (m)
K	Consistency Index in Power-law Viscosity Model ($Pa.s^n$)
M	Mass of Polymer in Solution (g)
M_n	Number Average Molecular Weight (g/mole)
n	Flow Index in Power-law Viscosity Model
N	Screw Speed (rpm)
$\Delta P/L$	Pressure Drop Across Length L in Single Screw Extruder (Pa/m)
Q	Volumetric Flow Rate (m^3/s)
RPH	Relative Peak Height of Peak in FT-IR Spectrum
Δt	Time Interval in RTD Calculations (s)
$\bar{t}$	Average Residence Time (s)
T	Temperature Reading of IR Probe (°C)
T^D	Dimensionless Temperature for Local RTD Measurement
T_g	Glass Transition Temperature (°C)
T_{max}	Maximum Temperature for Local RTD Measurement (°C)
T_{min}	Minimum Temperature for Local RTD Measurement (°C)
U	Barrel Velocity with Respect to a Stationary Screw (m/s)
V_{HCl}^{Blank}	Volume of HCl Solution Used to Neutralize the Blank (mL)
V_{HCl}^{Sample}	Volume of HCl Solution Used to Neutralize Sample with Polymer (mL)
W	Channel Width of Single Screw Extruder (m)
W(t)	Washout Function
X	Selectivity of Competitive-Consecutive Reaction

CHAPTER 1
INTRODUCTION AND OBJECTIVES

1.1. Introduction

The purpose of a mixing process is to increase the randomness, or the uniformity, of the mixture. It is a critical process because the final material properties of a polymer product depend on its uniformity (Hold, 1982). Turbulent mixing of polymers is not possible due to their high viscosities, and diffusion is very limited during the short times used in common processing applications. Therefore, mixing of polymers is solely completed by the deformation of the material during laminar flow. Nearly all polymers pass through an extruder prior to the production of their finished products. In particular, twin screw extruders are used in applications that require mixing, such as polymer blending, compounding, and reactive extrusion. In the case of immiscible polymer blending, the rheological and mechanical properties depend on the morphology, which is affected by the conditions of the mixing process as well as the properties of the blended polymers.

Dispersive and distributive mixing are required to produce an useful polymer product. The former results in the breakup of cohesive agglomerates, while the latter increases the homogeneity of the mixture. Using a wide variety of experimental techniques, dispersive mixing has been extensively investigated during polymer blending in twin screw extruders (Gogos *et al.*, 1996; Lee and White, 1997; Franzheim *et al.*, 1997b). Following the decrease in the size of the agglomerates is a simple method to quantitatively investigate the dispersive mixing process. Distributive mixing during liquid-liquid blending is characterized by the generation of interfacial area between the distinct phases. Interfacial area is very difficult to

quantitatively measure, and therefore, there is a lack of experimental data on distributive mixing in extruders during polymer blending.

In conventional chemical reactors, such as batch reactors and continuous stirred tank reactors (CSTR), the state of mixing on the molecular level has been studied using various special chemical reactions (Fournier *et al.*, 1996). In particular, the conversion of a fast bimolecular reaction and the selectivity of a competitive-consecutive reaction were used to quantitatively measure the micromixing (Chella and Ottino, 1984; Ou and Ranz, 1983a; 1983b). Application of these methods to the analysis of mixing during polymer processing is very limited. Wu (1994) attempted to use a competitive-consecutive reaction between small molecule anhydride and amine compounds to investigate micromixing during the melt-melt blending of segregated streams of a PE wax in kneading blocks of a co-rotating twin screw extruder. Small molecule polar compounds are not compatible with hydrophobic polyolefins, such as PE and PP, and therefore, their reactions are not well suited to the analysis of mixing during polymer blending in extruders. In this research, a fast bimolecular reaction between two low molecular weight reactive polymers was used to study micromixing during melt-melt blending of PP in a co-rotating twin screw extruder. The conversion of the interfacial reaction is also a direct measurement of the distributive mixing.

1.2. Research Objectives

The research described in this thesis investigated a novel method to quantitatively measure distributive mixing during polymer blending in a twin screw extruder. The motivation for this research was the lack of experimental data on distributive mixing in extruders because of the difficulty in directly measuring interfacial area generation. The

research was divided into the following three objectives: i) preparation of the reactive polymer tracers, ii) validation of the method, and iii) application of the method to the analysis of distributive mixing during melt-melt blending of PP in a co-rotating twin screw extruder. For the first objective, anhydride and primary amine functional groups were selected because their fast coupling reaction is mixing limited during polymer processing applications (Maier *et al.*, 1994). Targeted functionalization of existing terminal double bonds in a low molecular polyolefin was completed. In contrast to conventional free radical functionalization techniques, targeted functionalization results in site specific grafting of the functional group without undesired side reactions, such as crosslinking and degradation. For the mixing experiments, the reactive polymers were separately blended into PP resins at a concentration of 5wt%. To accomplish the second objective, model interfacial reactions between the reactive polymers in molten PP were completed. In particular, the kinetics of the anhydride – amine reaction and the diffusion rates of the reactive polymers in molten PP were investigated. Finally, the novel method was used to quantitatively measure distributive mixing by analyzing the conversion of the anhydride functional groups during melt-melt blending of segregated PP streams in a twin screw extruder. Investigated factors included the operating conditions, the screw configuration, and the polymer viscosity. In addition, RTD measurements were completed to gain a complete understanding of the mixing in the extruder on both the macroscopic and microscopic levels.

1.3. Dissertation Outline

This thesis is divided into nine chapters including the introduction. Chapter 2 discusses the classifications of extruders and the types of mixing that occur during polymer

processing. A separate review of dispersive mixing, distributive mixing, and RTD in twin screw extruders is presented. In addition, the use of special chemical reactions to investigate micromixing in conventional chemical reactors as well as their limited applications to the analysis of polymer mixing is described. Chapter 3 presents the methods used to prepare the anhydride and amine reactive polymers. A detailed review of both conventional free radical functionalization and targeted functionalization techniques is presented. The functionalized polymers as well as their reaction product are then characterized. Chapter 4 is an overview of the materials, equipment, procedures, and analysis methods used in the mixing experiments. The experimental method is validated using model interfacial reactions and preliminary melt-melt blending experiments in Chapter 5. A detailed investigation of the effects of operating conditions and kneading block geometry on the overall distributive mixing of the twin screw extruder is presented in Chapter 6. Particular attention is given to the identification of the controlling variables for distributive mixing as well as the determination of the relationships between distributive mixing and RTD measurements. Chapter 7 describes the analysis of the distributive mixing profile along the length of the melt-melt blending section of the twin screw extruder. Specially designed sampling devices were used to extract samples of the polymer melt at desired positions along the extruder during its continuous operation. The mixing in conveying sections and kneading blocks were compared at various operating conditions. In addition, local residence time, fill distribution, and temperature rise measurements were completed to gain a better understanding of the mixing process in the extruder. Chapter 8 presents the conclusions of this research as well as recommendations for further work. Finally, the references cited in this thesis are compiled in Chapter 9.

CHAPTER 2
LITERATURE REVIEW

Mixing is a process that involves the intermingling of initially segregated components by mechanical means (Erwin, 1992), with the objective of obtaining an uniform product. Turbulence in polymer melts is not achievable due to their high viscosities and diffusion is very limited. In polymer processing applications, the desired uniformity is achieved by convective mixing during laminar flow. This chapter discusses the processing of polymers in extruders and the different classifications of mixing that are required to obtain an useful polymer product. Particular attention is then given to the investigations of each classification of mixing in extruders. Finally, the analysis of mixing in conventional chemical reactors using special chemical reactions is discussed as well as the limited applications of these methods to the analysis of mixing during polymer processing.

2.1. Classifications of Extruders and Mixing

Nearly all polymers pass through an extruder between their polymerization and the fabrication of the finished product. The processing steps that can be completed in an extruder are: solid conveying, melting, mixing, melt sealing, devolatilization, and pumping. Twin screw extruders are most often used in operations that require mixing because their modular design allows for tailoring the screw configuration to the desired process. The geometry of a single screw extruder is defined by the following: barrel diameter, screw lead (pitch), channel depth, flight width, and radial clearance between the barrel wall and the top of the flight. Conversely, the design of twin screw extruders is more complex due to their different possible operation modes. Twin screw extruder classifications are based on the

direction of the screw rotation and the degree of flight intermeshing. Another classification method is based on the possible flow paths in the longitudinal direction (down the unwound screw channel) and the crosswise direction (rotating around a single screw). The most common classifications of twin screw extruders are presented in Table 2.1 and Figure 2.1 (Sakai, 1994).

Table 2.1. Classifications of Twin Screw Extruders

Screw Rotation Mode	Degree of Flight Intermeshing	Longitudinal Flow	Crosswise Flow
Co-rotation	Fully	Open	Closed
Counter-rotation	Fully	Closed	Closed
Counter-rotation	Tangential	Open	Open

Fully intermeshing counter-rotating twin screw extruders have been extensively investigated by Janssen (1978). The closed C-chambers formed between the surfaces of the screws and barrel, depicted in Figure 2.2 (Janssen, 1991), result in positive displacement flow. This flow mechanism results in efficient pumping characteristics, but the pressure arising from lubrication flow through the calendaring gap causes a low maximum operating screw speed. Fully intermeshing co-rotating twin screw extruders are described as self cleaning due to their complete flight penetration. Figure 2.3 (White, 1990) depicts the flow path in the conveying elements of a fully intermeshing co-rotating twin screw extruder, which is a figure-8 caused by the drag flow between the screws and barrel surfaces.

Screw design and operating conditions determine the flow patterns in the twin screw extruder, which affect its mixing capability. The screw configuration of a modular twin screw extruder consists of a number of elements placed along the two shafts in a desired order. There are many different types of screw and mixing elements, but the most common

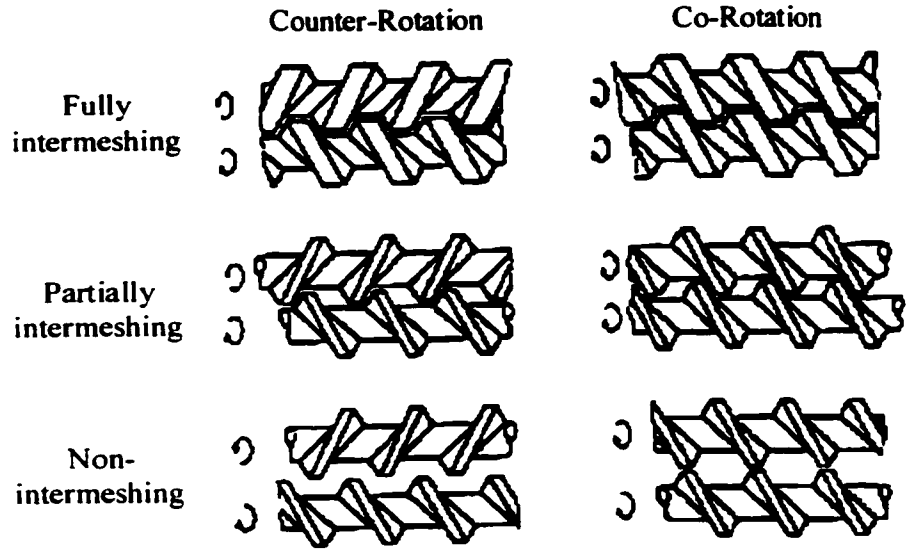

Figure 2.1. Examples of Twin Screw Extruder Classifications (Sakai, 1994)

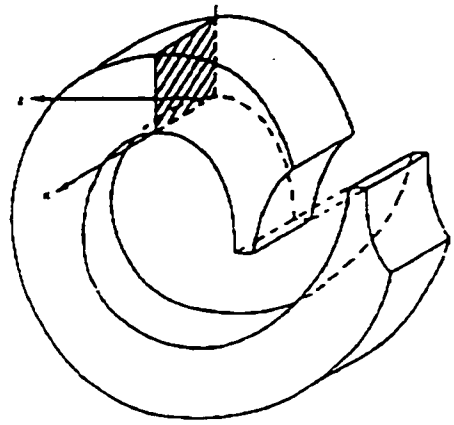

Figure 2.2. Closed C-chamber of Counter-rotating Twin Screw Extruder (Janssen, 1991)

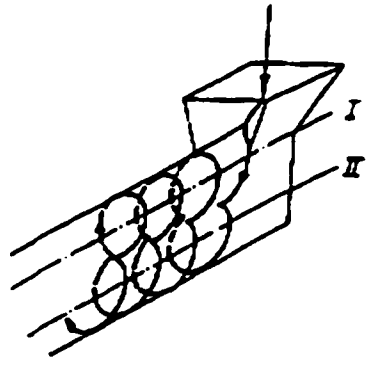

Figure 2.3. Flow Path in Fully Intermeshing Co-rotating Twin Screw Extruder (White, 1990)

are conveying elements and kneading discs, which are depicted in Figure 2.4. The pumping capacity of a conveying element is determined by its pitch. A series of adjacent kneading discs is referred to as a kneading block, which are the elements predominately used to perform the required melting and mixing in twin screw extruders. The stagger angle between adjacent kneading discs can be varied, which affects its pumping characteristics (White and Szydlowski, 1987).

Macroscopic simulations of polymer processing in co-rotating twin screw extruders have been presented by Potente *et al.* (1994), White and Szydlowski (1987), White and Chen (1994), Bawiskar and White (1997), Strutt (1998), and Vergnes *et al.* (1998). These composite models allow for the calculation of the profiles of melting, temperature, pressure, residence time, and degree of fill along the length of the extruder. The simulation programs can be used to aid polymer processors in the selection of the screw configuration, which is usually considered more art than science, and the operating conditions for a desired extrusion process. These methods are based on 1-D approximations of the flow in the extruder, which results in short computation times. Conversely, the flow patterns in twin screw extruders are 3-D, and therefore, the simulations cannot effectively predict the mixing capability. Thus, the simulations sacrifice detail for their simplicity.

Mixing during polymer blending, compounding, and reactive extrusion applications is critical because the final properties of a polymer product depend on the quality of mixing achieved by the extruder. For example, composition uniformity is required to obtain good final properties (Hold, 1982). In their review on the mixing of polymers during laminar flow, Ottino and Chella (1983) noted that the final properties of a polymer blend depend on the properties of the individual polymers, their compatibility, and the processing conditions

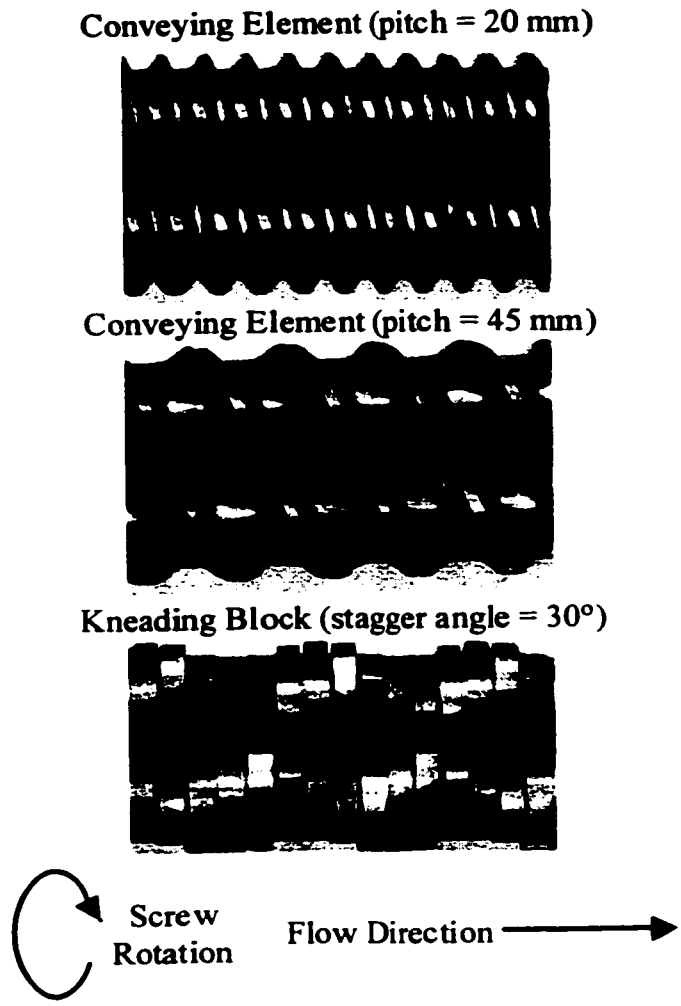

Figure 2.4. Common Elements for Co-rotating Twin Screw Extruders

(which determine the quality of mixing). In the case of an immiscible polymer blend, its morphology determines the physical properties (Franzheim *et al.*, 1997a). For example, a laminar morphology (distinct layers of the minor phase in the matrix), which was generated in a twin screw extruder during the blending of HDPE and PA6, exhibited excellent barrier properties, such as reduced toluene permeability (Rodriguez-Veloz and Kamal, 1999). Finally, the conversion of a chemical reaction between a polymer melt and incompatible small molecule polar reactants during a reactive extrusion process, is dependent on the mass transfer, which is enhanced by effective mixing of the distinct phases (Ganzeveld and Janssen, 1990; 1994).

There are two general categories of mixing that occur during polymer processing. The first is dispersive mixing, which results in the breakup of cohesive agglomerates. These cohesive agglomerates can be filler particles or the minor component of an immiscible polymer blend. Due to the cohesive nature of the agglomerates, both applied stress and shear rate are important in the dispersive mixing process. The dispersive mixing efficiency depends on the viscosity ratio of the minor and continuous phases as well as the type of deformation. For all viscosity ratios, elongational flow results in more efficient dispersive mixing (Meijer and Janssen, 1994). Consider the breakup of a droplet of an immiscible fluid in a continuous matrix. Shear flows result in less efficient dispersive mixing because of the internal circulatory flow that develops inside the droplet due to its rotation in the shear field (Karam and Bellinger, 1968). This internal circulation causes a high internal pressure that resists droplet pinching, which is required for the breakup. In some instances, Karam and Bellinger (1968) observed breakup of the droplets after the shearing stress was ceased because the pinching was no longer resisted by the internal pressure.

The second classification of mixing is convective mixing by laminar flow, which yields the homogenization of a mixture of components. This type of mixing is often referred to as distributive mixing, which is convective mixing obtained through fluid rearrangement without deformation. In an extruder, the mixing is caused by deformation from the laminar flow, but the common terminology will be used in this thesis. While dispersive mixing is required only in applications involving a cohesive phase, distributive mixing is required to ensure product uniformity in all applications. As well, distributive mixing is the only type of mixing required when blending miscible polymers. During liquid-liquid blending, distributive mixing is characterized by the generation of interfacial area, which is directly related to the initial interfacial area, the applied strain, and the orientation of the interface in the flow field (Spencer and Wiley, 1951).

Similar to dispersive mixing, the efficiency of distributive mixing depends on the type of deformation. Efficiency is investigated by considering the stretching of a line connecting two points in the flow field. Elongational flow results in an exponential growth of the line as a function of the applied strain, while in shear flow only a linear growth is obtained (Meijer and Janssen, 1994). Rotation of the line in the shear flow field decreases the efficiency as the line orients with the direction of the streamlines. An exponential dependence is obtained in shear flows with a periodic rearrangement of the line, which results in randomization of its orientation (Rauwendaal, 1994).

The mixing of a droplet of an immiscible polymer in a continuous matrix is commonly evaluated using the capillary number, which is the ratio of the shear stress and the interfacial stress. A detailed review of the experimental and theoretical analyses of drop deformation and breakup has been presented by Meijer and Janssen (1994). Below a critical

capillary number, which depends on the type of flow (shear versus elongation) and the viscosity ratio of the dispersed and continuous phases, the drop is stable. Distributive mixing, or deformation via stretching of the droplet into a thread or filament, occurs for large capillary numbers because the shear stresses dominate the interfacial stresses. Conversely, dispersive mixing occurs when the capillary number approaches the critical value because the interfacial stresses compete with the shear stresses. Rayleigh disturbances then grow at the interface and the polymer filament disintegrates into small droplets.

During polymer processing in extruders, dispersive and distributive mixing occur simultaneously. Both types of mixing are required to obtain good properties in the final product, and Figure 2.5 depicts the possible scenarios that can occur if a proper balance of both classifications of mixing are not achieved (adapted from Gale, 1997). The process that is depicted in Figure 2.5 represents the mixing of a cohesive agglomerate, such as a filler, into a continuous polymer matrix. Dispersive mixing is required to reduce the agglomerate size, and distributive mixing is required to improve the uniformity of the mixture. The stresses applied on the agglomerates from the matrix results in the dispersive mixing, and convection due to the fluid motion results in the distributive mixing. It is important to note, that interfacial area is not generated during the distribution of the particles in the matrix. This mixing process is completely different from the distributive mixing that occurs during polymer blending. As previously mentioned, distributive mixing is characterized by the generation of interfacial area during liquid-liquid mixing. Area generation is caused by the deformation of the fluids, which is directly related to the applied strain. In this thesis, distributive mixing refers to the homogenization of a mixture via the generation of interfacial area between distinct liquid phases.

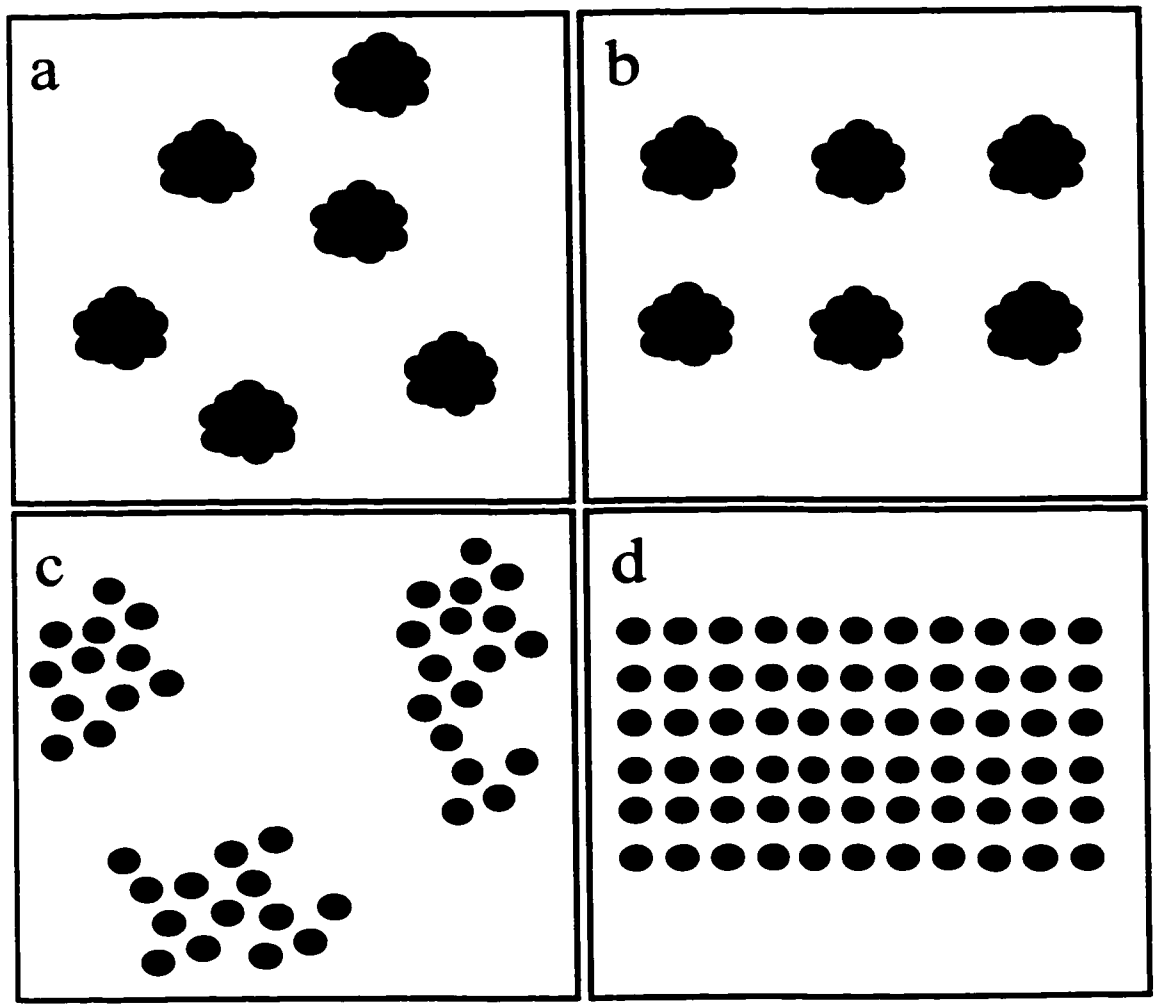

Figure 2.5. Scenarios of Dispersive and Distributive Mixing During the Blending of an Agglomerate into a Polymer Matrix (adapted from Gale, 1997)

a) bad dispersive mixing, bad distributive mixing
b) bad dispersive mixing, good distributive mixing
c) good dispersive mixing, bad distributive mixing
d) good dispersive mixing, good distributive mixing

A measurement of the mixing quality is required to quantitatively investigate a mixing process. To define the goodness of mixing, one must choose a scale of scrutiny (Danckwerts, 1953a) because all mixtures are poorly mixed if one considers a sufficiently small scale. Danckwerts (1952) proposed the now classical measurements of the scale and intensity of segregation of a mixture. These indices describe the mixing quality of a fine-grained mixture, in which the scale of scrutiny is significantly smaller than the total system volume, but consists of many particles of the components to be mixed (Danckwerts, 1953a). The scale of segregation is a measure of the size of the undistributed domains and the intensity of segregation is a measure of the difference between the composition of the undistributed domains and the average composition of the mixture. The intensity of segregation is reduced by diffusion of the material at the interfaces between the distinct domains. As previously mentioned, diffusion of polymers during processing operations is negligible. Therefore, polymer mixing is accomplished by reducing the scale of segregation through mechanical means. During polymer blending, the mechanical mixing is achieved by deforming the fluid in shear or elongational flows.

Mohr *et al.* (1957) proposed that the striation thickness, which is the characteristic distance between segregated phases, is a better measurement of the mixing quality of polymer blends. The striation thickness, which is directly related to the interfacial area between the segregated phases, was a function of the applied strain, the initial striation thickness, and the orientation of the interface to the flow direction. Bigio and Stry (1990) reported that a characteristic direction of the flow pattern is required to produce a striation pattern that can easily be quantified for analysis of the mixing. For unidirectional flows, a

simple quantitative measure of the mixing quality was the number of striations in a cross section of the flow.

A significant amount of research has been completed to determine the mixing capability of twin screw extruders. Rauwendaal (1981) performed an experimental comparison of co-rotating and counter-rotating twin screw extruders and observed that the former was superior for distributive mixing and the latter was superior for dispersive mixing. Flow through the calendaring gap, which is a high shear rate region due to the tight clearance between the screws of the counter-rotating twin screw extruder, was proposed to result in its superior dispersive mixing capability. Andersen (1994) presented two figures, which have been reproduced in Figure 2.6, that indicate the mixing capabilities of different kneading block configurations in the co-rotation mode. The figures were presented without experimental data to confirm the proposed trends. Using dynamic pressure measurements, Christiano and Lindenfelzer (1997) investigated the effect of the kneading disc stagger angle on the pressure profile and flow patterns in a co-rotating twin screw extruder. Based on the results, they proposed a dispersive and distributive mixing capability to each kneading block design, but no direct measurements of the mixing quality were offered to confirm their proposed trends. Most polymer mixing research has focused on one mixing classification, and therefore, a separate review of dispersive and distributive mixing is now presented.

2.2. Investigations of Dispersive Mixing

Dispersive mixing is relatively easy to measure using optical microscopy, scanning electron microscopy (SEM), or transmission electron microscopy (TEM) to follow the reduction in the size of the cohesive agglomerates. The majority of the research on

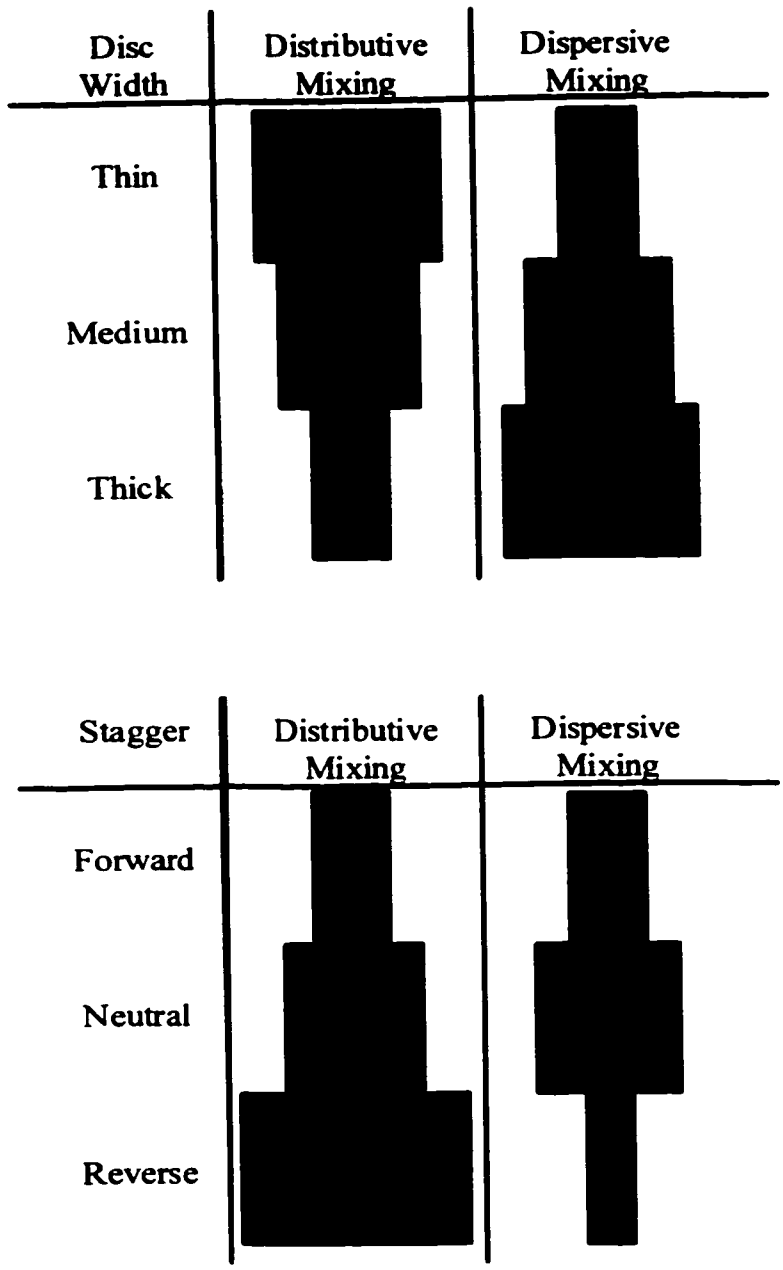

Figure 2.6. Kneading Block Mixing Capability Proposed by Andersen (1994)

dispersive mixing has focused on the blending of immiscible polymers and the evolution of the morphology from the initial pellet state to the final product obtained from the extruder. The largest amount of dispersive mixing (reduction in minor phase domain size) was observed in the melting zone of a twin screw extruder, while only a small change in the domain size was observed in the molten polymer mixing zone (Sakai, 1995). These observations were attributed to the large stresses applied to the polymer during the melting transition. Conversely, Favis and Therrien (1991) observed that the morphology of PP / PC blends was most significantly affected by the flow through the die at the end of the twin screw extruder. Sundararaj *et al.* (1995) proposed that the morphology development during melting involves the formation of sheets from pellets, which then breakup into cylinders and droplets. Rapid morphology development was also observed during melt blending of segregated streams of PE and PS in a co-rotating twin screw extruder, which indicated that the overall polymer blend morphology is not solely determined during the melting transition (Bourry and Favis, 1998). In addition, Huneault (1998) observed identical morphologies from both the conventional compounding of premixed solids and the blending of segregated polymer melts in a co-rotating twin screw extruder. Melt-melt blending exhibited a similar mixing efficiency even for the dispersion of a significantly higher viscosity polymer melt into the matrix. Melt blending of segregated polymer melts has also been investigated in single screw extruders (Gale, 1997; Esseghir *et al.* 1998).

Using a dead stop / freeze polymer / screw extraction procedure, the evolution of the morphology during the blending of HDPE and PS (25/75) was investigated in a co-rotating twin screw extruder (Cho and White, 1995). The most rapid reduction in the size of the PE domains was achieved by kneading blocks placed early in the screw configuration. The

results confirmed the importance of the melting zone on the overall dispersive mixing. Using the same procedure, Lee and White (1997) observed faster morphology development and smaller minor phase domains when additional kneading blocks were added to the screw configuration. As well, slower morphology development was observed during the blending of resins with greatly different viscosities. Comparing different types of mixing elements indicated that the dispersive mixing performance of turbine elements was superior to that of kneading blocks with various stagger angles.

Using three sampling nozzles (specially designed barrels with a screw valve), Nishio *et al.* (1991) investigated the morphology development of PP / PA6 blends with the addition of maleic anhydride grafted PP (PP-g-mAh). These sampling nozzles allowed for direct sampling of the polymer melt during continuous operation of the extruder, and the domain size of the minor phase decreased along the length of the extruder. Simultaneously, the amount of copolymer formed by the reaction between PA6 and PP-g-mAh increased along the length of the extruder. Recently, Cartier and Hu (1999) investigated the morphology development during the reactive compatibilized blending of PP and PA6 using PP-g-mAh in a co-rotating twin screw extruder. Morphology development was extremely rapid and the final minor phase (PA6) domain size was achieved at the end of the melting section. The experimental results were attributed to the apparent instantaneous reaction kinetics of the first step of the reaction between anhydride and primary amine functional groups. Operating conditions and additional kneading blocks in the melt mixing section did not significantly affect the final morphology.

Direct polymer melt sampling using specially designed barrel plates was also used by Franzheim *et al.* (1997a; 1997b) to investigate dispersive mixing during the blending PP and

PA6 in a co-rotating twin screw extruder. Sampling was completed at various positions along a kneading block, and a reduction in the minor phase domain size was observed. The kneading block was located at the end of the extruder and the morphology development prior to the kneading block was not investigated (1997a; 1997b). The kneading block design (disc width and stagger angle) did not significantly affect the reduction in the minor phase domain size (Franzheim *et al.*, 1997a). In further work, operating conditions did not significantly affect the dispersive mixing process, and it was noted that most of the morphology development occurred during the melting transition prior to the sampling positions in the melt blending section of the twin screw extruder (Potente *et al.*, 1999).

Gogos *et al.* (1994; 1996) used a co-rotating twin screw extruder with a clam shell barrel, which allowed for rapid sampling of the polymer melt directly from the screws upon stopping the extruder and opening the barrel, to investigate dispersive mixing. Sampling was completed along a kneading block, and the dispersion quality improved as the screw speed was increased from 60 to 120 rpm. As well, blending of LDPE and PS resins with different viscosity ratios was completed, and four different dispersion mechanisms were observed. Along with the viscosity ratio, the Deborah number, or the ratio of the relaxation time and the experiment time, was a critical factor for understanding the final blend morphology.

Huneault *et al.* (1996a) investigated the blending of PE and PS in a co-rotating twin screw extruder using open ports to remove samples during continuous processing. Immediately after the melting zone, the minor phase was observed in fibrillar form, which remained stable during the melt conveying and mixing zone in the extruder. Rapid cooling was required to accurately investigate the morphology development because a slow cooling rate allows the fibers to relax into spherical domains. As well, breakup of the fibers into

droplets was proposed to occur predominately in the fully filled pressurized zones of the extruder.

Elongational flow results in more efficient dispersive mixing, which is especially important when blending polymers with a high viscosity ratio (dispersed phase / continuous phase >> 1). Luciani and Utracki (1996) designed an extensional flow mixer (EFM) that promotes converging / diverging flow and connects to the end of a single screw extruder. As compared with a co-rotating twin screw extruder, the EFM (fed by a single screw extruder) achieved similar levels of dispersion. Thus, the EFM offers a reasonable alternative to twin screw extruders for polymer blending, but the modular twin screw extruder remains more flexible for use in other applications, such as reactive extrusion.

A significant amount of numerical modeling of the flow patterns in kneading blocks has been completed to predict their mixing capabilities. Finite element (FEM) simulations were performed and the dispersive mixing capabilities of bilobal and trilobal kneading discs was quantified using a mixing efficiency (Cheng and Manas-Zloczower, 1997). This mixing efficiency was the ratio of the magnitude of the rate of deformation tensor and the sum of the magnitude of the rate of deformation tensor and the magnitude of the vorticity tensor. In the extreme cases, the efficiency parameter is equal to 0 for pure rotational flow and 1 for pure elongational flow. The basis of this numerical method is that a larger elongational flow component (higher efficiency) results in improved dispersive mixing. The elongational flow component was predicted to be independent of the processing conditions. In addition, the mixing efficiencies of forward and reverse staggered kneading discs were not significantly different. Comparing the trilobal and bilobal designs, the former exhibited a slightly higher elongational flow component. FEM simulations of the flow in trilobal kneading discs and

staggered mixing discs have also been completed by Bruce *et al.* (1997). Using the same mixing efficiency as previously described, the elongation flow components were calculated. Rios *et al.* (1998) used the boundary element method (BEM) to numerically investigate the flow of a Newtonian fluid in fully filled co-rotating twin screw conveying elements. Changing the geometry of the screw elements by varying the centerline distance and screw tip angle did not significantly affect the elongation flow component. As well, Rios *et al.* (1999) attempted to include non-linear effects into the BEM simulations, but the numerical simulations deviated from analytical solutions for simple flow situations (for example, pressure flow in a tube) when the power-law index was lower than 0.7. Most polymer melts exhibit greater shear thinning behavior, and therefore, the BEM simulation method cannot be effectively extended from Newtonian materials to realistic polymer melts.

2.3. Investigations of Distributive Mixing

Distributive mixing of polymer melts is characterized by the generation of interfacial area, which is much more difficult to experimentally measure as compared to the particle size of a minor phase component for the analysis of dispersive mixing. Due to this difficulty, distributive mixing has not been extensively investigated. Shearer (1973) proposed that bulk mixing, or convective mixing, of high viscosity fluids requires subdivision and redistribution of the flow. In laminar flow, the fluid moves along streamlines and mixing is very limited without effective flow rearrangement. In addition, distributive mixing efficiency decreases as the stretching area aligns with the streamlines. Bigio *et al.* (1985) verified that the addition of a mixing pin in the screw channel of a conventional single screw extruder reoriented the streamlines, which tend to align with the directions of the shear field in the

screw channel. The interfacial area generation was linearly related to the applied strain, but the addition of a mixing pin resulted in a faster rate of mixing due to this fluid rearrangement. Numerical investigations of the fluid streamline rearrangement caused by mixing pins have been completed by Erwin and Mokhtarian (1983) and Yao *et al.* (1995).

Bigio and Conner (1995) presented an analysis of distributive mixing based on the calculation of two different efficiencies. The line efficiency is a measure of the orientation of the line to the optimum direction for maximum growth in the flow field (referred to as the direction of the maximum principal rate of deformation). In contrast, the flow efficiency indicates the ability of the flow to transfer energy into the direction of optimum mixing. Thus, the two efficiencies isolate the effects of the flow field and line orientation on distributive mixing.

Measuring the interfacial area between two liquid phases is very difficult. Alternatively, it is easier to count the number of striations in a cross section of the flow. Relationships between the striation count in a cross section of the flow and the interfacial area have been presented by Bigio and Stry (1990), but the relationship is only valid if there is a characteristic direction to the mixing pattern. Despite the limitations of this method, striation counting has been used to investigate distributive mixing in co-rotating twin screw extruders. Bigio and Erwin (1985) blended segregated streams of a silicone fluid with black and white pigments. After establishing steady-state flow, the co-rotating twin screw extruder was stopped and the silicone fluids were cured and then pealed from the screws. The striation count in a cross section of the cured silicone rubber scaled linearly with the applied strain, and the rate of mixing was faster in a kneading block as compared to a conventional conveying element.

Due to the difficulties in directly measuring distributive mixing in twin screw extruders, flow visualization experiments in co-rotating twin screw extruders with transparent barrels have been completed to investigate the mixing of model materials (Bigio *et al.* 1992; Bigio and Erwin, 1992; Bigio *et al.*, 1994; Sanchez *et al.*, 1997). Using a Newtonian silicone fluid as the continuous phase and an injected line of a black dyed silicone fluid, the line growth was followed along partially filled conveying elements (Bigio *et al.*, 1992, Bigio *et al.*, 1994). Improved mixing, or faster line stretching, was observed at higher degrees of fill. The specific throughput, or the ratio of the flow rate and screw speed, was proposed to be a controlling factor for the distributive mixing process. Visual investigations of the mixing of a low molecular weight additive into corn syrup indicated that mixing in kneading blocks is improved when a restrictive element is placed at the end of the kneading block to increase the back pressure (Sanchez *et al.*, 1997). Similar visualization techniques were used to investigate the mixing in non-intermeshing counter-rotating twin screw extruders (Bigio and Erwin, 1989; Bigio *et al.*, 1991; Baim and Bigio, 1994). The stagger between the flights of the two adjacent screws (Bigio *et al.*, 1991) as well as the volume fraction and viscosity ratio of the segregated phases (Baim and Bigio, 1994) exhibited significant effects on the distributive mixing.

The incorporation of a low viscosity silicone oil into PE was experimentally investigated in a co-rotating twin screw extruder (Burbank *et al.*, 1991). This process requires distributive mixing to incorporate the oil uniformly into the polymer melt. Comparing turbine mixing elements with a block of narrow kneading discs staggered in the forward direction indicated that the former was more effective for incorporating the oil. The mixing of miscible polymers in a twin screw extruder was experimentally investigated using

differential scanning calorimetry (DSC) to follow the mixing process (Klinger *et al.*, 1997). During the blending of miscible polymers, the glass transition temperature (T_g) approaches a single value. Thus, the evolution to a single value of the T_g along the length of the extruder is a direct measurement of the distributive mixing profile. Faster mixing was observed upon increasing the screw speed from 75 to 150 rpm due to the corresponding increase in the shear rate. Kalyon and Sangani (1989) investigated the distributive mixing of a thermoplastic elastomer in a kneading block of a co-rotating twin screw extruder. Using a tracer of pigmented thermoplastic elastomer, the rate of interfacial area generation was qualitatively higher in a reverse kneading block (stagger angle = -30°) as compared with a forward kneading block (stagger angle = 30°). Conversely, the forward spreading, which is an indication of the breadth of the residence time distribution (RTD), was greatest for the forward kneading block and smallest for the reverse kneading block.

Using particle tracking methods, the distributive mixing and RTD in kneading discs staggered in the forward direction were numerically investigated (Lawal and Kalyon, 1995a). Distributive mixing in the kneading block was predicted to occur under chaotic dynamics, which indicated the possibility of an exponential growth in the interfacial area. Using a similar numerical technique, Lawal and Kalyon (1995b) calculated the intensity of segregation to compare the mixing capabilities of kneading blocks staggered at various forward stagger angles. Intensity of segregation is a measure of the homogeneity of the mixture, and it ranges from 0 for a perfectly uniform mixture to 1 for complete segregation. Smaller values of the intensity of segregation were predicted for the flow in kneading blocks with larger forward stagger angles. In addition, numerical analysis of the RTD indicated the

possibility of stagnant flow regions in forward kneading blocks with small stagger angles between the adjacent discs (Lawal and Kalyon, 1995a).

David and Tadmor (1988) used a co-rotating disk processor as a simple processing machine to investigate distributive mixing. Using a combination of experimental results and numerical predictions, it was shown that backflow, which is caused by a high pressure at the discharge, improved the mixing. Numerical methods for analyzing distributive mixing have been presented by Li and Manas-Zloczower (1995) based on the length stretching of a line and the pairwise correlation function. The former is an indication of the spreading that can be achieved, and the latter indicates the global uniformity or distribution. Nichetti and Manas-Zloczower (1999) numerically investigated melt extrusion in a single screw extruder. Distributive mixing was investigated using the length stretch distributions for the spreading of particles that are initially clustered together. Superior distributive mixing, or increased spreading of the clusters, was predicted for materials having lower average molecular weights and broader molecular weight distributions.

Using FEM simulations, Goffart *et al.* (1996) investigated the 3-D flow of a Newtonian fluid in fully filled conveying elements of a co-rotating twin screw extruder. The predicted shear and elongational rates were related to the backflow, which was dependent on the screw speed. In a similar fashion, the 3-D flow in a kneading block was investigated (van der Wal *et al.*, 1996). Pressure, backflow volume, shear rate, and elongational rate depended on the stagger angle between the adjacent kneading discs. Using the FAN (flow analysis network) simulation method, Szydlowski *et al.* (1987, 1988) investigated the flow in kneading blocks with various stagger angles. The backward flux of the flow exhibited a maximum for a forward stagger angle of 60° and reverse stagger angles in the range of –60°

to –75°. Bravo (1998) performed 3-D flow simulations of a Carreau fluid in conveying elements and kneading blocks of a co-rotating twin screw extruder to investigate the pressure profiles, velocity profiles, deformation rates, and RTD. Jaffer *et al.* (1999) compared the numerical predictions of the velocity profiles with experimental measurements completed using particle image velocimetry. Ordered helical type fluid motion was observed in both conveying elements and kneading blocks. Particle tracking was used to investigate the RTD and the deformation rates applied to the polymer (Bravo, 1998). It was predicted that the particles experience a wide distribution of shear rates as they travel through the kneading block. A fraction of the material travels through multiple high shear rate regions, while a significant amount of the material travels through the kneading block without experiencing large deformation rates. Therefore, the average flow characteristics in the kneading block are not sufficient to describe its complex flow and mixing. These simulation methods do not quantify the distributive mixing capability, but the deformation rates affect the mixing process through the applied strain. As well, the backflow or recirculation of the flow may also play an important role in the distributive mixing process.

2.4. Investigations of Residence Time Distributions in Extruders

Residence time distributions (RTD) in extruders is another area of emphasis in polymer mixing research. RTD measurements offer insight on the degree of macromixing, or the axial mixing between packets of particles of different ages. This information is valuable for designing reactive extrusion processes and the processing of degradable polymers. The distribution of residence times resulted in a distribution of conversions during the reaction between diepoxy and diamine groups to form acrylic oligomers in a co-rotating

twin screw extruder (Titier *et al.*, 1996). Macromixing does not reveal information on the state of mixing at the microscopic level, which is also critical in reactive extrusion processes because chemical reactions are molecular events.

Danckwerts (1953b) discussed the relationship between the shape of the F-curve (cumulative RTD) and the mixing efficiency of a continuous system. It was noted that the mixing investigated in this manner is the mixing of materials of different ages at the exit of the system, and perfect mixing (ideal stirred tank) does not imply that the output is homogeneous (depends on the state of mixing at the molecular level). Bigg (1975) verified that distributive mixing during polymer extrusion is directly related to the applied strain, which is predominately determined by the transverse flow in the extruder channel. Conversely, RTD measurements were shown to quantify the distribution of the material in the primary flow direction (down the extruder channel, axial mixing). This axial mixing was not related to the applied strain or the homogeneity of the polymer product. Through the strain applied to the polymer, transverse mixing and product homogeneity is affected by the average residence time. Regardless of these limitations, RTD measurements have been extensively completed to understand the flow and mixing in extruders. In recent work, Shih (1999) proposed that the breadth of the RTD affects the composition uniformity of the polymer product. Composition fluctuations in the feed to the extruder were purposely created, and a broader RTD was able to effectively compensate for these fluctuations by mixing the materials in the primary flow direction.

The most common methods for RTD measurements are pulse and step tests of a tracer, but the former has been predominately used due to the significantly smaller amount of required tracer. A perfect tracer exhibits identical flow properties to the material being

investigated with an attribute (i.e. color, functional group) that allows for its detection. A review of the large amount of RTD research in extrusion applications is presented in Table 2.2 (the literature is grouped according to similar experimental techniques). All the research described in Table 2.2 was completed using a pulse test method.

Table 2.2. Summary of the Literature on RTD Measurement in Extruders

Reference	Extruder Type	Tracer Employed / Measurement Completed
Janssen et al. (1979)	Counter-Rotating (fully intermeshing)	Manganese Dioxide / Off-Line
Tzoganakis et al., (1989)	Single Screw	Manganese Dioxide / Off-Line
Wolf et al. (1986)	Counter-Rotating (fully intermeshing)	Neutron Activated Manganese Dioxide / In-Line
Thompson et al. (1995)	Counter-Rotating (non-intermeshing)	Neutron Activated Manganese Dioxide / In-Line
Huneault et al. (1996b)	Co-rotating (fully intermeshing)	Calcium Carbonate (Ultrasonic Detected) / In-Line
Gendron et al. (1996)	Co-rotating (fully intermeshing)	Calcium Carbonate (Ultrasonic Detected) / In-Line
Wetzel et al. (1997)	Co-rotating (fully intermeshing)	Titanium Oxide (Optical Probe) / In-Line
Xie et al. (1997)	Co-rotating (fully intermeshing)	Fluorescent Dye / In-Line
Bur and Gallant (1991)	Co-rotating (fully intermeshing)	Fluorescent Dye / In-Line
Nietsch *et al.* (1997)	Co-rotating (fully intermeshing)	Carbon Black / In-Line (IR Temperature Probe)
Donoian and Christiano (1999)	Co-rotating (fully intermeshing)	Carbon Black / In-Line (IR Temperature Probe)
Polance and Jayaraman (1995)	Co-rotating (fully intermeshing)	Red Dye (Color detected) / Off-Line
Gasner et al. (1996)	Co-rotating (fully intermeshing)	Visual Detection of Colored Polymer Tracer
Strutt et al. (1997)	Co-rotating (fully intermeshing)	Benzophenone (FT-IR Detected) / Off-Line
Kao and Allison (1984)	Co-rotating (fully intermeshing)	Yellow Dye, Carbon Black (UV Detected) / Off-Line

Reference	Extruder Type	Tracer Employed / Measurement Completed
Weiss and Stamato (1989)	Single Screw	Glass Spheres, Carbon Black, Sulfonated Polystyrene (UV Detected) / Off-Line
Cassagnau et al. (1991)	Co-rotating / Counter-rotating (fully intermeshing)	Phenyl, Anthracene Grafted PVC (UV Detected) / Off-Line
Chen et al. (1995)	Counter-rotating (non-intermeshing)	1-Aminoanthraquinone (UV Detected) / Off-Line
Oberlehner et al. (1994)	Co-rotating (fully intermeshing)	Anthracenemethanol (UV Detected) / Off-Line
Hu and Kadri (1999)	Co-rotating (fully intermeshing)	9-(methylamino-methyl)-antracene, Antracene Grafted PS and PMMA (UV Detected) / Off-Line
Brouwer *et al.* (1999)	Co-rotating (fully intermeshing)	Methylene Blue (UV Detected) / Off-Line

Off-line measurement techniques are usually limited to the analysis of the exit age distribution from samples collected at the die at the end of the extruder. In-line techniques, which require a probe to detect the tracer in the flowing polymer melt, offer the capability of determining the local RTD inside the extruder. Of particular interest is the method of Nietsch *et al.* (1997) that employs a carbon black tracer and an infrared (IR) temperature probe for the measurement of the local RTD in the extruder. Using this method, a temperature change is detected, which according to Nietsch *et al.* (1997) is directly related to the concentration of the carbon black tracer. The underlying principle of this measurement technique is the addition of carbon black changes the surface emissivity of the polymer melt. When there is a high concentration of carbon black, the polymer melt acts like a black body, and the IR probe receives radiation only from the surface of the polymer melt. As the concentration of carbon black decreases, the probe receives radiation from within the polymer melt, which results in a higher detected temperature. The carbon black tracer does

not actually change the melt temperature, but the IR probe is deceived by the changing surface emissivity. According to Nietsch *et al.* (1997), a pulse of carbon black doped polymer yields the residence time density function through the measurement of the dimensionless change in the temperature.

RTD research in the literature has focused on the following two areas: investigation of the effects of experimental factors on the RTD and investigation of the effects of the tracer properties on the RTD results. Relationships between RTD results and the screw speed and flow rate were presented (Kao and Allison, 1984; Gendron *et al.*, 1996; Xie *et al.*, 1997; Strutt *et al.*, 1997). As expected, longer average residence times were observed at lower screw speeds and flow rates. Differences between the RTD in conveying elements and mixing elements were investigated (Oberlehner *et al.*, 1994; Huneault *et al.*, 1996b) as well as differences between different kneading block designs (Wetzel *et al.*, 1997). RTD of special slotted screw elements and gear mixing elements were recently determined for model materials (Brouwer *et al.*, 1999).

Weiss and Stamato (1989) and Cassagnau *et al.* (1991) observed longer average residence times and broader distributions when using particulate tracers as compared with polymeric tracers (polymer chains with a detectable functional group). It is assumed that the tracer has identical flow properties to the polymer, but these results indicated that the particulate tracers exhibited greater axial mixing in the extruder. Recently Hu and Kadri (1999) showed that both particulate and polymeric tracers (including polymeric tracers that are thermodynamically immiscible with the investigated polymer) yield identical RTD results if the following conditions are maintained: a small amount of tracer is used in the experiment, the tracer is well mixed into the polymer prior to its use, and the tracer / polymer

blend has an identical geometric shape with the investigated polymer particles. Most polymers are fed to extruders in the form of pellets, powders, or flakes. The tracer is preblended into the polymer at a sufficient concentration for its detection, and the final blend must have an identical geometric shape to the investigated polymer resin.

Suppose that the local residence time distributions in two adjacent sections in an extruder are experimentally measured. Statistical superposition of the individual distributions yields the overall distribution in the extruder (Chen *et al.*, 1995). The only requirement for this numerical superposition is that the flow must be made sufficiently random between each adjacent section to ensure that the RTD in each section is independent. Chen *et al.* (1995) argued that this assumption is valid in non-intermeshing twin screw extruders, which offer sufficient randomization of the flow in the apex region between the screws. The superposition results agreed with direct experimental measurements of the overall RTD, which confirmed the statistical independence of the adjacent sections. As well, it was proposed that the method is valid for long, shallow screw channels where randomization across the screw channel cross section is easily accomplished.

A more interesting problem is the determination of the local RTD in a small section of the extruder. Huneault *et al.* (1996) used a numerical deconvolution method to calculate the local RTD in different sections a co-rotating twin screw extruder. First, overall distributions were measured by injecting the tracer pulse at different locations along the extruder, and analyzing the tracer concentration in the extrudate collected at the die. The overall distributions were then numerically deconvoluted to yield the local RTD in different sections of the extruder. These sections were assumed to be statistically independent, but this key assumption was not verified. In the work of Chen *et al.* (1995) the superposition results

were directly compared with the overall RTD, which was easily measured. Conversely, Huneault *et al.* (1996) did not make direct experimental measurements of the local RTD to compare with the deconvolution results.

Wetzel *et al.* (1997) used a dual probe technique to determine the local RTD in a small section of a co-rotating twin screw extruder during the processing of polybutene, which is a Newtonian fluid at the investigated shear rates. A pulse of a titanium oxide (TiO_2) tracer was injected at a single location and detected with optical probes at two desired positions along the twin screw extruder. At each detection point, an overall RTD from the injection point to the probe location was determined. Numerical deconvolution was then completed to obtain the local RTD (between the two probes), but once again, no comparison with direct experimental results was completed. Thus, the assumption of statistical independence between the two sections was not verified. The deconvolution results identified significant differences in the RTD of conveying elements and various kneading block geometries.

2.5. Analysis of the Micromixing in Conventional Chemical Reactors Using Special Chemical Reactions

As previously mentioned, RTD measurements do not reveal information on the state of mixing at the microscopic level (micromixing), which directly affects chemical reactions and the product homogeneity. Danckwerts (1958) showed that the conversion of a second order reaction in a stirred tank depends on both the RTD and the state of mixing at the molecular level. There is some confusion in the literature concerning the effect of segregation on the reaction rate. First consider a second order reaction that is completed in a stirred tank with one inlet stream. Danckwerts (1958) identified two possible limiting cases concerning the state of mixing at the molecular level. In one case, the fluid entering the

reactor is instantaneously mixed at the molecular level with the fluid in the reactor. In the second case, the entering fluid remains in separate globules that travel through the reactor. In this situation, the material inside the globule is homogeneously mixed, but there is no mixing between separate globules. Thus, there is segregation of fluid of different ages in the reactor, and it was shown by Danckwerts (1958) that this segregation results in a higher conversion for reaction orders greater than unity. Perfect instantaneous mixing at the molecular scale dilutes the reactant concentrations in the reactor, which correspondingly reduces the reaction rate.

Now consider a reaction occurring in a stirred tank between two components, which are fed in separate inlet streams. In this situation, segregation occurs between the two reacting components, and the reaction only proceeds when they are brought into contact. In contrast to the segregation of fluid of different ages, the segregation of the reacting components always decreases the conversion (Bourne, 1983). The focus of the remaining discussion concerns the effects of the segregation of the components on chemical reactions. Many experimental methods have been developed to investigate micromixing in conventional chemical reactors using special chemical reactions. These chemical reactions are molecular probes that yield information on the state of micromixing that cannot be obtained using other techniques, such as optical methods (Fournier *et al.*, 1996). As well, a significant amount of theoretical modeling has been completed to better understand the effects of imperfect micromixing on chemical reactions.

Ottino (1980) presented a laminar mixing model, which considers the fluid to consist of microelements that have a lamellar structure. The effects of deformation from the fluid flow, diffusion, and chemical reaction are considered in this model. Chella and Ottino

(1984) used the laminar mixing model and presented numerical predictions for different types of chemical reactions. Conversion of a simple bimolecular reaction and selectivity of more complex competitive-consecutive reactions depended on the characteristic times for diffusion, chemical reaction, and mixing. Similar results were presented by Ou and Ranz (1983a), which indicated significant differences between the conversion profiles of fast and slow reactions. The model of Ou and Ranz (1983a) considered the fluid to consist of alternating layers of the two segregated phases, with simultaneous diffusion within the layers and stretching by mechanical mixing.

Consider an arbitrary single step bimolecular chemical reaction. Segregation occurs when there are concentration gradients at the molecular level, and the striation thickness is defined as the characteristic distance between two adjacent segregated phases. Chella and Ottino (1984) showed that the degree of segregation reduces the conversion of a fast bimolecular reaction. Therefore, the conversion of a fast reaction is a quantitative indicator of the degree of segregation, which was used by Ottino (1981) to analyze the micromixing efficiency in multi-jet and stirred tank reactors. Similarly, Shenoy and Toor (1990) presented methods using instantaneous reactions to analyze micromixing in turbulent flows. Baldyga and Rohani (1987) proposed a method employing a step test of a fast or instantaneous bimolecular reaction to monitor the micromixing level of a CSTR. Mixing controls the conversion of a fast reaction, but in the case of a slow reaction, the mixing and diffusion occur prior to a significant conversion (Ou and Ranz, 1983a). Thus, the conversion of a slow reaction depends on the chemical kinetics. Danckwerts (1958) proposed that a slow bimolecular reaction can be used to analyze the state of mixing at the molecular level. The initial and average reaction rates were related to the intensity of segregation, but the reaction

kinetics must be sufficiently slow to minimize the actual depletion of the reactants. Bourne (1983) noted that slow reactions do not cause significant segregation, and therefore, the requirement for slow kinetics makes this method ineffective for investigating micromixing.

Models have been presented to describe the micromixing process of miscible fluids in turbulent flow (Bourne, 1983; Barresi *et al.*, 1992; Villermaux and Falk, 1994). For the mixing of a miscible minor component into an excess of the continuous phase, Bourne (1983) proposed that the first step of the mixing process is turbulent dispersion, which yields a reduction in the size of the minor phase down to the order of the Kolmogoroff scale. This size scale (λ_k) is defined as "the size of an eddy below which turbulent velocity fluctuations are highly damped" (Bourne *et al.*, 1981), and is related to the kinematic viscosity (ν) and the energy dissipation rate (ϵ, which depends on the power input to the fluid by the mixing device, i.e. a turbine) in equation 2.1.

$$\lambda_k = \left(\frac{\nu^3}{\epsilon}\right)^{1/4} \qquad (2.1)$$

The Kolmogoroff scale concerns the critical size of an eddy prior to the onset of decaying turbulence by the viscous dissipation of kinetic energy (Hinze, 1975). Below the Kolmogoroff scale, further mixing occurs through diffusion (Belevi *et al.*, 1981) and deformation (Angst *et al.*, 1982a). After turbulent dispersion of typical low viscosity fluids (1 – 5 mPa.s) in mixing vessels with turbines, Bourne *et al.* (1981b) estimated the spherical minor phase domains to have radii between 10 to 65 μm.

Barresi *et al.* (1992) proposed that turbulent micromixing proceeds according to the following three steps: distribution and reduction in the minor phase to the Kolmogoroff scale, striation thinning due to deformation, and diffusion / chemical reaction in the lamellar

structure. Villermaux and Falk (1994) presented a generalized mixing model for miscible fluids, which breaks down the mixing process into the following steps: erosion of the minor phase to a given size, dilution of the eroded material into smaller eddies that make up a reacting cloud around the eroded domain, incorporation of the bulk fluid into reacting cloud, and diffusion in the reacting cloud.

One special type of reaction that has shown great promise in the analysis of micromixing is the competitive-consecutive reaction, and the general form is depicted in equation 2.2.

$$\begin{aligned} A + B &\xrightarrow{k1} R \\ R + B &\xrightarrow{k2} S \\ X &= \frac{2S}{2S + R} \end{aligned} \qquad (2.2)$$

The selectivity (X) describes the product distribution from the competitive-consecutive reaction. Ou and Ranz (1983b) and Chella and Ottino (1984) showed that the selectivity depends on the rate of reaction (k1 and k2) and the micromixing. Consider a reaction between initially segregated phases of the components A and B. If there is instantaneous, perfect micromixing prior to a significant extent of the reaction, then the reactions are controlled by the chemical kinetics. The selectivity approaches a kinetic limit, which depends on the ratio of the reaction rate constants. For k1 / k2 equal to 10, the chemical kinetic limit of the selectivity is 0.23 (Wu, 1994). If the reaction is completed under complete segregation of the components, all the reactions occur at the interfaces between the phases. Complete segregation results in a selectivity of 1 because all the R that is formed at the interfaces further reacts to form S. Thus, the selectivity can be used to investigate the micromixing, which in most situations will lie somewhere between the two limiting cases.

Bourne and co-workers used a competitive-consecutive reaction to analyze the micromixing performance of stirred tanks operated in semi-batch and continuous operation modes (Bourne *et al.*, 1981a; Belevi *et al.*, 1981; Bourne *et al.*, 1981b; Angst *et al.*, 1982a; Angst *et al.*, 1982b; Bolzern and Bourne, 1983; Bourne and Rohani, 1983; Baldyga and Bourne, 1984; Angst *et al.*, 1984), and jet reactors (Baldyga *et al.*, 1994; Baldyga *et al.*, 1995). The employed competitive-consecutive reaction was the coupling of 1-naphthol (A) and diazotised sulphanilic acid (B) in dilute alkaline solutions at room temperature under turbulent flow conditions. The reactions were adequately fast to produce inhomogeneity at the microscopic level, and selectivities significantly higher than the perfect micromixing limit were observed. Numerical investigation of the reactions indicated that the selectivity was a function of the initial concentrations of the reactive species, the volumetric ratio of the segregated phases, the kinetic rate constants, the diffusion rate, and the rate of deformation (Belevi *et al.*, 1981; Angst *et al.*, 1982a). As well, extensional deformation of the fluid elements resulted in faster striation thinning as compared to simple shear deformation at a given energy dissipation rate. Faster striation thinning improved the micromixing and resulted in less secondary product (S) formation (Bolzern and Bourne, 1983). Employing the competitive-consecutive reaction between 1-naphthol and diazotised sulphanilic acid, Bennington and Thangavel (1993) investigated the micromixing in a suspension of pulp fibers in an aqueous solution. The fibrous suspension exhibited a yield stress, and the presence of the fibers significantly affected the micromixing by influencing the turbulence in the system. A correction was included in their work to account for the adsorption of the products onto the fibers.

Baldyga and Bourne (1990) extended the investigation of micromixing to the analysis of irreversible second order parallel reactions. Micromixing affected the product distributions, with corresponding limits for perfect mixing and complete segregation. As well, a model was presented to predict the product distribution for a given degree of segregation. The model considered the limiting step of the micromixing process to be the growth of the lamellar reaction zone through the engulfment of the minor phase into the continuous phase (turbulent dispersion, which yields the small eddies where the reaction occurs). A parallel reaction system for the analysis of micromixing was also offered by Fournier *et al.* (1996). The authors have presented a detailed review of the large number of different reaction systems that have been used to analyze micromixing. The new parallel competitive reaction was based on an acid-base neutralization and an oxidation reaction, which is depicted in equation 2.3.

$$\begin{aligned} &H_2BO_3^- + H^+ \rightarrow H_3BO_3 \\ &5I^- + IO_3^- + 6H^+ \rightarrow 3I_2 + 3H_2O \\ &I_2 + I^- \leftrightarrow I_3^- \end{aligned} \qquad (2.3)$$

In regions that have poor micromixing, the accumulation of excess acid resulted in the formation of iodine, which was detected in the visible and UV regions by spectrophotometric analysis. The reaction system was used to determine the micromixing quality of a stirred vessel using a glycerin-water solution to vary the viscosity (Guichardon *et al.*, 1996). Turbulent micromixing was less effective as the viscosity was increased from 0.001 Pa.s to 0.170 Pa.s.

2.6. Applications of Chemical Reaction Methods to the Analysis of Mixing During Polymer Processing

As previously described, a significant amount of research has been completed using special chemical reactions as molecular probes to measure micromixing under turbulent flow conditions in conventional chemical reactors. Application of these methods to the analysis of mixing during polymer processing is very limited. Agarwal and Campbell (1995) employed the competitive-consecutive reaction between 1-naphthol and diazotised sulphanilic acid to the analysis of the micromixing quality during the formation of filled reaction injection molded composites. Model experiments were completed using a transparent apparatus to visually investigate the mixing process. The filler significantly reduced the micromixedness (higher selectivity), but increasing the shear rate improved the micromixing.

Chella and Ottino (1982) applied their laminar mixing model to the analysis of simultaneous mixing, diffusion, and chemical reaction in a single screw extruder. Once again, the conversion of a fast bimolecular reaction and the product distribution of a competitive-consecutive reaction depended on the state of mixing at the molecular level. In the extruder, the mixing conditions were varied by considering various ratios of the drag flow and pressure flow, which is related to the degree of backflow or recirculation. Attention has been given to the effects of mixing on chemical reactions in counter-rotating twin screw extruders (Ganzeveld and Janssen, 1992a; 1992b) and co-rotating twin screw extruders (Kim and White, 1997). These reactions were not used to analyze the state of mixing, but some interesting observations were presented concerning the effects of mixing on reactive extrusion applications. For example, increasing the screw speed exhibited a complicated effect on the grafting of maleic anhydride onto HDPE, which was attributed to the competing contributions of reduced residence time and increased mixing rate (Ganzeveld and Janssen,

1992b). Using numerical simulations, Kim and White (1997) predicted rapid conversion during thermal degradation, peroxide induced degradation, and maleation of PP in kneading blocks due to their intensive mixing.

Wu (1994) applied the competitive-consecutive reaction between p-phenylene diamine and phthalic anhydride to the analysis of micromixing in a co-rotating twin screw extruder. The reaction kinetics were determined by Frey and Denson (1988), and the ratio of the kinetic rate constants was determined to be 10 at 150 °C. This ratio resulted in a chemical kinetic limit of 0.23 for the selectivity. Wu (1994) applied the reaction system to the analysis of micromixing during the blending of segregated melt streams of a low molecular weight PE wax (M_n = 12000) in a block of trilobal kneading discs staggered in the forward, neutral, and reverse directions. The experimental results were compared with a numerical model based on the laminar mixing model of Chella and Ottino (1984). A major assumption in the model was that the mixing in the kneading block was predominately caused by elongational flow, which resulted in efficient striation thinning. van der Wal *et al.* (1996) and Goffart *et al.* (1996) predicted that the average shear rates in conveying elements and kneading blocks are approximately 10 times greater than the average elongational rates. Although more efficient mixing occurs during elongational flow, the contribution of the shear flow to the mixing cannot be ignored to obtain realistic predictions.

In the experiments of Wu (1994), the kneading disc stagger angle and disc width were changed simultaneously. Although, Wu (1994) concluded that neutral staggered kneading discs yield the best micromixing, the separate contributions of the stagger angle and disc width on the micromixing cannot be evaluated. The numerical simulations underestimated the experimental measurements of the selectivity (predicting better micromixing), but the

effect of incompatibility between the hydrophobic PE melt and the polar small molecule reactants was not discussed. The large difference in polarity between the PE and the small molecule tracers may cause phase separation. Migration of the polar tracers to the interfaces due to the phase separation followed by their reaction at the interfaces (resulting in greater S formation) may account for the discrepancy between the numerical predictions and the experimental results.

Relationships between mixing and conversion were investigated by Maier *et al.* (1994) for the reactions between maleic anhydride grafted ethylene-propylene rubber (EPR-g-mAh) and long chain alcohols and primary amines in co-rotating twin screw extruders. In the case of the amine - anhydride reaction, the conversion was assumed to be mixing limited. Injection of a low molecular weight oligomeric amine resulted in rapid conversion of the anhydride functional groups, which indicated that the migration of the low molecular weight molecule in the rubber was very fast. Increasing the molecular weight of the oligomeric amine decreased the rate of consumption of the anhydride functional groups. Higher conversions were observed at lower screw speeds, which was attributed to improved mixing of the oligomer in the rubber. No screw configuration offered superior mixing (highest conversion) over all the investigated operating conditions.

Curry and Andersen (1990; 1991/1992) investigated the effects of the extruder operating conditions on the mass transfer controlled reaction between oxazoline functionalized PS and acid functionalized PE in a co-rotating twin screw extruder. It was proposed that the reaction conversion was sensitive to the quality of mixing. The crosslinks formed between the two reactive polymers resulted in a viscosity increase, which was related to the screw speed and throughput. Increasing the flow rate significantly reduced the

crosslink density and viscosity because of the corresponding decrease in the residence time. Two maximum viscosities were observed at higher screw speeds, which were attributed to the effects of screw speed on the residence time and the dispersive mixing in the extruder. Surprisingly, at the same extent of the reaction, two different polymer morphologies were observed, and therefore, the crosslink density was not directly related to the quality of mixing. A similar investigation of the crosslinks formed during the blending of ethylene vinyl alcohol (EVA) and styrenic maleic anhydride copolymer (SMA) was completed by Curry (1995). Higher viscosities due to crosslink formation were observed at higher screw speeds and lower flow rates.

CHAPTER 3
REACTIVE POLYMER TRACER PREPARATION AND CHARACTERIZATION

Of the great number of different polymers used in everyday consumer plastic products, thermoplastic polyolefins are used extensively due to their good mechanical properties, chemical inertness, and processability. Thus, polyolefins, such as PP, lend themselves towards film, bottle, and packaging applications. In addition, commodity PP has recently experienced extensive growth as it is used as a substitute for more expensive engineering resins (Pardos, 1999). The lack of functional groups in polyolefins, which gives them their hydrophobicity, limits their possible applications. Therefore, extensive research has been completed on the grafting of polar functional groups onto polyolefins via reactive extrusion. The most common functionalization method is the maleation of PE and PP, which vastly improves the adhesive properties of the polymers to metal surfaces. The first section of this chapter presents a review of different functionalization techniques, and particular attention is given to both free radical and targeted methods. As well, the reactions between anhydride and amine functional groups are reviewed. Following the literature review, the materials, equipment, and preparation methods that were used to prepare the reactive polymer tracers are described. Finally, characterization of the reactive polymers and the product from their coupling reaction is presented.

3.1. Review of Polymer Functionalization via Reactive Extrusion

Functional groups can be incorporated onto polymers by the following general methods (Liu and Baker, 1992): incorporation into the polymer (either backbone, side group, or at the chain end) during polymerization, copolymerization with a monomer that contains

the functional group, and modification of the polymer by some chemical method. Of the three methods, the modification of existing polymers is the most promising because it does not require a change in the polymerization process. Reactive extrusion, which combines polymer processing and polymer modification into a single operation, offers the advantage of performing the chemical modification in the absence of solvents. The extruder is used as a chemical reactor, and as previously mentioned, twin screw extruders offer superior flexibility because of their modular screw design. Polymer functionalization usually involves chemical reactions between a polymer melt and various incompatible small molecule reactants. Thus, the overall efficiency of the process is greatly affected by the mixing of the incompatible phases achieved by the extruder. In particular, distributive mixing, which results in the generation of interfacial area between the incompatible phases, is critical during reactive extrusion. The most common functional groups introduced to polyolefins are acidic and basic monomers. Free radical methods have been extensively used to graft monomers onto polyolefins, but the use of free radicals causes many undesired side reactions. An alternative functionalization method is the targeted modification of existing unsaturation in the polymer.

3.1.1. Free Radical Methods for the Functionalization of Polyolefins

At sufficiently high temperatures, organic peroxides decompose to form free radicals (RO•), which are extremely reactive species. These radicals abstract hydrogens from the polymer backbone, resulting in the formation of polymer radicals. A monomer containing the desired functional group can be grafted onto the polymer backbone via its addition to a polymer radical. Unfortunately, the following side reactions can occur during free radical functionalization of polymers: crosslinking of the polymer through the combination of two

polymer radicals, degradation via scission of the polymer radical, homopolymerization of the monomer, and oxidation of the polymer in the presence of peroxy radicals. A simplified reaction mechanism for the free radical functionalization of a polymer is depicted in Figure 3.1.

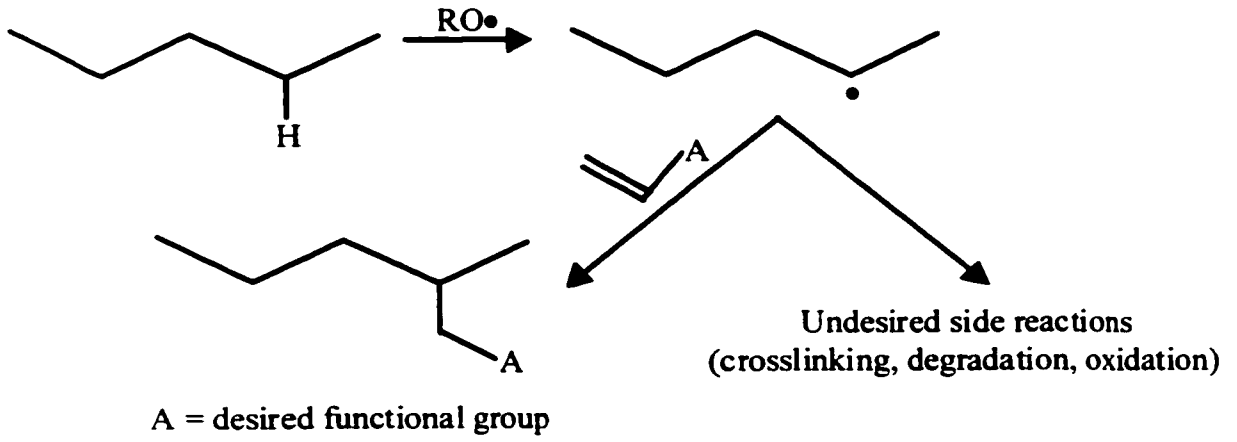

Figure 3.1. Simplified Reaction Mechanism for the Grafting of a Monomer onto a Polymer Backbone using Free Radicals

Maleic anhydride (mAh) is the most common acidic monomer grafted to polyolefins via free radical methods. Gaylord and Mishra (1983) investigated the maleation of PP in the melt-phase using peroxides as catalysts. The reactions caused severe polymer degradation due to the disproportionation (β-scission) of the tertiary polymer radicals. The tertiary hydrogens on the PP backbone were preferentially abstracted due to the greater stability of the tertiary polymer radicals. Grafting of single succinic anhydride units along the PP backbone occurred via addition of maleic anhydride to the polymer radicals. As well, maleic anhydride excimers (excited monomers) formed in the presence of the radicals produced by the rapid decomposition of the peroxide. The excimers also abstracted hydrogens from the polymer backbone, which resulted in further degradation of the PP as well as further sites for

the addition of maleic anhydride. This proposed mechanism effectively explains the observation that the degree of PP degradation is significantly greater in the presence of maleic anhydride and a peroxide as compared to only the peroxide. As well, homopolymerization of the maleic anhydride occurred via ionic coupling or electron transfer between the excimer and free maleic anhydride. This observation is very interesting because the reactions were carried out at 180 °C, which is well above the reported ceiling temperature of 150 °C for maleic anhydride (Gaylord *et al.*, 1992). Homopolymerization of the maleic anhydride may result in the grafting of poly(maleic anhydride) segments to the polymer backbone, but the addition of an electron donating species (such as dimethylformamide) prevented homopolymerization (Gaylord and Mishra, 1983).

Maleation of LLDPE was investigated by Gaylord *et al.* (1992) in the melt-phase with peroxide catalysts. A reaction mechanism was proposed that attributes the reactive species to the excimer (excited monomer). As compared with the maleation of PP, crosslinking via coupling of two polymer radicals dominated the side reactions for PE. Along with the crosslinking, approximately 0.2 to 1.4wt% grafted maleic anhydride was observed in the soluble fraction of the functionalized polymer. Liu *et al.* (1990) investigated the maleation of LDPE in solution with a peroxide, and the addition of maleic anhydride greatly increased the amount of crosslinking as indicated by a decrease in the melt index.

At a low maleic anhydride concentration, Borsig *et al.* (1995) observed an increase in the molecular weight of atactic PP during functionalization. This increase was attributed to crosslinking of two polymer radicals through a maleic anhydride unit. Ho *et al.* (1993) investigated the effects of maleic anhydride concentration and peroxide concentration on the degree of degradation during melt-phase functionalization of PP in an internal mixer. Similar

to the observation of Gaylord and Mishra (1983), the initial addition of maleic anhydride to the polymer / peroxide mixture resulted in further degradation as indicated by a decrease in the mixer torque. Surprisingly, the amount of degradation decreased as the maleic anhydride concentration was increased from 1 to 10wt%. This observation was attributed to competition between the β-scission (resulting in degradation), combination (resulting in crosslinking), and chain transfer (donation of a hydrogen from a free maleic anhydride to a polymer radical) reactions. Recently, Nachtigall *et al.* (1999) investigated the free radical functionalization of PP with maleic anhydride using a factorial experimental design. The reactions were carried out in a batch mixer, and the investigated factors were: run time, temperature, maleic anhydride concentration, and peroxide concentration. The product containing the highest degree of maleic anhydride incorporation also had the lowest molecular weight, which suggested that the grafting occurred predominately at the chain ends of the PP.

In the case of the free radical grafting of maleic anhydride onto EPR in an internal mixer, Wu and Su (1991) observed a complex interaction between crosslinking, scission, and grafting reactions. Addition of maleic anhydride resulted in an initial increase in the amount of crosslinking as indicated by a torque increase. The torque slowly decreased at latter reaction times, which was attributed to polymer degradation. The competition between the two side reactions resulted in the formation of highly crosslinked and extremely low molecular weight chains in the functionalized product. The highest grafting extent was achieved using moderate concentrations of the maleic anhydride (around 1wt%) and peroxide (less than 1wt%). No improvements in the grafting were observed at higher maleic anhydride concentrations, which was attributed to the limited mixing intensity of the internal

mixer. Wu and Su (1992) also investigated the effects of the addition of stearamide on the free radical maleation of EPR in an internal mixer. At low peroxide concentrations (less than 0.5wt%), the addition of stearamide effectively suppressed the crosslinking and scission side reactions. This suppression was attributed to the stearamide acting as a chain transfer agent, which can donate a hydrogen to a polymer radical.

There has been great interest in the detailed characterization of maleic anhydride grafted polymers to confirm the proposed reaction mechanisms. De Roover *et al.* (1995) characterized PP-g-mAh using FT-IR analysis and proposed a reaction mechanism. The characterization was completed by comparing the FT-IR spectrum of the grafted polymer with the FT-IR spectra of the following model compounds: citraconic anhydride, 2,3-dimethylmaleic anhydride, n-octodacylsuccinic anhydride, poly(maleic anhydride), and maleic anhydride. In particular, the carbonyl stretching vibration of the cyclic anhydride in the region of 1780-1792 cm^{-1} was compared. From this comparison, it was concluded that PP-g-mAh consists of single succinic anhydride units and poly(maleic anhydride) units at the terminal site (chain end). Surprisingly, it was reported that the grafting did not occur along the PP backbone. The homopolymerization of maleic anhydride during the functionalization of PP at temperatures well above the reported ceiling temperature of maleic anhydride was confirmed in additional experiments (De Roover *et al.*, 1996).

In contrast to the conclusions of De Roover *et al.* (1995), Heinen *et al.* (1996) used ^{13}C NMR to identify the grafting positions of maleic anhydride along the backbones of PP, PE, and EPR. To elucidate the grafting positions, ^{13}C labeled maleic anhydride was used. The following is a summary of their results: maleic anhydride was attached to the PE (both high and low density) backbone in the form of single succinic anhydride units and short

poly(maleic anhydride) oligomers, maleic anhydride was attached to the EPR backbone solely as single succinic anhydride units (attached at the tertiary carbon position), and maleic anhydride was attached to PP as single succinic anhydride units along the polymer backbone and at the terminal site. Attachment of succinic anhydride to the chain end of PP was attributed to hydrogen abstraction follow by chain scission of the maleic anhydride radical along the polymer backbone. Comparing the characterization work of Heinen *et al.* (1996) and De Roover *et al.* (1995), the former appears more experimentally justified and agrees well with the majority of the proposed reaction mechanisms in the literature.

Along with acidic functional groups, a lot of interest has been given to the grafting of basic functional groups onto polyolefins. Simmons and Baker (1989) functionalized LLDPE with dimethylamine ethyl methacrylate, which contains a tertiary amino functional group, in the presence of a peroxide using a batch mixer. For reaction times of 20 minutes, a maximum of 3wt% of the monomer was grafted onto the PE. Similarly, Song and Baker (1990) performed the basic functionalization of PE in a co-rotating twin screw extruder. A concentration of 1.5wt% of dimethylamine ethyl methacrylate was grafted onto the polymer without significant polymer crosslinking when a low concentration of peroxide and a high concentration of monomer was employed. The grafting reaction competed with the homopolymerization of the monomer. Free radical functionalization of PE in the melt-phase with t-butylaminoethyl methacrylate was investigated by Song and Baker (1992a). This monomer contains a secondary amine functional group, which can react with acidic functionalized polymers. The addition of *p*-benzoquinone as a chain terminator greatly suppressed the homopolymerization of the monomer, and therefore, improved the grafting efficiency. Carbon tetrabromide, which is a chain transfer agent, suppressed crosslinking at

the cost of decreased monomer grafting due to the fewer polymer radicals that were available for the grafting reaction.

Free radical grafting of glycidyl methacrylate onto PP in a co-rotating twin screw extruder was investigated, with particular attention given to the effects of the feeding protocol of the reactants on the grafting efficiency (Hu and Cartier, 1998). To promote mixing of the incompatible phases, the low molecular weight reactants were best added in a fully filled region of the extruder. Melt-phase grafting of glycidyl methacrylate onto PE using a peroxide initiator was experimentally and numerically investigated by Hojabr *et al.* (1998). Good agreement between the experimental results and the numerical predictions was observed when the reaction kinetics were determined from batch mixer experiments and the transport parameters in the extruder, such as the average residence time and the degree of macromixing (Peclet number), were measured under actual reaction conditions.

Another basic functional group that has been grafted via free radical methods onto PP is oxazoline. Liu and Baker (1994) melt grafted 0.19wt% oxazoline functional groups onto PP in a batch mixer with a peroxide initiator. The functionalized polymer was used to improve the properties of a blend of PP and 20wt% acrylonitrile-*co*-butadiene-*co*-acrylic acid rubber (NBR). An interfacial reaction between the oxazoline functional groups on the PP and the acid functional groups on the rubber phase occurred, which resulted in toughening of the blend. Without this interfacial reaction, no improvement over the impact properties of pure PP were observed. Vainio *et al.* (1996; 1997) also investigated the free radical functionalization of PP with oxazoline functional groups in a batch mixer (1996) and a co-rotating twin screw extruder (1997). Grafting levels of 1.5wt% in the batch mixer and 2.1wt% in the twin screw extruder were achieved. The addition of styrene as a comonomer

greatly reduced the degree of degradation of the PP, but it also decreased the grafting yield. The grafted polymer was used in an attempt to improve the properties of a PP / PBT blend (70/30). In the batch mixer, the reaction between the basic oxazoline functional groups of the PP and the carboxylic acidic functional groups of the PBT was observed to be extremely fast, with the equilibrium conversion being achieved in approximately 3 minutes at temperatures between 165 to 195 °C. The properties of the blends produced in the twin screw extruder depended on the degree of degradation of the PP that occurred during the functionalization process. The impact properties and the elongation at break were significantly improved, but an optimum concentration of the functionalized PP existed. The optimum concentration depended on both the processing conditions and the functionalization parameters, which included the degree of degradation, the grafting yield, and the concentration of residual (free) monomer present in the functionalized polymer.

Liu *et al.* (1993) functionalized PP with glycidyl methacrylate, a monomer containing a tertiary amine, a monomer containing a secondary amine, and a monomer containing oxazoline. The functionalized polymers were compared by determining their ability to compatibilize PP / NBR (80/20) blends. The most effective functionalized polymers (added at a concentration of 25wt% of the PP phase) contained the oxazoline and glycidyl methacrlyate functional groups, which reacted with the acidic functional groups of the rubber phase. A tenfold improvement in the impact properties were observed as compared with an uncompatibilized blend.

Basic functionalization of EPR was accomplished by two different methods by Immirzi *et al.* (1987). The first method was the free radical grafting of 2-(dimethylamino)ethyl methacrylate onto the rubber in solution, which is a complicated

process due to the competing reactions of grafting, crosslinking, degradation, and homopolymerization of the monomer. An alternative functionalization method was the reaction of succinic anhydride grafted EPR with *N,N*-dimethylethylenediamine, which contains one terminal primary amine and one terminal tertiary amine functional group. This fast reaction resulted in the formation of an imide, with the pendant tertiary amine functional group left unreacted. The second functionalization method was proposed to offer superior control of the amine content in the final polymer. In further work (Greco *et al.*, 1987), acidic and basic functionalized rubbers formed network structures through polar crosslinks between their functional groups, which significantly improved the tensile properties of the rubber. Dharmarajan *et al.* (1995) prepared secondary amine functionalized PP by reacting PP-g-mAh with a 100% excess of an unsymmetrical diamine (one pendant primary amine functional group and one pendant secondary amine functional group). The primary amine group preferentially reacted with the anhydride functional groups along the PP backbone in a non-intermeshing twin screw extruder, which left the secondary amine functional group unreacted. The functionalized polymer was then used to compatibilize PP / SMA blends through the amidation reaction of the amine and anhydride functional groups of the two reactive polymers.

3.1.2. Targeted Functionalization of the Existing Unsaturation in Polymers

Targeted functionalization of the existing unsaturation in polymers offers the advantage of site specific functionalization without the undesired side reactions that occur during free radical functionalization. For example, the terminal double bond (vinylidene) of PP, which is a 1,1-disubsituted double bond, can be targeted for the location of the desired

functional group. Mülhaupt *et al.* (1991) functionalized low molecular weight metallocene catalyzed PP containing terminal double bonds with the following functional groups: anhydrides, esters, amines, carboxylic acids, silanes, boranes, alcohols, and thiols. Thus, a wide variety of possible functional groups can be selectively added to the terminal site of PP. In the case of conventional high molecular weight isotactic PP, the concentration of terminal double bonds available for the targeted reaction is very low. Free radical degradation or thermal degradation of PP can be performed to increase the terminal double bond content, with a corresponding decrease in the molecular weight.

A very promising targeted functionalization method is the hydrosilylation of carbon – carbon double bonds, resulting in the addition of a silicon hydride. Lewis *et al.* (1991) showed that rhodium and platinum catalyzed hydrosilylation reactions are heterogeneous. The morphology of the metal colloid, which is formed between the catalyst and the silane compound, affected its catalytic activity. As well, the heterogeneous nature was confirmed using mercury inhibition tests of the catalyst. Catalytic hydrosilylation of terminal double bonds in PP was completed in the melt-phase (Malz and Tzoganakis, 1998; Tzoganakis and Malz, 1997). t-butylhydroperoxide was an effective cocatalyst, which is required to supply oxygen to the melt-phase reaction to stabilize the colloid between the silane and the catalyst. A method employing hydrosilylation chemistry to introduce terminal functional groups to PP was proposed and tested using styrene as a model monomer (Malz and Tzoganakis, 1998). Similarly, Hazziza-Laskar *et al.* (1991) attached tertiary amine functional groups to polybutadiene by hydrosilylation in solution. In both of these functionalization examples, a functionalized silane was produced using a large excess of a bifunctional silane (containing two silicon hydrides) and a monomer containing the desired functional group via catalytic

hydrosilylation. Using distillation, the functionalized silane was separated from the unreacted silane. The functionalized silane was then added to the unsaturated polymers via a second catalytic hydrosilylation step. Recently, catalytic hydrosilylation was used to introduce succinic anhydride and epoxy functional groups onto a silane (Maric and Macosko, 1999). The functionalized silanes were used in an attempt to compatibilize blends of PDMS in PS or PA6 via reactions with amine functional groups (terminal functional group on PS chain or the end groups of the nylon).

Hydrosilylation of terminal double bonds in PP was also accomplished via a free radical method in the melt-phase (Shearer and Tzoganakis, 1997). Although free radicals were used in this reaction method, the grafting was targeted to the terminal double bonds. The non-catalytic method involved the simultaneous peroxide degradation of PP to produce terminal double bonds, and the addition of silyl radicals to these double bonds. The silyl radicals were formed by abstraction of the hydrogen from the silicon hydride by the peroxide radicals. The reactions were carried out in a single screw extruder, and the grafting extent was related to the concentrations of the reactants and the average residence time.

Oostenbrink and Gaymans (1992) investigated the maleation of EPDM rubber in a co-rotating twin screw extruder, and grafting was observed without the addition of a peroxide. In the absence of the peroxide, the thermal grafting occurred via the Alder Ene reaction between the maleic anhydride and the existing double bonds of the dicyclopentene units of the rubber. At the investigated reaction conditions, the grafting efficiency was greatly improved by the addition of the peroxide. In contrast to the grafting via the Alder Ene reaction, side reactions with the peroxide radicals caused a simultaneous viscosity increase due to the crosslinking of the rubber. The Alder Ene reaction has been defined by

Hoffmann (1969) as the "indirect substituting addition of a compound with a double bond (enophile) to an olefin with an allylic hydrogen (ene)". This reaction is similar to the Diels-Alder reaction since it is pericyclic, or occurs in a single step through a cyclic transition state. A simple example of the Alder Ene reaction is depicted in Figure 3.2, with the allylic hydrogen identified to highlight its transfer from the ene to the enophile.

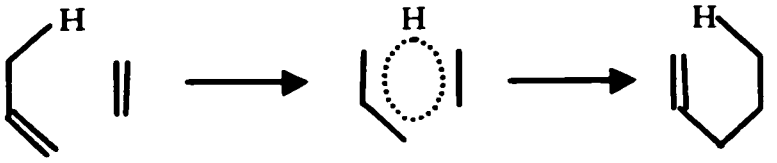

Figure 3.2. Example of the Alder Ene Reaction

The Alder Ene reaction requires elevated temperatures (200 to 600 °C) to proceed, but it is also reversible, with the retro-ene reaction favored at high temperatures and the forward reaction favored at high pressures (Hoffmann, 1969). Therefore, an optimum temperature exists for the forward reaction. The reaction is also favored when the ene is electron rich and the enophile is electron deficient, which depends on the substituents bonded to the reacting species. Maleic anhydride is well suited as an enophile to react with alkenes because of its two carbonyl electron withdrawing groups (Hoffmann, 1969). Typical reaction conditions for the maleation of simple alkenes via the Alder Ene reaction are reaction times of 20 hours at 220 °C in an aromatic solvent using an autoclave reactor (Hoffmann, 1969). Benn *et al.* (1977) showed that the maleation of alkenes via the Alder Ene reaction follows second order kinetics. As well, a concerted reaction mechanism (all bonds broken and formed simultaneously, no long lived intermediates) was proposed over a diradical mechanism.

Steric hindrance of the reaction site affected the favored transition state, which is either exo or endo, and the configuration of the product.

Thompson *et al.* (1998a; 1998b) studied the terminal functionalization of a low molecular weight amorphous PP wax with maleic anhydride via a catalyzed Alder Ene reaction at temperatures between 220 to 250 °C in a small high pressure autoclave. Anhydride incorporation at the terminal site was favored at high temperatures and high maleic anhydride concentrations. The reaction was catalyzed with various Lewis acids, which were observed to cause their largest effects at low concentrations. The objective of the research was to promote the Alder Ene reaction to occur at the processing temperatures of polymers and within the residence time of conventional extruders. Possible free radical grafting of the maleic anhydride onto the PP was suppressed using TEMPO as a free radical trapping species. The reaction kinetics deviated from the second order kinetic model at high temperatures, which was attributed to the complications from side reactions, such as homopolymerization of the maleic anhydride. The reaction method was applied to the anhydride functionalization of EPDM rubber in a co-rotating twin screw extruder (Thompson *et al.*, 1998c). Grafting via the Alder Ene reaction occurred at the double bonds of the 5-ethylidene-2-norbornene (ENB) segments of the rubber. Depending on the temperature, maleic anhydride concentration, Lewis acid type, and Lewis acid concentration, the incorporated succinic anhydride content in the rubber was 0.1 to 0.3wt%. The most significant factors were the temperature (210 to 230 °C) and the maleic anhydride concentration (0.5 to 2.0 mole equivalence with respect to the double bonds of the rubber).

Hydroboration is a well known chemical reaction that is defined as the addition of a boron-hydrogen bond to an olefin, which has been extensively reviewed by Brown (1962). A

simple example of the hydroboration of an olefin with borane is depicted in Figure 3.3 (the product is referred to as an organoborane).

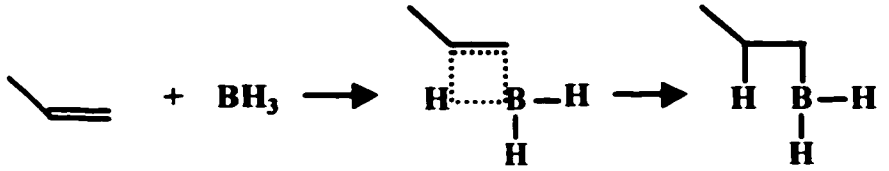

Figure 3.3. Example of the Hydroboration of an Olefin

All three of the boron – hydrogen bonds of borane can react with olefins resulting in the formation of a trialkylborane. The reaction occurs through a four-membered ring transition state, and the boron and hydrogen add to the same side of the double bond. Hydroboration of substituted alkenes is directed to a large extent to the less hindered carbon of the double bond (Brown, 1962). To ensure exclusive bonding to the less substituted carbon, hydroboration can be completed using dialkylboranes, with 9-borabicyclononane (9-BBN, depicted in Figure 3.4) offering the most selective bonding (Pelter *et al.*, 1988).

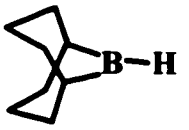

Figure 3.4. Structure of 9-BBN (Hindered Dialkylborane)

The vast applications of organoboranes in chemical synthesis have been reviewed by Pelter *et al.* (1988). Two of the most important reactions are the oxidation and amination of organoboranes to yield hydroxyl and amino groups attached to the organic compound with complete retention of the configuration (the boron is replaced with the hydroxyl or amino

group without a change in the structure). These reactions result in anti-Markovnikov addition of the hydroxyl or amino groups because the boron was attached to the less substituted carbon of the olefin. Conversely, alkene addition reactions that proceed through a carbocation or a radical intermediate result in Markovnikov addition to these cations or radicals of the more substituted carbon of the olefin due to their greater stability. An example of a Markovnikov addition is the reaction between hydrogen bromide (HBr) and a substituted alkene, which results in the bonding of the bromide to the more substituted carbon of the alkene. This reaction proceeds through a carbocation intermediate, and the cation of the more substituted carbon is more stable due to hyperconjugation and inductive effects.

Ramakrishnan (1991) polymerized cyclic olefins to produce polyalkenylenes with controlled spacing between the methylene units. Hydroboration with 9-BBN followed by oxidation of the borane containing polymer with sodium hydroxide (NaOH) and hydrogen peroxide (H_2O_2) was completed. All the reactions were completed in solution with THF. The product was PE with hydroxyl groups positioned along the backbone at controlled positions (the position of the reacted methylene units). This product is chemically identical to conventional ethylene - vinyl alcohol copolymer (EVAL). It was proposed that this new method results in superior control of the composition and structure of EVAL as compared with the conventional production method, which involves the alcoholysis of ethylene – vinyl acetate random copolymer. Nemes *et al.* (1992) used hydroboration followed by oxidation to produce hydroxyl terminally functionalized low molecular weight PP. Similarly, Chung and Rhubright (1993) functionalized the double bonds with hydroxyl groups in poly(propylene-*co*-1,4-hexadiene) by hydroboration followed by oxidation.

The general reaction mechanism for the oxidation of an organoborane (the boron center is bonded to three alkyl groups) using a hydrogen peroxide is depicted in Figure 3.5 (adapted from Pelter *et al.*, 1988).

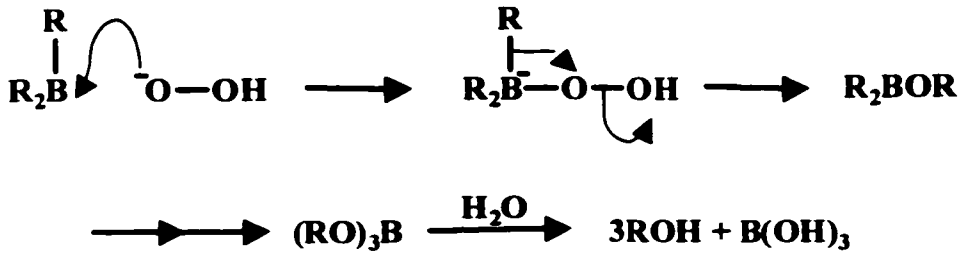

Figure 3.5. Reaction Mechanism for the Oxidation of a Trialkylborane (adapted from Pelter *et al.*, 1988)

The reaction involves the migration of the alkyl groups from the boron to the oxygen, with complete retention of the product configuration. Upon hydrolysis, the hydroxyl groups and boric acid are formed. The reaction is driven by the formation of the strong boron – oxygen bonds and all three of the alkyl groups attached to the boron center can react (referred to as a quantitative reaction).

Brown *et al.* (1964; 1987) reported that amination of an organoborane does not involve all three of the alkyl groups attached to the boron center. A limiting conversion of 66% suggested that only two of the alkyl groups can migrate to the nitrogen to form the amine compound. As well, the reaction was attempted using hydroxylamine, which is the nitrogen analog of hydrogen peroxide, but only simple addition compounds with the organoborane were formed (Brown *et al.*, 1987). Thus, the nitrogen containing compound used to perform the amination required a good leaving group to drive the reaction. Hydroxylamine-*o*-sulfonic acid, a commercially available compound, was used to perform the amination of an organoborane, with a limiting conversion of 66%. The reaction

mechanism for the amination of an organoborane is depicted in Figure 3.6 (adapted from Pelter *et al.*, 1988).

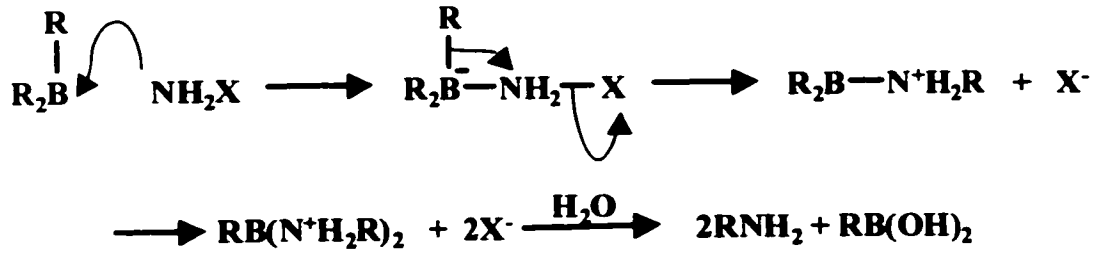

Figure 3.6. Reaction Mechanism for the Amination of a Trialkylborane (adapted from Pelter *et al.*, 1988)

Similar to the oxidation of an organoborane, amination involves the migration of the alkyl groups to the incoming atom. The limiting conversion was attributed by Brown *et al.* (1987) to the high electron density on the boron due to the two nitrogen or two oxygen groups (after hydrolysis) preventing the third hydroxylamine-*o*-sulfonic acid from coordinating with the boron center. This coordination must occur for the migration of the last alkyl group to the nitrogen. The product is a mixture of the desired alkyl primary amine and monoalkyl boronic acid.

Chung *et al.* (1994) functionalized unsaturated PE (copolymer of ethylene and 1,4-hexadiene) by hydroboration followed by amination with hydroxylamine-*o*-sulfonic acid. The reactions were completed in solution with THF under N_2 to prevent side reactions with water and oxygen. Once again, amination of a trialkylborane is not quantitative because the borane adduct becomes too stable after one or two of the alkyl groups migrate to the nitrogen centers. Therefore, boron can remain attached to the polymer chain. To ensure selective amination of the polymer, hydroboration was completed using lithium dimethylborohydride.

The methyl groups do not react in the amination step, and therefore, selective amination of the polymer occurred as indicated by ^{1}H NMR analysis. Secondary amine functional groups were attached to the terminal site of low molecular weight atactic and isotactic PP (Shiono *et al.*, 1993). The terminally functionalized polymers were prepared by performing hydroboration of the terminal double bonds followed by the addition of 1-butylazide. Prior to the reaction with the azide, the trialkylboranes were disproportionated to form alkyldichlorideborane to ensure selective addition of the secondary amine to the polymer chain. The yield of the secondary amine functionalized PP from the alkyldichlorideborane was greater than 80%.

Chung *et al.* (1995) and Chung (1995) prepared functionalized polyolefins by copolymerizing the olefin with a borane containing monomer, followed by conversion of the borane to a variety of functional groups (hydroxyl, amino). A homogeneous metallocene catalyst resulted in the highest incorporation of the borane monomers into the copolymer. As well, the formation of graft copolymers was investigated using a polymer containing 9-BBN side groups (Chung, 1995). In the presence of oxygen, the attached borane groups formed radicals, which were available to react with methyl methacrylate to propagate poly(methyl methacrylate) side chains on the polyolefin backbone.

3.1.3. Applications of Functionalized Polymers and Anhydride - Amine Reactions

Functionalized polymers are extensively used as compatibilizers to improve the properties of immiscible polymer blends (Liu and Baker, 1994; Vainio *et al.*, 1996, 1997; Liu *et al.*, 1993; Dharmarajan *et al.*, 1995). Polymer compatibilization has been reviewed by Gaylord (1989) and Liu and Baker (1992). Immiscible blends often exhibit poor properties

due to their unstable morphologies. Compatibilization greatly improves the polymer morphology (smaller minor phase domain sizes) by reducing the interfacial tension and promoting adhesion between the incompatible phases (Gaylord, 1989). The compatibilization can be completed by adding a preformed block copolymer containing segments that are similar to the two homopolymers being blended. A second technique is the *in situ* formation of the block copolymer at the interface between the two immiscible phases using two reactive polymers (one reactive polymer being compatible with each immiscible phase). Liu and Baker (1992) identified six categories of reactive polymers and their possible coupling reactions. The application of functionalized polymers in the compatibilization of polymer blends is now briefly described, with the focus on reactions between acidic and basic reactive polymers.

Ide and Hasegawa (1974) used PP-g-mAh to compatibilize the immiscible blend of PP and PA6. The formation of the graft copolymer through the reaction of the anhydride functional groups and the terminal primary amine groups of the PA6 resulted in a much finer morphology and a corresponding improvement in the mechanical properties. Rösch and Mülhaupt (1993) compared the effectiveness of PP-g-mAh and maleic anhydride grafted polystyrene-*block*-poly(ethene-*co*-but-1-ene)-*block*-polystyrene as compatibilizers for the immiscible blend of PP and PA6. The latter was observed to outperform the conventional PP-g-mAh in producing a finer morphology and a corresponding improvement in the mechanical properties of the compatibilized blend. It was proposed that the conventional PP-g-mAh was miscible with the PP phase, and therefore, only a small amount of the anhydride functional groups reacted with the amine end groups of the PA6 at the interfaces. Conversely, maleic anhydride grafted polystyrene-*block*-poly(ethylene-*co*-but-1-ene)-*block*-

polystyrene was immiscible with both polymer phases, and therefore, it accumulated at the interfaces between the PP and PA6 phases. This accumulation at the interface resulted in greater coupling between the immiscible phases.

Reactive compatibilization of PP / PA6 blends with an acrylic acid grafted PP was affected by the screw speed, the presence of venting, and the feeding sequence of the components in a co-rotating twin screw extruder (Dagli *et al.*, 1994). From preliminary experiments in a batch mixer, the reaction rate increased with the rotor speed, which indicated that the mixing of the components plays a critical role in the compatibilization process. Polyoxypropylenediamine was used in an attempt to compatibilize a blend of PP and EPDM rubber (Phan *et al.*, 1997). Both polymer phases contained grafted maleic anhydride functional groups, and therefore, crosslinks were formed between the two phases with the diamine at the interface. The diamine concentration was varied between 0 to 6wt%, and the impact strength of the blends exhibited a maximum at 3wt%. Primary amine terminated PS was used an a reactive compatibilizer for the blend of impact modified SMA and PPO in a twin screw extruder (Koning *et al.*, 1997). The amine terminated PS reacted with the anhydride units of SMA, which formed PS grafts that were miscible with the PPO phase. As compared to a conventional block copolymer, the reactive method resulted in superior mechanical properties, except for the elongation at break. This decrease in elongation at break was attributed to a partial crosslinking of the SMA phase because the reactive PS contained primary amine groups at both chain ends.

Using a one step reactive extrusion process in a co-rotating twin screw extruder, the reactive compatibilization of PP / PBT blends was accomplished (Sun *et al.*, 1996). The process involved the free radical functionalization of PP followed by the addition of the PBT.

Grafted glycidyl methacrylate functional groups were superior to acrylic acid and maleic anhydride functional groups for the compatibilization reaction with the carboxylic acid and/or hydroxyl groups at the chain ends of the PBT. Optimization of the process considered the functionalization procedure, the removal of residual monomer prior to the addition of the second polymer via venting, and the processing conditions. After optimization, the compatibilization resulted in a fifteen fold increase in the impact strength and the elongation at break as compared with a non-reactive blend.

A comparison of the morphology development during reactive and non-reactive blending was completed in a batch mixer by Scott and Macosko (1994b). The investigated blends were nylon / EPR and PS / EPR (the rubber was the dispersed phase). The functionalized polymers were maleic anhydride grafted EPR, amine terminated nylon, and oxazoline grafted PS. Morphology development in all the experiments occurred predominately during the melting transition. Interfacial reactions resulted in smaller dispersed domain sizes, faster dispersions of the rubber, and narrower size distributions in the final blends. Similarly, Cartier and Hu (1999) showed that the morphology development during the reactive blending of PP-g-mAh and PA6 occurred exclusively in the melting section of a co-rotating twin screw extruder.

A common reaction used in polymer compatibilization is the coupling of cyclic anhydride and amine functional groups. Model interfacial reactions between SMA and amine terminated polymers were investigated by Scott and Macosko (1994a) using a heatable IR cell, which allowed for in-line FT-IR analysis of the reactions. A reaction mechanism (depicted in Figure 3.7) for the coupling a primary amine terminated polymer and the maleic anhydride units of SMA was proposed. The reaction between the functional groups is

completed in two steps. In solution, the intermediate was identified as the secondary amide carboxylic acid salt (A), although in the melt-phase it is more likely to be the amic acid (B). As well, it was proposed that the reaction kinetics of the first step in the melt-phase at polymer processing temperatures is extremely fast, and therefore, the overall kinetics are dominated by the second step of the reaction (cyclization of the intermediate to the imide). Faster reaction kinetics (a combination of chemical kinetics and the diffusion) were observed at higher temperatures and lower polymer molecular weights.

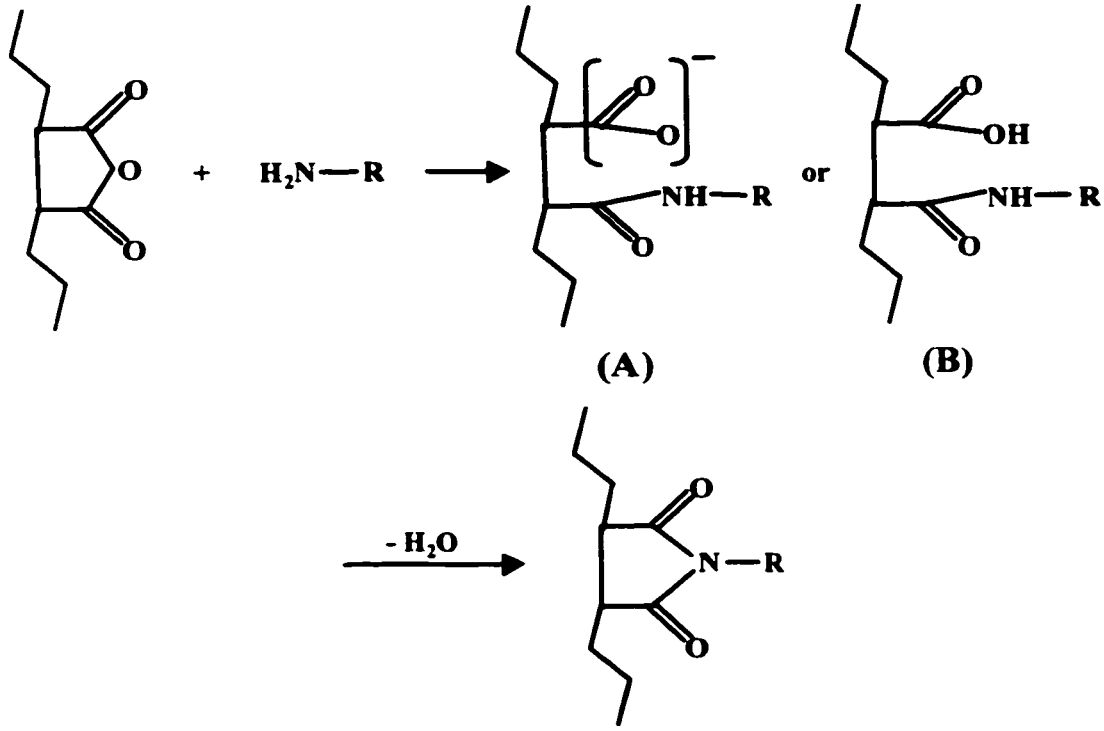

Figure 3.7. Reaction Mechanism For the Coupling of Cyclic Anhydride and Primary Amine Functional Groups (adapted from Scott and Macosko, 1994a)

Reactions between SMA and various primary amines were investigated at low temperatures (0 – 40 °C) in solution with THF (Hu and Lindt, 1992). At the investigated temperatures, the reaction proceeded only to the acid amide intermediate. In addition, the reaction was reversible at elevated temperatures (140 °C). Tessier and Marechal (1988) and

Maréchal *et al.* (1995) investigated the reactions of anhydrides with amines and amides. In solution, the anhydride – amine reaction was almost instantaneous, and the imide formation rate increased with temperature (Tessier and Marechal, 1988). The anhydride – amide reaction between model small molecules and oligomers (Tessier and Marechal, 1988) and between polyamides and anhydrides (Maréchal *et al.*, 1995) was significantly slower.

Melt-phase reactions between primary, secondary, and tertiary small molecule diamines and carboxylic acid grafted PE and SMA were completed to investigate the amine relative reactivities (Song and Baker, 1992b). As expected, the reactivity was primary > secondary > tertiary. In addition, the amine functional groups were more reactive with the anhydride functional groups as compared with the carboxylic acid functional groups. Rapid reaction between SMA and the primary diamine in a batch mixer at 180 °C resulted in complete crosslinking of the polymer in less than two minutes of blending. Recently, the aminolysis kinetics of polymer bond cyclic anhydride units with a small molecule secondary amine were investigated (Ferrari and Baker, 1998). As compared to the reaction between a model small molecule anhydride and the secondary amine in the presence of molten PE, the aminolysis of the polymer bond anhydride functional groups exhibited significantly slower kinetics. This decrease in the reaction rate was attributed to a collapsed coil effect, which results in shielding of the attached anhydride units by the polymer chain. Polymer entanglements in the melt significantly limit the ability of the polymer chain to reorient and expose the attached anhydride units to the secondary amine for the reaction.

Poly(styrene-*co*-*N*-maleimide) copolymers were prepared by reactive extrusion of SMA and ammonia in a co-rotating twin screw extruder (Vermeesch *et al.*, 1993). Rapid imidation was observed during residence times of two minutes when devolatilization was

applied to remove the water and drive the cyclization. Similarly, SMA was reacted with primary *N*-alkylamines in a co-rotating twin screw extruder (Vermeesch and Groeninckx, 1994). To obtain high yields of the imide product within the 2 to 7 min residence time of the extruder, venting was required to drive the cyclization. The grafts along the polymer backbone decreased the T_g of the product as compared to the original copolymer. Wang *et al.* (1994) branched acrylic acid grafted PP with hexadecylamine in solution and via reactive extrusion in a co-rotating twin screw extruder. FT-IR analysis indicated the formation of the imide, and the grafts resulted in a similar depression of the T_g.

3.2. Experimental

As discussed in the literature review section, the first step of the reaction between a cyclic anhydride and a primary amine is extremely fast under the conditions employed during polymer processing. Therefore, the coupling reaction of anhydride and primary amine terminally functionalized polymers is well suited for the proposed application of employing reactive polymers to investigate mixing during polymer blending. The procedure for the anhydride functionalization of terminal double bonds was adapted from the research of Thompson *et al.* (1998a; 1998b; 1998c). Similarly, the procedure for the primary amine functionalization of terminal double bonds was adapted from the research of Chung *et al.* (1994). The materials, equipment, and procedures for the preparation of the reactive polymers are described. Finally, characterization of the functionalized polymers and their reaction product is presented to confirm the attachment of the desired functional groups.

3.2.1. Materials and Equipment

Two low molecular weight amorphous polyolefin waxes were compared as base materials for the reactive polymer tracers. The polymers were graciously donated by Crowley Chemical Co., and they are commonly employed as tackifiers. Polypol-19 is an amorphous atactic PP, and Polymer C-SYN is an ethylene – propylene (5/95) copolymer. A comparison of their material properties is presented in Table 3.1 (except for the vinylidene concentration, the other values were supplied by Crowley Chemical Co.).

Table 3.1. Base Polymers for the Reactive Tracers

Property (Units)	Polypol-19	Polymer C-SYN
Softening Point (^{o}C)	85	104
Specific Gravity at 60^{o}F	0.840	0.850
Number Average MW (g/mole)	2010	3500
Weight Average MW (g/mole)	10300	12000
Ethylene Content (wt%)	3-5	5
Vinylidene Concentration (mole/g polymer*10^{4})	1.8	3.0

The vinylidene contents were estimated using the FT-IR calibration technique of Thompson *et al.* (1997). This technique is based on a calibration of the FT-IR relative peak height for the vinylidene functional group with ^{1}H NMR results of the vinylidene content of Polypol-19. The product of the number average molecular weight and the vinylidene concentration of Polymer C-SYN estimated that approximately every polymer chain contains one terminal double bond (1.05 mole of vinylidene per mole of polymer).

A list of the other reagents used in the preparation of the reactive polymer tracers is presented in Table 3.2.

Table 3.2. Experimental Reagents

Name of Chemical	Source	Grade
Acetone	BDH	Wash
9-BBN, 0.5M in THF	Aldrich	Anhydrous Solution
Benzoquinone	Aldrich	98% Pure
Hydroxylamine-*o*-sulfonic acid, 95%	Fluka	95% Pure
Maleic Anhydride	Aldrich	99% Pure
Tetrahydrofuran (THF)	Caledon	99% Pure

Preliminary functionalization experiments were completed in small scale quantities to determine the feasibility of the reactions and to evaluate the experimental procedures. Terminal anhydride functionalization was completed in a 300 mL Parr batch reactor. The batch reactor was heated with a heating jacket, and agitation was completed using a turbine rotor. Terminal primary amine functionalization was completed in a 500 mL three-necked glass flask. Heating was completed using a heating mantle, and agitation was introduced using a magnetic stir bar. After successful completion of the preliminary reactions, scale-up of the functionalization methods to produce large quantities of the reactive polymers was completed using a 2 L Parr pressurized batch reactor and a 5 L three-necked glass flask.

3.2.2. Functionalization Procedures

Anhydride functionalization of the terminal double bonds of the low molecular weight polymers was completed by a melt-phase Alder Ene reaction, and a simplified reaction mechanism is depicted in Figure 3.8. The functionalized polymer contains a terminal succinic anhydride group, which is a saturated cyclic anhydride. As well, the unsaturation in the reaction product may be in the form of an internal double bond (A) or a pendant vinylidene (B).

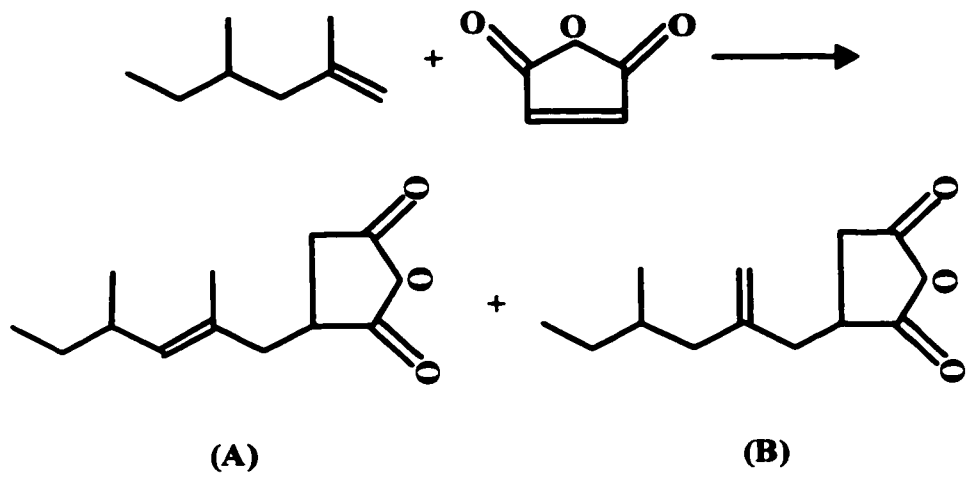

(A) (B)

Figure 3.8. Simplified Mechanism for the Functionalization of a Terminal Double Bond with Maleic Anhydride via the Alder Ene Reaction

600 g of low molecular weight polymer wax, 80 g of maleic anhydride (approximately 5 times the available vinylidene concentration), and 1 g of benzoquinone were charged to the 2L Parr batch reactor (depicted in Figure 3.9) at room temperature. The benzoquinone was used as a radical scavenger to minimize the homopolymerization of the maleic anhydride. The reactor contents were purged with N_2 for 30 min, after which, the reactor was pressurized to 0.69 MPa (100 psi). The reactor was then heated to 230 °C using a heating jacket connected to a Thermolyne type 45550 input controller (initially heated at setting 5, then lowered to setting 2.6 to maintain the desired temperature). A thermocouple was positioned in the reactor to measure the polymer melt temperature, and it took approximately 1.5 hours to reach the desired setpoint from room temperature. After reaching 150 °C, agitation was provided using a rotor containing two turbine blades, and a motor speed of approximately 200 rpm was used. The reaction was run for approximately 14 hours (overnight) at the desired setpoint temperature. Using a valve at the bottom of the reactor, the reactor contents were poured into a ceramic bowl. The functionalized polymer

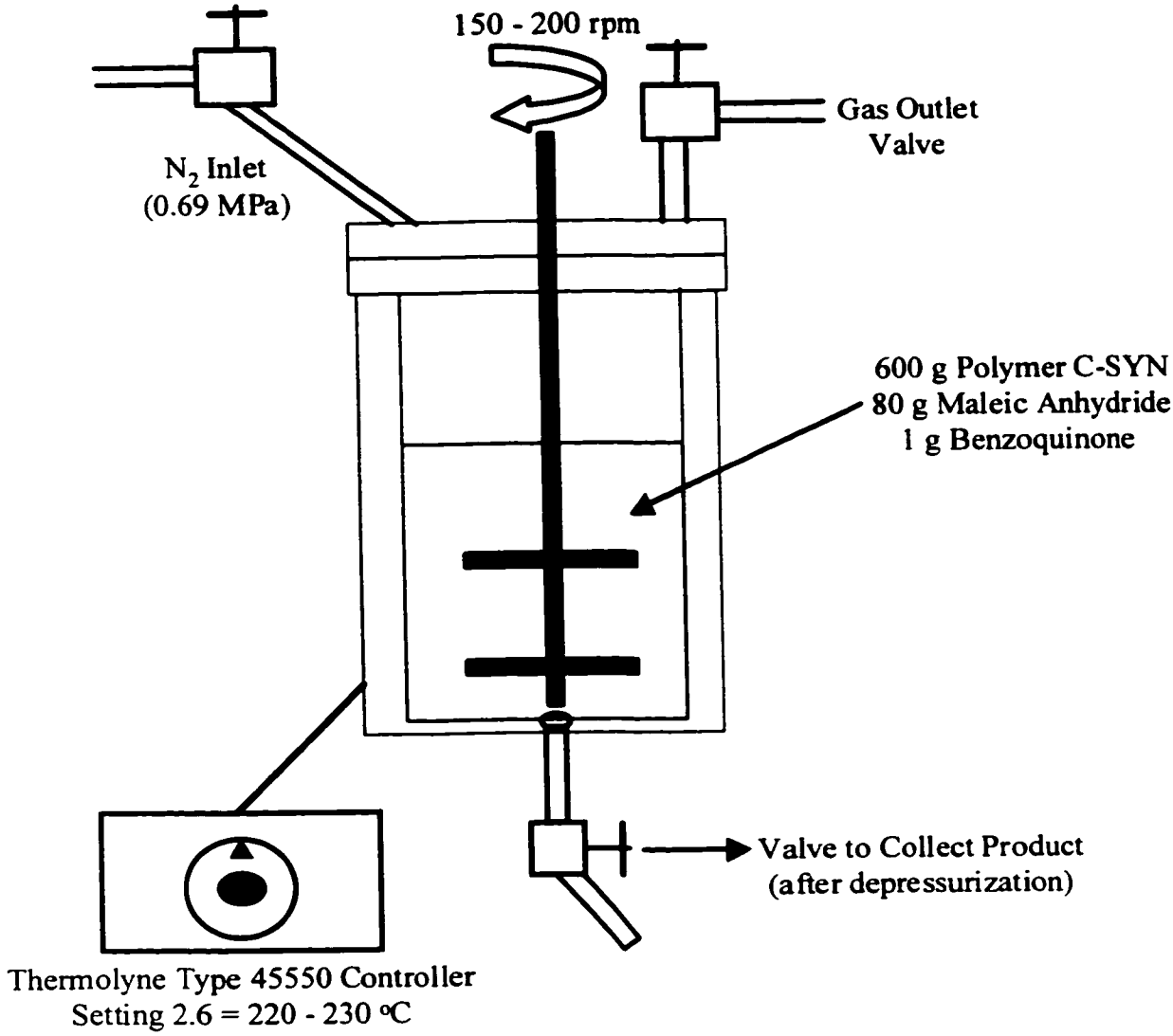

Figure 3.9. Parr Batch Reactor Apparatus for the Preparation of the Anhydride Reactive Polymer

was dark brown due to the formation of poly(maleic anhydride). Prior to using the functionalized polymer in the mixing experiments it was purified to remove free maleic anhydride and poly(maleic anhydride). This purification was completed by leaching out the undesired compounds with hot acetone. The method was repeated until the acetone no longer turned brown, which indicated that all the undesired compounds were removed from the polymer. Purification required approximately 20 L of wash acetone per 1 kg of polymer. Finally, the purified polymer was dried in a vacuum oven for 12 hours at 120 to 140 °C to remove the acetone. The dried polymer was stored in a dessicator to minimize its exposure to water, which hydrolyzes the succinic anhydride functional groups to their corresponding di-acid.

Primary amine functionalization of the terminal double bonds of the low molecular weight polymers was completed by hydroboration with 9-BBN followed by amination of the trialkylborane with hydroxylamine-*o*-sulfonic acid. As previously mentioned, 9-BBN selectively adds to the less hindered carbon of the terminal double bond, which ensures that the functionalization will result in terminal placement of the functional group. Amination of the trialkylborane is not quantitative, with a limiting conversion of 66% (Brown *et al.*, 1988). Therefore, the product contains both primary amine and boronic acid (B-OH) terminally functionalized polymer chains. The simplified reaction mechanism for the formation of a terminal primary amine functionalized polymer chain is depicted in Figure 3.10 (the formation of the undesired monoalkyl boronic acid is also included).

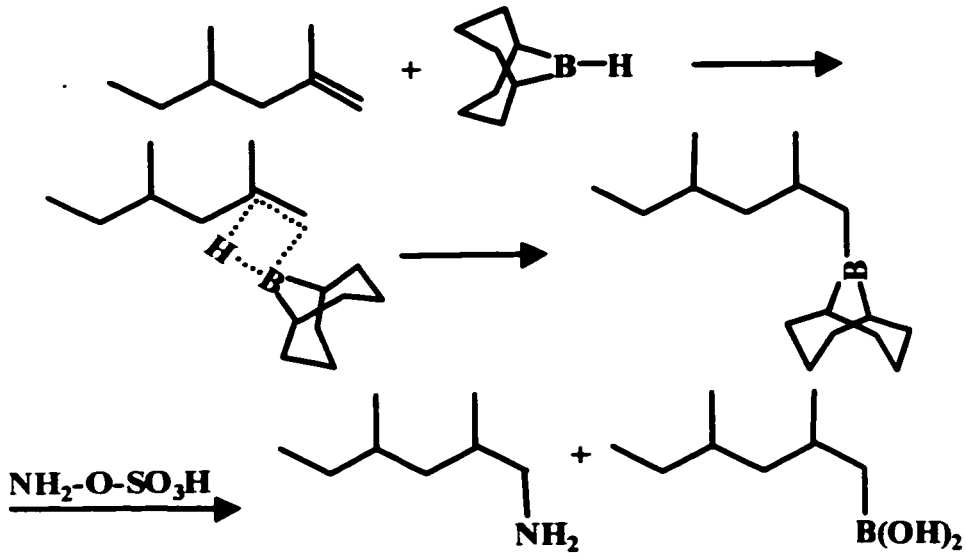

Figure 3.10. Simplified Mechanism for the Functionalization of a Terminal Double Bond with a Primary Amine via Hydroboration / Amination

A solution of 400 g of the low molecular weight polymer in 4 L of THF was prepared in the 5 L three-necked glass flask (apparatus depicted in Figure 3.11). The polymer was dissolved into the solvent under refluxing conditions (66 °C) using the heating mantle. A water cooled condenser was connected to the middle neck to condense the THF vapors. The solution was continuously purged with N_2, which was introduced by a tube through one of the side necks of the flask, to prevent side reactions with oxygen. The solution was maintained at reflux conditions (66 °C) during the dissolving and hydroboration stages. After all the polymer was dissolved, a total of 250 mL of 0.5 M 9-BBN solution in THF was added to the reactor (total borane concentration equivalent to approximately 1.1 to 1.17 times the available vinylidene concentration). Preliminary experiments on the primary amine functionalization of terminal double bonds in Polymer C-SYN indicated the need for a small excess of borane solution. This required excess was attributed to the consumption of a small portion of the borane in side reactions with oxygen or water. The borane solution was

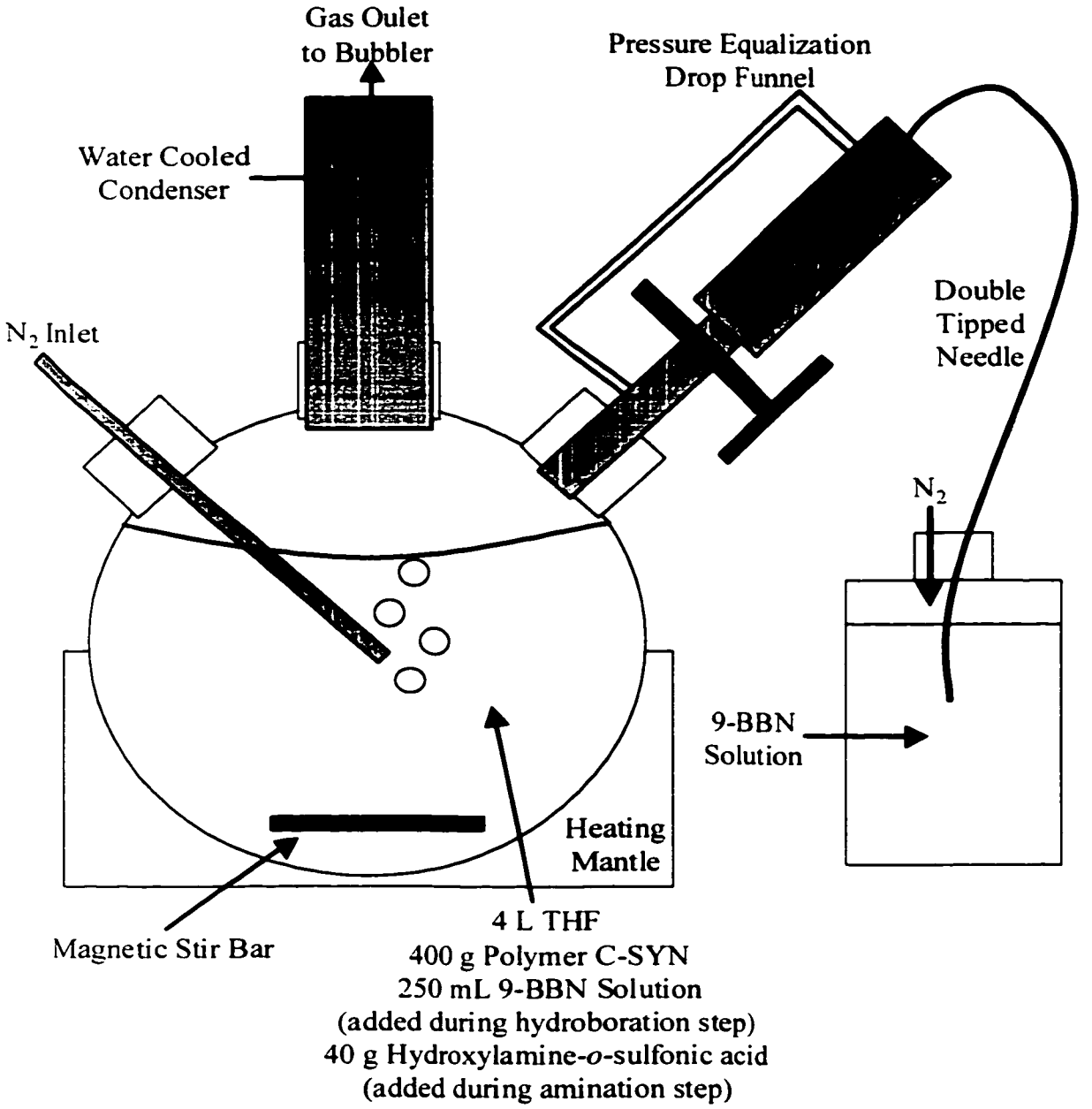

Figure 3.11. Apparatus for the Preparation of the Amine Reactive Polymer via Hydroboration / Amination in Solution

transferred directly from its bottle to a pressure equalization drop funnel that was connected to the reactor through the third neck of the glass flask. Transferring of the borane solution was completed using a double tipped needle and a N_2 purge to force the solution from its bottle to the funnel. The borane solution was added dropwise to the reactor contents over a period of 1 hour, and the hydroboration step was run for a total of 6 hours.

After hydroboration, the reactor contents were cooled to approximately room temperature. Amination was then completed by adding 40 g hydroxylamine-*o*-sulfonic acid (3:1 molar ratio of the hydroxylamine-*o*-sulfonic acid to the borane concentration used in the hydroboration stage) mixed with 100 mL THF to the reactor contents. The 3:1 molar ratio of the hydroxylamine-*o*-sulfonic acid to the borane was used to maximize the amination of the trialkylborane, but only two of the alkyl groups can transfer to the nitrogen groups. The hydroxylamine-*o*-sulfonic acid / THF mixture was added directly through the large middle neck of the glass flask after quickly removing the condenser. The transfer procedure was completed in approximately 15 seconds. After 30 min, the reactor contents were heated to refluxing conditions, and the reaction was run for 12 hours (overnight). The amination reaction was killed by pouring the reactor contents into 4 L of distilled water. The white polymer precipitated, and it was easily separated from the liquids. The collected polymer was purified by leaching out the residual boric acid and free hydroxylamine-*o*-sulfonic acid with hot distilled water, and then acetone. Finally, the purified polymer was dried in a vacuum oven for 12 hours at 120 °C, and then stored in 125 mL jars.

3.2.3. Characterization of the Reactive Polymers

The products from the functionalization reactions were characterized using Fourier-transform infrared spectroscopy (FT-IR). A Nicolet 520 mid-range (400-4000 cm^{-1}) spectrometer was used, with a resolution of 2 cm^{-1}. The low molecular weight polymer waxes and their functionalized products were analyzed by smearing a thin layer of the material on a NaCl disc. The most important region of the FT-IR spectrum was the carbonyl region between 1700 and 1900 cm^{-1}, which was used to follow the reactions of the cyclic anhydride functional groups.

FT-IR analysis was used to obtain relative measurements of the anhydride functional group concentration. To obtain an absolute anhydride concentration measurement, a colorimetric titration method described by Thompson *et al.* (1998a) was used. Titration solutions were prepared and standardized, with concentrations of 0.051 M HCl in isopropanol and 0.044 M KOH in ethanol. For each titration, approximately 0.3 g of maleic anhydride functionalized polymer was dissolved into 50 mL of boiling toluene in the presence of 200 μL of distilled water. The water was used to hydrolyze the cyclic anhydride to its di-acid, which guarantees that two molecules of base are neutralized by one cyclic anhydride functional group. The solution was heated for 1 hour and then cooled to room temperature. Upon cooling, toluene was added to the solution to bring the total volume to 100 mL. Three drops of thymol blue (1% solution in DMF) were added to the solution, and then the solution was divided into 3 aliquots of 25 mL. Into each aliquot, 2 mL of the base solution was added, which turned the indicator purple. The amount of base added to each aliquot was greater than the total concentration of the anhydride functional groups, and therefore, the remaining base was titrated against the acid solution. This method resulted in a

sharp end point for the titration, and the neutralization point occurred when the color changed from purple to yellow. For determination of the anhydride concentration in the samples, a blank consisting of 25 mL of toluene, 1 drop of indicator, and 2 mL of base was titrated against the HCl solution. The volume of acid required to neutralize the blank was 1.5 mL. The concentration of the succinic anhydride functional groups (in grams of succinic anhydride per gram of functionalized polymer) in the functionalized polymers is given by equation 3.1.

$$[\text{Anhydride Concentration}] = \frac{0.196 * C_{HCl}(V_{HCl}^{Blank} - V_{HCl}^{Sample})}{M} \qquad (3.1)$$

where: C_{HCl} : HCl concentration in acid solution (M)
M : Mass of polymer dissolved into 100 mL solution (g)
V_{HCl}^{Blank} : Volume of acid solution required to neutralized blank (mL)
V_{HCl}^{Sample} : Volume of acid solution required to neutralized 25 ml sample (mL)

Intrinsic viscosity of 0.4wt% solutions of the low molecular weight polymers in decahydronaphthalene was measured using ASTM method D 2857. The measurements were completed using a 75 mL Cannon-Ubbelhode dilution viscometer in a silicon oil bath, which was maintained at 60 °C. A blank of pure decahydronaphthalene was used to determine the average reflux time of the solvent. Three reflux times for the polymer solution were obtained by diluting the solution directly in the viscometer. Linear regression analysis of the inherent viscosity results was used to estimate the intrinsic viscosity.

3.3. Functionalization Results: Characterization of the Functionalized Polymers and Their Coupling Reaction Product

Preliminary melt-phase Alder Ene reactions between the terminal double bonds of Polypol-19 and Polymer C-SYN with maleic anhydride were completed in a 300 mL Parr batch reactor using a similar procedure as previously outlined. The products were analyzed

using the titration method, and the results are compared in Table 3.3 (all results are presented as ninety-five percent confidence intervals of the average values determined from 5 replicate titrations for each material).

Table 3.3. Titration Results for the Maleic Anhydride Functionalized Polymers

Material	g Succinic Anhydride / g Functionalized Polymer	Mole % Succinic Anhydride	Conversion (%) of Terminal Double Bonds
Functionalized Polypol-19	0.0141 ± 0.001	29.0 ± 1.9	80.1 ± 5.4
Functionalized Polymer C-SYN	0.0165 ± 0.001	58.9 ± 1.8	62.3 ± 1.9

The titration results indicated that the functionalized polymers were uniform due to the small observed confidence intervals. The anhydride reactive polymer based on Polymer C-SYN had a significantly higher anhydride content, which was attributed to its greater initial concentration of terminal double bonds available for the Alder Ene reaction. Therefore, all the reactive tracers used in the mixing experiments were based on Polymer C-SYN, and the remainder of the research on the reactive polymers will concern only the polymers based on Polymer C-SYN.

A comparison of the FT-IR spectra of the anhydride functionalized Polymer C-SYN and pure Polymer C-SYN is presented in Figure 3.12, and the important peaks in the succinic anhydride functionalized polymer are reviewed in Table 3.4. All the expected characteristic peaks for the succinic anhydride functional groups were observed in the FT-IR spectrum of the functionalized polymer. A small shoulder was apparent at 1784 cm^{-1}, which indicated that a very small amount of poly(maleic anhydride) remained in the purified polymer.

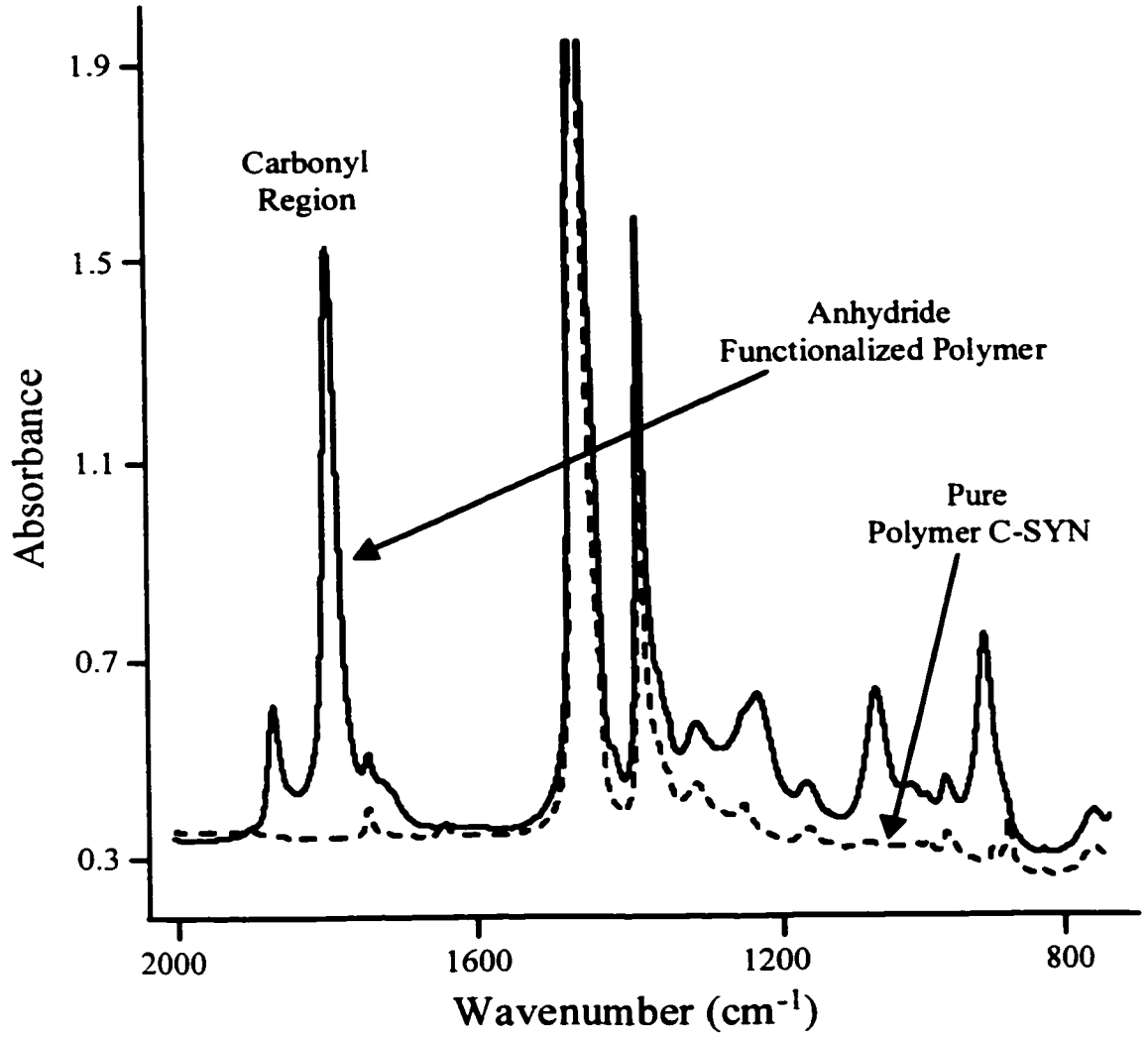

Figure 3.12. A Comparison of the FT-IR Spectra of Pure Polymer C-SYN and the Anhydride Functionalized Polymer

Conversion of the terminal double bonds cannot be estimated using the peak at 888 cm^{-1} because the product from the Alder Ene reaction also contains a double bond.

Table 3.4. Important Peaks in the FT-IR Spectrum of the Succinic Anhydride Functionalized Polymer

Peak (cm^{-1})	Group	Reference
1865	Antisymmetric C=O stretching vibration of anhydride	De Roover et al. (1995)
1792	Symmetric C=O stretching vibration of anhydride	De Roover et al. (1995)
1784	C=O stretching vibration of poly(maleic anhydride)	De Roover et al. (1995)
1228	Cyclic C-O vibrations of anhydride	Mirone and Chiorboli (1962)
1066	C-O stretching vibrations of anhydride	Mirone and Chiorboli (1962)
1022	CH bend, Ring bend of anhydride	Mirone and Chiorboli (1962)
922	C=O bend of anhydride	Mirone and Chiorboli (1962)
888	CH out-of-plane deformation of vinylidene	Bellamy (1958)

A comparison of the FT-IR spectra of pure Polymer C-SYN and the reacted polymer after the hydroboration and amination steps is presented in Figure 3.13. The important peaks after hydroboration are presented in Table 3.5, and the important peaks after amination are presented in Table 3.6. FT-IR analysis confirmed the attachment of the primary amine functional groups to the polymer chain. The peaks located at 1528 cm^{-1} and 1213 cm^{-1} indicated that the product may contain some attached boron groups, which is possible due to the limiting conversion of the amination reaction. According to the reaction mechanism presented in Figure 3.6 (adapted from Pelter *et al.*, 1988), boronic acid may remain terminally attached to some of the polymer chains in the product.

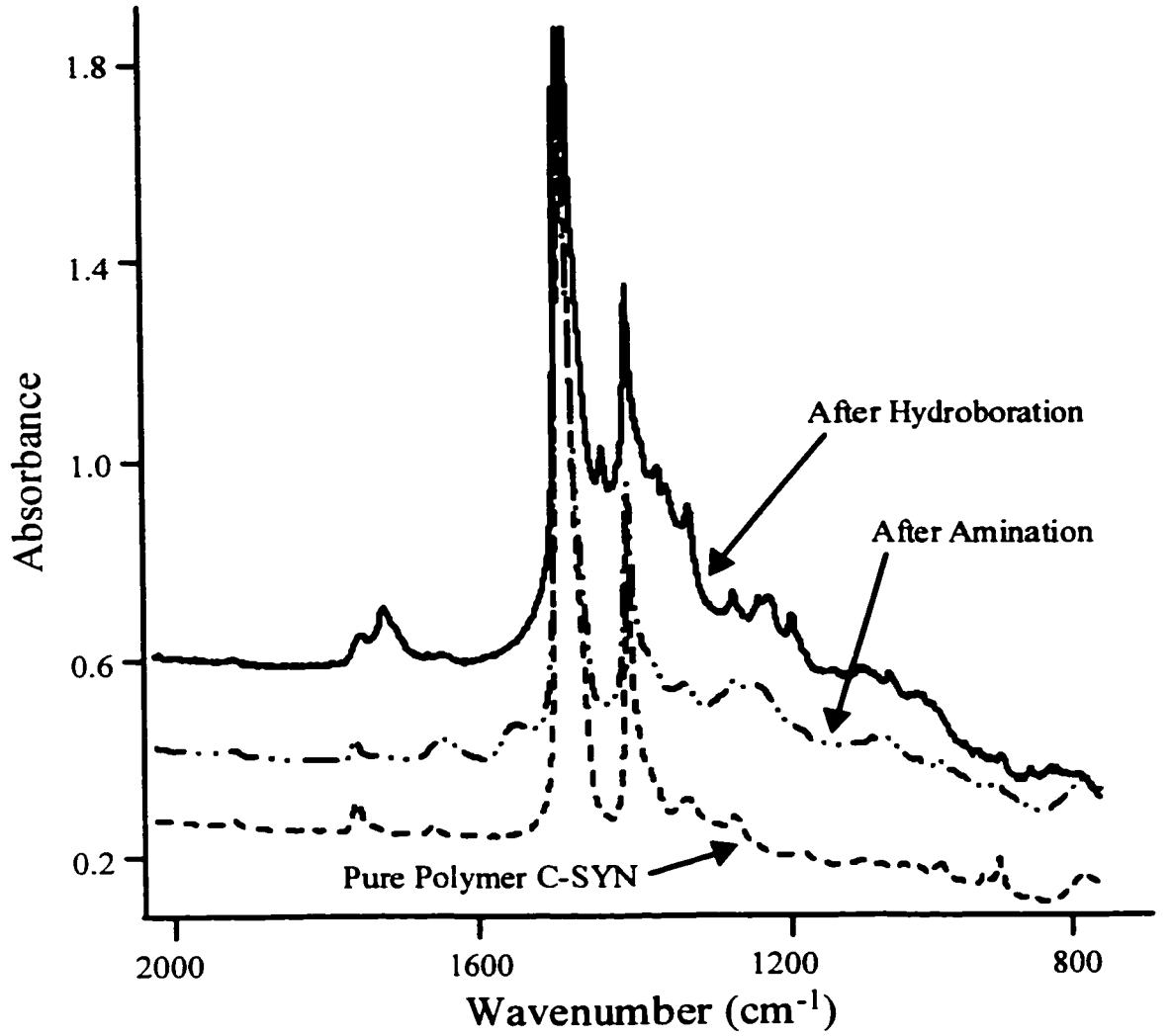

Figure 3.13. A Comparison of the FT-IR Spectra of Pure Polymer C-SYN and the Reacted Polymer After the Hydroboration and Amination Stages

Note: The baselines of the two reacted products are staggered upwards from the baseline of the pure Polymer C-SYN to allow for easier comparison of the spectra (the scale on the absorbance axis corresponds to the bottom spectrum only).

Table 3.5. Important Peaks in the FT-IR Spectrum After Hydroboration

Peak (cm^{-1})	Group	Reference
3208	O-H stretch of boric acid	Bellamy (1958)
2260	B-H stretch	Bellamy (1958)
1707	B-H-B bridging vibration	Bellamy (1958)
1412	B-C stretching	Bellamy (1958)
1301	$B-CH_3$ stretching	Bellamy (1958)
1242	B-R stretching	Bellamy (1958)
1200	B-H of free borane	Bellamy (1958)
1165	free B-H	Bellamy (1958)
1037	B-C stretching	Bellamy (1958)

Table 3.6. Important Peaks in the FT-IR Spectrum After Amination

Peak (cm^{-1})	Group	Reference
1630	NH_2 scissors	Lin-Vien et al. (1991)
1528	B-N stretching	Bellamy (1958)
1213	B-R stretching / C-N stretching	Bellamy (1958) / Lin-Vien (1991)
1046	C-N stretching	Lin-Vien et al. (1991)
861	NH_2 wagging	Lin-Vien et al. (1991)

FT-IR analysis indicated the successful attachment of the desired functional groups to the polymer. A preliminary reaction between the two reactive polymers was completed to investigate their reaction product. Bulk imidation of the two reactive tracers was completed using equal masses of the two polymers. Approximately 5 g of each reactive polymer was charged to a small three-necked glass flask. The contents were heated using a heating mantle to approximately 160 °C, and agitation was introduced using a magnetic stir bar. The flask was continuously purged with N_2 to prevent polymer degradation. The reaction was completed for a total of 2 hours, and a comparison of the FT-IR spectra from the beginning (obtained after complete melting of the two polymers, approximately 5 min) and the end of the reaction is presented in Figure 3.14.

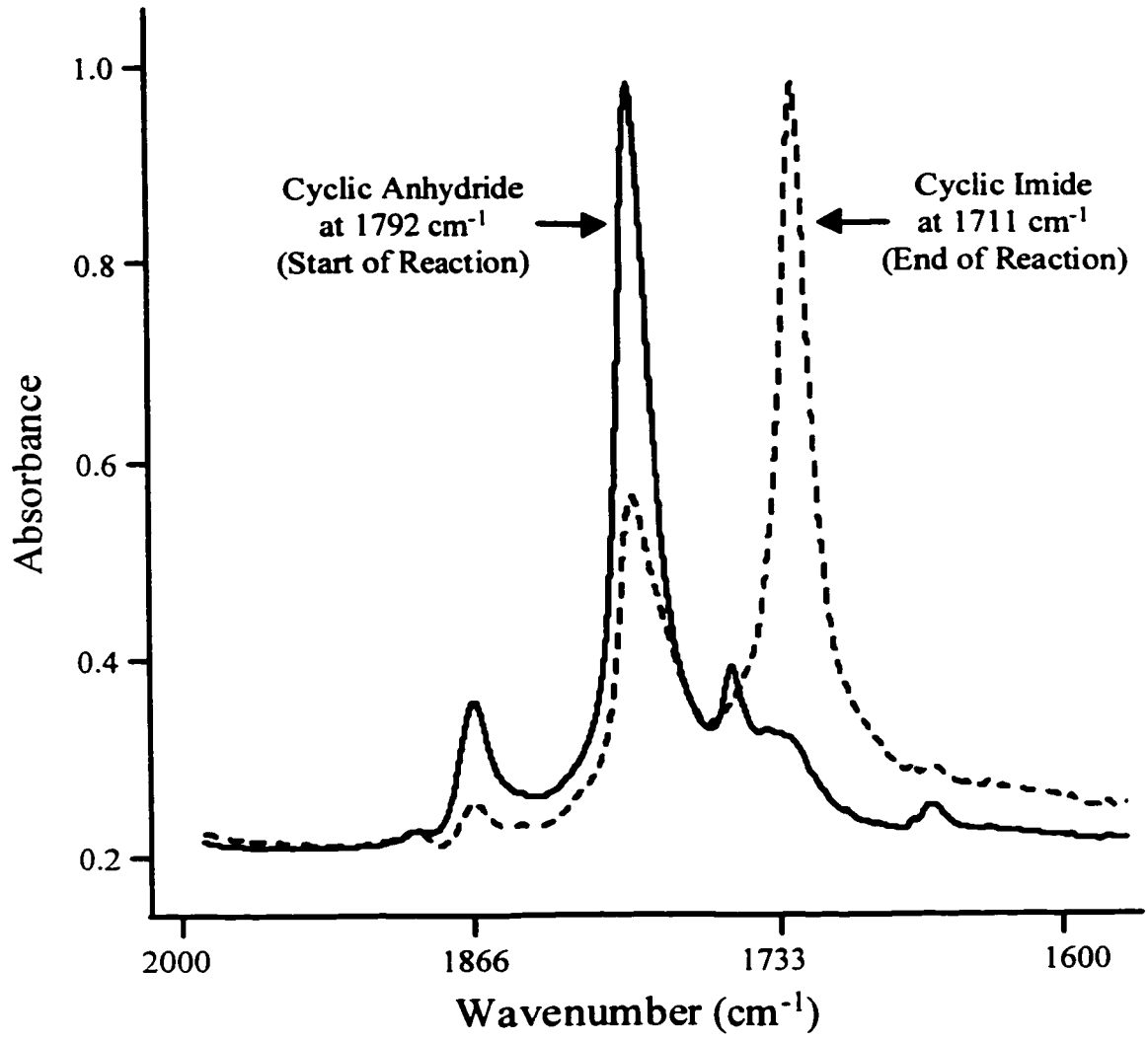

Figure 3.14. FT-IR Spectra of the Bulk Imidation of the Reactive Polymers

The polymer product was heated in a vacuum oven at 120 °C for 12 hours, and no further significant change in the FT-IR spectrum was observed. Therefore, complete conversion of the limiting functional group was accomplished during the imidation of the reactive polymers. In addition, the reported reversibility of the reaction by Hu and Lindt (1992) was not observed. As indicated in Figure 3.14, the limiting species was the amine functional group. The peak at 1792 cm^{-1} corresponds to the succinic anhydride functional group, and the peak at 1711 cm^{-1} corresponds to the cyclic imide formed during the reaction. Using the peak at 1792 cm^{-1} and an internal reference at 1378 cm^{-1}, which corresponds to the polymer backbone (Painter *et al.*, 1982), the conversion of the anhydride functional groups was estimated to be 47.4%. This calculation assumed that the conversion of the anhydride functional groups during the melting of the polymers (approximately 5 min) was negligible. Further amine – anhydride reactions are discussed in the Chapter 5.

Intrinsic viscosity of solutions of the two reactive polymers, Polymer C-SYN, and the imide product were measured using decahydronaphthalene as the solvent. The average reflux time of the solvent was 204.5 seconds, which is above the minimum value of 200 seconds required to ignore kinetic energy corrections. Linear regression was performed on the inherent viscosity data, and the intrinsic viscosities are presented in Table 3.7.

Table 3.7. Intrinsic Viscosity Results

Material	Intrinsic Viscosity (dl/g)	Standard Error
Polymer C-SYN	0.1823	0.0013
Anhydride Functionalized Polymer C-SYN	0.1799	0.0001
Amine Functionalized Polymer C-SYN	0.1799	0.0039
Imide Product of Reactive Tracers	0.2773	0.0015

The intrinsic viscosity results indicated that the functionalization methods (Alder Ene reaction, hydroboration / amination) did not degrade the Polymer C-SYN. The intrinsic viscosity of the product obtained from the bulk imidation was significantly higher than that of the individual reactive polymer tracers. The reaction resulted in chain extension, which suggested that the functional groups were terminally bound to the polymer chains. The intrinsic viscosity, which is an indication of the chain size, did not double due to the reaction because not all the polymer chains were functionalized in the reactive polymers.

3.4. Concluding Remarks on the Preparation of the Reactive Polymer Tracers and Possible Improvements

Characterization of the reactive polymers and their imidation product confirmed the successful attachment of the desired succinic anhydride and primary amine functional groups. Targeted functionalization of the existing terminal double bonds of Polymer C-SYN yielded reactive polymers containing precisely located functional groups. In addition, the reactions were non-degradative to the polymer because no free radicals were used. Large quantities of the succinic anhydride reactive polymer were easy to prepare using a batch reactor. Although no solvent was required in the melt-phase Alder Ene reaction, purification was required to remove the free maleic anhydride and poly(maleic anhydride). These species will react with the amine functionalized polymer if they are not removed from the product.

Preparation of the primary amine terminally functionalized polymer via hydroboration followed by amination was completed in solution. Large quantities of solvent were required to produce the amount of reactive polymer used in this research. The development of a simple melt-phase functionalization technique for introducing primary amine functional groups to polyolefins would be a great improvement for further research.

One possible method was attempted using a Diels-Alder reaction between the terminal double bonds of Polypol-19 and the 1,4 diene of 4-aminoquinaldine, which is constrained in the cis conformation. This conformation should allow the compound to react with the terminal double bond to form a Diels-Alder adduct. In all the experiments completed in the 300 mL Parr batch reactor at temperatures between 200 to 240 °C for 4 to 24 hours under N_2, no attachment of the 4-aminoquinaldine to the polymer was observed. Upon purification using hot acetone, the product exhibited no new peaks in the FT-IR spectrum.

There are many possible reasons for the failure of this Diels-Alder reaction. First, the Diels-Alder reaction is reversible, and therefore, the equilibrium may have been unfavorable towards the forward reaction at the investigated temperatures. Second, the mixing capability of the batch mixer may not be sufficient to bring the incompatible phases into contact for the reaction to occur. Upon opening the reactor, yellow crystalline flakes were observed at the top of the reactor, which were identified as 4-aminoquinaldine using FT-IR analysis. This observation confirmed that there was phase separation between the incompatible reactants in the batch mixer. Finally, the double bonds in the bi-cyclic structure of 4-aminoquinaldine may have been delocalized through possible resonance structures, which are depicted in Figure 3.15. This delocalization would limit the ability of the 4-aminoquinaldine to form the Diels-Alder adduct with the terminal double bonds of the polymer.

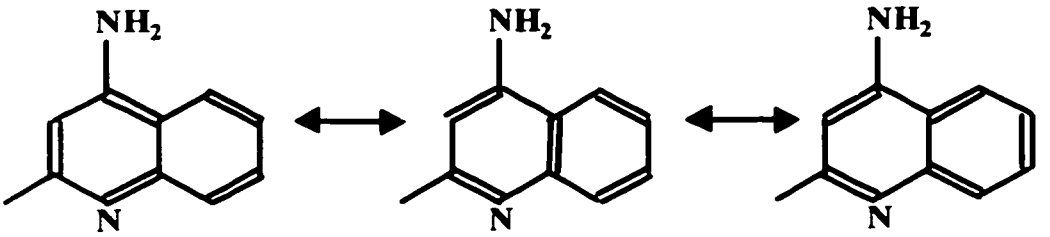

Figure 3.15. Possible Resonance Structures of 4-aminoquinaldine

Another possible functionalization method is the hydrosilylation of the terminal double bonds of Polymer C-SYN with a silane compound containing a primary amine functional group. A combination of the methods of Hazziza-Laskar *et al.* (1991) and Malz and Tzoganakis (1998) could be used to introduce primary amine functionalized silanes to unsaturated polymers via a melt-phase catalytic hydrosilylation reaction. Although this procedure must be completed in two steps, no solvent is required. The silane segment connecting the polymer chain and the functional group may affect the properties of the functionalized polymer, and therefore, it is recommended to use a similar functionalization method to prepare the anhydride functionalized polymer. As previously mentioned, Maric and Macosko (1999) used hydrosilylation to functionalize a silane with succinic anhydride. The proposed two step functionalization method via hydrosilylation is depicted in Figure 3.16. All the required chemicals are commercially available (tetramethyldisiloxane – Aldrich 23,573-3; hydrosilylation catalyst is platinum-divinyltetramethyldisiloxane complex in xylene – United Chemical Technologies PC072; hydrosilylation co-catalyst is t-butylhydroperoxide in decane – Aldrich 41,666-5; allylamine – Aldrich 14,583-1; allyl succinic anhydride – Polysciences). The reaction conditions proposed in Figure 3.16 are based on the conditions used by Hazziza-Laskar *et al.* (1991) and Malz and Tzoganakis (1998), but optimization of the conditions may result in higher yields of the reactive polymers. For application as reactive tracers in the analysis of polymer mixing, the reactive polymers must be compatible with PP resins. The siloxane segment may cause preferential migration of the reactive polymers to the interfaces and the metal surfaces of the extruder, and therefore, the compatibility of these tracers in PP must be confirmed.

Step 1: In glass reactor at 50 - 70 °C (depending of b.p. of reactants) for 6 hrs

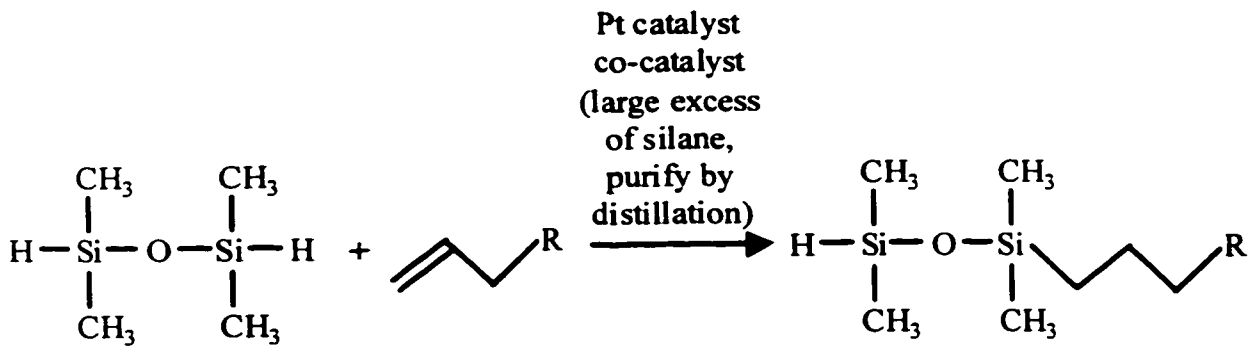

Step 2: In Parr batch reactor at 200 °C under N_2 for 6 hrs

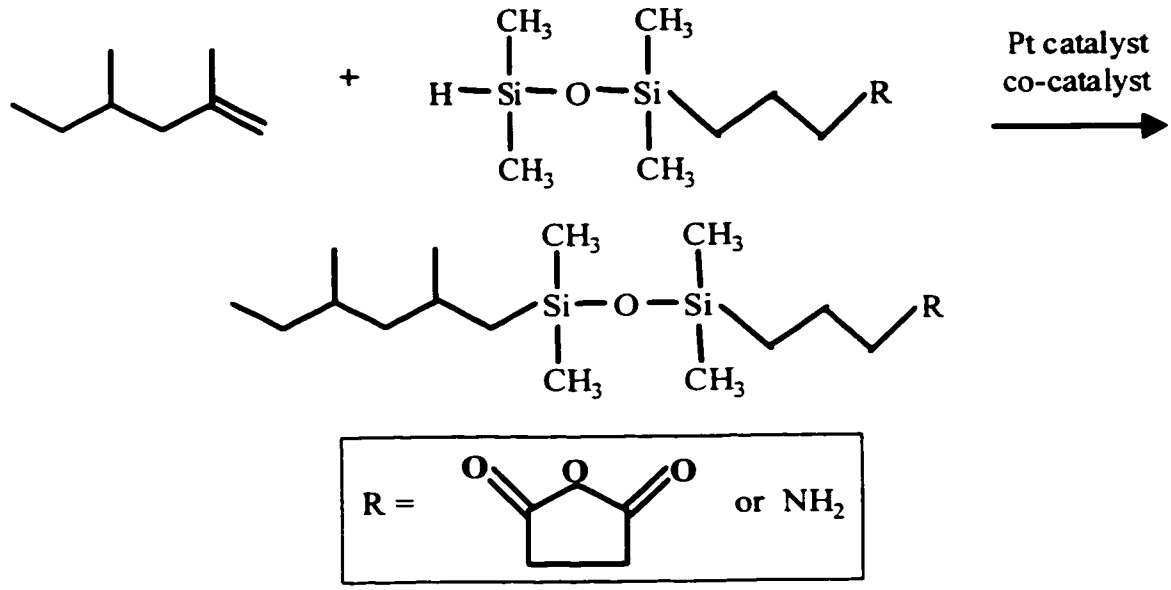

Figure 3.16. Possible Functionalization Method to Introduce Primary Amines and Anhydrides to Unsaturated Polymers Via Hydrosilylation

CHAPTER 4
EXPERIMENTAL

This chapter describes the materials, equipment, and procedures that were used in the novel analysis of mixing during polymer blending in a twin screw extruder using reactive polymer tracers. The preparation of the reactive polymer tracers and their characterization was discussed separately in Chapter 3. In addition, preliminary experiments on the reaction between the polymer tracers in molten PP are described. Finally, the methods used to analyze the mixing and RTD results are presented.

4.1. Materials

All the mixing experiments were completed using PP as the investigated polymer. Three different PP resins were obtained for the research, and some of their material properties are compared in Table 4.1.

Table 4.1. Material Properties of the Investigated PP Resins

Resin Name / Manufacturer	Melt Flow Index* (g / 10 min)	Number Average Molecular Weight** (g / mole)	Weight Average Molecular Weight** (g / mole)	Polydispersity (PDI)
HY6100 / Montell	1.2	64400	300600	4.67
KF6100 / Montell	3	48100	411300	8.55
Petrothene PP8000GK / Equistar	5	41900	246000	5.87

*Measured according to ASTM D-1238 Condition L
**Measured from GPC analysis of the molecular weight distribution

Excluding the PP resins and the reactive polymer tracers, the other materials used in this research are presented in Table 4.2.

Table 4.2. Other Materials Used in Research

Material	Source	Purpose
Hexadecylamine	Aldrich	Model amine compound for preliminary experiments on reaction kinetics in molten PP
Anhydrous Calcium Sulfate	Drierite	Desiccant used to minimize hydrolysis of anhydride functional groups
TiO_2	Kronos	Pigment used to increase contrast in photographs of the polymer melt on the screws of the twin screw extruder (fill distribution measurements)
Carbon Black	Cabot N660	Tracer for local residence time measurements

4.2. Equipment

A summary of the equipment used in this research is presented in Table 4.3.

Table 4.3. Equipment Used in Research

Name of Equipment	Model (Company)	Specifications
Batch Mixer	Rheomix 3000 attached to Rheocord 90 (Haake)	Batch mixer connected to torque rheometer, roller blades (non-intermeshing), processes approximately 200 g polymer per batch
Feeder	LWFD5-200 (K-TRON)	Operated in volumetric feeding mode, Mass flow rates of 15 – 500 g/min
Feeder	FW/18/5 (Brabender)	Operated in volumetric feeding mode, flexwall design to prevent bridging of pellets, mass flow rates of 5 – 50 g/min
Single Screw Extruder	Rheomex 252 attached to Rheocord 90 (Haake)	1.9 cm diameter single screw extruder connected to torque rheometer, L/D = 25, vibrating feeder, conventional screw (feed zone / compression zone / metering zone; L/D = 10/5/5)

Name of Equipment	Model (Company)	Specifications
Twin Screw Extruder	LSM 30.34 (Leistritz)	Co-rotating, fully intermeshing, L/D=35, total length = 1.2 m (10 barrel segments), screw diameter = 34 mm, centerline separation = 30 mm, forward conveying elements (pitch = 20, 30, 45 mm), reverse conveying elements (pitch = 20 mm), bilobal kneading discs (thickness = 7.5 mm) with possible stagger angles of –30°, -60°, 30°, 60°, and 90°
Water Bath	(Berlyn)	Length = 1.8 m, used to solidify the polymer extrudate from the twin screw extruder
Pelletizer	Pel-4 (Berlyn)	Strand pelletizer
Strand Die	In House Design	Connects to end of twin screw extruder, dual strands, diameter = 4 mm
Film Die	In House Design	Connects to end of twin screw extruder, width = 2.5 cm, gap = 0.75 mm film thickness (depends of draw rate) = 0.7 – 1.5 mm
Single / Twin Melt Adapter	In House Design	Connects output from single screw extruder to vent barrel segment of the twin screw extruder, length = 19 cm, inner diameter = 1.9 cm, heated with clam shell band heater, melt injection point directly above intermeshing region of twin screw extruder
Pressure Transducer	PT462E (Dynisco)	Connects to twin screw extruder through ½-20 UNF-2B mounting hole, tip is flush with barrel wall, measures melt pressure in range of 0 MPa to maximum of transducer (34.5, 51.7, 68.9 MPa), accuracy = ± 0.5%
Melt Temperature Probe	MTX922-6/24-1-C-0-10 (Dynisco)	Connects to twin screw extruder through ½-20 UNF-2B mounting hole, tip flush with barrel wall, measures melt temperature using infrared energy principle (range = 135 – 371 °C, accuracy = ± 1%)
Hot Press	(Pasadena Hydraulics)	Temperatures up to 300 °C, Pressing force up to 40,000 lbs., used to produce polymer films for FT-IR analysis, mold with thickness = 0.2, 0.3, 0.75, and 0.9 mm to produce circular films (diameter = 2.54 cm)

Name of Equipment	Model (Company)	Specifications
Grinder	Model 2 (Wiley Hill)	Rotating blade grinder for grinding plastic collected from batch mixer into coarse powder
Desiccator	F42027 (Scienceware)	Used for storage of anhydride reactive polymer and PP / anhydride reactive polymer blend to minimize hydrolysis of the functional groups
Heatable Infrared Cell	HTC 100 (Harrick)	Apparatus for in-line FT-IR analysis of model interfacial polymer reactions, positioned inside FT-IR spectrometer (Nicolet 520 mid-range)
GPC	150-CV+ (Waters)	High temperature GPC, TCB solvent at 140 °C, calibrated with linear polystyrene standards
Capillary Rheometer	Galaxy V Model 8052 (Kayeness)	Capillary rheometer for shear viscosity measurement, capillary die diameters = 0.015, 0.02, 0.03 in, L/D = 5, 10, 20, 40, 50, 60, force cell with 2000 lbs. Maximum load

4.3. Procedures

4.3.1. PP / Reactive Polymer Tracer Blending

From preliminary reactions between the reactive tracers in molten PP, it was determined that a tracer concentration of 5wt% was adequate for quantitative analysis of the conversion. In the case of the model interfacial reactions, 5wt% blends of each reactive tracer in the PP resins were prepared using the batch mixer. 200 g of PP pellets were processed in the batch mixer at 195 °C and 50 rpm. After complete melting of the PP and the establishment of a constant torque, 10.5 g of one of the reactive polymers was added to the mixer. The components were blended for approximately 10 min, and then removed from the mixer using brass spatulas. The solidified chunks of the blend were then ground into a coarse powder, and the blend containing the anhydride reactive polymer was stored in a desiccator.

In the case of the mixing experiments in the twin screw extruder, large quantities of the PP / reactive polymer tracer blends were required. The blending procedure was modified to significantly reduce the number of batches that were required to prepare these blends. Using the batch mixer, blends of each reactive polymer in PP were prepared with a tracer concentration of 25wt%. The blends did not have waxy textures, which indicated that the tracers were well distributed into the PP matrix. If the reactive polymers were incompatible with the PP resin, the low molecular weight tracer would migrate to the surface of the blend causing a waxy texture. The compatibility of the PP and the reactive tracers is further discussed in Chapter 5. The 25wt% blends were ground into a coarse powder and the blend containing the anhydride functionalized polymer was stored in a vacuum desiccator to minimize the hydrolysis of the anhydride functional groups. Prior to the mixing experiments, the 25wt% blends were letdown to 5wt% by extruding a premixed solid blend of the coarse powder with pure PP pellets in the twin screw extruder. Once again, the collected pellets of the PP / anhydride polymer tracer blend were stored in desiccators.

4.3.2. Preliminary Reactions Between the Reactive Polymer Tracers in the Presence of Molten PP

Preliminary reactions between the reactive polymers were completed to gain a better understanding of the anhydride - amine kinetics and the diffusion rates of the tracers in molten PP. Thin films (thickness = 0.15 mm – 0.8 mm, depending on mold thickness) of the PP / reactive polymer blends were compression molded using the hot press. These films were used to perform model reactions in the hot press and the heatable IR cell. The model reactions occurred at the interfaces between the PP layers, and the reaction rate was controlled by the diffusion of the tracers to the interfaces. For the reactions in the hot press, a

stack of thin films (a combination of two thin films or in some experiments multiple films to increase the number of interfaces available for the reaction) was compression molded. As depicted in Figure 4.1, the stack of films was held in a mold between aluminum foil and thin metal sheets. The hot press was preheated to 200 °C, and a pressure of 5.5 MPa was applied to the mold. After desired reaction times, the mold and its contents were rapidly cooled in a water bath to control the amount of crystallinity in the solidified film. The same procedure was used in all the hot press reactions because the degree of crystallinity significantly affects the peak absorbances in the FT-IR spectrum of PP (Zbinden, 1964). Off-line analysis of the reactions was completed using FT-IR analysis of the solidified film. Conversely, in-line analysis of the melt-phase reactions was completed using the heatable IR cell. A stack of thin polymer films (held between 2 NaCl discs, depicted in Figure 4.1) was placed in the heatable IR cell, which was positioned in the FT-IR spectrometer. It took approximately 8 min for the heatable IR cell to reach 200 °C from room temperature. At desired reaction times, direct FT-IR analysis of the melt was completed.

4.3.3. Analysis of Mixing During Melt-melt Blending in the Twin Screw Extruder

The primary objective of this research was to develop an experimental method to analyze distributive mixing during polymer blending. To eliminate the complications of the melting transition on the overall mixing process, melt-melt blending of segregated PP streams was performed. Each segregated stream contained one of the reactive polymer tracers homogeneously distributed into the melt. As the two polymer melts are blended together in the extruder, interfacial area is generated, and the reactive polymer tracers come into contact and react at the growing interface. Therefore, the conversion of this interfacial

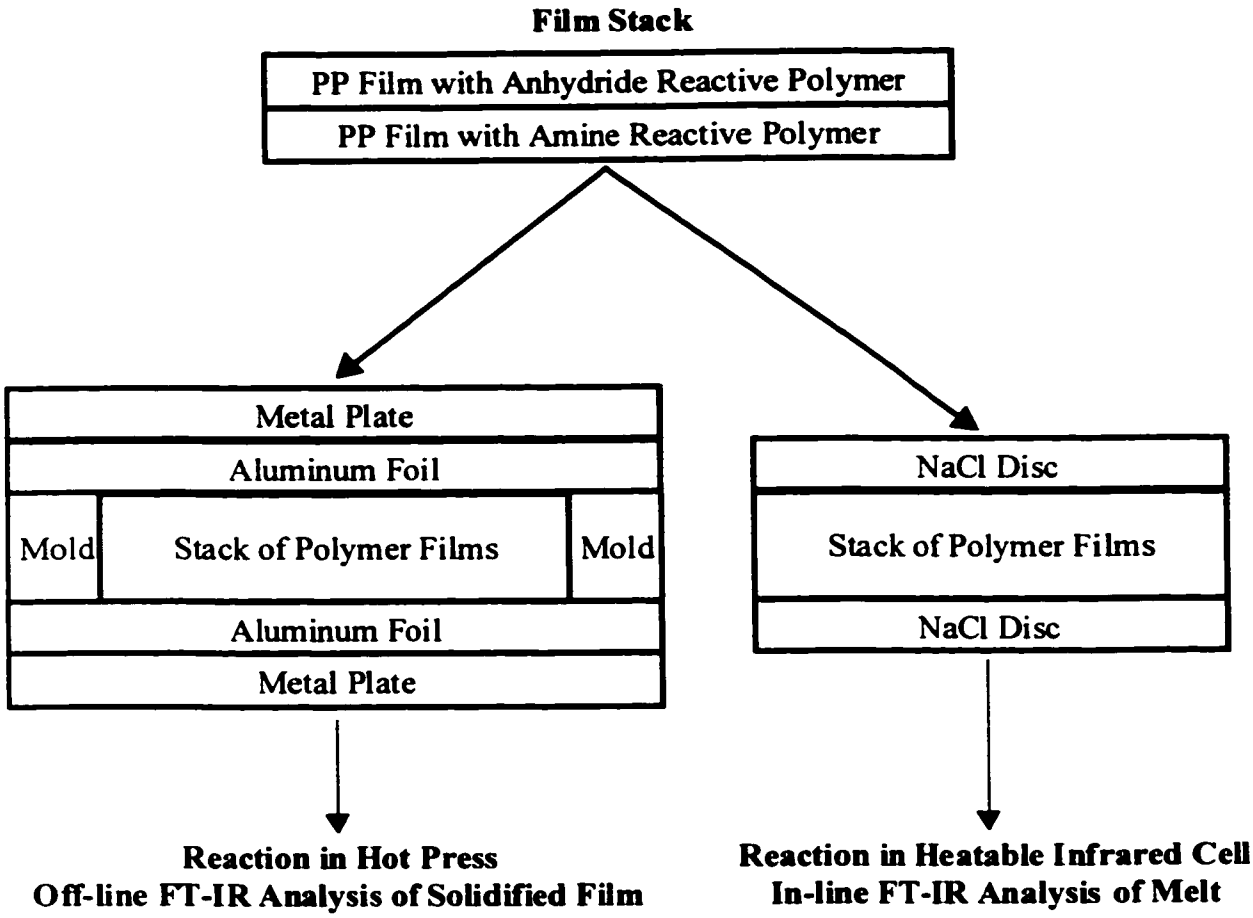

Figure 4.1. Model Interfacial Reactions Between Thin Polymer Films (Off-line and In-line Measurements)

reaction is directly related to the amount of interfacial area generated by the extruder, or the distributive mixing performance.

4.3.3.1. Analysis of the Overall Distributive Mixing

To perform melt-melt blending in the twin screw extruder, a tandem extruder apparatus was used (Figure 4.2). Output from the single screw extruder was fed to the twin screw extruder using an adapter. The PP / amine reactive polymer tracer blend was metered to the beginning of the twin screw extruder (barrel segment 1) using the K-TRON feeder. The PP / anhydride reactive polymer tracer blend was melt fed using the single screw extruder / adapter (Figure 4.3) to a desired downstream position of the twin screw extruder. Blending of the two polymer melts was completed from the melt feeding location to the end of the extruder. A slit die was used to produce a thin polymer film (average thickness = 1 mm) from the twin screw extruder, which was used directly for the FT-IR analysis of the reaction conversion. This conversion is directly related to the total amount of interfacial area generated during the processing of the polymer melts in the blending section of the twin screw extruder, or the overall distributive mixing. The polymer film was rapidly solidified in the water bath to prevent further reaction and to control the crystallinity. All the mixing experiments were completed using equal mass flow rates in the two segregated polymer melt streams, or a volumetric ratio of one.

An example of the screw configuration used in a mixing experiment is presented in Figure 4.4 (melt feeding location at barrel position 6 of 10). A typical barrel temperature profile was: 130 (solid feeding zone, barrel 1), 170, 200, 210 (melting zone with kneading block, barrel 4), 220, 220 (melt feeding zone, barrel 6), 220, 220, 220, 220, and 220 °C (die).

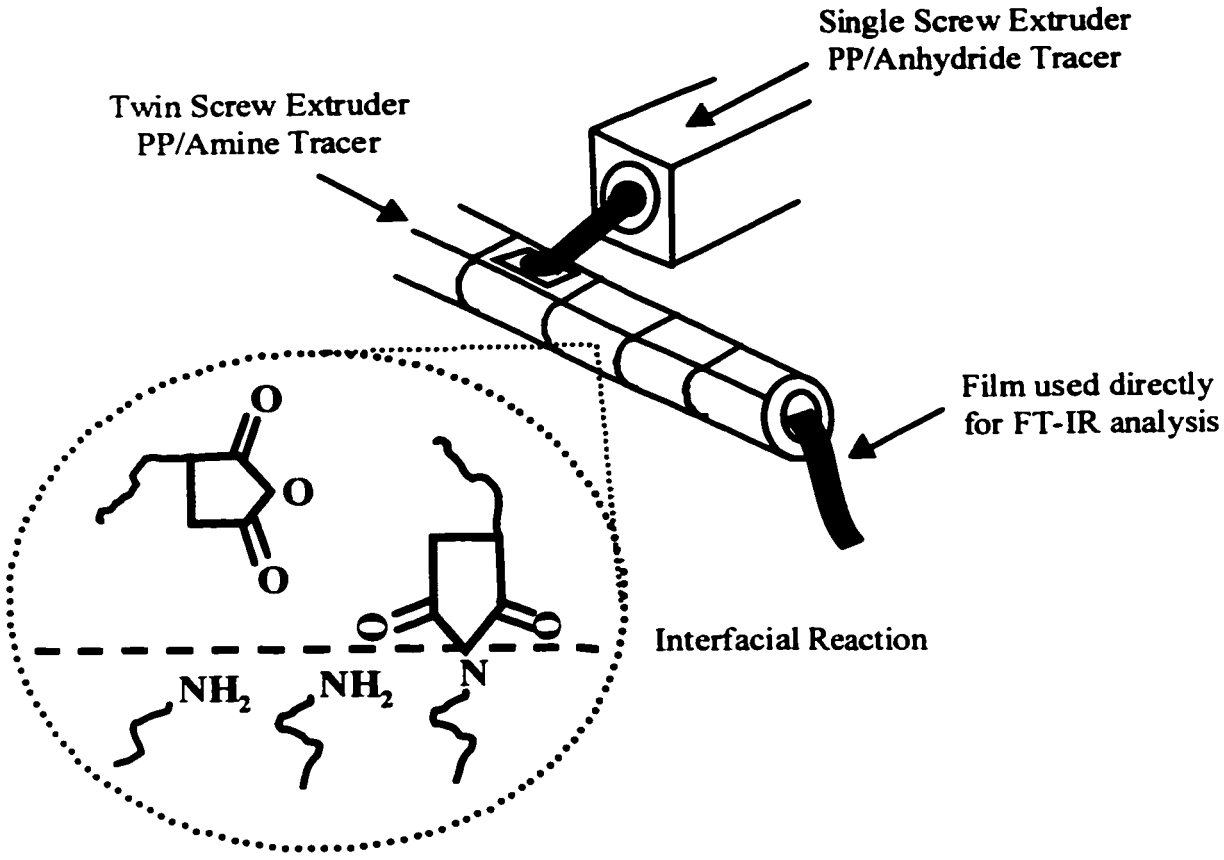

Figure 4.2. Apparatus for Melt-melt Blending with Segregated PP Melts Containing the Reactive Polymer Tracers

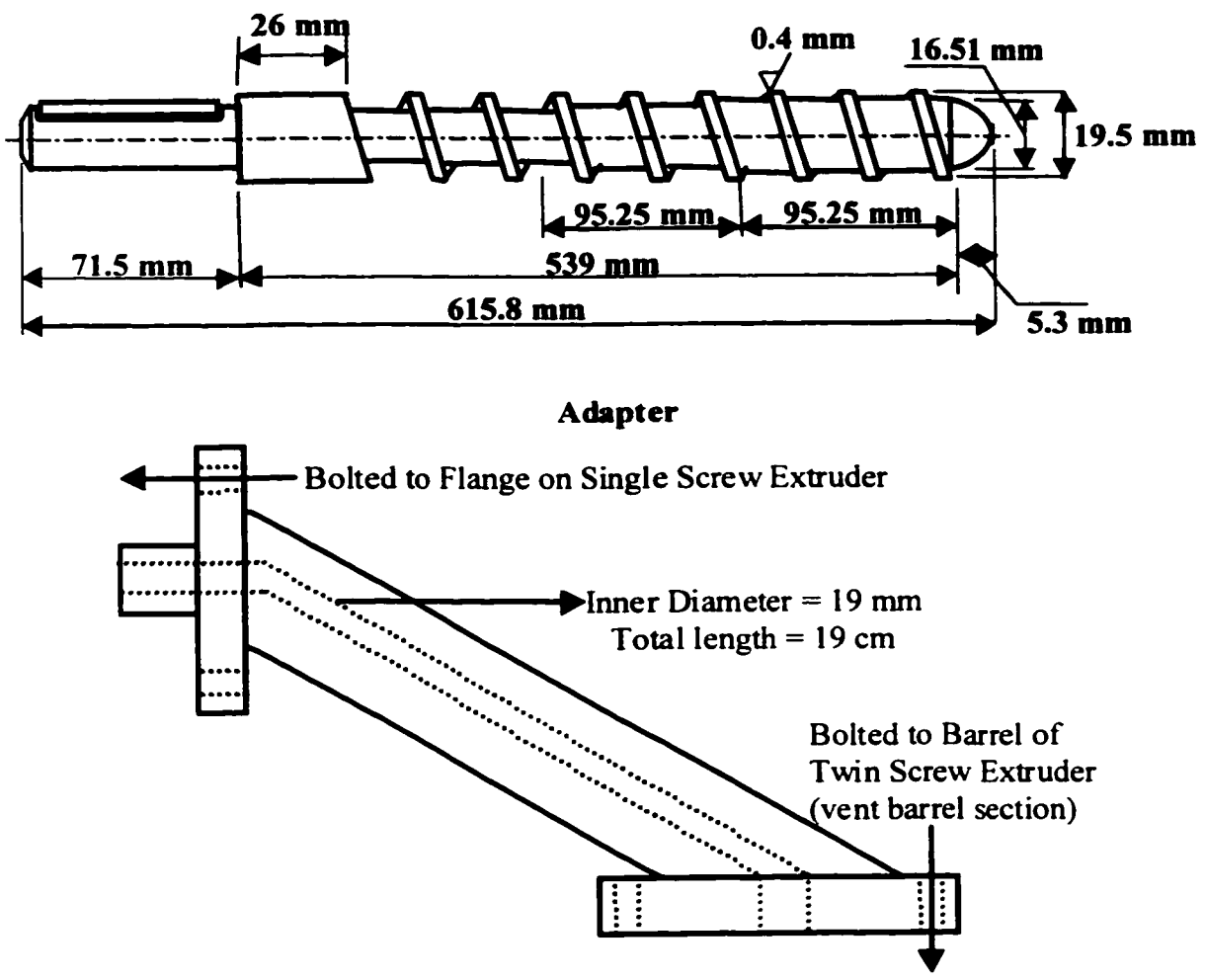

Figure 4.3. Single Screw Extruder and Adapter

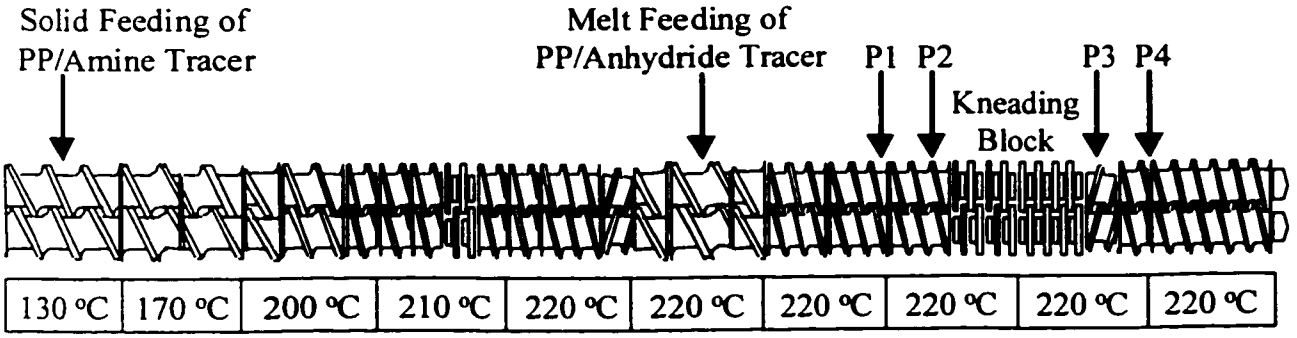

Figure 4.4. Example of Screw Configuration for Melt-melt Blending

The temperature profile of the single screw extruder was: 140 (solid feeding), 180 (transition), 220 (metering zone), and 220 °C (adapter). The screw configuration in the melt-melt blending section consisted of conveying elements and a kneading block. In all of the mixing experiments, the kneading block was made up of 16 adjacent bilobal kneading discs (thickness = 7.5 mm) with a total L/D of 3.5. The following three kneading disc stagger angles were investigated: 30° (forward), 90° (neutral), and −30° (reverse). The kneading block was immediately followed by a reverse conveying element (length = 30 mm, pitch = 20 mm). This restrictive element was used to maintain a high pressure and a high degree of fill in the kneading block section. Photographs of the three investigated kneading block geometries are presented in Figure 4.5. For the overall distributive mixing experiments, the investigated factors included the kneading block design, the screw speed (50 – 200 rpm), the total flow rate (50, 100 g/min), the barrel temperature in the blending section (190, 220 °C), and the viscosity of the PP resins.

Pressure transducers were positioned (identified as P1 – P4 in Figure 4.4) upstream and downstream of the kneading block to measure the pressure drop or gain over the kneading block section. The polymer melt temperature was measured using an IR melt temperature probe located at the die of the twin screw extruder. An OPTO22 data acquisition system was used to convert the analog signals from the pressure transducers and the temperature probe into digital signals. Each digital signal was sampled 25 times per 6 seconds using a LabVIEW program (version 4.0). The channel depth at a pressure transducer position changes as the screw rotates, which causes the pressure reading to fluctuate. A minimum pressure is measured at the largest channel depth, and a maximum pressure is measured when the screw flight passes the transducer surface. In a kneading

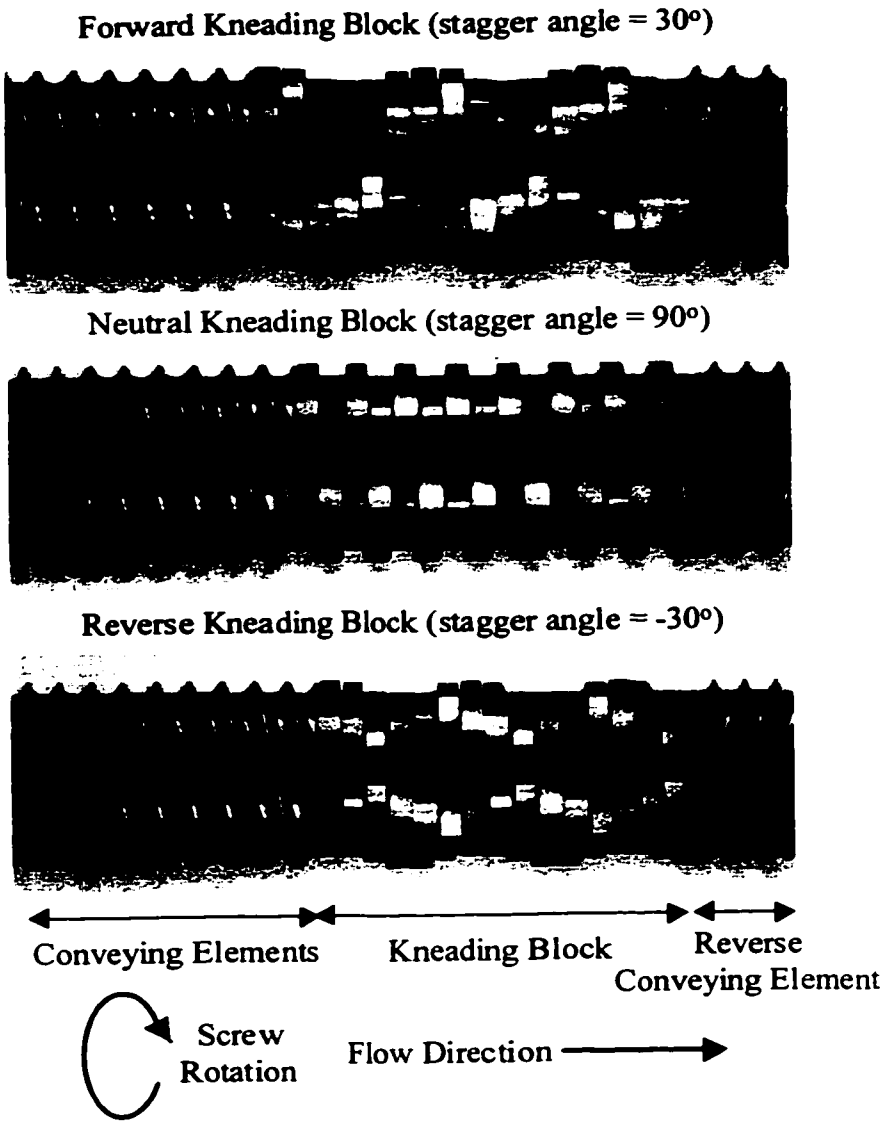

Figure 4.5. Photographs of the Investigated Kneading Block Geometries

block, a peak pressure is caused by the disc tip "sweeping" the transducer surface at the barrel (Bravo, 1998). The average pressure at the axial position of each transducer was calculated using the 25 readings collected during each 6 second time interval. Similarly, the melt temperature readings were averaged during each time interval.

The conveying elements positioned under the melt feeding location were partially filled in all the mixing experiments. Therefore, the output from the single screw extruder / adapter was independent of the pressure at the melt feeding location. Output curves for the single screw extruder / adapter versus screw speed were measured using a 5wt% blend of Polymer C-SYN in PP. An example of the output curve for the blend with KF6100 PP is presented in Figure 4.6. The output curve was used to determine the screw speed of the single screw extruder required to deliver the desired flow rate of the melt fed polymer stream to the twin screw extruder. The output from a single screw extruder is a combination of the drag flow and pressure flow, which is expressed in the simplified equation 4.1 (neglecting the shape factors). The decrease in the polymer viscosity at higher temperatures caused only a small increase in the output of the single screw extruder because the pressure drop across the adapter was relatively small (less than 0.15 MPa).

$$Q = \frac{WHU}{2} - \frac{WH^3}{12\eta}\left(\frac{\Delta P}{L}\right) \qquad (4.1)$$

where: Q : volumetric flow rate (m^3/s)
W : channel width (m); 14 mm for the screw presented in Figure 4.3
H : channel depth (m); 2 mm in the metering section for the screw presented in Figure 4.3
U : velocity of barrel rotating relative to stationary screw (m/s) = πDN
where: D : screw diameter (m); 19.5 mm for the screw presented in Figure 4.3
N : screw rotation speed (rev/s)
η : polymer viscosity (Pa.s)
$\Delta P/L$: pressure drop across screw length L (Pa/m)

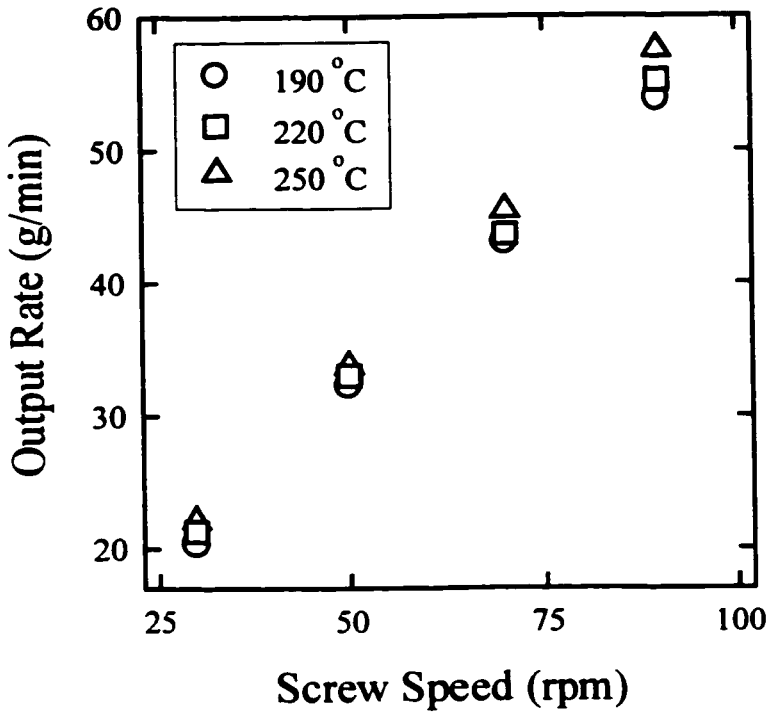

Figure 4.6. Example of Single Screw / Adapter Output Curve for KF6100 PP with 5wt% Polymer C-SYN

4.3.3.2. Analysis of the Distributive Mixing Profile

The experiments described in section 4.3.3.1 concern the analysis of the overall distributive mixing in the blending section of the twin screw extruder. Further experiments were completed to investigate the distributive mixing profile, or the development of the interfacial area along the length of this section. Specially designed barrel plates with sampling valves have been used by Nishio *et al.* (1991), Franzheim *et al.* (1997), and Potente *et al.* (1999) to investigate the dispersive mixing profile along the length of twin screw extruders. Four sampling plates (depicted in Figure 4.7) were designed and machined to allow for sampling of the polymer melt from the twin screw extruder during its continuous operation. Each plate had a thickness of 30 mm, and therefore, the combination of the four devices replaced one of the barrel segments of the twin screw extruder. The sampling plates were heated by conduction from the adjacent barrel segments of the twin screw extruder. Replacing a barrel segment with the sampling plates did not affect the melt temperature measured at the die. Polymer melt sampling was completed by retracting the threaded bolt in the sampling plate to the position indicated in Figure 4.7, after which, the polymer melt flowed out the indicated channel. This sampling process required pressure to force the material through the channel, and therefore, the method was limited to sampling in fully filled (pressurized) sections of the twin screw extruder.

An example of the screw configuration and the locations of the sampling plates is presented in Figure 4.8. The plates (S1 – S4) were positioned upstream and downstream of the kneading block (sampling port S2 was 15 mm upstream of the first kneading disc, and sampling port S3 was 15 mm downstream of the final kneading disc in the middle of the reverse conveying element). The mixing profile experiments were completed using equal

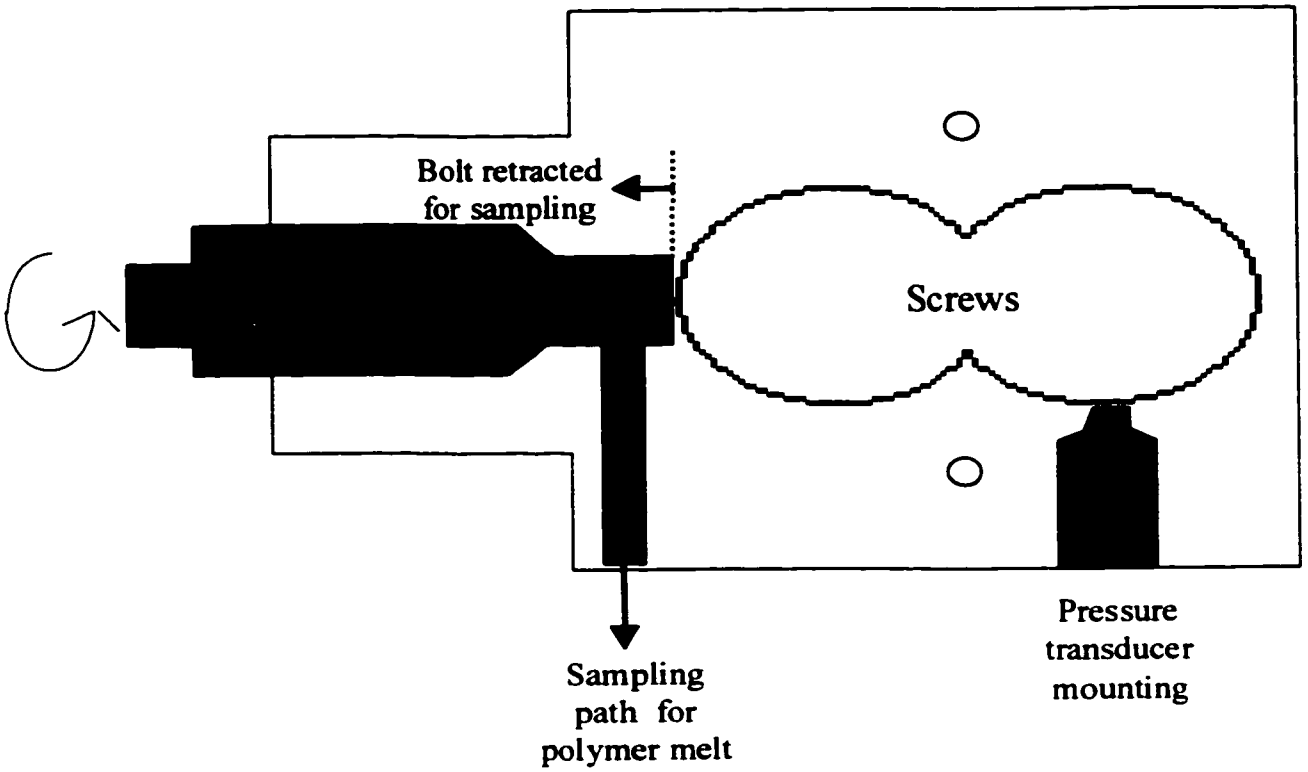

Figure 4.7. Sampling Plate Design

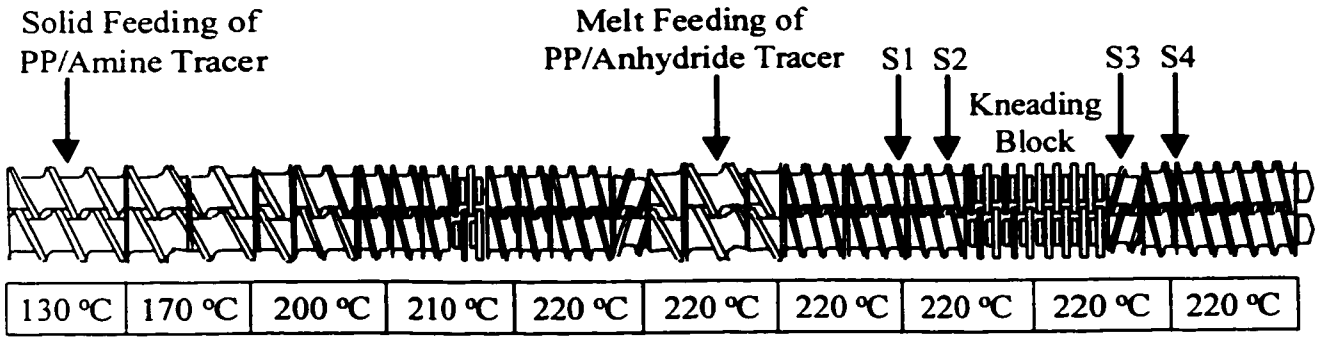

Figure 4.8. Screw Configuration and Sampling Plate Positions for Distributive Mixing Profile Experiments

mass flow rates in the two segregated streams (Petrothene PP + 5wt% tracer) and barrel temperatures of 220 °C in the blending section. Screw configurations with forward, neutral, and reverse kneading blocks were investigated at screw speeds of 50 to 100 rpm and total flow rates of 50 and 100 g/min. In all the experiments, the pressure at the reverse conveying element was sufficient to obtain a sample from S3. The polymer melt was also successfully sampled at position S2 upstream of the neutral and reverse kneading blocks, which are restrictive designs. Prior to collecting a sample of the polymer melt, the sampling channel was purged for 30 seconds to establish steady-state and to remove accumulated material from the sampling channel. After purging, samples of the melt were collected and quickly quenched in the water bath to produce a strand. For FT-IR analysis of the reaction, the strand was cut into small pieces and compression molded into thin films (thickness = 0.75 mm) using the hot press at 200 °C for 30 seconds. No significant further reaction between the reactive polymers occurred during this short pressing time. In the mixing profile experiments, the film die was replaced by the dual strand die (diameter = 4 mm). Similar to the sampling procedure for the sampling ports, short polymer strands from the die were collected and then compression molded into thin films. Therefore, all the analyzed films contained approximately the same degree of crystallinity.

In the case of the screw configuration containing the forward kneading block, the pressure upstream of the kneading block was insufficient to force the polymer melt through the sampling channel at S2. Sampling downstream of the kneading block at S3 and at the die was completed using the previously described method. To determine the mixing performance prior to the forward kneading block, the melt-melt blending experiments were repeated without the die at the end of the twin screw extruder. After establishing steady-state

flow, the extruder was dead stopped and the screws were extracted. Upon extracting the screws, polymer samples were collected from the positions of S2 and S3. Screw extraction and sampling was completed in approximately 2 min, after which, the collected polymers were pressed into thin films as previously described. For the screw configuration containing the forward kneading block, samples of the polymer melt were obtained directly from sampling plate S3 and from the extracted screws at the same position. The conversions measured from these two methods were not significantly different, and therefore, very little further reaction between the reactive polymer tracers occurred during the extraction procedure. This comparison verified that the reaction between the polymer tracers is very slow under diffusion control in molten PP.

Screw extraction was also used to investigate the fill distribution of the melt inside the extruder. In particular, the fully filled length prior to the kneading block was measured and used in the analysis of the mixing results. The fill length prior to the forward kneading block was measured during the mixing profile experiments previously mentioned. In separate experiments, the fill length was measured for the extrusion of pure PP in the same screw configuration. The results were identical, and therefore, the fill length prior to the kneading block was not affected by the addition of the polymer tracer and the corresponding decrease in the viscosity. To improve the contrast for photographs of the fill distribution, 0.5wt% TiO_2 was blended into the pure PP. The white pigmented PP was used to investigate the fill distribution in the screw configurations containing the forward, neutral, and reverse kneading blocks over a range of operating conditions.

4.3.3.3. Melt Feeding Directly into the Kneading Block

In all of the previously described mixing experiments, the melt fed stream was introduced into the twin screw extruder in a partially filled conveying section upstream of the kneading block. Experiments were also completed to investigate the mixing when the polymer melt was fed directly into the kneading block. These experiments were completed using the screw configuration presented in Figure 4.8 at operating conditions of 220 °C (barrel temperatures in the blending section), 50 g/min, and 50 rpm. The following stagger angles in the kneading block were investigated: 30°, 60°, 90°, and –30°. In contrast to the feeding arrangement presented in Figure 4.8, the single screw extruder and the adapter depicted in Figure 4.9 (used in the work of Lee, 1999) were used to melt feed the PP / anhydride polymer blend directly into the kneading block (40 mm downstream of the first kneading disc) through an injection port in a barrel segment of the twin screw extruder. The polymer melt was sampled at position S3 to investigate the mixing in the kneading block (total mixing length = 95 mm). The previously described procedure was used to prepare the collected samples for FT-IR analysis of the reaction conversion.

4.3.4. Residence Time Distribution Measurements

Residence time distribution (RTD) measurements were completed to investigate possible relationships between the distributive mixing results and the average residence time and the degree of macromixing. All the RTD experiments were completed using the Petrothene PP resin. In addition, the RTD experiments were completed using the same extruder apparatus, screw configurations, and operating conditions as the distributive mixing

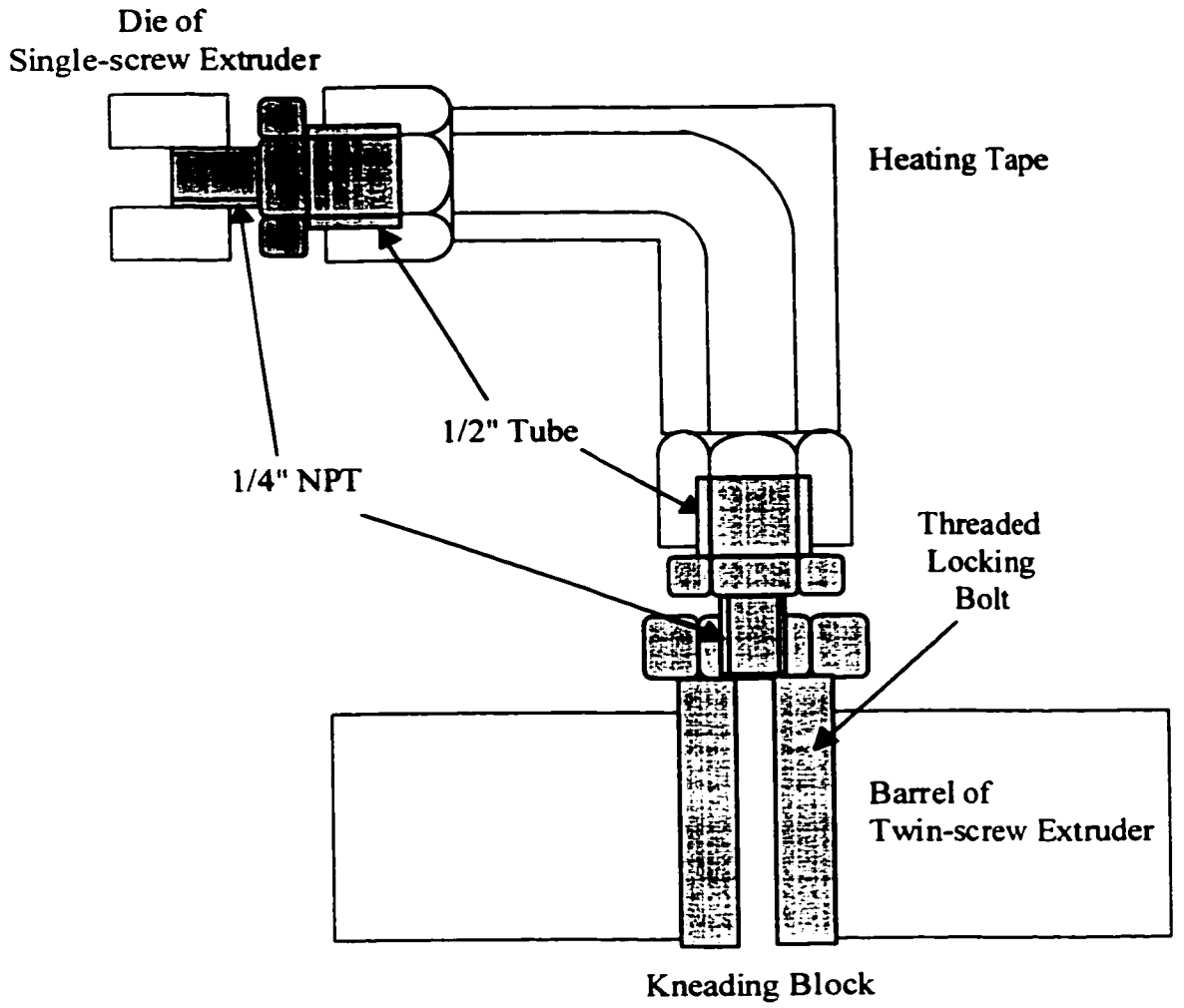

Figure 4.9. Adapter Used to Connect the Single Screw Extruder to the Injection Port of the Twin Screw Extruder for Melt Feeding Directly into the Kneading Block (from the work of Lee, 1999)

experiments. Two methods were used to examine the overall RTD as well as the local RTD in different sections of the twin screw extruder.

4.3.4.1. Determination of the Cumulative RTD in the Melt-melt Blending Section of the Twin Screw Extruder

To compare the RTD results and the overall distributive mixing measurements described in section 4.3.3.1, only the RTD in the melt-melt blending section (melt feeding location to the film die) was required. The same tandem extruder apparatus (Figure 4.2) was used, with equal mass flow rates in the two segregated polymer melt streams. Pure PP was metered to the beginning of the twin screw extruder, and a 5wt% blend of the anhydride functionalized polymer tracer in PP was melt fed using the single screw extruder / adapter (Figure 4.3). To measure the RTD in the melt-melt blending section, a washout of the anhydride tracer was implemented to yield the cumulative RTD. After melt-melt blending for 20 min to establish steady-state flow, the mass flow rate of the pure PP stream was doubled. A pressure transducer was positioned immediately prior to the melt feeding location in a fully filled region. This region was fully filled due to the reverse conveying element that was located immediately upstream of the conveying elements where the melt feeding was completed (screw configuration presented in Figure 4.4). A sharp increase in this pressure indicated the time when the new flow rate reached the melt feeding location. Immediately, the flow of the PP / anhydride functionalized polymer tracer from the single screw extruder / adapter was stopped, and a stop watch was started. No surging in the flow at the die was observed during the experiments, which indicated that the flow rate remained constant. Sampling of the polymer film at the slit die at the end of the twin screw extruder was completed every 5 s for 5 min, and then every 30 s for an additional 5 min for a total of

70 measurements for each distribution. The sampling was completed using a knife to make a small etch on the side of the film at the die face. FT-IR analysis was performed using the collected film, and the washout of the anhydride tracer was followed using its characteristic peak at 1793 cm^{-1}.

Although the washout technique required a significant amount of the anhydride reactive polymer, it is the best method for determining the moments of a RTD that has a significant tail (Nauman and Buffham, 1983). A disadvantage of the washout technique is that numerical differentiation of the experimental results is required to obtain the residence time density function. Small errors in the experimental measurements of the washout function can lead to large errors upon differentiating. Therefore, comparison of the RTD results was completed using the cumulative distributions only. The cumulative distribution is not as sensitive as the residence time density function to small changes in the degree of macromixing. As well, it is more difficult to identify stagnation and recirculation using the cumulative distribution.

4.3.4.2. Determination of the Local Residence Time Across Conveying and Kneading Sections of the Twin Screw Extruder

Local residence time measurements in conveying sections and kneading blocks were completed to investigate the possible relationship between the local distributive mixing measurements and the average residence time. The method of Nietsch *et al.* (1997) as described in Chapter 2 was used to perform the local RTD measurements. This method is based on the measurement of the polymer melt temperature using an IR temperature probe, which has been reviewed by Maier (1996). As described by Maier (1996), the IR probe receives thermal radiation from the polymer melt, or the source. The radiation is guided

along optical fibers to a detector, which converts it to a voltage. The voltage is then transformed into a temperature reading based on the calibration of the probe and detector. The probe window receives the radiation from an acceptance cone that has a penetration depth that can range from 5 μm to as great as 1 cm (Maier, 1996). This depth is very sensitive to the properties of the investigated material. Nietsch *et al.* (1997) showed that a pulse of carbon black pigmented polymer causes a significant decrease in the temperature reading. The tracer is added at a very low concentration (<0.4wt%), and it does not actually decrease the melt temperature. The carbon black increases the surface emissivity of the polymer melt, which causes the IR probe to detect a false lower temperature. The temperature decrease is directly related to the changing surface emissivity, which depends on the carbon black concentration. Therefore, Nietsch *et al.* (1997) proposed that the temperature change can be used to track the local RTD at the probe position.

As noted by Chen (1992), the IR temperature probe must be air cooled to ensure accurate measurement of the polymer melt temperature when the melt temperature is less than 28 °C hotter than the probe temperature, which will depend on the barrel temperature at the probe position. Air cooling lowers the temperature of the probe and it eliminates the contribution of the probe temperature to the temperature reading. In the experiments, 0.21 MPa (30 psi) of cooling air was applied to the air inlet on the probe. Without air cooling, the probe measured temperatures 4 to 10 °C hotter due to the contribution from the probe temperature. The tracer was a 25wt% blend of carbon black in Petrothene PP, which was prepared using the twin screw extruder. The local residence time measurements were completed using the screw configuration presented in Figure 4.10 (identical to configuration used in the distributive mixing profile experiments described in section 4.3.3.2), with the IR

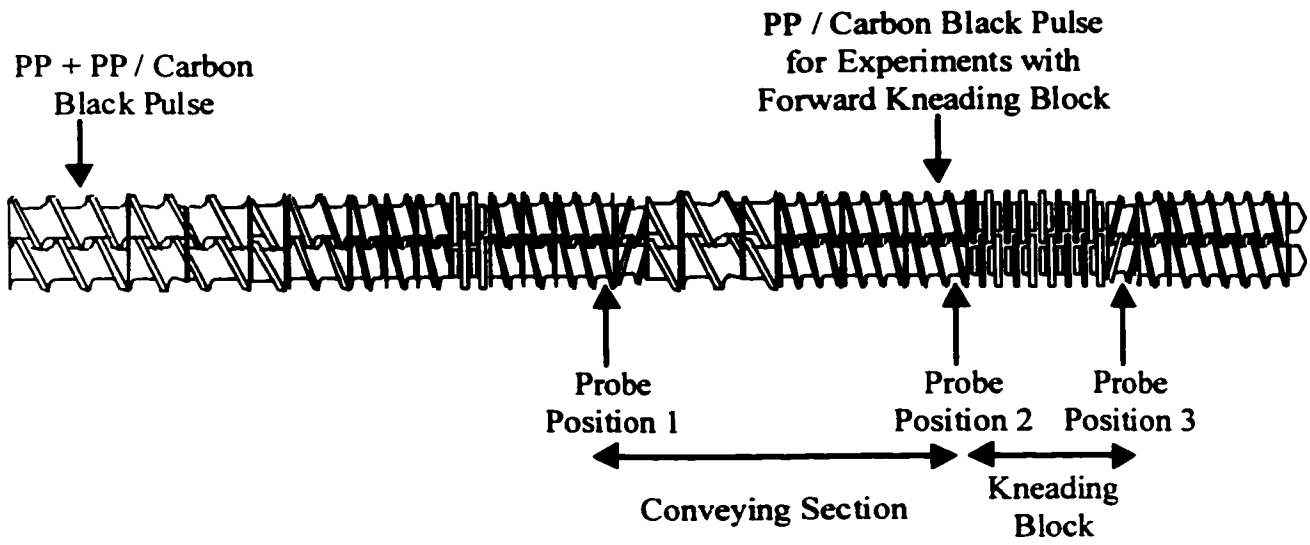

Temperature Profile

130 °C	170 °C	200 °C	210 °C	220 °C	220 °C	220 °C	220 °C	220 °C	220 °C

Figure 4.10. Screw Configuration for the Local RTD Measurements and the Infrared Temperature Probe Positions

temperature probe at the identified positions (position 1 was a mounting in barrel section 5, and positions 2 and 3 were mountings in the specially designed sampling plates located immediately upstream / downstream of the kneading block). Only one probe was used in the experiments, and therefore, the measurement of the RTD at each position was completed in a separate run. The experiments were completed for screw configurations containing forward, neutral, and reverse kneading blocks over a wide range of screw speeds (50 – 200 rpm) and flow rates (50 – 100 g/min).

The RTD experiments were completed by adding a pulse of 0.2 to 0.4 g of the PP / carbon black blend with the polymer feed to the beginning of the twin screw extruder (barrel section 1). Using an OPTO22 data acquisition system and a LabVIEW program, the IR temperature reading was recorded four times per second. In contrast to the average pressures and temperatures recorded during the mixing experiments, the temperature readings used to calculate the local RTD were not averaged over every 6 second time interval. Experiments were completed at probe positions 2 and 3 (Figure 4.10) to investigate the local residence time in the kneading block. The screw channel at probe position 1 (Figure 4.10) was fully filled due to the reverse conveying element. After the reverse conveying element, the screw channel was partially filled, and therefore, the residence time at probe position 1 does not depend on the downstream screw configuration. Thus, the RTD experiments at probe position 1 were completed only for the screw configuration containing the neutral kneading block. Comparison of the results at probe positions 1 and 2 was used to calculate the local residence time in the conveying section prior to the kneading block.

It was not possible to detect the temperature change caused by the carbon black tracer at probe position 2 prior to the forward kneading block except for the following operating

conditions: 100 g/min – 50 rpm and 75 g/min – 50 rpm. Except for these two sets of operating conditions, the pressure at probe position 2 was zero. To measure the local residence time across the forward kneading block, separate experiments were completed by injecting a pulse of 0.05 g PP / carbon black (2 pellets of the blend) immediately prior to the kneading block through an open vertical pressure transducer mounting (identified in Figure 4.10, the mounting was in a sampling plate). The addition of the solid tracer to the polymer melt did not affect the RTD analysis because it melted extremely rapidly, which is discussed in detail in Chapter 7. The IR temperature probe was placed at position 3 to directly measure the RTD across the forward kneading block.

4.4. Analysis of the Products from the Mixing and RTD Experiments

4.4.1. Polymer Characterization Methods

As reported in Table 4.1, GPC analysis was completed to measure the molecular weight distributions of the three investigated PP resins. The analysis was completed using TCB as the solvent at a temperature of 140 °C. The shear viscosity of the PP resins and their blends with 5wt% Polymer C-SYN were measured using a capillary rheometer (capillary die, die diameter = 0.03 in, L/D = 2, 20, 40, 50) at various temperatures (190 – 250 °C). Differential scanning calorimetry (DSC, TA Instruments 2920 cell) was used to investigate the compatibility of the low molecular weight polymer tracer in the high molecular weight PP resins. The DSC cell was cooled using liquid N_2 for the measurements to –120 °C and then heated at a ramp rate of 10 °C/min to a final temperature of 50 °C. Prior to the

measurements, the DSC samples were heated above their melting temperatures and then cooled to eliminate their thermal histories.

4.4.2. FT-IR Analysis of the Reaction Conversion for the Quantitative Measurement of the Mixing

FT-IR analysis was used to determine the conversion of the interfacial reaction between the reactive polymer tracers from the melt-melt blending experiments. Analysis was completed using the film directly obtained from the slit die at the end of the twin screw extruder to analyze the overall mixing or the thin films compression molded from the strands collected from the sampling ports and the dual strand die to analyze the mixing profile. The coupling reaction between the terminal succinic anhydride and primary amine functional groups was followed using the carbonyl stretching vibration of the cyclic anhydride at 1793 cm^{-1}. To quantitatively compare FT-IR spectra obtained from different films, an internal reference corresponding to the PP backbone was used. The internal references used in the FT-IR analysis were the C-C-C bending vibration at 459 cm^{-1} or the C-C-C bending, C-CH_3 stretching, and CH_2 rocking vibration at 528.5 cm^{-1} (Painter *et al.*, 1982). The peak heights of the anhydride functional group and the internal reference were measured from a common baseline extending from 411 to 2008 cm^{-1}. The ratio of the anhydride functional group peak height to the internal reference peak height is the relative peak height, which is independent of the film thickness.

During melt-melt blending, a certain amount of the anhydride functionalized polymer was consumed in the interfacial reaction with the primary amine functionalized polymer. To calculate this conversion, which is directly related to the amount of interfacial area generated, the anhydride relative peak height for zero conversion and full conversion were required. PP

containing 5wt% of the anhydride reactive polymer was melt blended with pure PP and then analyzed by FT-IR to determine the relative peak height at zero conversion. Three different methods were performed to obtain the full conversion of the interfacial reaction. Samples of the polymer film from randomly selected melt-melt blending experiments were compression molded in the hot press at 200 °C for over two hours. During this time, the reaction continued via diffusion of the reactive polymers until the full conversion of the amine functionalized polymer (the limiting species) was achieved. Equal mass concentrations of the two reactive polymers were used in all the mixing experiments, but as mentioned in Chapter 3, the limiting conversion of the amination of the trialkylborane during its preparation resulted in fewer primary amine functional groups per gram of the tracer. For the second method, randomly selected polymer films were heated in a vacuum oven at 120 to 140 °C for 3 days to drive the reaction to its completion. In this temperature range, the tracers were molten inside the solid PP matrix. The samples were then compression molded into thin films (pressing time = 5 min, thickness = 0.75 mm) and rapidly quenched in a water bath to control the degree of crystallinity in the films. Finally, equal masses of the PP / reactive tracer blends were melt mixed in a batch mixer for 45 min at 220 °C to drive the reaction to full conversion by the combination of mechanical mixing and diffusion. FT-IR analysis was completed to determine the relative peak height of the anhydride functional group after full conversion of the reaction, and the results from the three methods were not significantly different. Thus, the final conversion was achieved even without melting the PP matrix if sufficient time was given (second method). Migration of the polymer tracers in the solid PP matrix will occur extremely slowly. As indicated by FT-IR analysis, the degree of crystallinity in the polymer films increased during the three days they were maintained at

120 to 140 °C. To crystallize, the PP matrix must expel the low molecular weight amorphous polymer tracers. During this process, the polymer tracers may have come into contact and further reacted to achieve the final conversion.

Using the relative peak heights for zero and full conversion, the conversion from a melt-melt blending experiment was calculated using equation 4.2.

$$\text{Anhydride Conversion} = \frac{\text{RPH@1793(Zero)} - \text{RPH@1793(Sample)}}{\text{RPH@1793(Zero)} - \text{RPH@1793(Full)}} \qquad (4.2)$$

where: RPH@1793 (Zero) : anhydride relative peak height for zero conversion
RPH@1793 (Sample) : anhydride relative peak height for melt-melt blending sample
RPH@1793 (Full) : anhydride relative peak height for full conversion

An example of the FT-IR spectra used in the calculation of the anhydride conversion from a melt-melt blending experiment is presented in Figure 4.11. From Figure 4.11, the peak absorbance of the anhydride functional group at 1793 cm^{-1} was in the range of 0.5 to 0.8, which is within the recommended range for quantitative FT-IR analysis (Rabek, 1980). Similarly, the peak absorbance of the internal reference corresponding to the PP backbone was within the recommended range. In addition, the peak heights in all the spectra were carefully measured at the same wavenumber and from the same baseline using the OMNIC (version 1.2) software.

4.4.3. FT-IR Analysis of the Washout of the Anhydride Polymer Tracer for the Determination of the Cumulative RTD

In the cumulative RTD measurements using the anhydride reactive polymer as the tracer, the relative peak height at 1793 cm^{-1} was used to determine the dimensionless tracer concentration in the film obtained directly from the twin screw extruder. An example of

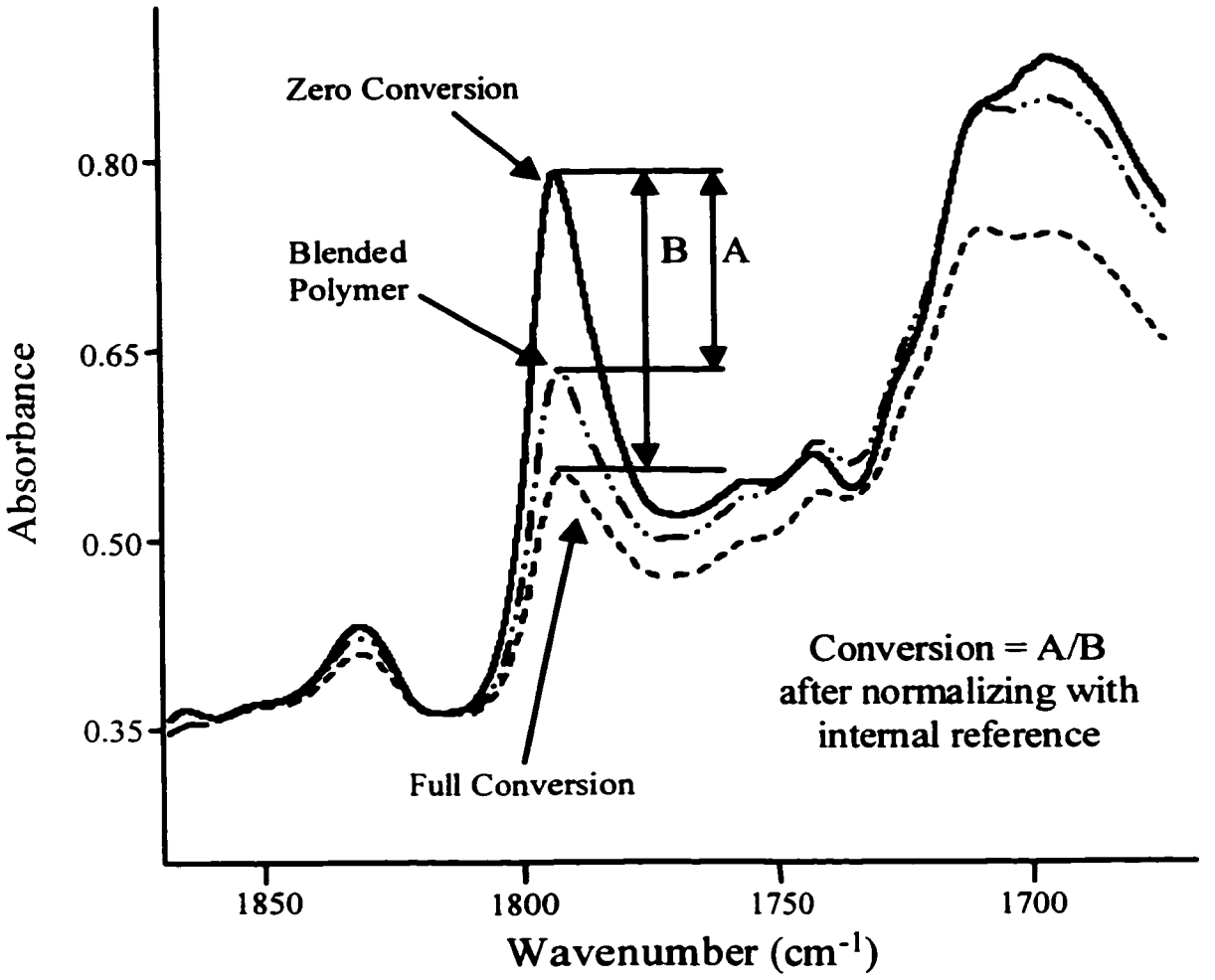

Figure 4.11. Example of the FT-IR Spectra Used to Determine the Anhydride Conversion from a Melt-melt Blending Experiment

some of the FT-IR spectra obtained from a RTD measurement is presented in Figure 4.12 for the screw configuration containing the neutral kneading block at 50 g/min and 50 rpm. The washout function of the tracer was calculated using equation 4.3, and the average residence time ($\bar{t}$) and the variance (σ^2) of the distributions were calculated using the well known moment equations 4.4 and 4.5 (Nauman and Buffham, 1983).

$$W(t) = \frac{RPH@1793(t) - RPH@1793(final\ t)}{RPH@1793(t=0) - RPH@1793(final\ t)} \tag{4.3}$$

where: W(t) : washout function, decreases from 1 to 0
RPH @ 1793(t) : anhydride relative peak height at time t
RPH @ 1793(final t) : anhydride relative peak height at final time (average of last five data points at end of experiment)
RPH @ 1793(t=0) : anhydride relative peak height at time zero (average of first five data points at beginning of experiment)

$$\bar{t} = \int_{t=0}^{final\ t} W(t)dt \tag{4.4}$$

$$\sigma^2 = 2\int_{t=0}^{final\ t} tW(t)dt - (\bar{t})^2 \tag{4.5}$$

Calculation of the anhydride conversion (equation 4.2) and the washout function (equation 4.3) assumed that the anhydride relative peak height was linearly related to its functional group concentration. Using a succinic anhydride terminally functionalized Polypol-19, Thompson *et al.* (1998b) developed a calibration between the relative peak height and the anhydride functional group concentration determined by a titration method. A linear relationship between the anhydride functional group concentration in the low molecular weight polymer and the relative peak height was observed. More important for this research, Thompson (1998) developed a calibration between the concentration of succinic anhydride functional groups and the relative peak height for a conventional isotactic PP. The calibration was completed using KF6100 PP and a highly maleated Polypol-19 wax,

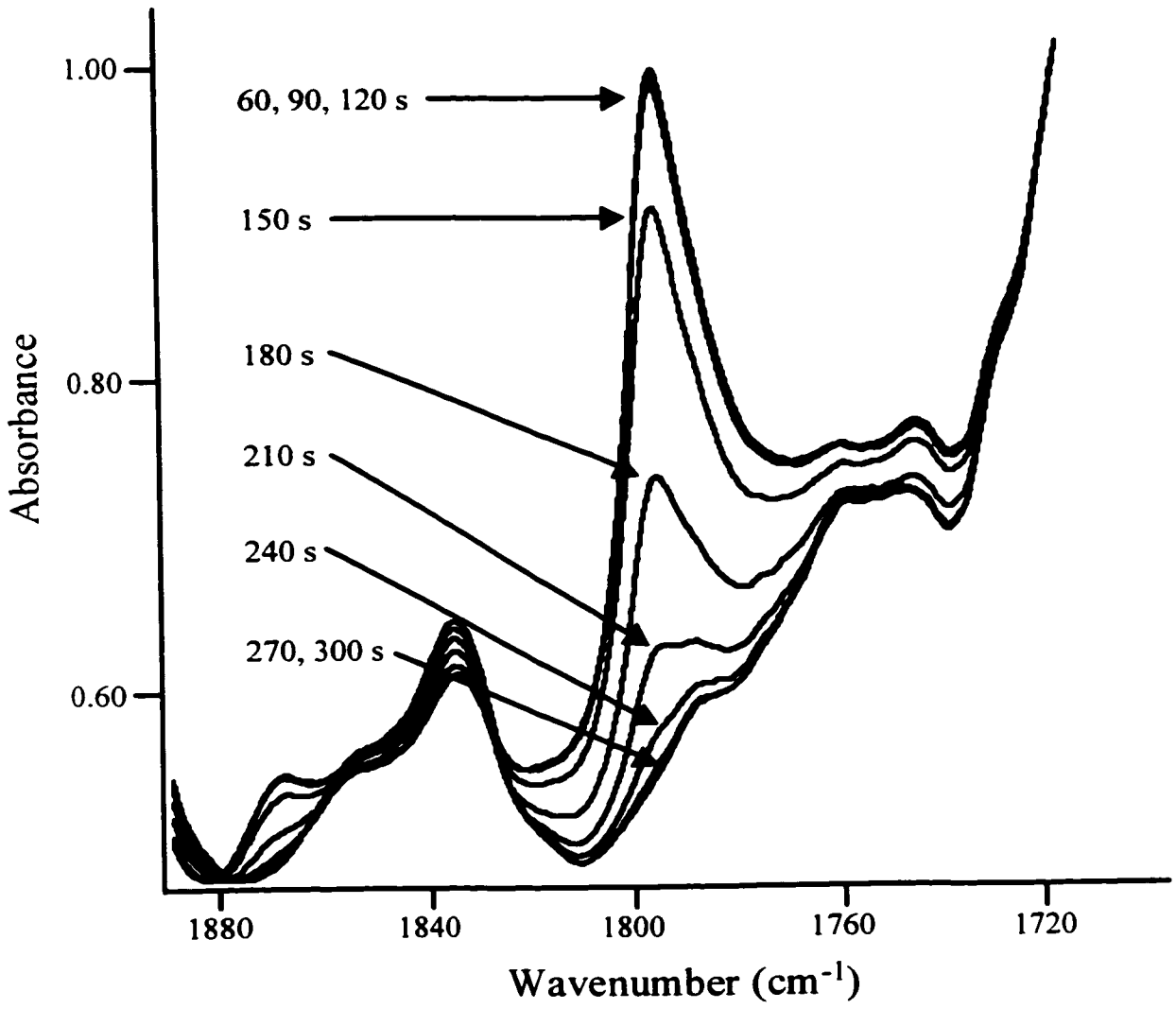

Figure 4.12. Example of the FT-IR Spectra Obtained from a RTD Experiment Using a Washout of the Anhydride Functionalized Polymer Tracer

with a known succinic anhydride content. The calibration curve is reproduced in Figure 4.13 and the linear regression equation is reported in equation 4.6.

$$C_{SAh} = 0.07 * \left(\frac{\text{Absorbance@1792}}{\text{Absorbance@459}}\right) + 0.007 \qquad (4.6)$$

where: C_{SAh} : succinic anhydride functional group concentration (wt%)

The correlation coefficient (r^2) was 0.97, which indicated that the linear regression equation was an adequate representation of the experimental results. The calibration of Thompson (1998) confirmed the linear relationship between the FT-IR measurements and the anhydride functional group concentration, which is a critical assumption in the calculation of the anhydride conversion and the washout function in this research.

4.4.4. Local Residence Time Calculations

An example of the temperature measurements from the IR temperature probe at positions 2 and 3 (Figure 4.10) for the screw configuration containing the neutral kneading block at 100 g/min and 100 rpm is presented in Figure 4.14. The pulse of 0.4 g PP / carbon black was added to the beginning of the twin screw extruder (barrel 1, Figure 4.10) at time equal to zero. As expected, the carbon black tracer required a longer time to reach probe position 3. Comparing the baseline temperatures (flow of pure PP before / after the carbon black tracer passes the probe position) at the two probe positions indicated that the melt temperature increased by approximately 8 °C as the polymer traveled through the neutral kneading block. The signal to noise ratio was significantly greater at probe position 3. In general (averaged over all the experiments completed at each probe position), the signal to noise ratio was 4.1 at probe position 1, 5.8 at probe position 2, and 12.3 at probe position 3. Nietsch *et al.* (1997) reported a noise value of 20% for their RTD measurements, which is

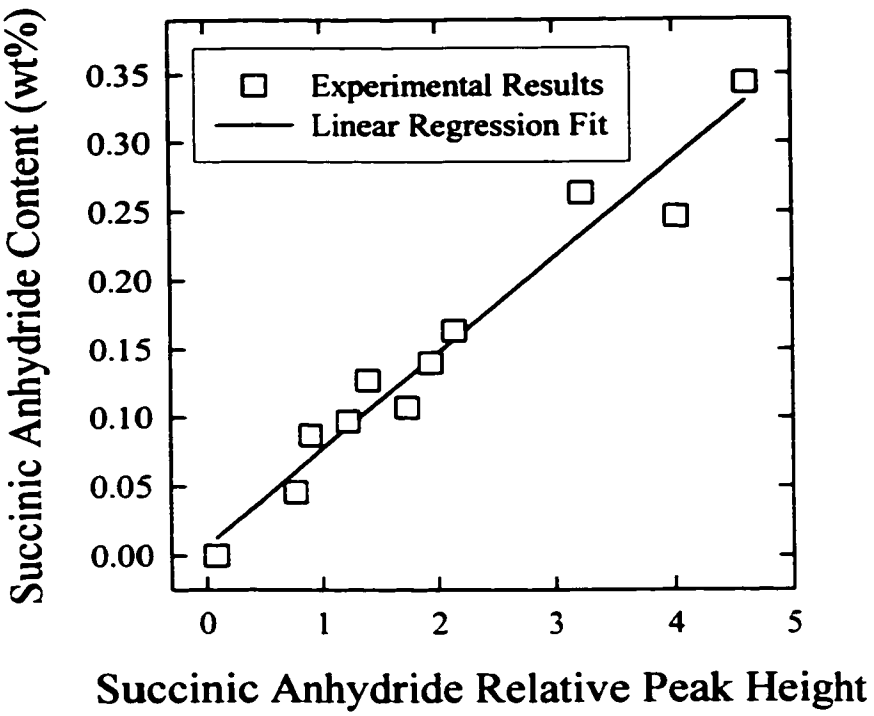

Figure 4.13. Thompson's (1998) Calibration of the Succinic Anhydride Functional Group Concentration in Isotactic PP with the Relative Peak Height

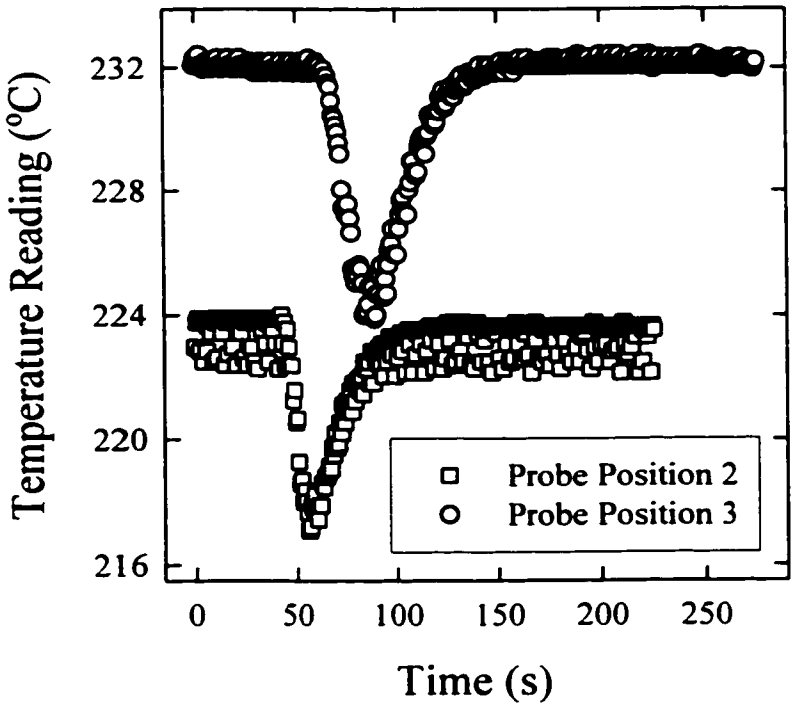

Figure 4.14. Temperature Readings from the Local Residence Time Experiments for the Screw Configuration Containing the Neutral Kneading Block (100 g/min, 100 rpm)

similar to the values observed in this research (the % noise is the inverse of the reported signal to noise ratio multiplied by 100). In addition, the signal to noise ratio generally increased with the melt temperature, and the highest melt temperatures were measured at the reverse conveying element at the end of the kneading block (probe position 3).

A dimensionless temperature was calculated using equation 4.7, and then converted into the residence time density function, f(t), according to equation 4.8. Average residence time ($\bar{t}$) and variance (σ^2) were then calculated using equations 4.9 and 4.10. Prior to the calculation of the RTD moments, the raw data in the baseline region (prior to and after the peak caused by the tracer), which contained significant noise, was replaced with a steady-state average value. This replacement did not significantly affect the calculation of the average residence time. Conversely, the calculation of the variance was much more sensitive to the noise (especially at longer times), and this baseline replacement improved the reproducibility of the calculated variances. In an extreme case, a negative variance, which is not physically possible, was calculated using a noisy raw data baseline.

$$T^D = \frac{T_{max} - T}{T_{max} - T_{min}} \tag{4.7}$$

where: T^D : dimensionless temperature
T : temperature reading (°C)
T_{max} : maximum temperature reading, replaced by the average steady-state baseline reading (°C)
T_{min} : minimum temperature reading (°C)

$$f(t) = \frac{T^D(t)}{\sum T^D \Delta t} \tag{4.8}$$

$$\bar{t} = \sum t\, f(t) \Delta t \tag{4.9}$$

$$\sigma^2 = \sum t^2\, f(t) \Delta t - (\bar{t})^2 \tag{4.10}$$

Using these equations, the average residence times at probe positions 2 and 3 for the experimental conditions presented in Figure 4.14 were 68.56 s and 96.11 s, respectively. Assuming additivity of the residence times in different sections of the twin screw extruder, which is discussed in Chapter 7, the local residence time in the neutral kneading block (between probe positions 2 and 3) was 27.55 s for the specified operating conditions.

CHAPTER 5
COUPLING OF ANHYDRIDE AND AMINE FUNCTIONALIZED POLYMERS AND ITS APPLICATION TO THE ANALYSIS OF MIXING DURING POLYMER BLENDING IN EXTRUDERS

A low molecular weight amorphous polyolefin was successfully functionalized with succinic anhydride and primary amine functional groups at the terminal site. This chapter describes the preliminary experiments completed using these two reactive polymers. First, model interfacial reactions between the reactive polymers in molten PP were completed to investigate the reaction kinetics and diffusion effects. After the model reactions, the reactive polymer tracers were used in an attempt to investigate the mixing during melt-melt blending of segregated PP streams in a co-rotating twin screw extruder. The investigated factors were the screw speed, the total flow rate, the kneading block design, and the viscosity ratio of the two segregated polymer melts.

5.1. Model Interfacial Reactions Between Anhydride and Amine Functionalized Polymers in Molten PP

Thin films of the anhydride and amine functionalized polymers in KF6100 PP (5wt% tracer) were prepared, and a comparison of their FT-IR spectra to that of pure Polymer PP is presented in Figure 5.1. The three spectra are staggered to allow for easier comparison, and the important differences between the spectra are indicated in the circled regions. A concentration of 5wt% anhydride reactive polymer in the KF6100 PP resulted in an adequate peak height at 1793 cm^{-1} for quantitative analysis of the anhydride / amine reaction. To investigate the uniformity of the PP blends containing the anhydride and amine reactive polymers, a total of six films of each blend were prepared and analyzed using FT-IR. Relative peak heights of some of the characteristic peaks were calculated using the peak at

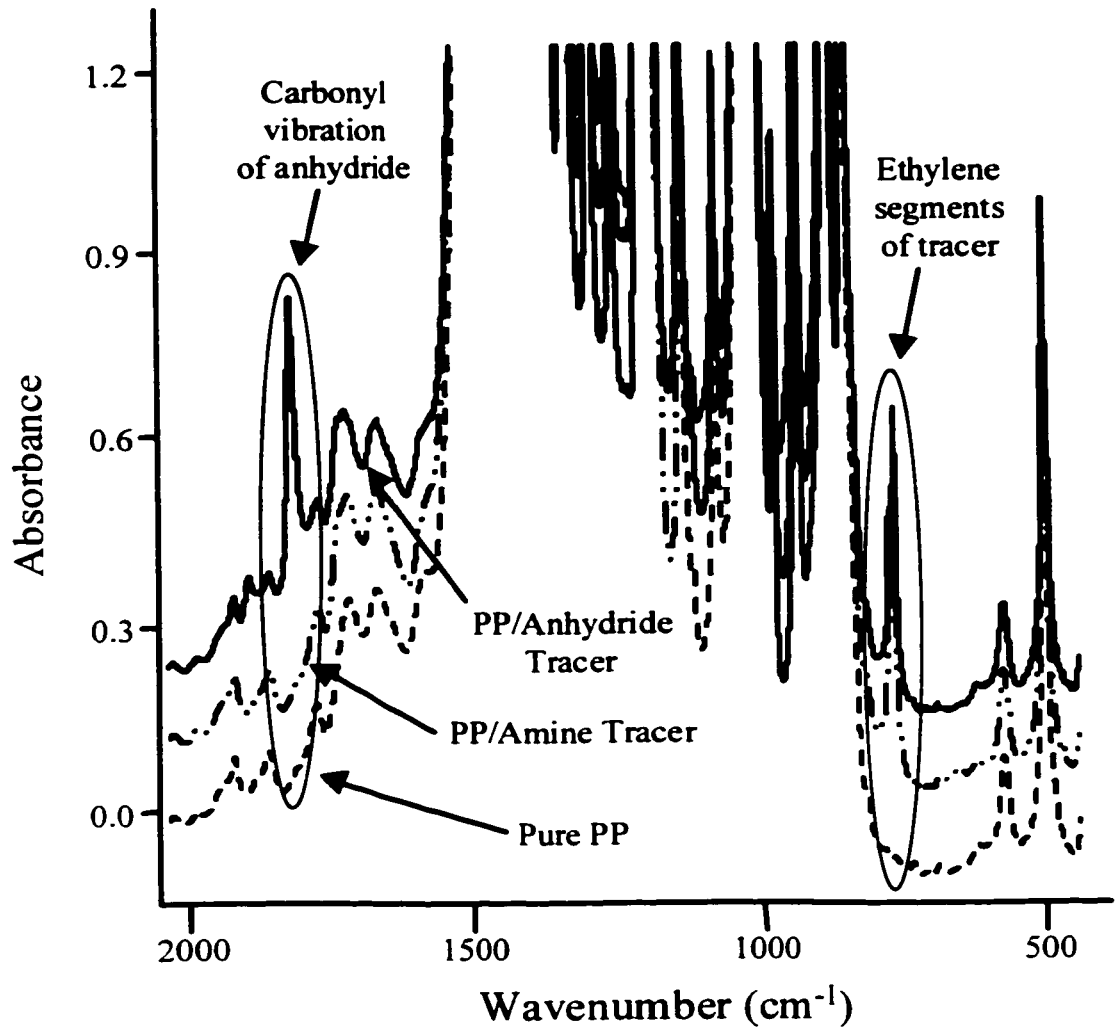

Figure 5.1. FT-IR Spectra of the Reactive Polymers in KF6100 PP (5wt% Tracer)

Note: The baselines of the two blends are staggered upwards from the baseline of the pure PP to allow for easier comparison of the spectra (the scale on the absorbance axis corresponds to the bottom spectrum only).

459.4 cm^{-1} as an internal reference. For the blend containing the anhydride reactive polymer, the relative peak height at 1793 cm^{-1} was 0.854 $\pm$ 0.018 (presented as a ninety-five percent confidence interval). The small confidence interval confirmed that the anhydride reactive polymer was uniformly distributed into the PP resin. The only visible peak in the FT-IR spectrum corresponding to the amine functionalized polymer in its blend with KF6100 PP was the doublet at 721 cm^{-1}, which corresponds to the ethylene units that are incorporated into Polymer C-SYN (Bellamy, 1958). The relative peak height at 721 cm^{-1} was 0.719 $\pm$ 0.005 (presented as a ninety-five percent confidence interval), and the small confidence interval confirmed that the amine reactive polymer was uniformly distributed in the blend. Finally, all the polymer films were transparent, which suggested that the reactive polymers were compatible with the PP resin.

To further investigate the compatibility between the low molecular weight polymer tracers and the PP resins, a blending experiment was completed using the batch reactor at 200 °C, with a motor speed of 50 rpm. In the first run, 150 g of Petrothene PP was charged to the preheated batch mixer. The PP was fully melted after 6 min, and then 5 g of Polymer C-SYN wax was added to the batch mixer. Every 1 to 2 minutes an additional 5 g of wax was added to the mixer until it was fully filled (total of 100 g of wax added). A separate experiment was completed with an initial mass of 100 g of Petrothene PP. The torque plots from these blending experiments are presented in Figure 5.2. Immediately after the addition of each 5 g quantity of wax, the torque sharply decreased, which was attributed to the lubrication of the barrel and rotor surfaces with the low molecular weight polymer. The torque then increased to a new steady-state value as the wax was incorporated into the blend. The steady-state torque decreased with each addition of the wax due to the corresponding

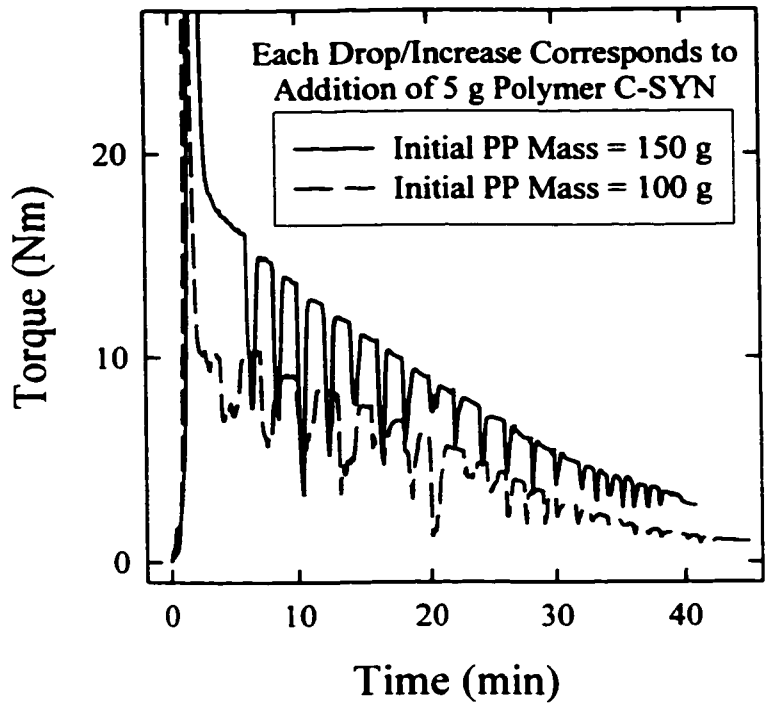

Figure 5.2. Torque Plots from the Blending of Polymer C-SYN and Petrothene PP in the Batch Mixer

dilution of the polymer viscosity. The final polymer blends were homogeneous, and there was no visible separation of the low molecular weight polymer from the blend. Upon solidifying, the surfaces of the final blends did not have slippery or waxy textures even though the final wax concentrations were 40wt% and 54.5wt%, respectively. These results suggested that the low molecular weight polyolefin wax was compatible with the PP resin. If the polymers were not compatible, phase separation would cause the low molecular wax to bloom to the metal walls of the mixer during the blending and the surfaces of the blends.

DSC analysis was attempted to further investigate the compatibility of the materials, and the heating scans are presented in Figure 5.3. Due to its extremely low molecular weight, Polymer C-SYN exhibited a significantly lower T_g as compared to the Petrothene PP. A common test for blend compatibility is the measurement of the T_g. A single T_g for the blend indicates that the polymer phases are homogeneously mixed at the molecular level. Although glass transitions are apparent in Figure 5.3 for the pure materials (-12.6 °C for Petrothene PP and –62.9 °C for Polymer C-SYN), the final blend containing 54.5wt% wax did not exhibit a distinct transition. The absence of the transitions of both phases (Polymer C-SYN and Petrothene PP) further suggested that the materials were compatible.

To gain a better understanding of the reaction kinetics between cyclic anhydride functional groups and primary amines in molten PP, hexadecylamine (molecular weight = 241.46) was used as a model primary amine compound. Hexadecylamine, CH_3-$(CH_2)_{15}$-NH_2, is a low molecular weight analog of the primary amine terminally functionalized polymer. As well, it exhibits a boiling point of 330 °C, which is adequate for performing melt-phase reactions in molten PP. Thin films of KF6100 PP and hexadecylamine were compression molded (thickness = 0.75 mm) using the hot press. As compared to the

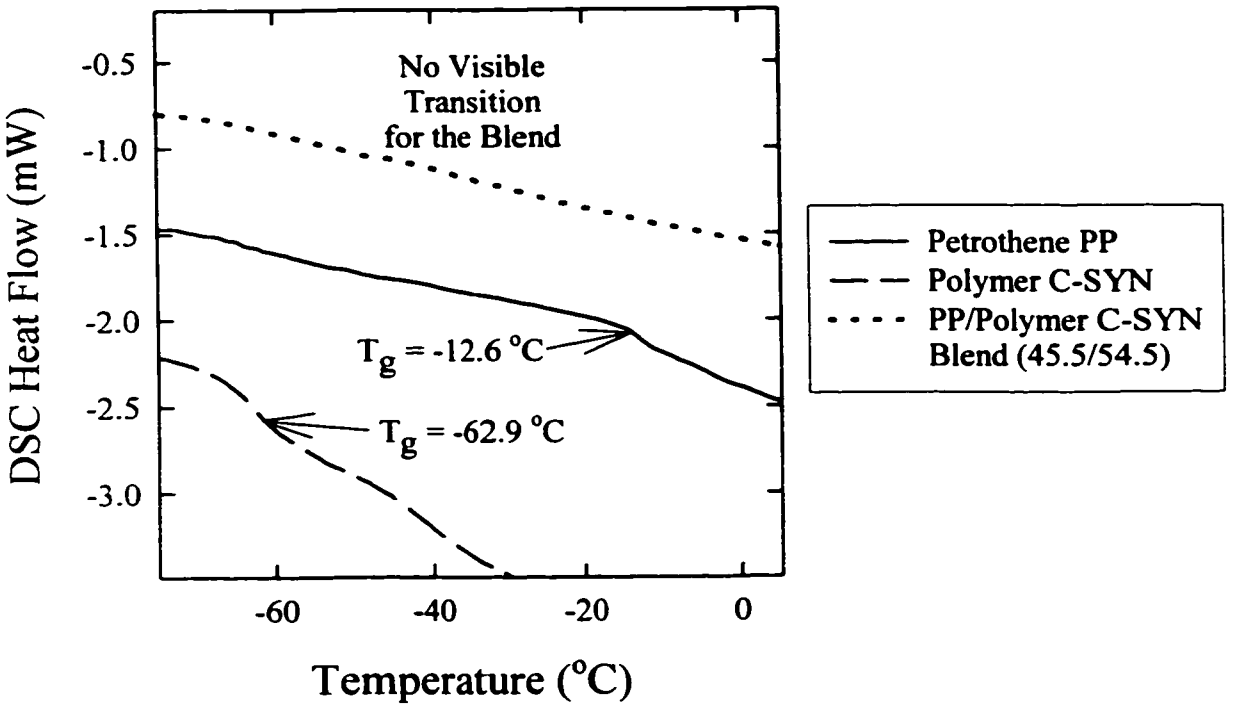

Figure 5.3. DSC Analysis of Petrothene PP, Polymer C-SYN, and their Blend Prepared in the Batch Mixer (54.5wt% Polymer C-SYN)

anhydride functional group concentration in its 5wt% blend in PP, an excess of hexadecylamine was used. The film containing hexadecylamine was opaque, which indicated poor compatibility between the polar small molecule compound and the hydrophobic PP. Incompatibility may lead to migration of the amine compound to the surface of the film, or phase separation.

The model interfacial reaction between hexadecylamine and the succinic anhydride reactive polymer in molten PP was completed using the heatable IR cell, which was positioned in the FT-IR spectrometer. A film containing hexadecylamine and a film containing the succinic anhydride functionalized polymer were positioned between NaCl discs, which were then placed into the heatable IR cell. Heating of the IR cell and its contents to 200 °C took approximately 8 min. After reaching the steady-state temperature, FT-IR spectra were obtained after desired time intervals up to a total of 2 hours. Conversion of the cyclic anhydride functional groups was followed using the peak at 1793 cm^{-1}, and formation of the cyclic imide was followed using the peak at 1712 cm^{-1}. Relative peak heights were calculated using the peak at 2399.4 cm^{-1} as an internal reference, which corresponds to an overtone of the backbone peaks of the PP (Liang and Pearson, 1960). The anhydride and imide peak heights were measured from a common baseline extending from 675 to 2008 cm^{-1}. This baseline differed from the baseline used to analyze the solid polymer films from the mixing experiments because the NaCl discs block out the IR spectrum below 600 cm^{-1}. The peak height of the internal reference was measured from a local baseline in its region (2290 to 2451 cm^{-1}). FT-IR spectra obtained from the reaction are presented in Figure 5.4 and the profiles of the anhydride and imide relative peak heights are presented in

Figure 5.5. The zero time in Figure 5.5 corresponds to the first measurement obtained after reaching the desired setpoint of 200 °C.

Complete conversion of the anhydride functional groups occurred prior to establishing the steady-state temperature of the heatable cell (within 8 min). The anhydride peak at 1793 cm^{-1} was not visible in the first FT-IR spectrum obtained after reaching the setpoint temperature. This extremely fast conversion of the anhydride functional groups was attributed to a rapid migration of the incompatible hexadecylamine in the molten PP, which is similar to the observation of Maier *et al.* (1994) for the migration of small molecule polar amine in EPR. The reaction was not isolated to the interface between the two PP layers. To achieve completed conversion in less than 8 min, the small molecule polar amine must have rapidly migrated into the PP layer containing the anhydride reactive polymer. The experimental results also confirmed the observation of Scott and Macosko (1994a) concerning the rapid kinetics of the first step of the anhydride - primary amine coupling reaction at polymer processing temperatures. In contrast to the rapid consumption of the anhydride functional groups, the formation of the cyclic imide occurred very slowly, with the final steady-state relative peak height achieved after 80 to 100 min. Cyclization to form the imide results in a water byproduct, which must diffuse away from the reaction sites. During typical reactive extrusion processes, the residence time is approximately 1 to 5 min. The results from the model reaction suggested that imide formation is negligible during this short processing time. High yields of the cyclic imide are achieved during reaction extrusion in twin screw extruders when devolatilization is used to remove the water byproduct (Vermeesch *et al.*, 1993; Vermeesch and Groeninckx, 1994). Therefore, the kinetics of the cyclization are very sensitive to the removal of the water byproduct via venting.

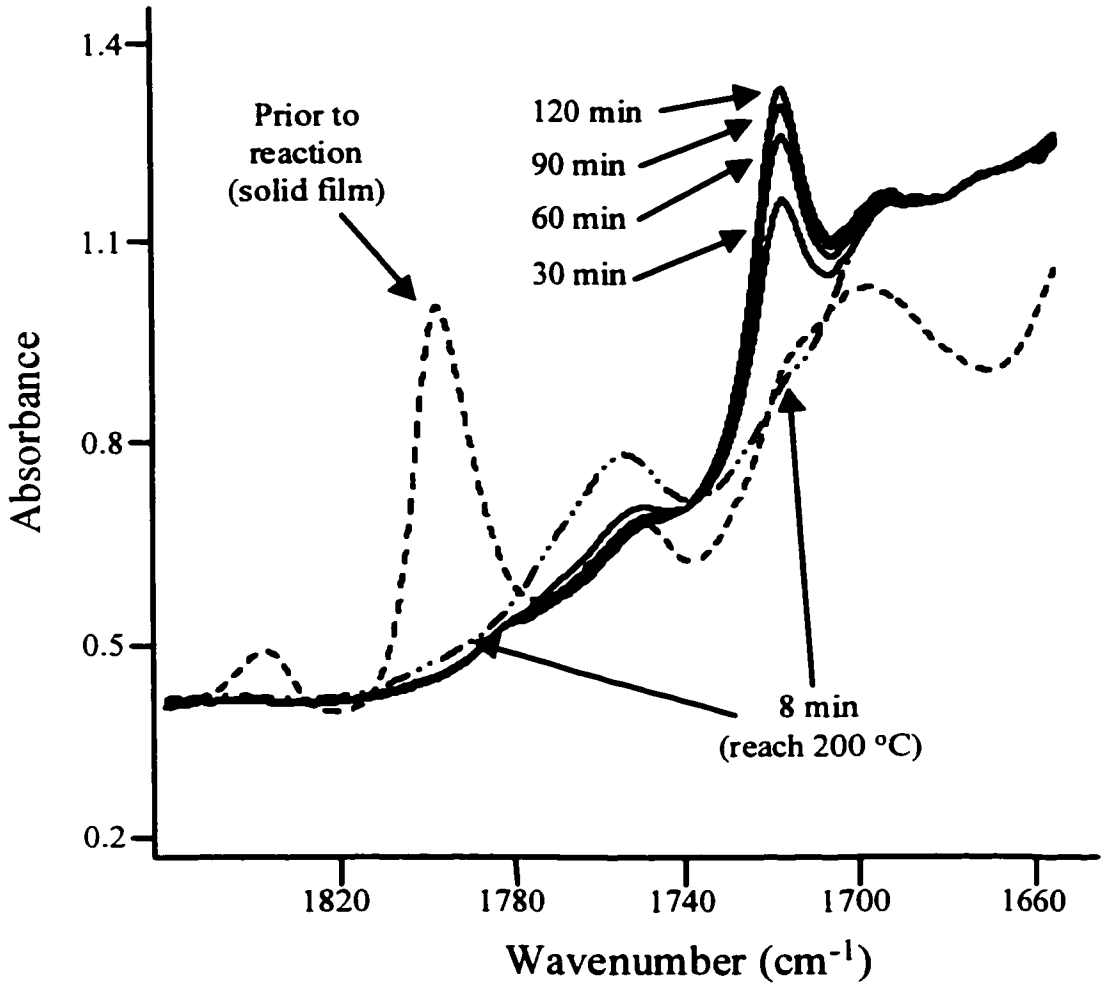

Figure 5.4. FT-IR Spectra of the Model Interfacial Reaction Between Hexadecylamine and the Anhydride Functionalized Polymer in Molten PP

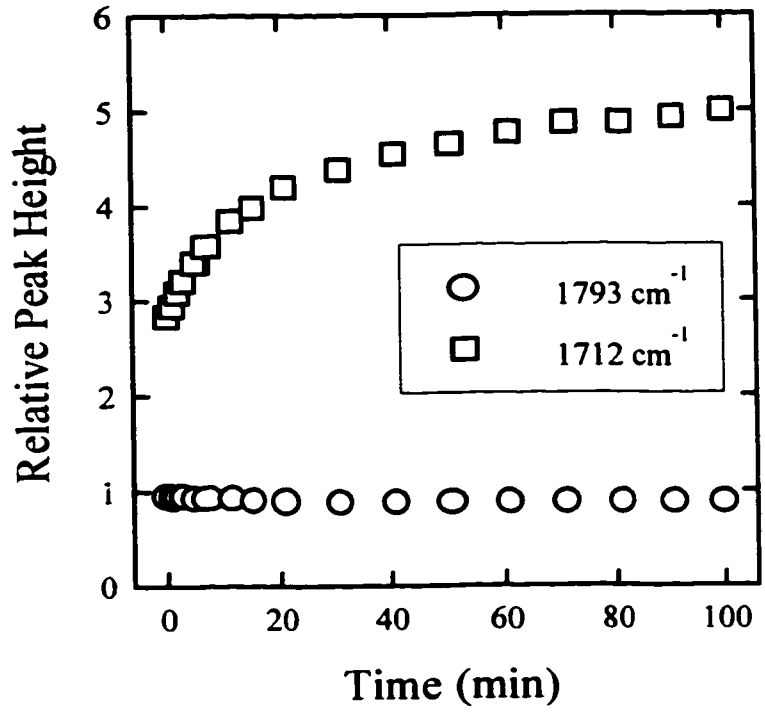

Figure 5.5. Relative Peak Height Profiles from the Reaction with Hexadecylamine

During the reaction with hexadecylamine, no peaks were observed in the FT-IR spectra corresponding to the reaction intermediate, which confirmed the observations of Scott and Macosko (1994a). It was proposed that the intermediate is an amic acid, which should exhibit a carbonyl stretching vibration for the acid functional group. Hydrolysis of the anhydride functionalized polymer to its di-acid was completed by exposing the polymer to the atmosphere for approximately three weeks. FT-IR analysis indicated that the carbonyl stretching vibration of the di-acid was located at 1715 cm^{-1}. The acid functional group of the amic acid intermediate should exhibit a peak near this wavenumber. Thus, the intermediate may overlap with the cyclic imide, which exhibits its carbonyl stretching vibration at 1712 cm^{-1}. During the model reaction, complete conversion of the anhydride functional groups occurred prior to the first FT-IR measurement, but the imide formation occurred slowly. If the amic acid intermediate was formed there should be a peak initially in the region of 1715 cm^{-1}. No peak was observed initially in this region, which suggested that the amic acid intermediate was not formed. Scott and Macosko (1994a) proposed that the intermediate is not visible in the FT-IR spectrum because the reaction may proceed quickly from the intermediate to the imide product. During the reaction with hexadecylamine, there was a significant delay between the anhydride conversion and the imide formation, and therefore, the proposed reaction mechanism of Scott and Macosko (1994a) through the amic acid intermediate may not be valid for the melt-phase reaction.

Model interfacial reactions between anhydride and amine reactive polymers in PP were completed by the two methods described in section 4.3.2. In both cases, thin films of the reactive polymers in KF6100 PP were compression molded (thickness = 0.31 mm). For the reactions, one film containing the anhydride reactive polymer was placed between two

films containing the amine reactive polymer. This method maintained a constant striation thickness of 0.31 mm during the reaction. Stacks of these three films were reacted in the hot press and the heatable IR cell at 200 °C. The reaction in the hot press was completed for times ranging from 2 to 240 min (for each time a separate stack of films was used). In the heatable IR cell, in-line analysis was completed at times up to 240 min. The results from the two different reaction methods cannot be quantitatively compared because there are significant differences in the peak positions and absorbances in solid and melted PP phases (Zbinden, 1964). In the case of the reaction completed in the hot press, the anhydride and imide relative peak heights were determined using the peak at 459.4 cm^{-1} as an internal reference, and a common baseline extending between 411 and 2008 cm^{-1}. For the in-line analysis using the heatable IR cell, the peak at 2399.4 cm^{-1} was used as an internal reference (its peak height measured using a local baseline). The anhydride and imide peak heights were measured from a baseline between 685 to 2020 cm^{-1}. The carbonyl stretching vibration of the cyclic imide formed in the reaction between the two reactive polymers was located at 1710 cm^{-1} as compared to 1712 cm^{-1} for the imide formed in the reaction between the anhydride reactive polymer and hexadecylamine. This peak shifting was attributed to the effect of the chain length on the carbonyl vibration of the imide. FT-IR spectra obtained from the reaction in the hot press are presented in Figure 5.6, and the relative peak profiles from the reaction in the hot press and heatable IR cell are presented in Figure 5.7.

The shapes of the relative peak height profiles obtained from the two different reaction methods are in qualitative agreement. Similar to the observations of Scott and Macosko (1994a), the consumption of the anhydride functional groups and the formation of the imide occurred simultaneously. This observation is in contrast to the reaction with

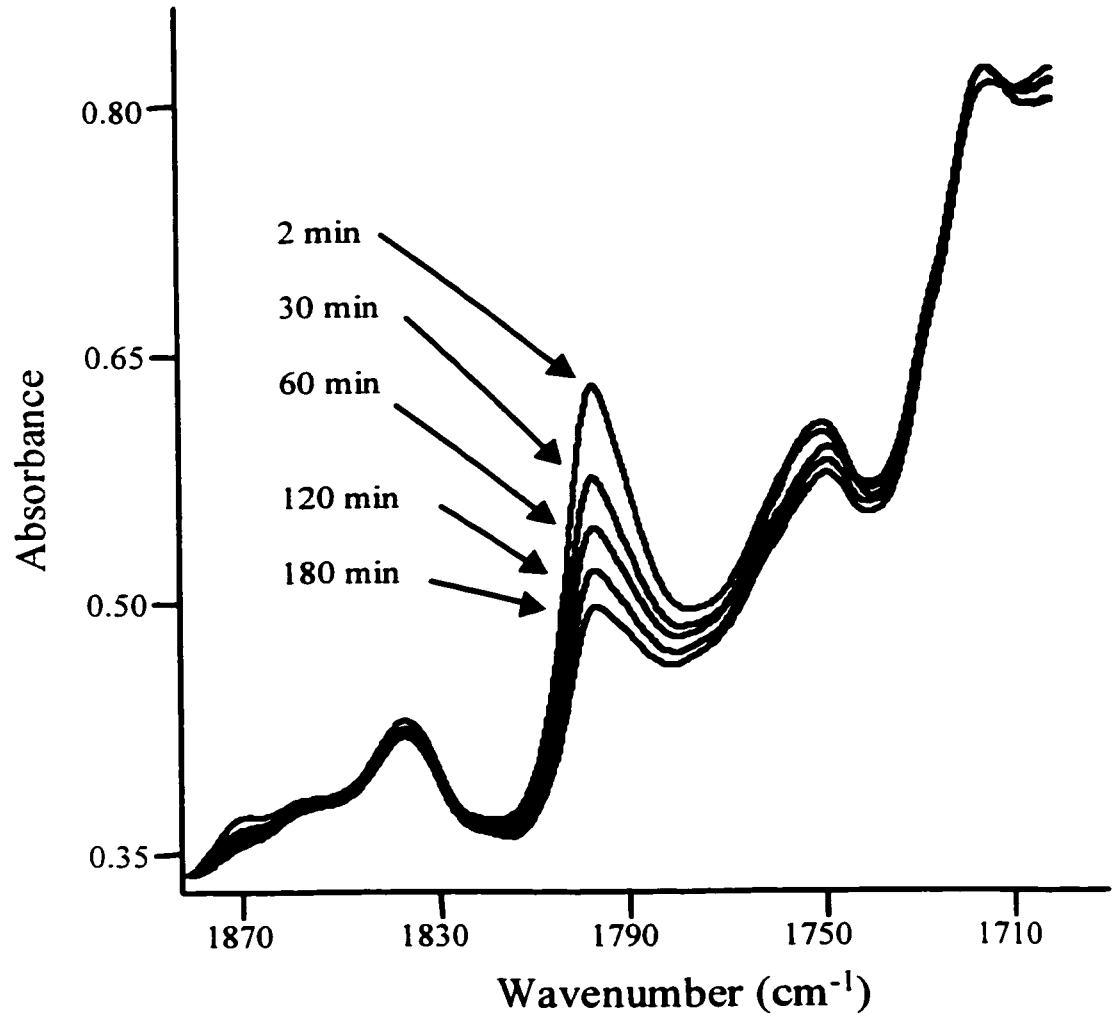

Figure 5.6. FT-IR Spectra Obtained from the Model Interfacial Reaction Between the Reactive Polymers in Molten PP

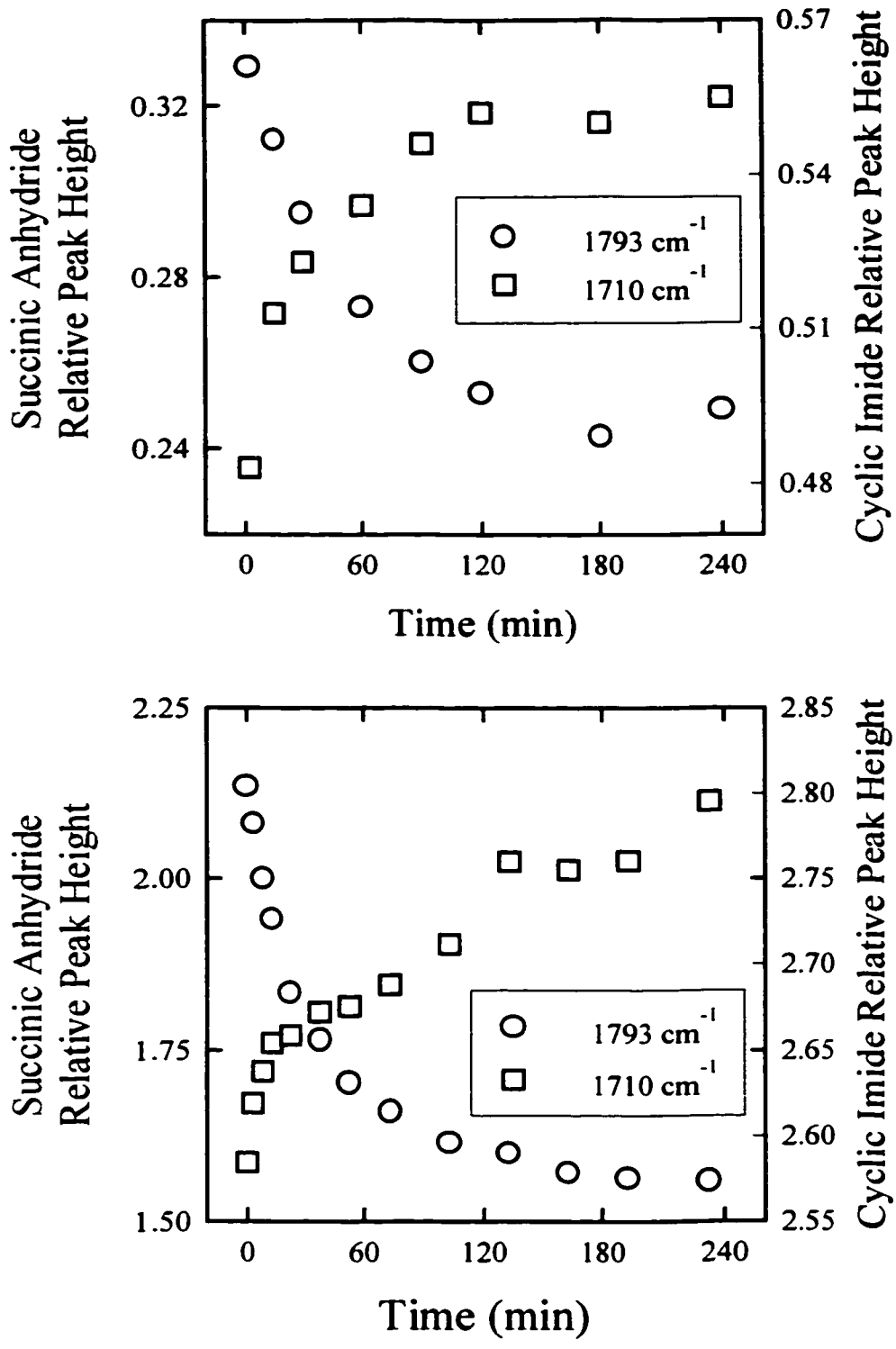

Figure 5.7. Relative Peak Height Profiles from the Model Interfacial Reactions Between the Reactive Polymers in Molten PP
(Top) Hot Press Reaction
(Bottom) Heatable IR Cell Reaction

hexadecylamine, which exhibited a significant time delay between the two steps of the reaction. The interfacial reaction between the reactive polymers in molten PP occurred slowly, with complete conversion in approximately 3 hours. As compared to the rapid migration of hexadecylamine, the diffusion of the reactive polymers in the PP matrix was extremely slow. The polymer tracers exhibit properties much more similar to that of the PP matrix. In addition, the reactive polymers were compatible with the PP resins while the polar hexadecylamine was not compatible. These advantages make the reactive polymers better candidates for reactive tracers in PP. As previously mentioned, compatibility issues between the hydrophobic polymer and polar small molecule reactants used in the research of Wu (1994) on micromixing were not considered.

The basic principle of the proposed method for analyzing polymer mixing is that the coupling of the two reactive polymers occurs at the interface, and the conversion is directly related to the total amount of interfacial area generated. A model interfacial reaction was completed to confirm this underlying principle. Thin films of the anhydride and amine reactive polymers in Petrothene PP were compression molded (thickness = 0.2 mm) using the hot press. Using a mold with three circular cavities (diameter = 2.54 cm, thickness = 1.5 mm), three model reactions were completed simultaneously in the hot press at 200 °C with an applied pressure of 5.5 MPa. A stack of 8 thin films, with 4 containing the anhydride reactive polymer and 4 containing the amine reactive polymer, were used in each reaction. The interfacial area available for the reaction was varied by changing the stacking order of the 8 films, which is depicted in Figure 5.8. The number of interfaces available for the reaction was varied between 1, 3, and 7 (each interface corresponds to 506.7 mm^2 of interfacial area). The reactions were run for 15 min, after which, the mold and its contents

were rapidly cooled in the water bath. The diffusion of the reactive polymers in molten PP is very slow (Figure 5.7), and therefore, only the reactive polymers in the vicinity of the interfaces react during the 15 min. Two separate experiments using this method were completed, and the relationship between the anhydride conversion determined from FT-IR analysis and the interfacial area available for the reaction is presented in Figure 5.9. The anhydride conversion was calculated using equation 4.2, and the internal reference was the peak at 528.5 cm^{-1}. Before the reaction, each film stack was analyzed using the FT-IR spectrometer to determine the anhydride relative peak height at zero conversion. To obtain full conversion of the interfacial reactions, the stacks were further reacted in a vacuum oven at 120 to 140 °C for 3 days. To maintain a constant degree of crystallinity, the fully reacted films were compression molded in the hot press for 3 min at 200 °C and then water quenched.

Using linear regression analysis, the relationship between the anhydride conversion and the interfacial area available (units = mm^2) for the reaction was quantified and it is presented in equation 5.1 (the intercept was not significant as indicated by its t-statistic).

$$\text{Anhydride Conversion} = 9.31 \times 10^{-5} * (\text{Interfacial Area}) \qquad (5.1)$$

The correlation coefficient (r^2) was 0.9985, which indicated that the regression equation adequately represented the experimental data. The experimental results were then normalized with respect to the conversion obtained with one interface (interfacial area = 506.7 mm^2), and the normalized results were 3.05 for three interfaces (interfacial area = 1520 mm^2) and 6.82 for seven interfaces (interfacial area = 3547 mm^2). These results confirmed that the conversion was linearly related to the interfacial area available for the reaction, which verified the basic principle of the experimental method.

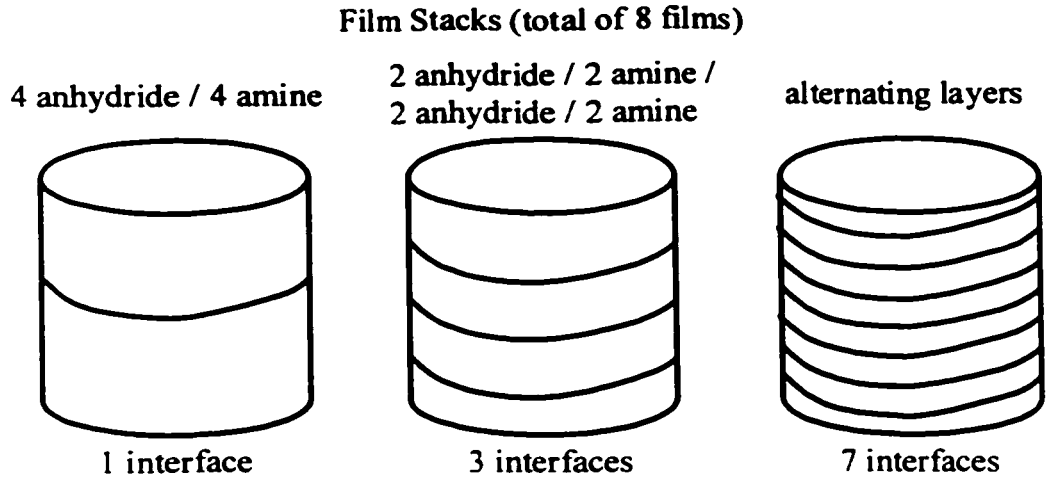

Figure 5.8. Stacking Method Used to Vary the Interfacial Area

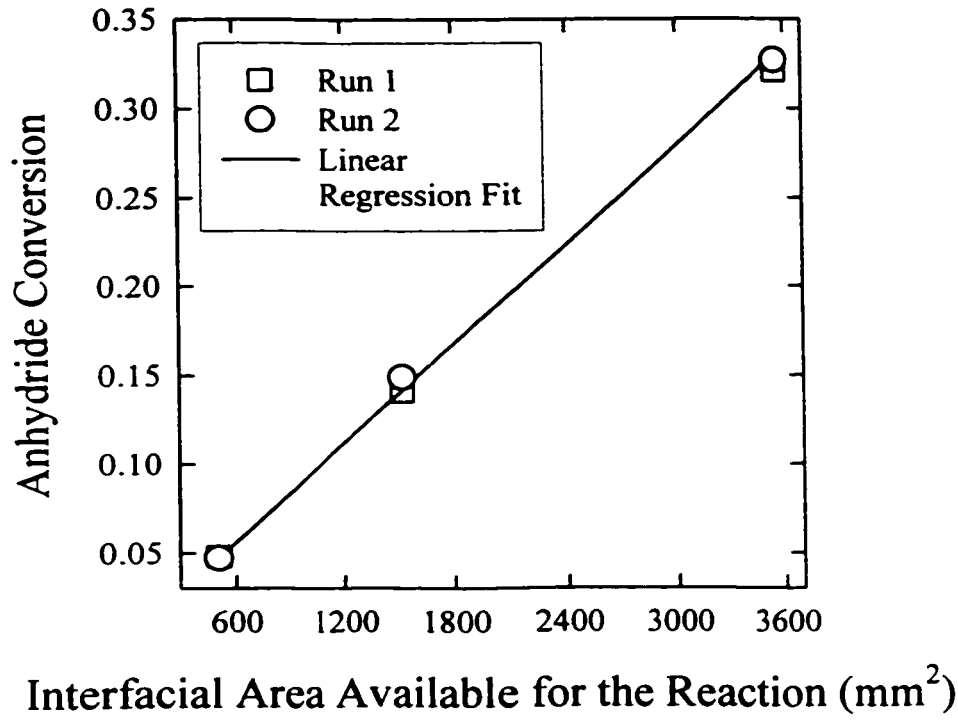

Figure 5.9. Relationship Between Anhydride Conversion and the Interfacial Area Available for the Reaction

An additional preliminary interfacial reaction was completed in the hot press to investigate the possible reversibility of the anhydride – amine reaction that was observed by Hu and Lindt (1992). Once again, a film of Petrothene / 5wt% anhydride polymer tracer was pressed between two films of the Petrothene / 5wt% amine polymer tracer (total thickness = 1.5 mm). The stack of films was reacted in the hot press according to the following steps: 2 min at 200 °C, 30 additional min at 200 °C, 30 additional min at 260 °C, 30 additional min at 300 °C, and annealed for 3 hrs at 140 °C in a vacuum oven. Between each reaction step, FT-IR analysis was completed, and the spectra are presented in Figure 5.10. As indicated in Figure 5.10, the peak height of the anhydride functional group at 1793 cm^{-1} decreased after each reaction step. The results confirmed that the reaction between the terminally functionalized anhydride and amine polymer tracers was irreversible in the temperature range commonly experienced during polymer processing in extruders. In addition, the reaction continued to proceed during the annealing step at 140 °C, which confirmed that the reaction may occur below the melting temperature of the PP matrix (approximately 175 °C). This reaction was attributed to the migration of the polymer tracers caused by the crystallization of the PP matrix.

Two significant differences were observed between the melt-phase anhydride – amine reactions completed in this work and the solution reactions completed by Hu and Lindt (1992) and Scott and Macosko (1994a). The first difference is the irreversibility of the melt-phase reaction as compared to the solution reaction of Hu and Lindt (1992). The second difference is the detection of the intermediate that is formed by the rapid coupling of the functional groups prior to the formation of the cyclic imide. In solution, a secondary amide acid salt intermediate was clearly visible prior to the imide formation by Hu and Lindt (1992)

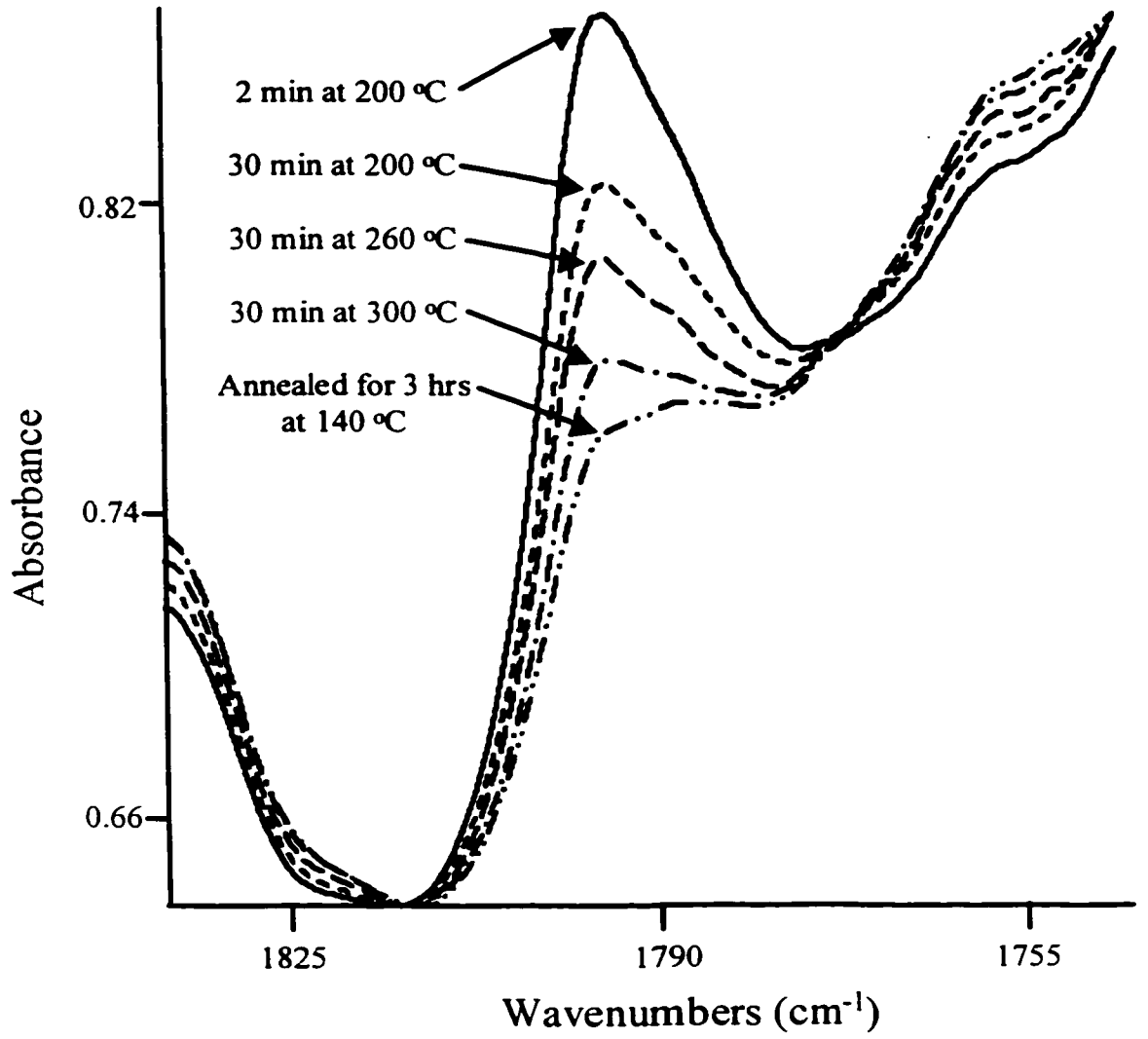

Figure 5.10. FT-IR Spectra of the Model Interfacial Reaction Between the Polymer Tracers in Molten PP at Different Temperatures to Investigate the Possibility of a Reverse Reaction

and Scott and Macosko (1994a). As previously mentioned, no intermediates were visible in the FT-IR spectra of the melt-phase reactions completed in this research. These two differences suggested that the melt-phase reaction does not proceed according to the reaction mechanism presented in Figure 3.7, which was proposed by Scott and Macosko (1994a). Regardless of the true reaction mechanism in the melt-phase, the coupling of the anhydride and amine functional groups occurred extremely fast and the conversion was linearly related to the interfacial area available for reaction. Therefore, the polymer tracers were used to analyze mixing during polymer blending in a twin screw extruder.

5.2. Preliminary Experiments on Mixing During Melt-melt Blending in a Twin Screw Extruder

Three sets of preliminary experiments on mixing during melt-melt blending in a twin screw extruder were completed to determine the feasibility of the experimental method and to investigate the importance of many different factors. All the experiments were completed using the tandem extruder apparatus (Figure 4.2), with equal mass flow rates in the two segregated melt streams. Prior to presenting the experimental results a few comments are offered concerning the interfacial reaction between the polymer tracers. The terminal coupling of the reactive polymers does not affect the interfacial properties because the molecular weight of the tracers is negligible as compared to the PP resin. Conversely, the crosslinks formed between high molecular weight reactive polymers, as in the work of Curry *et al.* (1990; 1991/1992), affect the interfacial properties and its deformability. As well, the crosslinks increase the polymer viscosity, which will have an effect on the pressures in the extruder. No viscosity increase was observed in the experiments with the low molecular weight reactive polymers. Scott and Macosko (1994a) observed a limiting conversion during

model interfacial reactions between SMA and primary amine terminated polymers. This limiting conversion, or a leveling off of the reaction, was attributed to the formation of a crosslinked interfacial layer, which inhibited further diffusion of the reactive polymers. Once again, due to the low molecular weight of the reactive polymer tracers used in this research, the interfacial properties were not significantly affected by the coupling reaction. Therefore, the low molecular weight reactive polymer tracers cannot be replaced by conventional high molecular weight reactive polymers because their reaction affects the overall mixing process. As well, conventional functionalized polymers may contain more than one functional group grafted to the backbone of each polymer chain. Therefore, more than one possible reaction can occur between two conventional reactive polymer chains at the interface. Conversely, only one reaction can occur between the terminally functionalized polymers used in this research. The conversion measures the number of reactions that occurred between separate pairs of the reactive tracers at the interface that is generated between the two segregated polymer melts in the twin screw extruder.

5.2.1. Factorial Screening Experiments

A simple 2^3 full factorial experiment design was implemented to investigate the effects of the total flow rate, the screw speed, and the viscosity ratio of the melt streams on the mixing performance of the twin screw extruder. The experiments were completed using the KF6100 PP resin, and the viscosity ratio was achieved using a temperature difference between the segregated melt streams. To estimate the viscosity ratio, the apparent shear viscosity of a 5wt% blend of Polymer C-SYN in KF6100 PP was measured at 190, 210, 230, and 250 °C. The measurements were completed in a capillary rheometer using a capillary die

(D = 0.508 mm, L/D = 60) over the apparent shear rate range of 100 to 1000 s^{-1}. The apparent shear viscosities of pure KF6100 PP and the blend containing the low molecular weight tracer are presented in Figure 5.11. For each material, the results were fitted to a temperature dependent power-law viscosity model and the coefficients of the regression equations are presented in Table 5.1. Linear regression was performed using the linear form of the power-law viscosity model (presented in Table 5.1, developed by taking the natural logarithm of both sides of the power-law viscosity model), and the r^2 values correspond to the results for the linear models.

Table 5.1. Coefficients of the Regression Equations of the Temperature Dependent Power-law Viscosity Model#

Material	K (Pa.s^n)	β (1/°C)	n	r^2
KF6100 PP	43914	0.0029	0.36	0.9983
KF6100 PP + 5wt% Polymer C-SYN	36169	0.0029	0.37	0.9982

$\eta = K * \exp(-\beta * T) * \dot{\gamma}^{(n-1)}$

Linear model : $\ln(\eta) = \ln(K) - \beta*T + (n-1)*\ln(\dot{\gamma})$

where: η : apparent shear viscosity (Pa.s)

K : consistency index (Pa.s^n)

β : temperature coefficient (1/°C)

n : flow index

$\dot{\gamma}$: apparent shear rate (s^{-1})

As expected, the addition of 5wt% Polymer C-SYN decreased the apparent shear viscosity of the PP by approximately 15%. The tracer did not affect the temperature coefficient or the flow index. Therefore, the shear thinning and temperature behavior of the polymer melt remained unchanged. The shear viscosity results estimated a viscosity ratio of approximately 1.5 using temperatures of 190 and 250 °C.

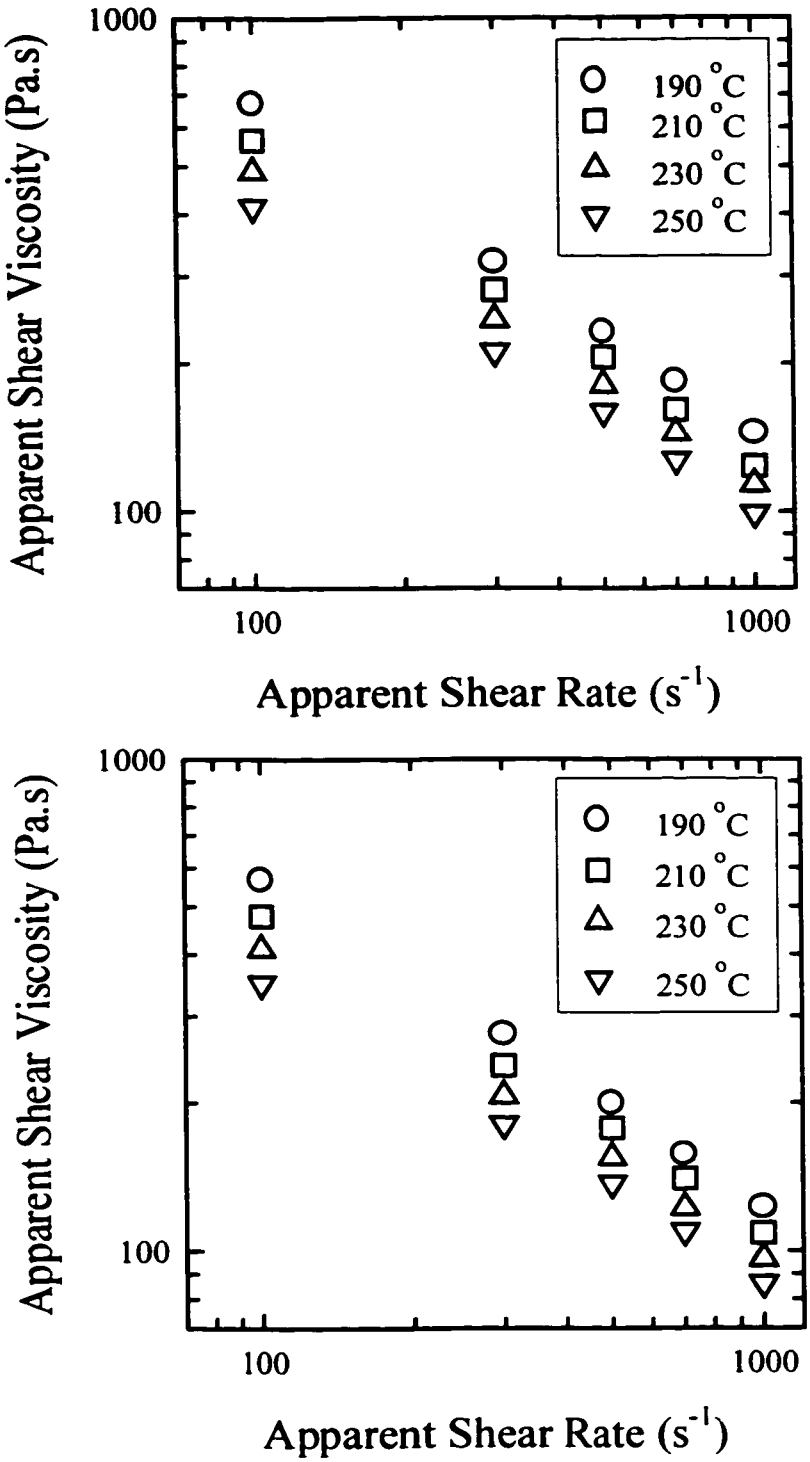

Figure 5.11. Apparent Shear Viscosity Results
(Top) Pure KF6100 PP
(Bottom) KF6100 PP + 5wt% Polymer C-SYN

The factor levels were: viscosity ratio of 1 and 1.5 (controlled using a temperature of 190 or 250 °C for the polymer melt fed using the single screw extruder), total flow rate of 50 and 100 g/min, and screw speeds of 50 and 150 rpm. The barrel temperatures in the melt-melt blending section of the twin screw extruder were maintained at 190 °C. The viscosity ratio cannot be controlled precisely using the temperature difference method, and it depends on the local shear rate and melt temperature in the extruder. The linear regression analysis of the experimental results was completed using codified factor levels (-1 for lower level, +1 for higher level). The experiment design and factor levels are presented in Table 5.2.

Table 5.2. Factorial Experiment Design and Factor Levels

Experiment #	Viscosity Ratio η(twin) / η(single)	Screw Speed (rpm)	Total Flow Rate (g/min)
1	1.5	150	100
2	1.5	150	50
3	1.5	50	100
4	1.5	50	50
5	1	150	100
6	1	150	50
7	1	50	100
8	1	50	50
Midpoint (MP)	1.25	100	75

As described in section 4.3.3, the PP / amine reactive polymer blend was metered to the beginning of the twin screw extruder and the PP / anhydride reactive polymer blend was melt fed to barrel position 7 using the single screw extruder / adapter. The screw configuration of the melt-melt blending section is depicted in Figure 5.12. The conveying elements located under the melt feeding location were partially filled, and therefore, the calibration method outlined in section 4.3.3 was used to determine the screw speeds of the single screw extruder that yielded the desired flow rates of 25 and 50 g/min in the melt fed

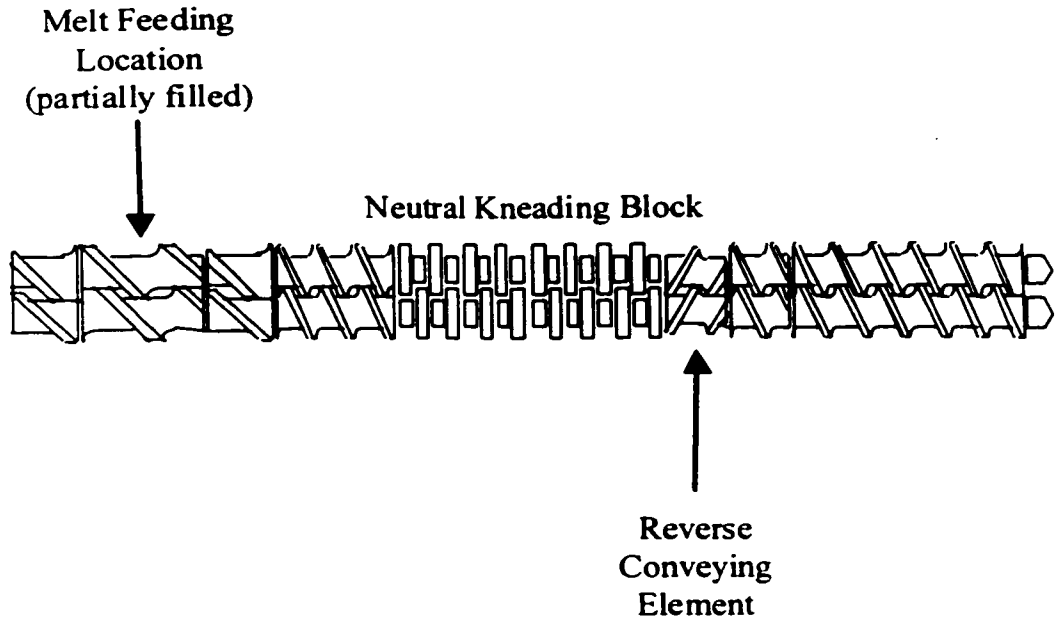

Figure 5.12. Screw Configuration in the Melt-melt Blending Section for the Factorial Screening Experiments

stream. The kneading block consisted of 16 adjacent bilobal kneading discs staggered in a neutral configuration (90°), which was followed by a reverse conveying element. A pressure transducer located immediately after the reverse conveying element measured a zero pressure in all the experiments, which indicated that the screw channel was partially filled at that location. The polymer backup length prior to the slit die did not affect the polymer fill in the kneading block, and therefore, the flow patterns and pressure in the kneading block were independent of the die restriction. This condition was maintained in all the mixing experiments presented in this thesis.

FT-IR analysis of the anhydride conversion was completed using the film produced by the slit die at the end of the twin screw extruder. Prior to sampling the polymer film, the extruders were run for a minimum of 20 min to establish steady-state. For calculation of the anhydride conversion using equation 4.2, the relative peak height of the anhydride peak at 1793 cm^{-1} (internal reference at 528.5 cm^{-1}) for the conditions of zero and full conversion were determined to be 2.558 and 2.005, respectively. The calculated anhydride conversions and standard errors are presented in Table 5.3. Five replicates were completed at the midpoint (MP) conditions to determine the experimental reproducibility, and a three level nested design as described by Box, Hunter, and Hunter (1978) was used to decompose the overall variance. The calculated standard errors were: overall = 0.021, batch-to-batch (between separate runs) = 0.009, sample inhomogeneity (within a single run) = 0.023, and FT-IR analysis reproducibility = 0.038. Although the replicate averages were in satisfactory agreement, there was an indication of poor FT-IR analysis reproducibility as well as sample inhomogeneity. The latter was attributed to a slight pulsing in the feed rate of the PP / amine reactive polymer blend from the K-TRON feeder to the beginning of the twin screw extruder.

Table 5.3. Experimental Results of Anhydride Conversion

Experiment #	Anhydride Conversion	Sample Standard Error
1	0.569	0.053
2	0.725	0.018
3	0.880	0.016
4	0.783	0.023
5	0.652	0.026
6	0.659	0.060
7	0.963	0.057
8	0.806	0.058
MP 1	0.688	0.035
MP 2	0.661	0.006
MP 3	0.704	0.038
MP 4	0.685	0.077
MP 5	0.654	0.040

Linear regression using codified factor levels was completed to quantify the factor effects as well as their interactions. Using the overall variance (prior to decomposition) from the midpoint analysis, F-statistics were calculated to determine the factor significance. The linear regression results of the significant factors are presented in Table 5.4. The correlation coefficient (r^2) of the linear model containing the three significant factors was 0.958, and all the remaining factors accounted for less than 3% of the total variability.

Table 5.4. Linear Regression Results and Statistical Analysis of the Significant Factors

Factor	Effect	% of Total Variance Explained by Effect	F-statistic*
Screw Speed	-0.207	72.8	201.8
Screw Speed – Flow Rate Interaction	-0.104	18.4	51.1
Viscosity Ratio – Flow Rate Interaction	-0.052	4.62	12.8

***F-distribution = 7.71 for 95% confidence (degrees of freedom =1,4)**

The three significant factors exhibited negative effects on the anhydride conversion, which is a direct indication of the distributive mixing performance of the melt blending section of the twin screw extruder. The reaction conversion is also a direct measurement of the micromixing of the polymer melts in the extruder because the chemical reaction between the polymer tracers is a molecular event. It was expected that increasing screw speed from 50 to 150 rpm would improve the mixing performance through an increase in the shear rate, which correspondingly increases the interfacial area generation rate. Conversely, the opposite effect was observed, which was attributed to the negative effect of reduced residence time. Distributive mixing of two segregated fluids, or the generation of interfacial area, is directly related to the total applied shear strain (Meijer and Janssen, 1994), which is dependent on the residence times and the shear rates in the extruder. Therefore, reduced residence time and increased shear rate were competing effects on the mixing performance at the higher screw speed.

In all the experiments completed at the screw speed of 150 rpm, shear heating in the kneading block section of the twin screw extruder was observed. This shear heating was manifested by a significant increase in the barrel temperature at the kneading block. The cooling system did not maintain the desired barrel setpoint temperature of 190 °C. As a result, the barrel temperatures in the kneading block section reached new steady values in the range of 205 to 215 °C. As well, the melt temperature measured at the die with the IR temperature probe increased by approximately 5 to 7 °C upon increasing the screw speed from 50 to 150 rpm. This temperature increase affected the reaction kinetics, but the reaction between the polymer tracers remained mixing limited. A decrease in the polymer viscosity at the higher temperature may have affected the stresses applied to the polymer melts.

Although the applied stresses are important in dispersive mixing, only the applied strain is important in distributive mixing. Thompson *et al.* (1995) observed small increases in the average residence time upon increasing the barrel temperature from 220 to 240 °C in a non-intermeshing twin screw extruder. Therefore, it is not likely that the temperature increase caused a significant change in the residence time. Using FEM simulations, van der Wal *et al.* (1996) predicted that the polymer viscosity does not affect the shear or elongational rates applied to the polymer in the extruder except for extremely low viscosities (< 1 Pa.s, the viscosity in the experiments was > 100 Pa.s and depended on the shear rate, Figure 5.11). Therefore, the temperature increase and the corresponding viscosity decrease at 150 rpm did not affect the distributive mixing process.

The interaction between screw speed and flow rate (Q*N) was attributed to the effect of residence time on the mixing process. Increasing screw speed or flow rate reduces the residence time, which correspondingly decreases the applied shear strain. Bigio *et al.* (1994) showed that the specific throughput (Q/N), which is an indication of screw channel fill, affected distributive mixing. In all the experiments, the neutral kneading block and the reverse conveying element were fully filled due to their restrictive natures. Conversely, the degree of fill in the conveying elements preceding the kneading block and the die decreased with a decrease in flow rate or an increase in screw speed. Mixing is expected to be more efficient in fully filled conveying elements as compared to partially filled conveying elements due to the higher shear rates applied to the polymer (verified in the mixing profile experiments described in Chapter 7). Therefore, the negative interaction of flow rate and screw speed may have also incorporated this channel fill effect. Using codified factor levels

in the regression analysis, the interactions of Q*N and Q/N are confounded, and therefore, both contribute to the observed interaction between screw speed and flow rate.

The viscosity ratio - flow rate interaction indicated that the viscosity ratio exhibited a small negative effect on the mixing performance. Increasing the single screw extruder / adapter temperature from 190 to 250 °C did not significantly increase the polymer melt temperature measured at the end of the twin screw extruder. This surprising observation indicated that the hot melt stream supplied by the single screw extruder rapidly cooled in the twin screw extruder. Therefore, the temperature difference method did not produce a significant viscosity ratio. In additional experiments, blending of two different PP resins was completed to further investigate the viscosity ratio effect. This method allowed for better control over the viscosity ratio of the segregated melt streams, and the results are presented in the section 5.2.3.

5.2.2. Closer Examination of the Screw Speed Effect on Mixing During Melt-melt Blending

The feasibility of the novel experimental method using reactive polymers to quantitatively measure mixing during polymer melt blending was confirmed by the preliminary screening experiments. Further experiments were completed using the same screw configuration to gain a more detailed understanding of the effect of screw speed on the mixing process. The experiments were completed using a total flow rate of 50 g/min and barrel temperatures of 220 °C in both the twin and single screw extruders. Screw speeds between 50 and 175 rpm were investigated and the experimental results are presented in Figure 5.13. The error bars represent the standard errors calculated from 5 samples collected over a time interval of 10 minutes at each screw speed, and replicate experiments were

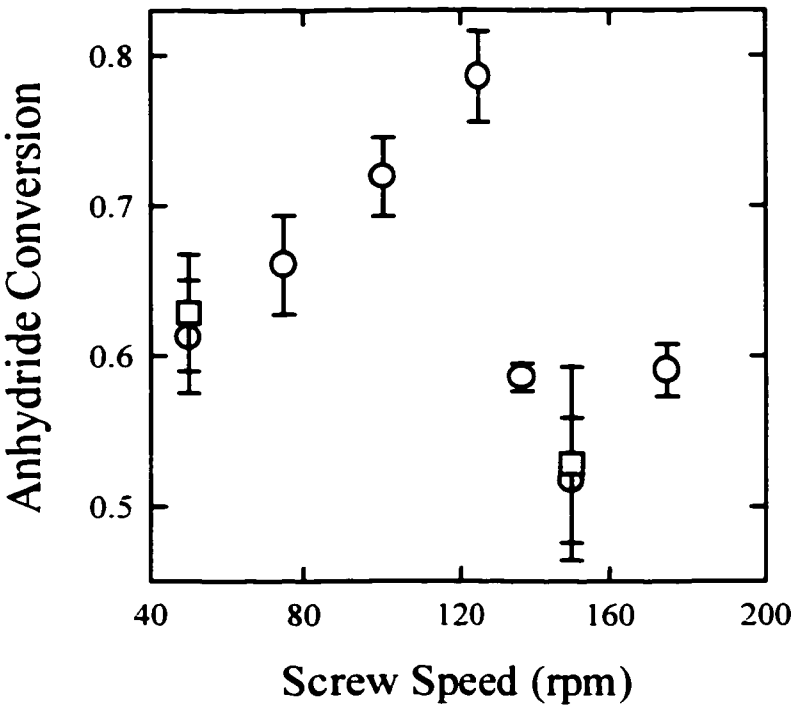

Figure 5.13. Screw Speed Effect on Mixing During Polymer Melt-melt Blending

completed at 50 and 150 rpm (square symbols in Figure 5.13). The average errors between the replicated experiments were less than 2%, which indicated adequate experimental reproducibility.

The mixing performance initially increased with screw speed, which was attributed to a corresponding increase in the shear rate. The sharp drop in the mixing performance between 125 and 137 rpm corresponded to the onset of shear heating in the kneading block section. The barrel temperature of the kneading block section increased from 220 °C to the following values: 227 °C for 137 rpm, 229 °C for 150 rpm, and 233 °C for 175 rpm. As previously mentioned, this temperature increase does not significantly affect the residence time or shear rate, and therefore, it does not affect distributive mixing. Conversely, the decrease in the mixing performance was attributed to the effects of reduced residence time and channel fill at the high screw speeds. Ganzeveld and Janssen (1992a; 1992b) investigated the complicated effect of screw speed on reactive extrusion processes in counter-rotating twin screw extruders. Distributive mixing is critical during reactive extrusion because the reactions occur at the interfaces between the incompatible phases. It was proposed that screw speed exhibits a non-linear effect on the reactions due to the competing contributions of residence time and mixing rate (deformation rate). The experimental results confirmed this complicated non-linear screw speed effect on distributive mixing in extruders because it incorporates the contributions of many different competing factors.

5.2.3. Investigation of the Effects of Polymer Viscosity and Kneading Block Design on the Mixing During Melt-melt Blending

Implementing a temperature difference between the two segregated streams did not effectively produce a large viscosity ratio. Therefore, blending of different viscosity PP melt

streams was attempted. The screw configuration used in these experiments is presented in Figure 4.4, which has a longer melt blending section than in the previously discussed mixing experiments (the melt feeding location was barrel segment 6). As in the previous experiments, the melt feeding location in the twin screw extruder was partially filled. Pressure transducers were positioned upstream and downstream of the kneading block to determine the pressure generation or consumption across this section. The investigated factors were the kneading disc stagger angle (30°, forwarding; 90°, neutral; -30°, reversing) and the polymer material properties.

The PP resins used in the experiments were Petrothene and HY6100, and the apparent shear viscosities of their blends with 5wt% Polymer C-SYN at 220 °C are presented in Figure 5.14. The viscosity data were fitted to power law models (the linear regression models are included in Figure 5.14 for comparison with the experimental data) and the calculated power law indices were: 0.35 for the HY6100 blend, 0.45 for the Petrothene blend, and 0.39 for the Petrothene/HY6100 (50:50) blend. GPC analysis of the molecular weight distributions of the PP resins was completed, and the average molecular weights and polydispersities (PDI) are presented in Table 4.1. As expected, the higher viscosity HY6100 PP resin also had the highest average molecular weights.

All experiments were completed with barrel temperatures of 220 °C in the melt-melt blending section and the metering section of the single screw extruder / adapter. A total mass flow rate of 50 g/min (25 g/min from each of the two segregated streams) and a screw speed of 75 rpm were used. For each kneading block design, experiments were completed to investigate the blending of identical melt streams and the blending of Petrothene and HY6100 melt streams (viscosity ratio = 2.3 at 10 s^{-1}). The polymer film collected at the slit

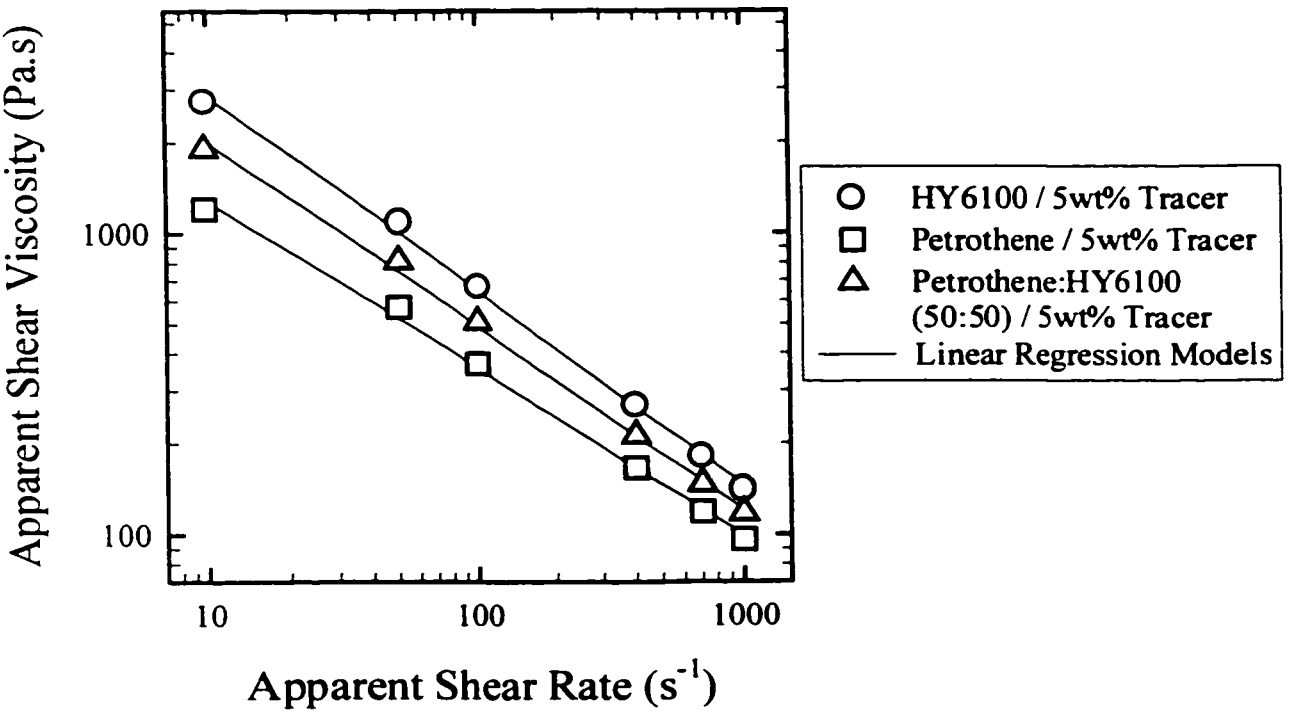

Figure 5.14. Apparent Shear Viscosity of the Investigated PP Resins with 5wt% Polymer C-SYN

die was used directly for FT-IR analysis of the anhydride conversion. Equation 4.2 was used to calculate the conversion from the relative peak heights, and the experimentally measured relative peak heights at zero and full conversion are presented in Table 5.5. The average pressures and net specific energy consumptions (Net SEC) are presented in Table 5.6. Net SEC, which is the net motor load divided by the mass throughput, is a measure of the total energy inputted into the polymer per unit mass (Rauwendaal, 1981).

Table 5.5. Relative Peak Heights Used in the Calculation of the Anhydride Conversion

Polymers Blended	RPH (Zero Conversion)	RPH (Full Conversion)
Petrothene / Petrothene	2.11	1.61
Petrothene / HY6100	2.36	1.75
HY6100 / Petrothene	2.38	1.80
HY6100 / HY6100	2.64	1.94

Table 5.6. Measured Net SEC and Average Pressure Values

Material Fed by Single/ Adapter	Material Fed by K-tron	Kneading Block Design	Net SEC (kW-hr/kg)	Pressure Upstream of Kneading Block* (MPa)	Pressure Upstream of Kneading Block** (MPa)	Die Pressure (MPa)
Petrothene	Petrothene	Neutral	0.48	1.83	1.14	2.02
Petrothene	Petrothene	Neutral	0.48	1.79	1.14	2.00
Petrothene	Petrothene	Neutral	0.48	1.83	1.14	2.02
HY6100	Petrothene	Neutral	0.48	2.34	1.45	2.55
Petrothene	HY6100	Neutral	0.56	2.28	1.45	2.65
HY6100	HY6100	Neutral	0.64	2.83	1.75	3.34
Petrothene	Petrothene	Forward	0.48	0.07	1.04	1.93
HY6100	Petrothene	Forward	0.48	0.04	1.26	2.52
Petrothene	HY6100	Forward	0.56	0.05	1.38	2.65
HY6100	HY6100	Forward	0.64	0.05	1.62	3.24
Petrothene	Petrothene	Reverse	0.48	3.54	1.01	2.00
HY6100	Petrothene	Reverse	0.60	4.52	1.28	2.55
Petrothene	HY6100	Reverse	0.68	4.62	1.28	2.55
HY6100	HY6100	Reverse	0.80	5.71	1.60	3.14

* Measured 15 mm upstream of first kneading disc, average over 10 minute time interval

**Measured 15 mm downstream of final kneading disc, located in the middle of the reverse conveying element, average over 10 minute time interval

Experimental results of the anhydride conversion are presented in Figure 5.15 (for each pair of polymers appearing in the legend, the first one refers to the stream fed to the twin screw extruder using the single screw extruder / adapter, and the second one was fed directly into the twin screw extruder using the K-tron feeder). From the replicated experiments, the reproducibility of the anhydride conversion was calculated to be 0.03, which is indicated by the error bar at the conditions of Petrothene / Petrothene blending with a stagger angle of 90°. For the blending of Petrothene PP and HY6100 PP, the feeding locations of the high viscosity and low viscosity polymer streams did not affect the mixing performance. From Figure 5.15, the blending of each combination of polymers indicated that the mixing performance of a kneading block followed by a reverse conveying element followed the trend of: forward (30°) > reverse (-30°) > neutral (90°). The experimental trend suggested that flow recirculation in the kneading block section was required to obtain good distributive mixing. In the case of forward and reverse kneading blocks, the flow directions of the drag and pressure components are in opposite directions. Conversely, the flow in a neutral kneading block is by pressure alone.

The most efficient mixing is expected to occur in the fully filled kneading block and the fully filled conveying elements (Chapter 7 discusses the mixing profile along the length of the extruder). As an example, the average pressure upstream of the kneading block for the blending of two HY6100 PP melt streams was 5.71 MPa (reverse), 2.83 MPa (neutral), and 0.05 MPa (forward). Therefore, the fully filled length prior to the kneading block followed the trend of: reverse > neutral > forward. As well, the Net SEC was greatest in the case of the screw configuration containing the reverse kneading block. With a lower amount of

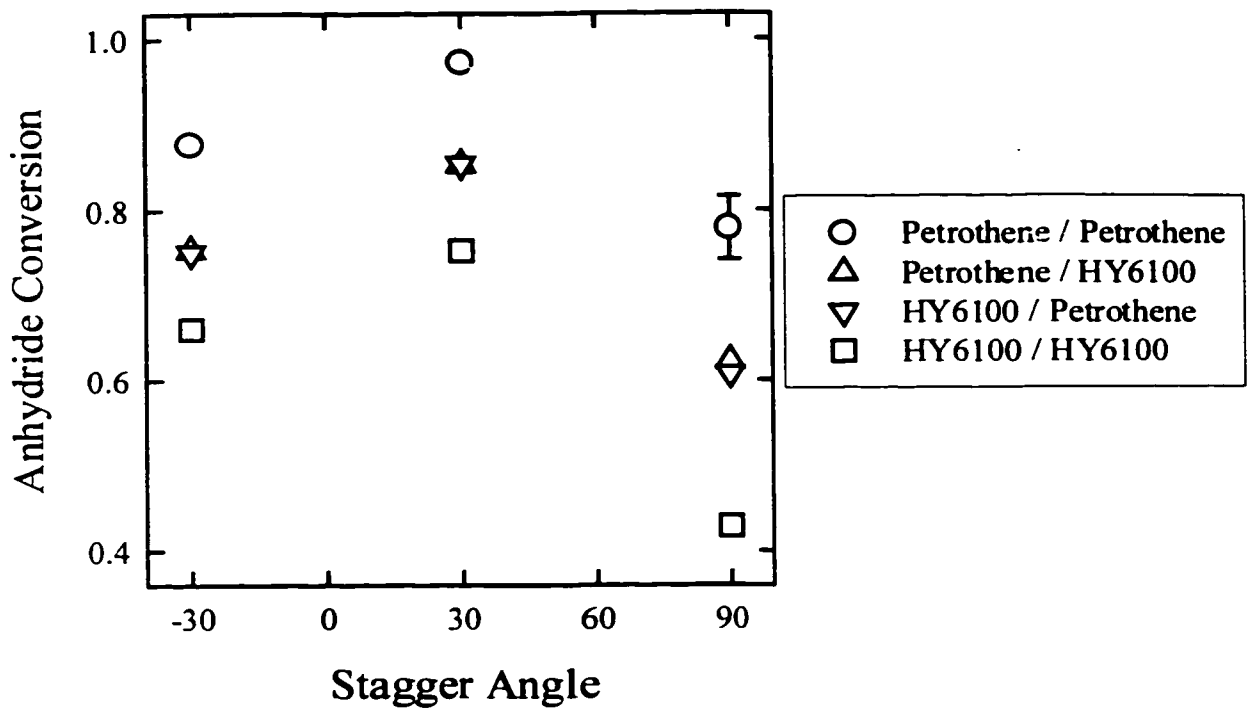

Figure 5.15. The Effects of Polymer Properties and Kneading Block Design on the Distributive Mixing During Melt-melt Blending

inputted energy and a shorter fully filled length prior to the kneading block, the forward kneading block section outperformed the reverse kneading block section.

The pressure upstream of the forward kneading block approached a zero value, which suggested that the forward kneading was partially filled. A break point position between the partially filled and the fully filled regions in the forward kneading block may have contributed to its superior mixing. After steady-state flow was established, the screws from the twin screw extruder were dead stopped and extracted to investigate the fill distribution in the kneading block section. Although a zero pressure was measured upstream of the forward kneading block, 2 to 3 conveying element channels were fully filled immediately upstream of the forward kneading block. The fill distribution in the melt-melt blending section is discussed in detail in Chapter 7. From visual inspection, the break point position was located in the conveying elements preceding the forward kneading block. As described in detail in Chapters 6 and 7, a possible reason for the superior mixing of the forward kneading block is the existence of stagnant regions in the flow.

The average channel depth in the kneading block was approximately 2 mm, which corresponds to an average shear rate of 66.8 s^{-1} at 75 rpm. The relationship between mixing performance and polymer viscosity at 66.8 s^{-1} is presented in Figure 5.16 (for each kneading block design, the lowest viscosity corresponds to the blending of two Petrothene streams, and the highest viscosity to the blending of two HY6100 streams). For each screw configuration, the mixing performance decreased with an increase in polymer viscosity. As reviewed by Meijer and Janssen (1994), droplet breakup during immiscible polymer blending in shear flows is most easily accomplished when the viscosities of the dispersed phase and the matrix are matched (viscosity ratio = 1). The viscosity ratio was equal to one for the blending of

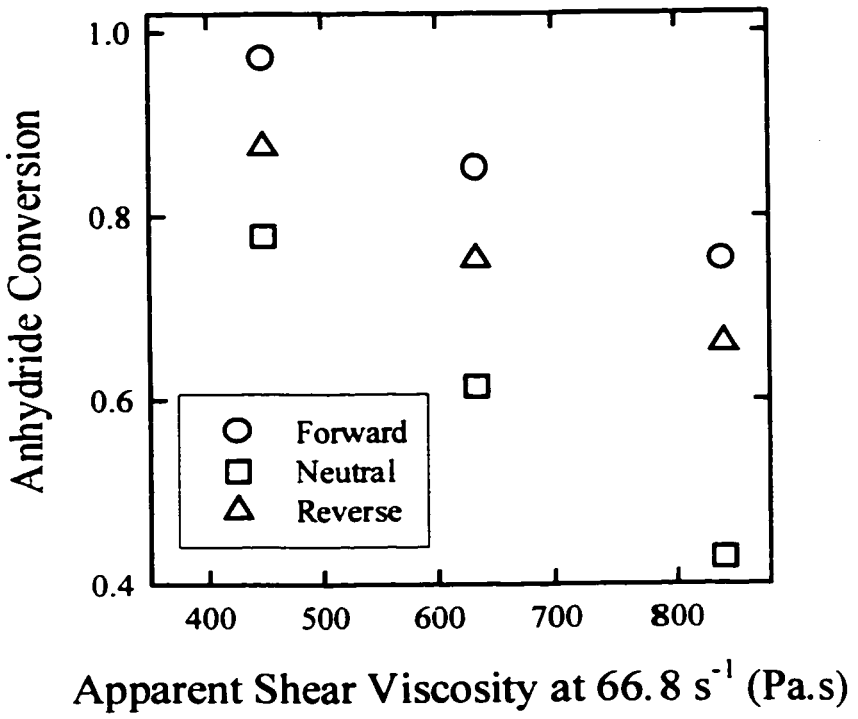

Figure 5.16. Relationships Between Mixing Performance and Polymer Viscosity

two Petrothene streams and the blending of two HY6100 streams, but the distributive mixing performances were significantly different.

Polymer viscosity affects the pressure flow in the kneading discs. The mixing performance of the screw configuration containing the neutral kneading block was the most sensitive to changes in the viscosity because the flow in the neutral kneading block is by pressure alone. White and Szydlowski (1987) presented screw characteristic curves of the dimensionless flow rate versus the dimensionless pressure in forward, neutral, and reverse staggered kneading discs. Similar to the mixing performance trends, the flow in the neutral kneading discs was predicted to be more sensitive to changes in the pressure and polymer viscosity than the flow in forward or reverse kneading discs.

As previously discussed, distributive mixing in twin screw extruders depends on the applied strain, which is related to the shear rates, residence times, and degree of fill. Using the local residence time method described in section 4.3.4.2, the average residence time from the melt feeding location to the end of the kneading block section (middle of the reverse conveying element) was measured for the flow of pure Petrothene and HY6100 in the screw configuration containing the neutral kneading block at 50 g/min and 75 rpm. The local residence time measurements are discussed in detail in Chapter 7. The average residence times were 107.3 s for Petrothene and 110.8 s for HY6100. As well, the fully filled length in the conveying section prior to the neutral kneading block was measured by visual inspection of the extracted screws of the twin screw extruder. The axial fully filled length prior to the neutral kneading block was 55 mm for the flow of both PP resins. Therefore, the polymer viscosity did not significantly affect the residence time or the fill distribution in the twin screw extruder.

Based on the comparison of the residence times and fill distributions, a similar strain was applied to both PP melts during their flow in the extruder. According to the classical investigation of distributive mixing by Spencer and Wiley (1951), the generation of interfacial area is related to the applied strain, the initial interfacial area, and its orientation in the flow field. Thus, a similar generation of interfacial area is expected during melt-melt blending of either Petrothene or HY6100 PP. From Figure 5.15, the anhydride conversions for the screw configuration with the neutral kneading block were 0.779 for melt-melt blending Petrothene and 0.429 for melt-melt blending HY6100. The anhydride conversion was linearly related to the total amount of interfacial area generated in the extruder, and therefore, 1.8 times more area was generated during the melt-melt blending of the lower viscosity Petrothene PP. This significant difference in the distributive mixing indicated that the mixing process also depended on the polymer properties.

Numerical simulations of Nichetti and Manas-Zloczower (1999) predicted that distributive mixing is easier to complete using lower molecular weight and broader MWD polymers. The numerical predictions were based on the analysis of the line stretch distributions from particle tracking of initial clusters of particles in the channel of a single screw extruder. The particle spreading was significantly greater in lower molecular weight polymers. In addition, Erwin (1978) showed that the energy required to generate an increase in the interfacial area is linearly related to the polymer viscosity. The experimental comparison of the melt-melt blending of Petrothene and HY6100 PP resins confirmed the proposed trends of Nichetti and Manas-Zloczower (1999) and Erwin (1978). Therefore, both material properties and the applied strain must be considered when evaluating the distributive mixing process. Owing to its lower viscosity and molecular weight, interfacial area was

significantly easier to generate during the melt-melt blending of Petrothene PP in the extruder.

As indicated in Figure 5.9, the anhydride conversion was linearly related to the interfacial area available for reaction when the same material was used in all the PP layers. The diffusion rates of the tracers in different viscosity PP melts may influence the conversion of the interfacial reaction. Therefore, model interfacial reactions were completed in the hot press to investigate the diffusion rates of the polymer tracers in the Petrothene and HY6100 PP resins. Using a similar method as described in section 4.3.2, two stacks of thin films were compression molded in the hot press to complete the model reactions. Each film stack consisted of: one layer of Petrothene containing 5wt% anhydride polymer tracer (thickness = 0.9 mm), one layer of pure Petrothene or HY6100 PP (thickness = 0.4 mm), and one layer of Petrothene containing 5wt% amine polymer tracer (thickness = 0.9 mm). The only difference between the two film stacks was the PP used in the middle layer. The reactions were controlled by the diffusion of the polymer tracers in the pure PP layer followed by their rapid coupling. Both reactions were completed at 200 °C, with an applied pressure of 5.5 MPa. At desired reactions times, the mold and its contents were rapidly cooled in a water bath and off-line FT-IR analysis of the anhydride conversion was completed. After each analysis, the films were further reacted in the hot press for a total reaction time of 6 hrs. The anhydride conversion profiles with respect to reaction time are presented in Figure 5.17.

The conversion profiles were very similar, and the viscosity of the PP resin in the middle layer only affected the conversion during reaction times between 15 to 60 min. During these reaction times, the conversion was slightly higher (average conversion difference = 0.06, experimental error = 0.03) in the case of the lower viscosity Petrothene PP

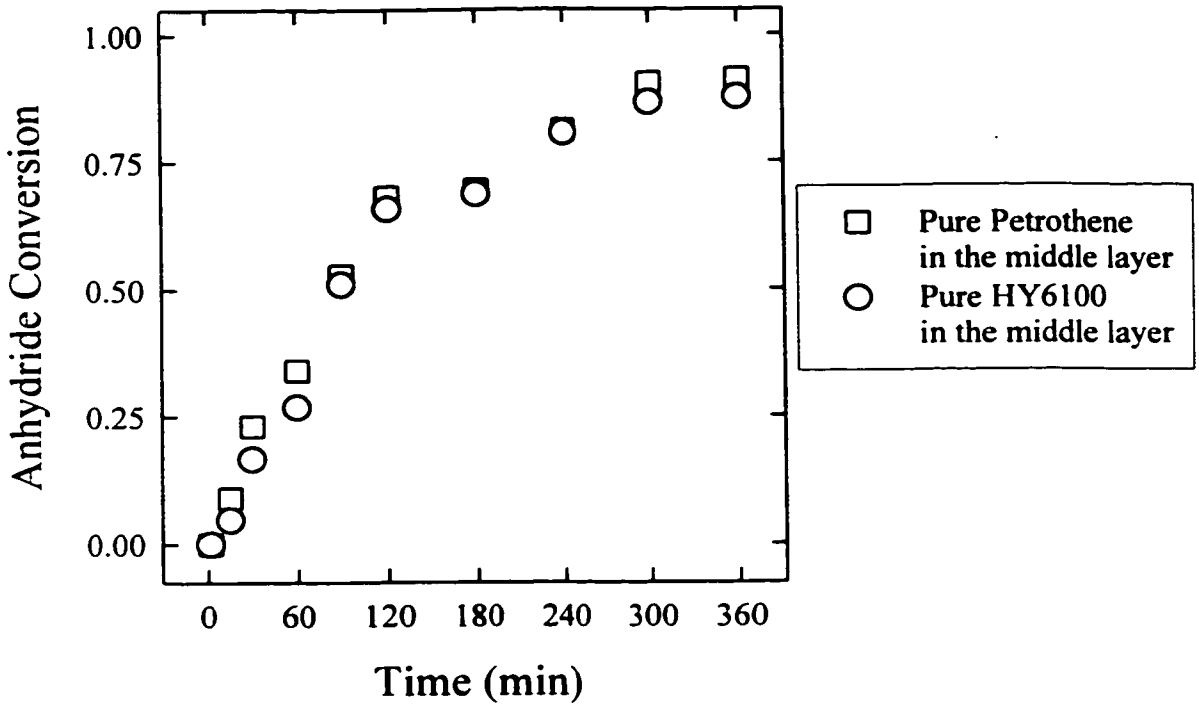

Figure 5.17. Conversion Profiles for the Model Reactions Investigating the Diffusion of the Polymer Tracers in Different Viscosity PP Resins

middle layer. Overall, the experimental results suggested that the diffusion rates of the polymer tracers in the molten PP were not significantly different. Therefore, the significantly lower anhydride conversion that was measured during the melt-melt blending of the higher viscosity HY6100 PP was not caused by a diffusion limitation of the polymer tracers in this higher viscosity PP. As well, diffusion of the tracers during typical residence times in the extruder (approximately 1 to 3 min, results presented in Chapters 6 and 7) is very limited. In the model interfacial reactions controlled by the diffusion of the polymer tracers in the molten PP (Figure 5.17), the anhydride conversions were less than 0.09 for reaction times of 15 min.

Two PP resins were studied in the experiments, and therefore, only limited conclusions can be drawn concerning the effects of polymer properties on the distributive mixing process. Differences in the elastic properties of Petrothene and HY6100 PP may also have affected the mixing performance. A capillary rheometer with four dies of different L/D ratios (diameter = 0.508 mm, L/ D = 2, 20, 40, 50) was used to determine the Bagley corrections and entrance pressure drops for the two investigated PP resins. The capillary experiments were completed using the pure resins at 220 °C at shear rates from 10 to 1000 s^{-1}. In the entry region of the capillary, the flow profile is not fully developed. A large entrance pressure drop results from the following three contributions: addition of kinetic energy to accelerate the polymer melt from the barrel into the capillary, viscous dissipation of energy due to rearrangement of the velocity profile at the capillary entrance, and storage of a certain amount of energy in the viscoelastic polymer melt as it undergoes elongational flow at the entrance (Rosen, 1993). The first two contributions occur during the flow of both non-viscoelastic and viscoelastic materials into a capillary, and the storage of elastic energy arises

from chain uncoiling (Brydson, 1981). If two polymers are compared, the polymer with the highest elasticity will store the most elastic energy at the capillary entrance and exhibit a corresponding higher entrance pressure drop. Shida *et al.* (1977) showed that the entrance pressure drop can be used as a relative measurement of elasticity, which depends on the degree of long chain branching or the fraction of high molecular weight polymer chains in the material, if the comparison of the materials is completed at a constant shear stress. At a constant shear rate, polymers with different viscosities exhibit different entrance pressure drops even if the degree of long chain branching and the fraction of high molecular weight polymer are identical. Therefore, the entrance pressure drop must be plotted with respect to the shear stress to eliminate its dependence on the polymer viscosity. The measured entrance pressure drops for the investigated PP resins are related to the apparent shear rate and corrected shear stress in Figure 5.18.

The entrance pressure drops of the two PP resins converged at low shear rates. In the range of shear rates commonly experienced in the twin screw extruder (approximately 50 to 500 s^{-1}), HY6100 PP exhibited an entrance pressure drop approximately twice the value of Petrothene PP. The entrance pressure drops for both PP resins followed the same curve with respect to the Bagley corrected shear stress. According to Shida *et al.* (1977), this overlapping indicated that there is no relative difference in the elastic properties of the two investigate PP resins. In a twin screw extruder, the shear rates are determined by the screw geometry and the screw speed. If two polymers of different viscosities are extruded at the same screw speed, similar shear rates will be applied to both polymers. Small differences in the shear rates may arise due to differences in the degree of fill. Conversely, the shear stress that is applied to each polymer depends on the shear rate and the polymer viscosity.

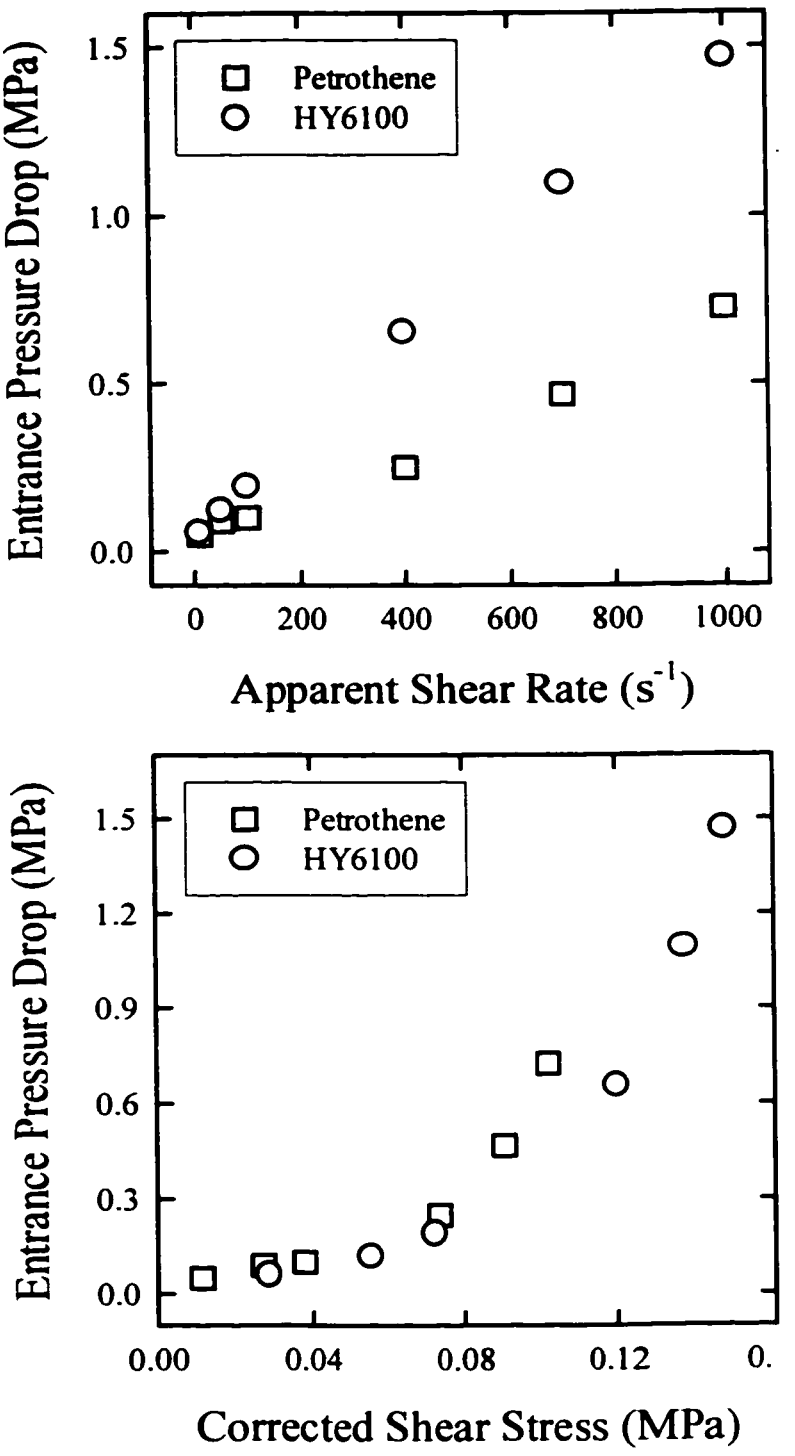

Figure 5.18. Entrance Pressure Drops of the Investigated PP Resins

Therefore, it may be more realistic to compare the elastic properties of the two polymers at a constant shear rate to understand the behavior of the polymers during extrusion. The method of Shida *et al.* (1977) is more effective for polymer characterization because it separates the effects of elasticity from viscosity, but it may not accurately represent the conditions experienced by the polymers during extrusion. Therefore, differences in the elastic properties of the two PP resins at constant shear rates may have contributed to the effect of the material properties on the mixing performance during melt-melt blending.

5.2.4. Validation of the Experimental Method and Final Comments

The main assumptions of the experimental method used in this research to analyze distributive mixing are: the reaction occurs at the interface, the reaction is irreversible, the conversion is not limited by the diffusion of the tracers, the reaction does not affect the interfacial properties, and the reaction rate is not controlled by the chemical kinetics. Model interfacial reactions verified the first three assumptions, and it was shown that the conversion was linearly related to the interfacial area available for the reaction (Figure 5.9). As well, the coupling of the tracers does not affect the interfacial properties because of their low molecular weight. The final assumption was tested by performing a melt-melt blending experiment in the twin screw extruder. Melt-melt blending of Petrothene with 5wt% anhydride reactive polymer and Petrothene with 10wt% amine reactive polymer was completed using the screw configuration with the neutral kneading block (same screw configuration as used in the experiments discussed in section 5.2.3). If chemical kinetics controls the reaction, the anhydride conversion will be higher when 10wt% amine reactive polymer is used as compared with 5wt% amine reactive polymer. The calculated anhydride

conversion for blending with 10wt% amine reactive polymer was 0.797. From the previous experiments with the same screw configuration and operating conditions, the anhydride conversion for blending with 5wt% amine reactive polymer was 0.779. These two conversions were not significantly different because the measured experimental error in the anhydride conversion was 0.03. The anhydride conversion was not dependent on the amine tracer concentration, and therefore, it was not controlled by the chemical kinetics.

Wu (1994) used low molecular weight anhydride and amine compounds to investigate micromixing in a twin screw extruder, and bubbles were observed in the analyzed samples. These bubbles were caused by the evolution of water during the cyclization reactions, which vaporized when the pressure in the extruder became lower than the vapor pressure of water. It was proposed that the bubbles may significantly interfere with the mixing analysis by causing secondary flows in the polymer melt and limiting diffusion of the reactants at the interfaces. In all the melt-melt blending experiments in the twin screw extruder with the polymer tracers, no bubbles were observed in the collected films. FT-IR analysis of the characteristic peak of the imide at 1710 cm^{-1} confirmed that there was no imide formation during the melt-melt blending process in the extruder. This result was expected because of the short residence times in the extruder and the slow kinetics of the cyclization. Vermeesch *et al.* (1993) and Vermeesch and Groeninckx (1994) achieved imidation of SMA during the short residence time of the twin screw extruder at elevated temperatures (240 – 265 °C), with venting to remove the water byproduct. In the absence of venting, such as in the melt-melt blending experiments completed in this research, there is no strong driving force for the cyclization and the corresponding evolution of water.

The novel experimental method for analyzing distributive mixing using reactive polymer tracers has two limitations. The first limitation is the inability to account for demixing during the processing in the extruder. Using numerical methods, Bigio and Conner (1995) predicted that sections of a line connecting two points in the flow of a single screw extruder grow, or stretch, while other sections of the line shrink. Therefore, it is possible for interfacial area to continuously grow and shrink as the polymer travels through the twin screw extruder. During the melt-melt blending experiments, the polymer tracers instantaneously reacted when brought into contact at the grow interfaces. This chemical reaction did not proceed in the reverse direction if the generated interfacial area demixed (shrunk) upon further processing in the extruder. Therefore, the reaction conversion actually measured the maximum amount of interfacial area generated during the blending process in the twin screw extruder.

Spencer and Wiley (1951) proposed that viscous fluid mixing involves the following two processes: the generation of interfacial area via deformation of the fluids in the flow field and the distribution of the interface throughout the volume of the mixing fluid. The conversion of the interfacial reaction between the polymer tracers is a direct measurement of the generation of interfacial area, but it does not indicate how the interface is distributed throughout the blended polymer. The distribution of the interfaces can be visually investigated by blending two polymers with different colors (similar to the blending of white and black pigmented streams of a silicone fluid by Bigio and Erwin, 1985). After steady-state flow is established, the polymer in the extruder is quickly frozen. The polymer carcass is then removed from the screws, and the distribution of the interfaces in different cross sections of the flow can be visually investigated. As previously mentioned, Bigio and Erwin

(1985) attempted to count the number of striations in the flow cross sections of a twin screw extruder to measure the distributive mixing. This method was limited to the analysis of distributive mixing in small sections of the extruder due to the complex striation patterns that were formed. In addition, "greying" of the black and white fluids or an inability to resolve thin striations also severely limited the analysis of the mixing. Clearly, the reactive polymer tracer method is superior for the analysis of interfacial area generation during the complex flow in twin screw extruders.

5.3. Concluding Remarks

The mixing limited reaction between the reactive polymers was effectively used as a microscopic probe to gain direct measurements of the mixing performance during polymer blending of segregated melt streams in a co-rotating twin screw extruder. Hexadecylamine, a small molecule analog of the amine reactive polymer, rapidly migrated through the molten PP and reacted with the anhydride functional groups. Owing to this rapid migration and possible incompatibility with the PP matrix, small molecule polar compounds cannot be used as reactive tracers in PP resins. Using model interfacial reactions and preliminary blending experiments, the key assumptions concerning the reactive polymer tracer method for analyzing distributive mixing were verified. In particular, the anhydride functional group conversion measured by FT-IR analysis was confirmed to be a direct indication of the interfacial area available for the reaction. Therefore, the conversion at the end of the twin screw extruder was a direct measurement of the overall distributive mixing performance as well as the micromixing because the chemical reaction is a molecular event.

From preliminary melt-melt blending experiments, a temperature difference of 60 °C between the segregated polymer melts did not significantly affect the mixing. This indicated that the temperature difference was an ineffective method for producing a viscosity ratio. Blending of different PP resins indicated that the distributive mixing performance was related to the polymer viscosity and not the viscosity ratio. The best mixing was achieved during the blending of two low viscosity segregated polymer melt streams. As well, the elastic properties of the PP resin may contribute to the observed difference in the mixing performances. The experimental results with different viscosity PP resins indicated that distributive mixing depends on both the applied strain and the material properties.

No interaction was observed between the effects of polymer properties and kneading block design on the distributive mixing performance. For each combination of the polymer melt streams, the mixing performance followed the trend of: forward > reverse > neutral. This trend was attributed to the positive effect of flow recirculation in the kneading block section on distributive mixing. Finally, the non-linear effect of screw speed on distributive mixing was attributed to the competing contributions of shear rate, residence time, and channel fill on the mixing process.

CHAPTER 6
THE EFFECTS OF KNEADING BLOCK DESIGN AND OPERATING CONDITIONS ON DISTRIBUTIVE MIXING AND RESIDENCE TIME DISTRIBUTION

The experimental method for analyzing distributive mixing during polymer blending in a twin screw extruder was validated by the model interfacial reactions and the preliminary melt-melt blending experiments. In particular, the coupling of the reactive polymers is controlled by the generation of interfacial area. This chapter presents a detailed analysis of distributive mixing and residence time distributions (RTD) during melt-melt blending in the twin screw extruder. The focus of the experiments was to determine the effects of kneading block design and operating conditions on the distributive mixing and the degree of macromixing. Combining these two measurements yielded a complete picture of the mixing at both the microscopic and macroscopic scales in the extruder. Possible relationships between distributive mixing and the RTD variables were investigated, and particular attention was given to the identification of the controlling factors for distributive mixing during polymer blending.

6.1. Distributive Mixing Measurements

As in the previous melt-melt blending experiments, the tandem extruder apparatus (Figure 4.2) was used to perform the experiments with equal mass flow rates in the two segregated polymer melt streams. The experiments were completed using Petrothene PP in both segregated streams with 5wt% reactive polymer tracer. Blending two identical polymer melts (identical PP resin, different reactive polymer tracer in each stream) eliminated the effects of interfacial tension on the mixing process. Therefore, the experimental results

indicated the maximum distributive mixing capability of the melt-melt blending section of the twin screw extruder. Generation of interfacial area between two incompatible polymer melts is resisted by the interfacial tension. The screw configuration, feeding arrangement, and location of the pressure transducers are depicted in Figure 6.1. The barrel temperatures in the melt-melt blending section and the metering zone / adapter of the single screw extruder were maintained at 220 °C. As in the previous experiments, the melt feeding location was partially filled, the kneading block consisted of 16 adjacent bilobal kneading discs, and the pressure immediately downstream of the reverse conveying element (P4) after the kneading block was zero. Determination of the anhydride conversion was completed by FT-IR analysis of the film collected at the slit die. Equation 4.2 was used to calculate the conversion, and the measured relative peak heights (ratio of absorbances at 1793 cm^{-1} and 528.5 cm^{-1}, presented as ninety-five percent conversion) for zero conversion and full conversion were 2.170 $\pm$ 0.020 and 1.451 $\pm$ 0.023, respectively. The experimental factors were: the design of the kneading block (stagger angles of 30°, forward; 90°, neutral; -30°, reverse), the screw speed of the twin screw extruder (50 – 200 rpm), and the total flow rate (50 or 100 g/min).

The experimental results of the anhydride conversion are presented for each screw configuration in Figure 6.2. The experimental results (symbols) are compared with regression models (lines), and the regression results are discussed at the end of this section. The error bars represent the standard errors obtained from five films collected at every set of operating conditions (error bars smaller than the data symbols are not visible in Figure 6.2). The average estimate of the experimental error for the anhydride conversion was 0.019. As well, replicate experiments were completed with the screw configuration containing the

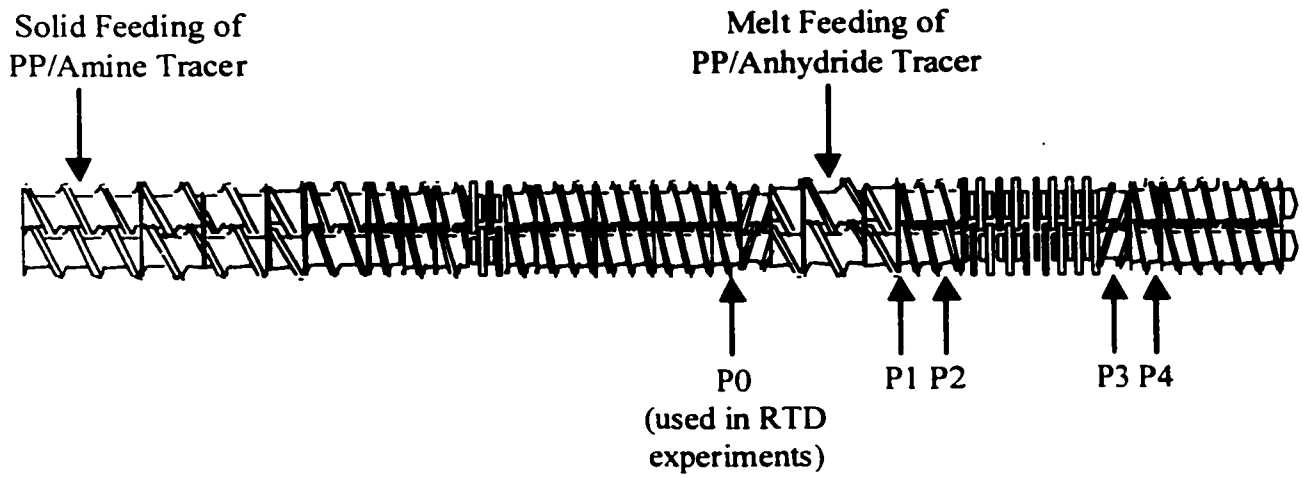

Temperature Profile

130 °C	170 °C	200 °C	210 °C	220 °C	220 °C	220 °C	220 °C	220 °C	220 °C

Figure 6.1. Screw Configuration, Feeding Arrangement, and Locations of the Pressure Transducers for Melt-melt Blending

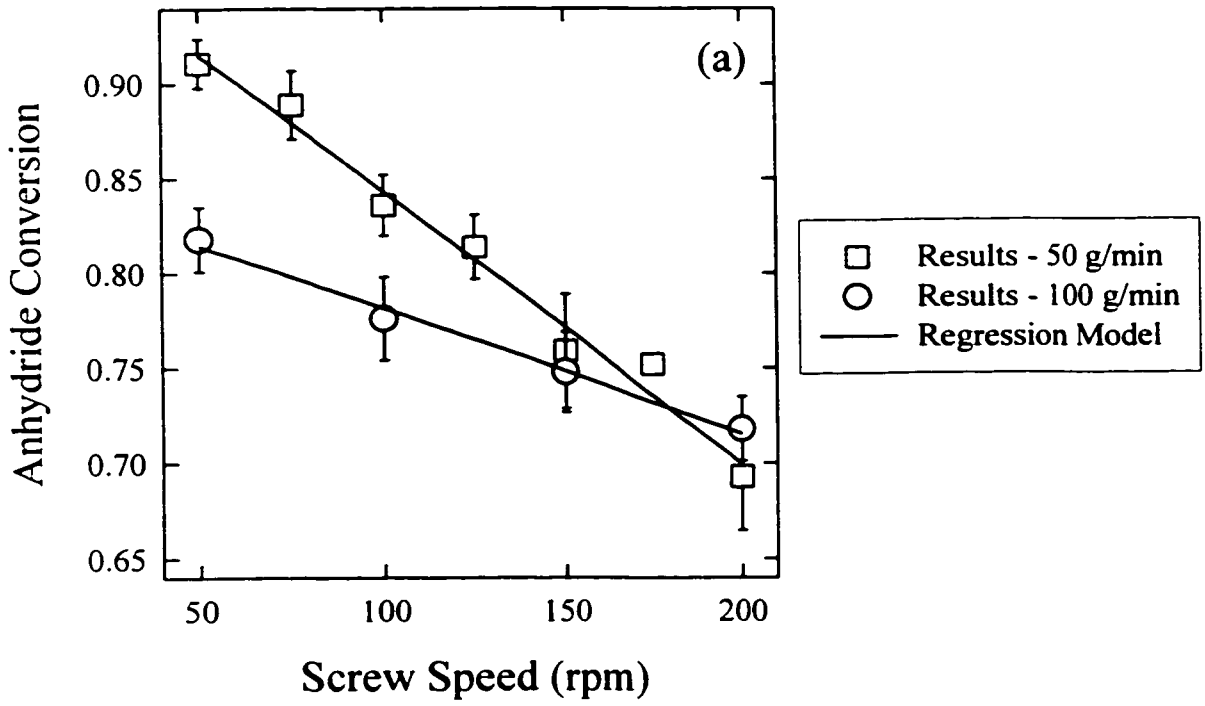

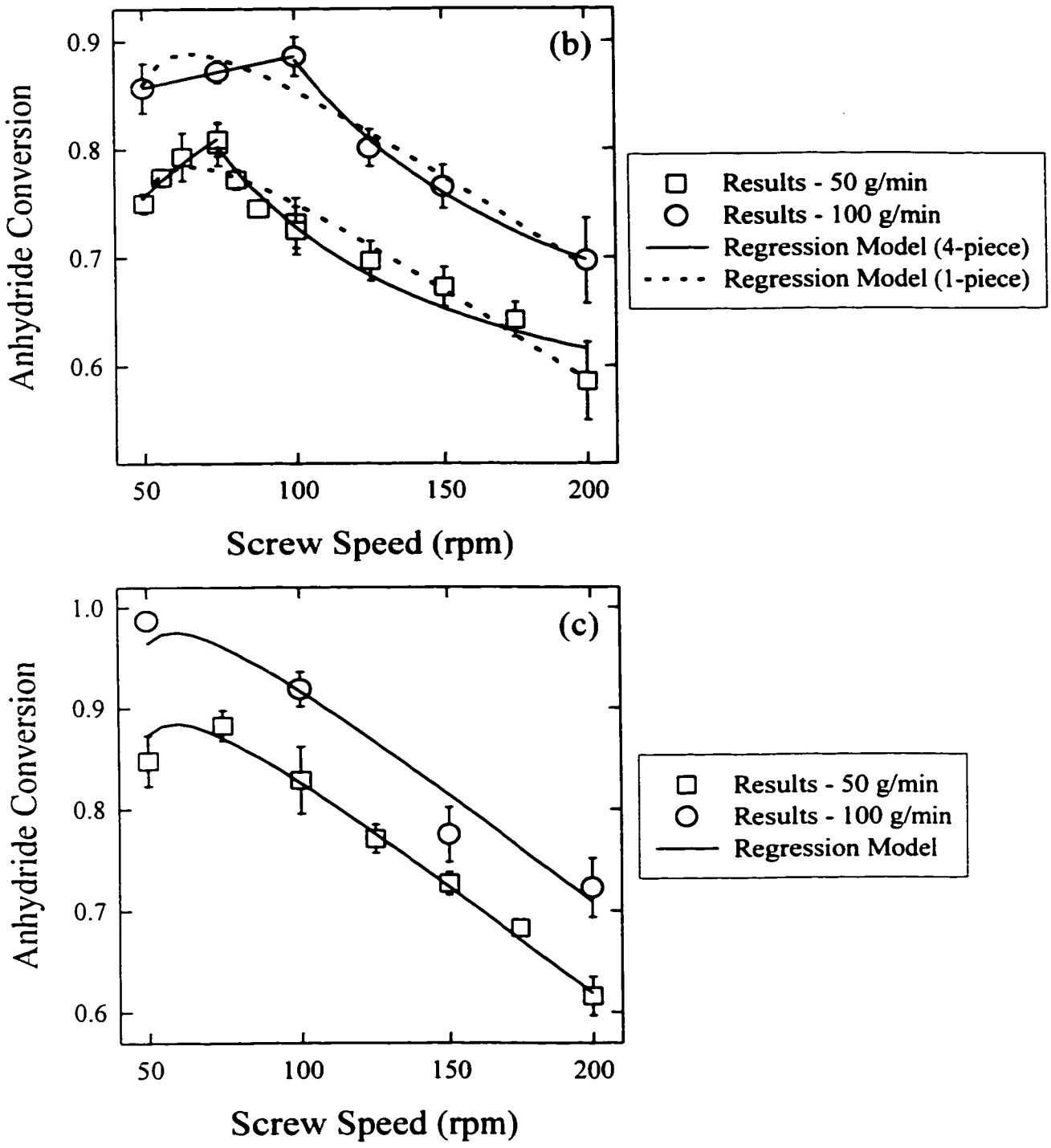

Figure 6.2. Anhydride Conversion Results from the Distributive Mixing Experiments
(a) Screw Configuration with Forward Kneading Block
(b) Screw Configuration with Neutral Kneading Block
(c) Screw Configuration with Reverse Kneading Block

neutral kneading block at the conditions of 50 g/min and 75 and 100 rpm. Comparison of the replicate averages indicated that the error between separate experiments was less than 2%. Screw speed and flow rate exhibited negative effects on the mixing performance of the screw configuration with the forward kneading block. Conversely, screw speed exhibited a non-linear effect on the mixing performances of the screw configurations with the neutral and the reverse kneading blocks. As well, flow rate exhibited a positive effect on the mixing performances of these two configurations. Clearly, mixing performance was dependent on the combination of the kneading block design and the operating conditions.

Efficient mixing occurs predominately in kneading blocks and fully filled conveying elements, which exhibit flow recirculation because of the negative pressure flow component (verified during the mixing profile experiments discussed in Chapter 7). The average pressure upstream of the kneading block (transducer P2 was located 15 mm upstream of the first kneading disc, pressure was averaged over a 10 minute time interval for each set of operating conditions) is presented in Figure 6.3. A higher pressure upstream of the kneading block corresponds to a longer polymer backup length, or a larger fully filled volume prior to the kneading block. As expected, the fully filled volume prior to the kneading block followed the trend of: reverse > neutral > forward. The average pressure at the reverse conveying element following the kneading block (P3) was the same for all three screw configurations at equal operating conditions. Screw speed and flow rate exhibited small positive effects on the pressure at P3, with the pressure increasing from a minimum of 1.1 MPa at 50g/min and 50 rpm to a maximum of 1.38 MPa at 100 g/min and 200 rpm. The pressure difference between P2 and P3 indicated that the forward kneading block generated pressure, and as expected, the neutral and reverse kneading blocks consumed pressure.

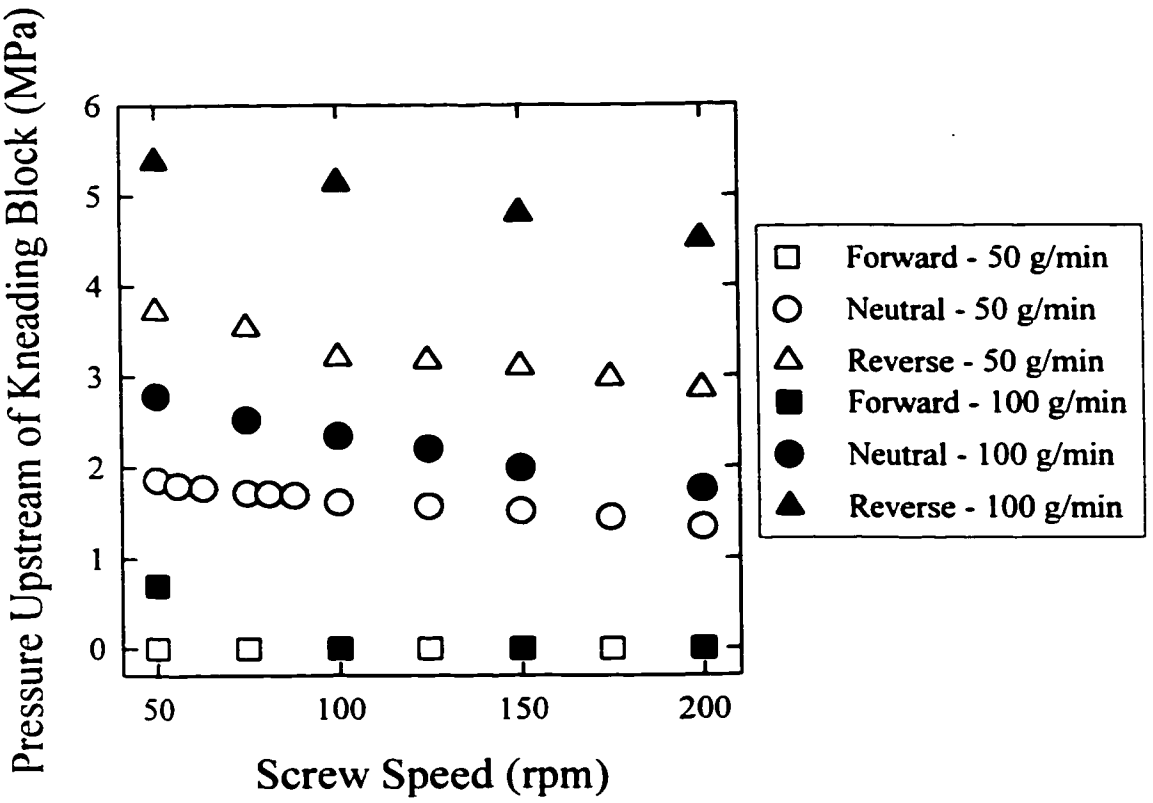

Figure 6.3. Average Pressure Upstream (P2) of the Kneading Block

Screw speed affects the distributive mixing process through the applied strain by the following contributions: shear rate, residence time, and fully filled volume. A more detailed explanation of the effect of average residence time is discussed in section 6.3. From Figure 6.3, the fully filled volume in the melt-melt blending section with the neutral and reverse kneading blocks decreased with an increase in screw speed. The non-linear screw speed effects (Figures 6.2 b and c) observed for the screw configurations with the neutral and reverse kneading blocks were attributed in part to the competing effects of shear rate, residence time, and fully filled volume. Conversely, the mixing performance of the screw configuration with the forward kneading block may have been dominated by the effect of reduced residence time at higher screw speeds and flow rates.

Flow rate affects the average residence time and the fully filled volume, which exhibit competing effects on the distributive mixing process. The screw configurations with the restrictive neutral and reverse kneading blocks exhibited improved mixing at the higher flow rate, which suggested that the increase in the fully filled volume dominated the effect of reduced residence time. A simultaneous increase in productivity and product uniformity was achieved by increasing the flow rate. Conversely, the mixing performance of the screw configuration with the forward kneading block decreased as the flow rate was increased. Thus, there is a fundamental difference between the effects of operating conditions on the mixing performances of screw configurations containing pressure consuming and pressure generating kneading blocks.

The experiments were not completed under isothermal conditions, and all three screw configurations exhibited viscous (shear) heating at screw speeds between 125 and 200 rpm. Viscous heating was manifested by an increase of 8 to 30 ^{o}C in the barrel temperature at the

location of the kneading block. As well, the melt temperature at the die (measured using an infrared temperature probe) increased by 6 to 12 °C. This temperature increase affected the reaction kinetics, but the interfacial reaction remained mixing limited. The magnitude of the temperature increase depended on the screw speed and flow rate. In the previous experiments discussed in section 5.2.2, which were completed using the KF6100 PP and a screw configuration containing a neutral kneading block at 50 g/min, the sharp decrease in the mixing performance occurred simultaneously with the onset of viscous heating. Conversely, the maximum mixing performance was observed at 75 rpm, and the onset of the viscous heating occurred at 125 rpm for the new experiments with the Petrothene PP at the same experimental conditions. Therefore, viscous heating was not the direct cause of the sharp decrease in the mixing performance at higher screw speeds.

The mixing performances of the three screw configurations are compared in Figure 6.4. At 50 g/min, the mixing performance followed the trend of: forward > reverse > neutral. Conversely, at 100 g/min, the mixing performance followed the trend of: reverse > neutral > forward at the screw speeds of 50 and 100 rpm. At the screw speeds of 150 and 200 rpm, the mixing performances of all three screw configurations were approximately equal. From Figure 6.4, the same level of distributive mixing was obtained from many different combinations of the experimental factors. For example, an anhydride conversion of approximately 80% was obtained using a forward kneading block with a flow rate of 100 g/min and a screw speed of 75 rpm, or a flow rate of 50 g/min and a screw speed of 130 rpm. The same level of mixing was obtained using a neutral kneading block with a flow rate of 100 g/min and a screw speed of 140 rpm, or a flow rate of 50 g/min and a screw speed of 75 rpm. Finally, the same level of mixing was obtained using a reverse kneading block

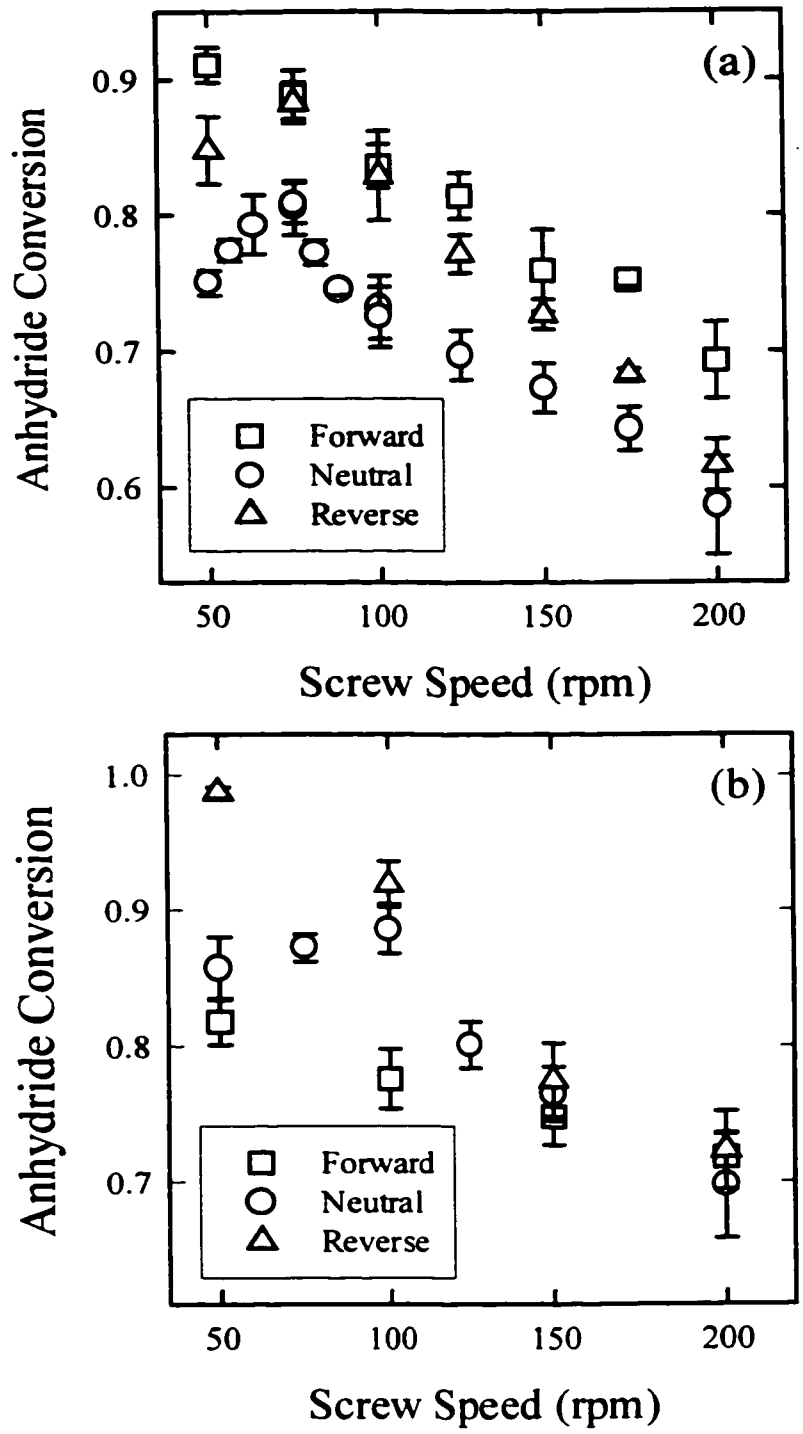

Figure 6.4. Comparison of the Mixing Results from the Three Screw Configurations
(a) 50 g/min
(b) 100 g/min

with a flow rate of 100 g/min and a screw speed of 155 rpm, or a flow rate of 50 g/min and a screw speed of 115 rpm.

Using the results obtained from the screw configuration with the neutral kneading block as a basis, the relative mixing performances of the screw configurations containing the forward and reverse kneading blocks are presented in Figure 6.5. The linear relationship between interfacial area and anhydride conversion was verified in Chapter 5 (Figure 5.9). Therefore, the maximum relative difference between the distributive mixing performances of the three screw configurations was 35%.

As compared with the screw configurations containing the pressure consuming kneading blocks, the mixing performance of the screw configuration with the forward kneading block was superior at 50 g/min and inferior at 100 g/min (at screw speeds of 50 and 100 rpm). In Chapter 5, it was proposed that a break point position located in the forward kneading block may contribute to its superior mixing performance. From Figure 6.3, pressure measurements suggested that the forward kneading block was partially filled for all the combinations of the operating conditions expect at 100 g/min and 50 rpm. After establishing steady-state flow, the screws were dead stopped and extracted from the extruder to inspect the fill distribution. From visual inspection, the forward kneading block appeared to be fully filled for all of the operating conditions, and a detailed analysis of the fill distribution is presented in Chapter 7. Therefore, the position of the break point does not explain the mixing performance of the screw configuration with the forward kneading block, an alternative explanation is offered in section 6.3.

Linear regression analysis was completed to quantify the effects of screw speed (N) and flow rate (Q) on the mixing performance of each screw configuration. The regression

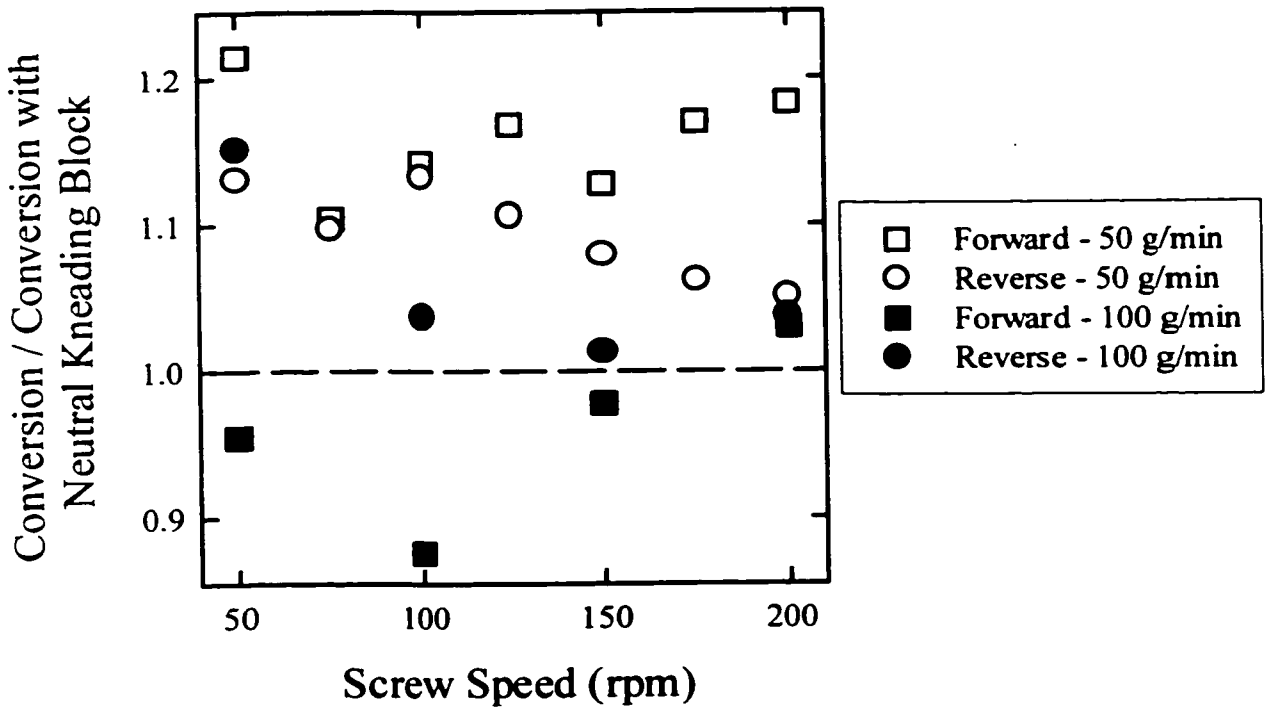

Figure 6.5. Relative Mixing Performances Using the Results from the Screw Configuration with the Neutral Kneading Block as a Basis

models are compared with the experimental results in Figure 6.2 (except in the case of the 4-piece model for the screw configuration with the neutral kneading block, the two regression lines in each figure represent a single model with one line for each value of the flow rate), and the model equations are presented in Table 6.1. All the terms included in the model equations were significant at the 95% confidence level.

Table 6.1. Regression Models of the Distributive Mixing Results for the Three Screw Configurations with Different Kneading Block (KB) Designs

KB Design	Model Equation		r^2
Forward	Conversion = $1.13 - 2.22*10^{-3}(N) - 2.80*10^{-3}(Q) + 1.56*10^{-5}(N*Q)$		0.9845
Neutral (1-piece)	Conversion = $0.82 - 1.67*10^{-3}(N) + 2.09*10^{-3}(Q) - 516000/(N^4)$		0.9547
Neutral (4-piece)	Conversion = $2.34*10^{-2} + 0.31*\log(N)$	; 50 g/min, 50 - 75 rpm	0.9548
	Conversion = $0.50 + 22.4/(N)$	; 50 g/min, 75 - 200 rpm	0.9575
	Conversion = $0.83 + 5.8*10^{-3}(N)$	; 100 g/min, 50 - 100 rpm	0.9996
	Conversion = $0.51 + 37.11/(N)$	; 100 g/min, 100 - 200 rpm	0.9945
Reverse	Conversion = $0.95 - 2.11*10^{-3}(N) + 1.82*10^{-3}(Q) - 387000/(N^4)$		0.9727

Units: N [=] rpm, Q [=] g/min

In the case of the neutral kneading block experimental results, regression analysis was completed using all the data in a single model (1-piece) and with data partitioning (4-piece). As indicated in Figure 6.2 (b), the 1-piece model cannot account for the sharp decrease in the mixing performance immediately after the maximum conversion. As well, the 1-piece model cannot account for the effect of flow rate on the location of the maximum conversion.

Therefore, the experimental results were partitioned into 4 pieces to improve the fit quality by including the discontinuities in the results at the maxima. The residual sum of squares for the 1-piece and 4-piece models were $4.85*10^{-3}$ and $2.12*10^{-3}$, respectively. The 56.3% reduction in the residual sum of squares indicated that data partitioning resulted in a much better fit to the experimental results.

The non-linear effect of screw speed on mixing with the neutral kneading block was incorporated into the 1-piece model with the $1/N^4$ term, but the screw speed coefficients lacked physical meaning. Conversely, data partitioning revealed the true non-linear screw speed effect. At each flow rate, screw speed exhibited an initial positive effect on the mixing performance, which was attributed to an increase in shear rate. The sharp drop in the mixing performance after the maximum conversion was attributed to the decreases in residence time and fully filled volume, which may have dominated the effect of an increase in shear rate. The position of the maximum conversion increased from 75 rpm at 50 g/min to 100 rpm at 100 g/min. This shifting was attributed to an increase in the fully filled volume at the higher flow rate, which may have delayed the sharp decrease in mixing. The only disadvantage of data partitioning was that the effect of flow rate cannot be quantified. As compared to the screw configuration with the neutral kneading block, the non-linear screw speed effect on mixing with the reverse kneading block was not as well defined. In the case of the screw configuration containing the forward kneading block, the effects of screw speed and flow rate were linear, but their interaction was also significant. Regression analysis of the experimental data confirmed the fundamental difference between the mixing behavior of the forward kneading block and the restrictive neutral and reverse kneading block designs.

6.2. Residence Time Distribution (RTD) Measurements

RTD measurements were completed to investigate the relationships between the distributive mixing results and both the average residence time and the degree of macromixing. For comparison with the distributive mixing experiments, only the RTD in the melt-melt blending section was required. The experimental procedure for measuring the RTD in the melt-melt blending section using a washout of the anhydride functionalized polymer tracer was described in section 4.3.4.1. This method involved a switchover from melt-melt blending with equal mass flow rates of pure PP and PP with 5wt% anhydride polymer tracer to the flow of only pure PP in the extruder. The flow rate of the pure PP to the beginning of the twin screw extruder was doubled, and a pressure transducer P0 (Figure 6.1) was used to determine when this new flow rate reached the melt feeding location. The flow from the single screw extruder was then stopped, and the washout of the tracer was followed using off-line FT-IR analysis of the anhydride functional group relative peak height in the film collected from the end of the extruder. Examples of pressure profiles from transducers P0, P2, and P3 are presented in Figure 6.6 for the screw configuration (depicted in Figure 6.1) containing the forward kneading block at 50 rpm and 100 g/min. The sharp increase in the pressure P0 corresponded to the time when the new flow rate of pure PP reached the melt feeding location. The switchover from melt-melt blending to the flow of pure PP did not significantly affect the pressures measured upstream and downstream of the forward kneading block (P2 and P3). Therefore, the flow rate in the melt-melt blending section of the extruder remained constant during the RTD experiment.

The RTD experiments were completed using the screw configurations and operating conditions investigated in the overall distributive mixing measurements. It is important to

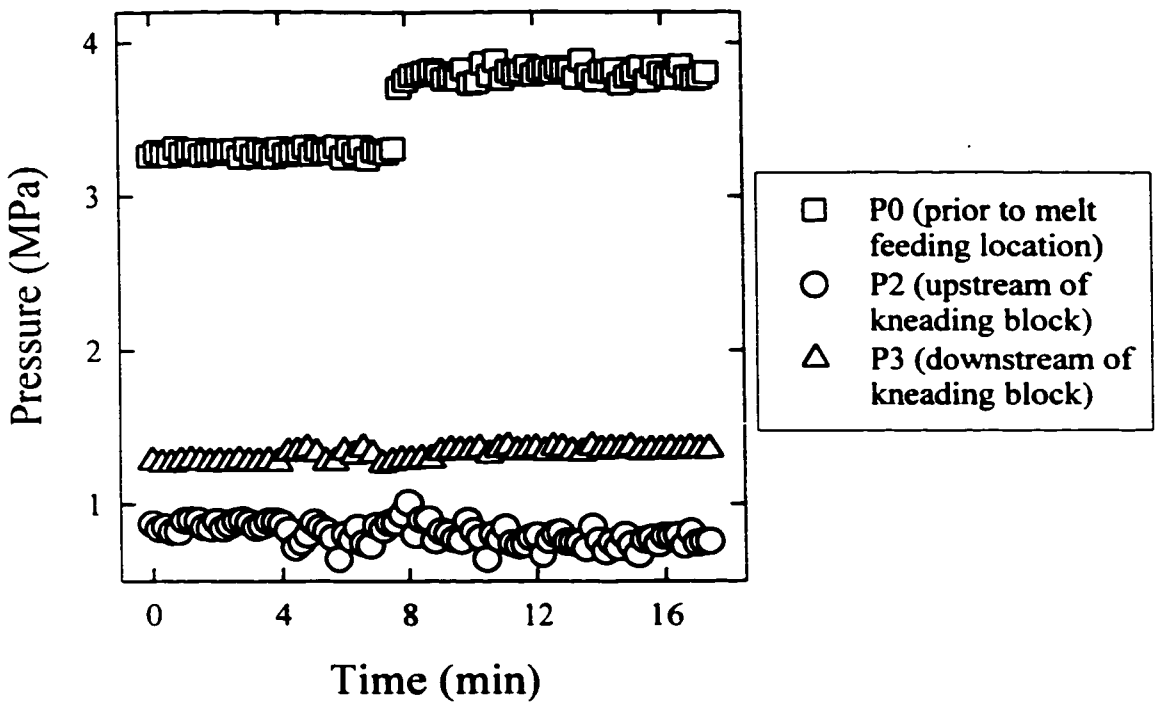

Figure 6.6. Pressure Profiles from a RTD Experiment Using the Washout Technique

note that the distributive mixing and RTD measurements were not completed under isothermal conditions. Increasing the screw speed results in greater viscous dissipation and higher melt temperatures. The melt temperature may affect the RTD results through the pressures and degree of fill in the extruder. Examples of the measured washout distributions are presented in Figure 6.7 for the screw configuration with the neutral kneading block at a flow rate of 50 g/min. The small fluctuations in the washout curves were within the expected experimental error of the FT-IR measurements. Shifting of the washout curves to lower times as the screw speed was increased indicated the expected decrease in the average residence time.

The dimensionless washout distributions for the screw configuration with the neutral kneading block at 50 g/min are presented in Figure 6.8, and a comparison of the dimensionless washout distributions for the three screw configurations is presented in Figure 6.9 for a screw speed of 50 rpm. All the dimensionless curves overlapped significantly, and therefore, the degree of macromixing was approximately the same in all the experiments. This observation was consistent for all the investigated values of the experimental factors. Numerical differentiation of the washout results was attempted to obtain the residence time density function, which is more sensitive to changes in the degree of macromixing as well as flow stagnation and recirculation. Examples of the dimensionless residence time density functions obtained from the numerical differentiation of the washout results for the screw configuration with the forward kneading block are presented in Figure 6.10. The small fluctuations in the washout results, which were attributed to the error in the FT-IR measurements, resulted in large errors upon differentiating. Regardless of these large fluctuations in the residence time density functions, all the distributions presented in Figure

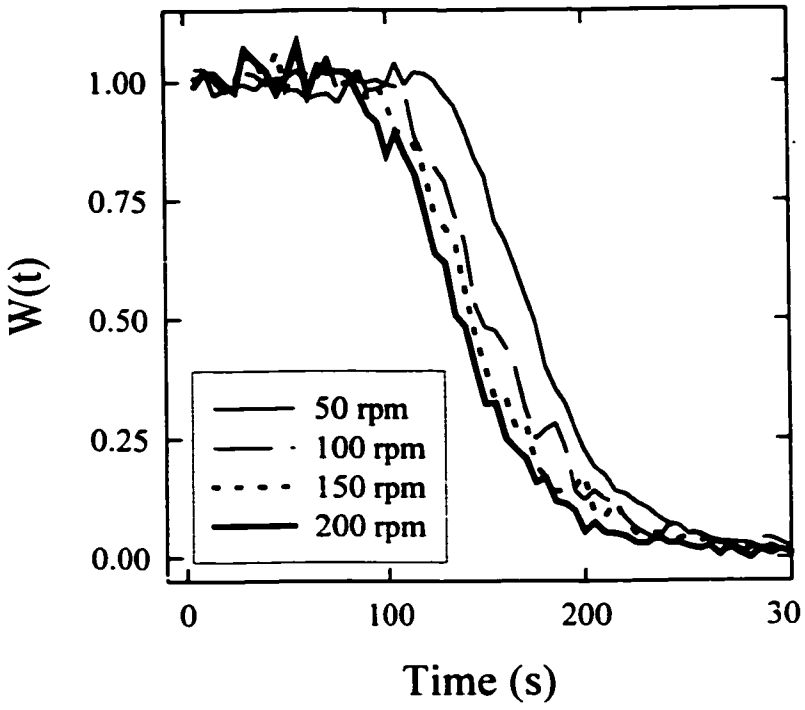

Figure 6.7. Washout Distributions for the Screw Configuration with the Neutral Kneading Block at 50 g/min

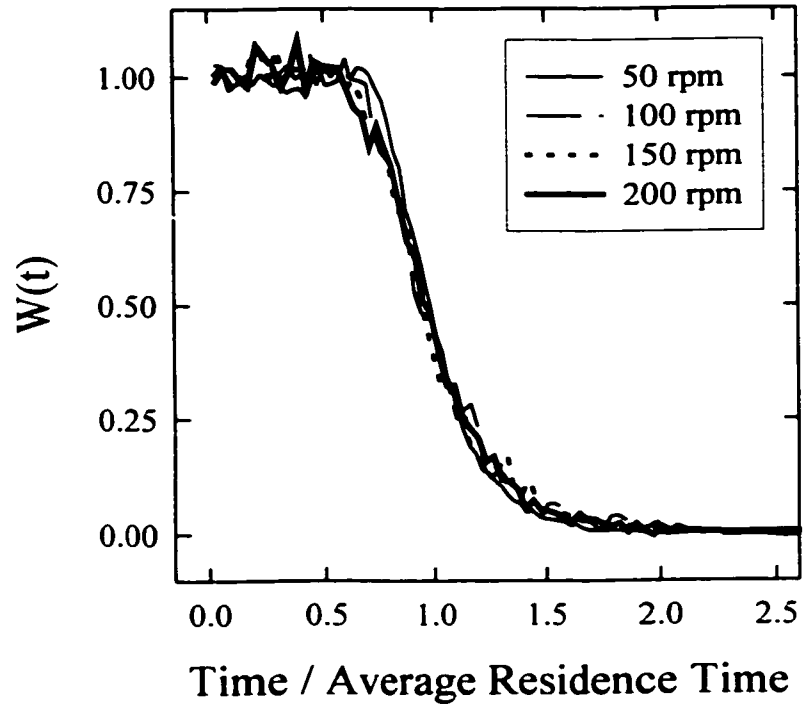

Figure 6.8. Dimensionless Washout Distributions for the Screw Configuration with the Neutral Kneading Block at 50 g/min

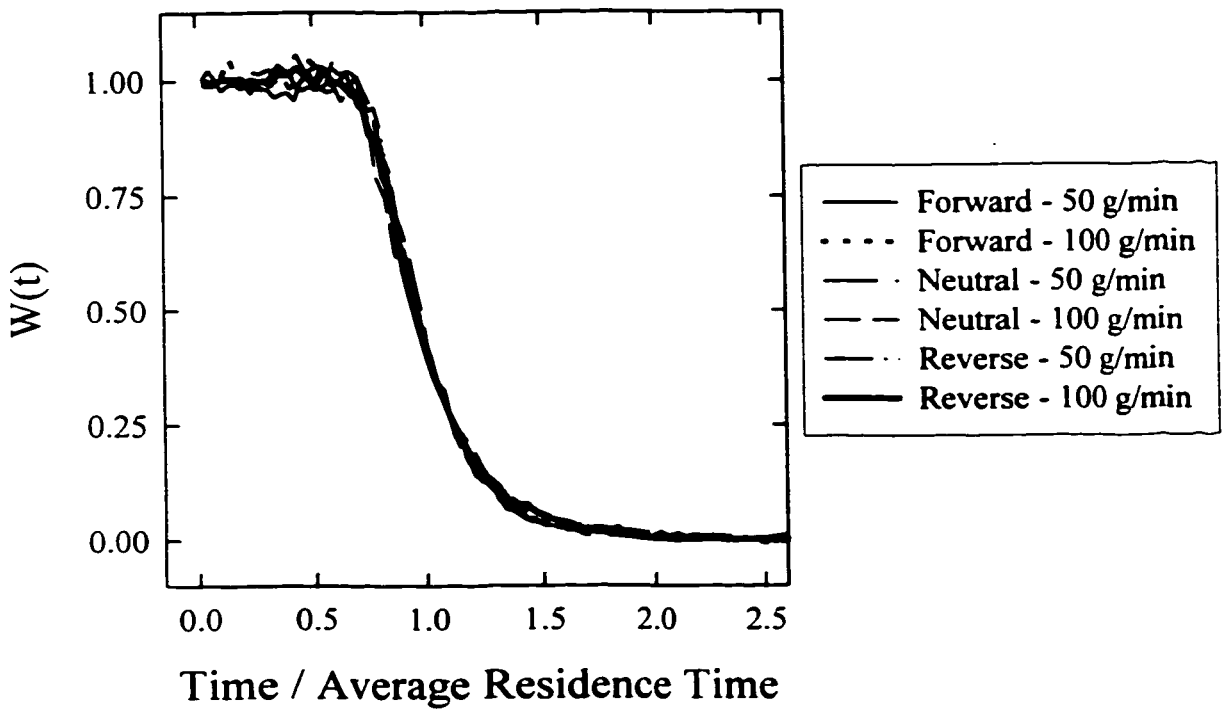

Figure 6.9. Comparison of the Dimensionless Washout Distributions for all Three Screw Configurations at 50 rpm

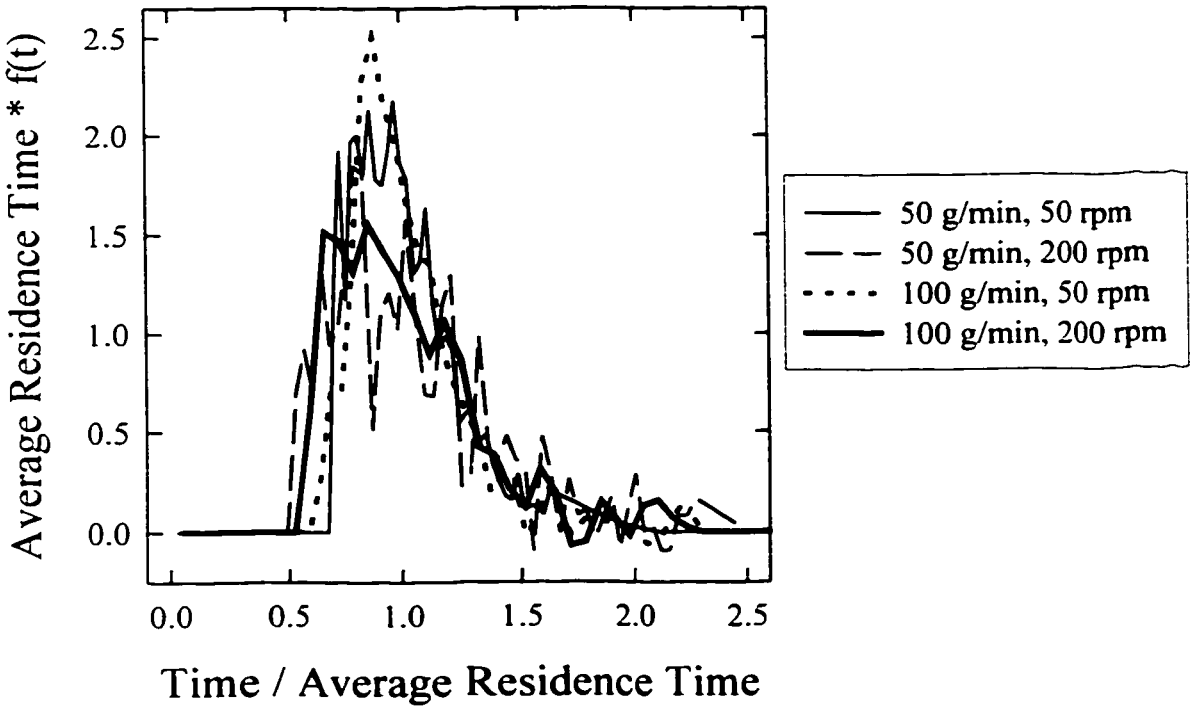

Figure 6.10. Dimensionless Residence Time Density Functions for the Screw Configuration with the Forward Kneading Block

6.10 exhibited similar breadths. Surprisingly, all the dimensionless washout curves and residence time density functions had similar shapes and overlapped. From visual inspection of the experimental RTD results, the investigated factors did not significantly affect the degree of macromixing in the melt-melt blending section of the twin screw extruder.

Using equation 4.4, the average residence times were calculated from the washout distributions and the results for all three screw configurations are compared in Figure 6.11. Replicate experiments were completed with the screw configuration containing the neutral kneading block at 50 g/min and 50 rpm. The calculated experimental error for the average residence time was less than 1%, which indicated that the experiment procedure was adequate. Linear regression was performed to quantify the factor effects, and the results are presented in Table 6.2. Comparison of the t-statistics with the corresponding values of the t-distribution indicated that all the factors were significant at the 95% confidence level. Additional comments on the regression analysis of average residence time data is presented in Appendix I, with particular attention given to the new analysis method proposed by Gasner *et al.* (1999).

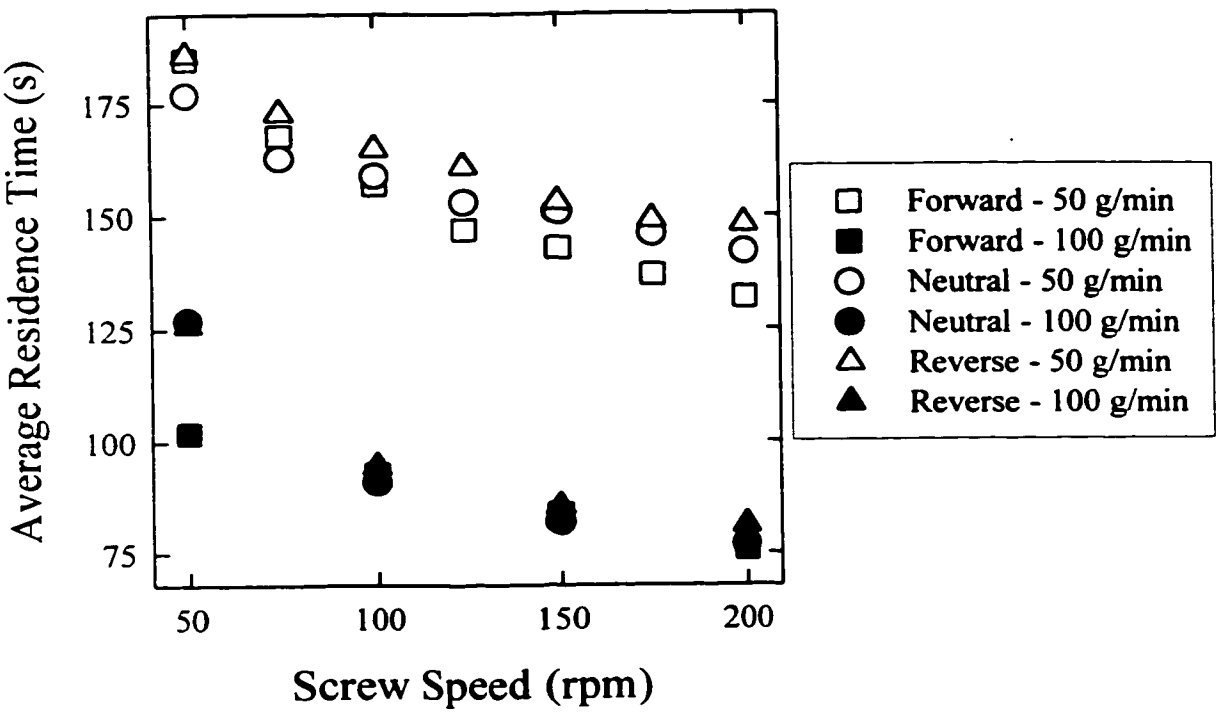

Figure 6.11. Average Residence Time Results for all Three Screw Configurations

Table 6.2. Linear Regression Results for the Regression Models* of the Average Residence Time Results

Kneading Block Design	Constant (β_0)	Specific Throughput (Q/N) Coefficient (β_1) / t-statistic#	Flow Rate (Q) Coefficient (β_2) / t-statistic	Q/N * Q Coefficient (β_{12}) / t-statistic##	r^2
Neutral	220	36.0 / 17.1	-1.63 / -38.7	Not Included	0.9948
Reverse	230	35.2 / 9.80	-1.70 / -23.6	Not Included	0.9862
Forward No Interaction	218	28.6 / 3.36	-1.60 / -9.37	Not Included	0.9203
Forward With Interaction	165	123 / 10.3	-0.93 / -9.32	-1.07 / 8.15	0.9924

* Average Residence Time $= \beta_0 + \beta_1\left(\frac{Q}{N}\right) + \beta_2(Q) + \beta_{12}\left(\frac{Q}{N}\right)(Q)$

Units: N [=] rpm, Q [=] g/min ; # $t_{0.975,8} = 2.306$; ## $t_{0.975,7} = 2.365$

As expected, an increase in the flow rate decreased the average residence time. The non-linear effect of screw speed on average residence time was incorporated into the specific throughput (Q/N) term, which is an indication of the degree of channel fill in conveying elements. Surprisingly, all three screw configurations exhibited similar average residence times at 100 g/min for screw speeds between 100 and 200 rpm. As indicated by pressure measurements upstream of the kneading block (Figure 6.3), there were significant differences in the fully filled volume prior to the different kneading block designs. This observation suggested that the degree of fill in the conveying section prior to the kneading block was a less significant factor for the average residence time at 100 g/min. The local residence times in the conveying section and kneading block are discussed in Chapter 7. The trends for the screw configurations with the neutral and reverse kneading blocks were similar, with slightly higher average residence times for the more restrictive reverse kneading block (larger fully filled volume preceding the reverse kneading block). The average residence times did not

follow the same trend for the screw configuration with the forward kneading block. Along with the effects of specific throughput and flow rate, their interaction was also significant. Without this interaction term, the linear regression fit quality decreased significantly as indicated by the decrease in r^2. As previously observed in the distributive mixing measurements, the average residence time results for the screw configurations containing the pressure generating kneading block and the pressure consuming kneading block designs were significantly different.

The RTD spreads (σ) and relative axial dispersions ($\bar{t}/\sigma$) are presented in Figures 6.12 and 6.13, respectively. The RTD spread, calculated using equation 4.5, quantifies the magnitude of the breadth of the distribution. The relative axial dispersion, which is the ratio of the spread and the average residence time, quantifies the relative level of macromixing. In the extreme cases, the relative axial dispersion is equal to zero for plug flow, and it is equal to one for perfect macromixing. From the replicate experiments completed with the screw configuration containing the neutral kneading block, the experimental errors in the RTD spread and relative axial dispersion were less than 2%. The RTD spread significantly decreased for each screw configuration as the flow rate was increased from 50 g/min to 100 g/min. Conversely, the spread exhibited no clear relationship with screw speed or specific throughput at each flow rate. Similar results have been discussed in the literature for the RTD in twin screw extruders (Gendron *et al.*, 1996).

In contrast to the RTD spread, the relative axial dispersion increased with the flow rate for the screw configurations containing the neutral and reverse kneading blocks. In general, the relative axial dispersion increased with screw speed at both flow rates. Similar trends were observed for the dimensionless variance and the Peclet number, which are also

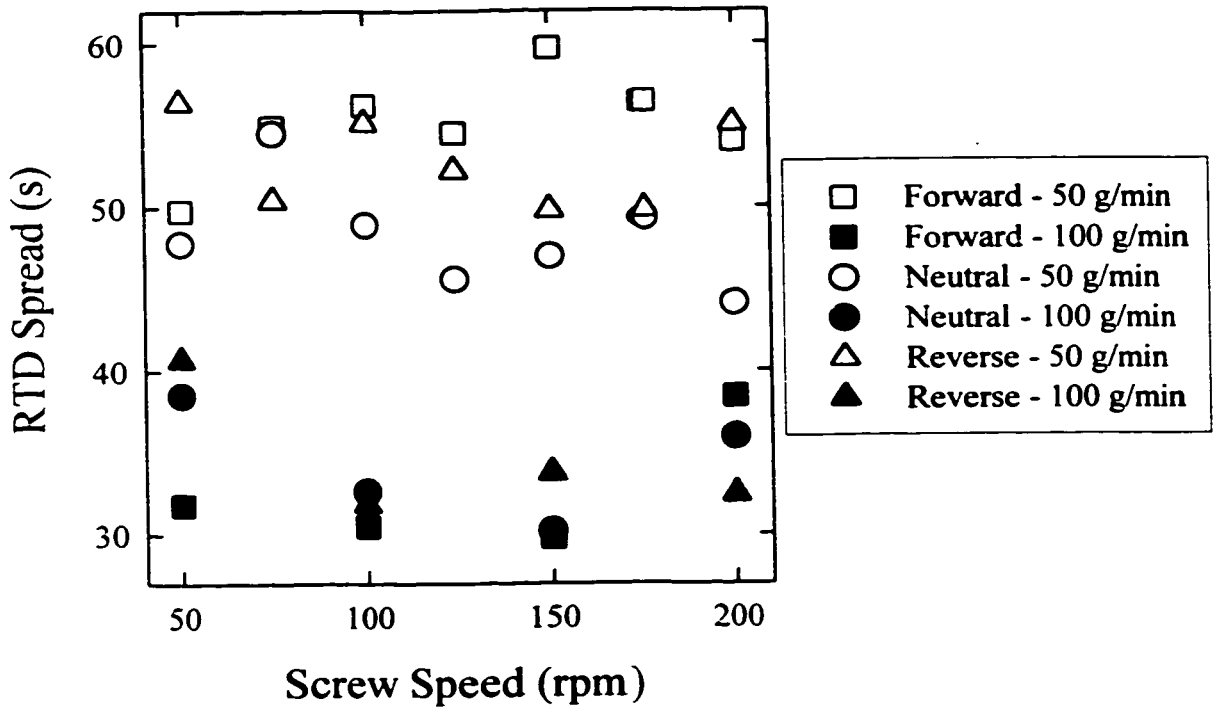

Figure 6.12. RTD Spread Results for all Three Screw Configurations

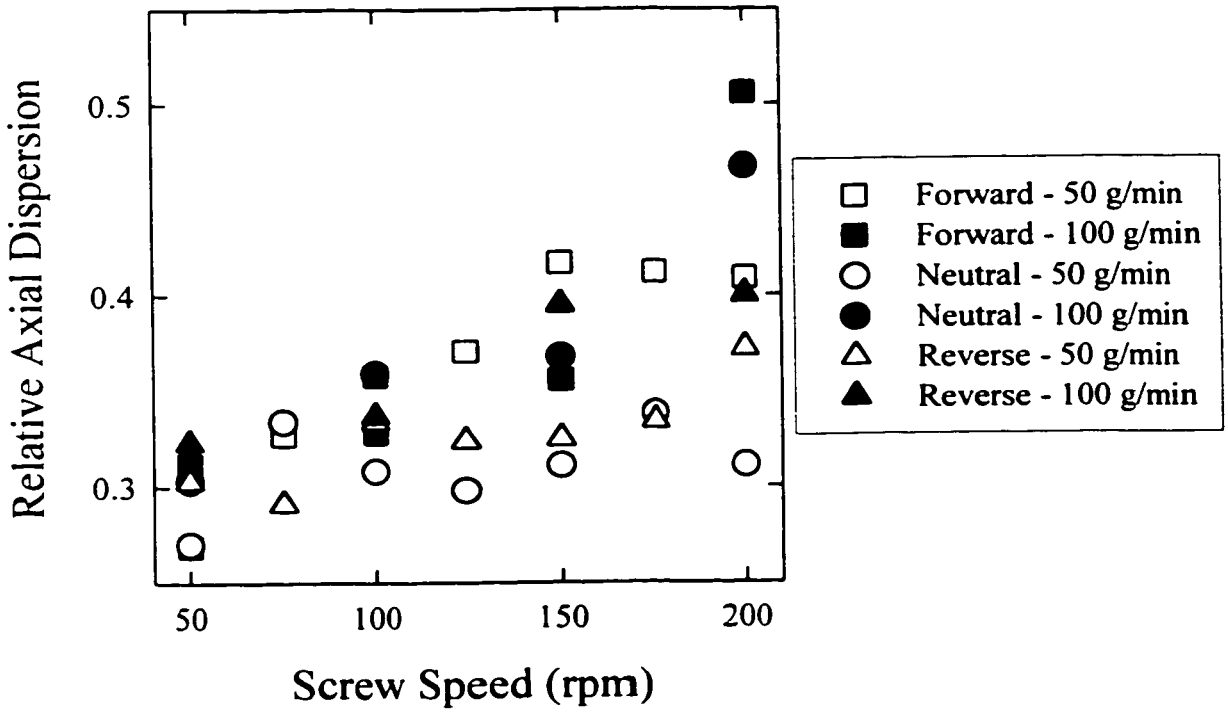

Figure 6.13. Relative Axial Dispersion Results for all Three Screw Configurations

used to characterize the relative degree of macromixing. From Figure 6.12, the RTD spread remained nearly constant with respect to the screw speed, and therefore, the increase in the relative axial dispersion was caused by the decrease in the average residence time at higher screw speeds. As previously discussed, visual inspection of the dimensionless distributions suggested that the experimental factors did not significantly affect the degree of macromixing. Therefore, an increase in the relative axial dispersion may not be a true indication of a change in the degree of macromixing. RTD spread, an absolute measurement of the breadth of the distribution, may be a better indicator of the degree of macromixing in the extruder.

The RTD spreads and relative axial dispersions were averaged for each flow rate and screw configuration, and the results are presented in Table 6.3. The average breadth of the RTD followed the trend of: forward > reverse > neutral at 50 g/min. This trend is identical to the distributive mixing performance trend at the low flow rate. These differences between the average RTD breadths for the three screw configurations were not large enough to be observed by visual inspection of the dimensionless distributions. At 100 g/min, the average breadth of the RTD did not depend on the kneading block design, and therefore, no general relationship existed between the distributive mixing and the degree of macromixing.

Table 6.3. Average Values of the RTD Spread and Relative Axial Dispersion

Kneading Block Design	Average RTD Spread (min)		Average Relative Axial Dispersion	
	50 g/min	100 g/min	50 g/min	100 g/min
Neutral	48.2	34.3	0.31	0.37
Reverse	52.7	34.7	0.33	0.36
Forward	55.1	32.6	0.37	0.37

6.3. Comparison of Distributive Mixing and RTD Results and Identification of the Controlling Factors for Distributive Mixing During Polymer Blending

One of the primary research objectives was to investigate the possible relationship between the distributive mixing results and the degree of macromixing, and comparisons of the anhydride conversions and the RTD spread and relative axial dispersion are presented in Figure 6.14. Distributive mixing was not related to the RTD spread, but it tended to decrease with an increase in the relative axial dispersion. It was previously proposed that the relative axial dispersion was not a true indicator of the degree of macromixing because no significant differences were observed in the dimensionless distributions. The negative effect of the relative axial dispersion on the distributive mixing performance was caused by the decreasing average residence time at higher screw speeds. Therefore, distributive mixing during polymer melt blending in the twin screw extruder was not related to the degree of macromixing. A similar result was presented by Bigg (1975) for the mixing of polymers in single screw extruders and static mixers. Bigg (1975) proposed that RTD measurements characterize the mixing of the polymer in the primary flow direction, or the direction down the unwound screw channel. Conversely, homogenization of the polymer product was achieved by distributive mixing, which was dominated by the transverse mixing caused by the cross channel flow in the single screw extruder. According to Figure 6.14, distributive mixing in the twin screw extruder does not depend on the mixing in the primary flow direction. The anhydride conversion is also an indication of the micromixing because the chemical reaction is a molecular event. Therefore, combining the experimental micromixing and RTD results indicated that the macromixing of the polymer in the extruder does not affect the micromixing.

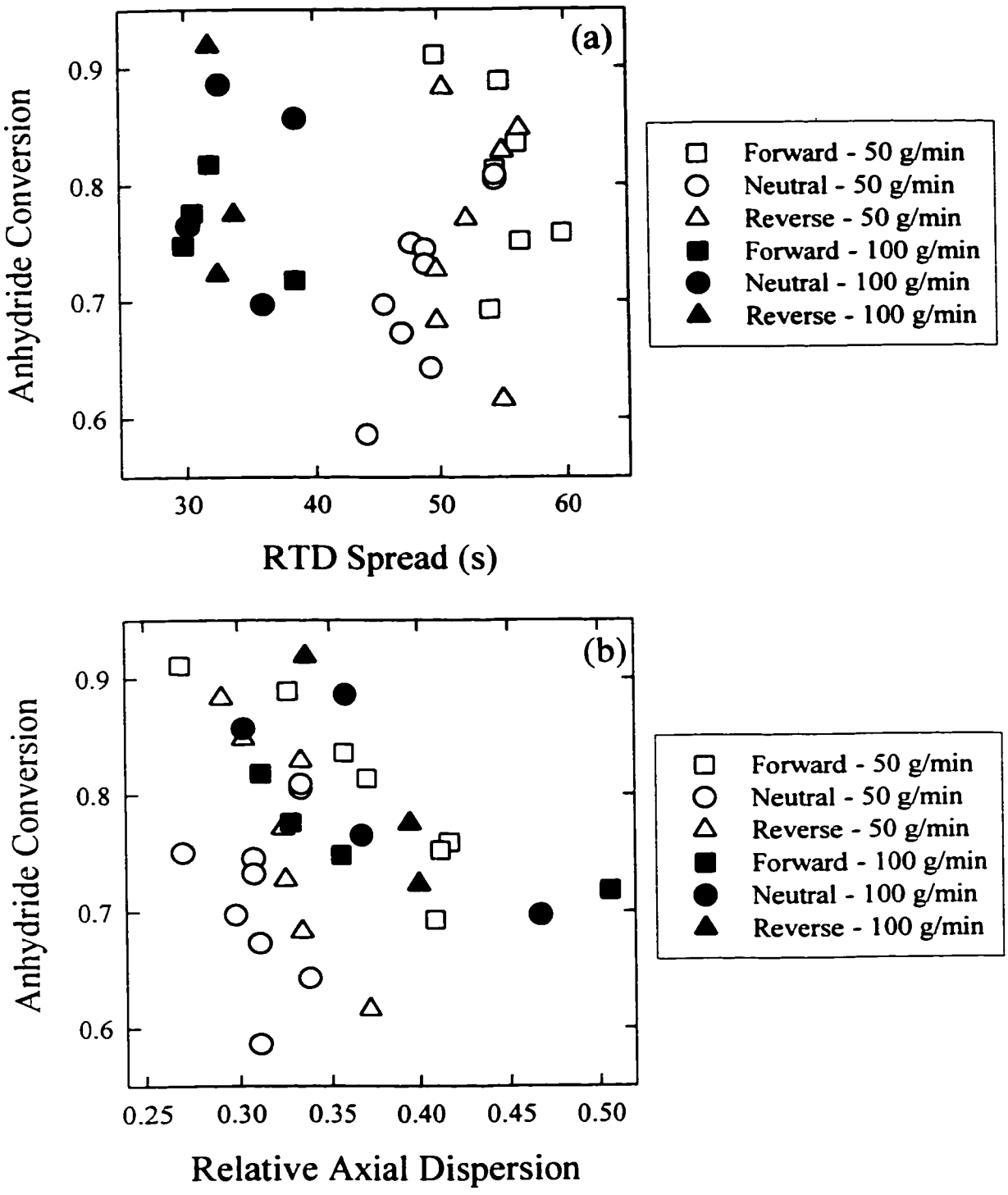

Figure 6.14. Comparison of the Distributive Mixing and RTD Results
(a) Relationship with RTD Spread
(b) Relationship with Relative Axial Dispersion

The degree of macromixing did not affect the distributive mixing, which raises the following question: are RTD measurements useful for analyzing mixing during polymer blending in twin screw extruders? As discussed by Bigg (1975), the average residence time is an important factor because it directly affects the applied strain. The relationship between the measured distributive mixing performances and the average residence times is presented in Figure 6.15. In general, the distributive mixing performance increased with average residence time, which confirmed the importance of average residence time in the mixing process. The mixing results from the three screw configurations formed a group at each flow rate, which indicated that average residence time was not the only important factor. Two lines highlighting the experimental trends are included in Figure 6.15, which show that the distributive mixing performances of the screw configurations with the neutral and reverse kneading blocks followed the same trend with respect to the average residence time over some interval at each flow rate. The overlapping of the mixing results from these two screw configurations suggested that the average residence time was the controlling variable in those intervals. After the maximum conversions for the screw configurations with the neutral and reverse kneading blocks, the mixing results deviated from the linear trends. From Figure 6.11, the average residence decreased with an increase in the screw speed. At each flow rate, an increase in the residence time in Figure 6.15 corresponds to decrease in the screw speed. The deviations from the linear trends after the maximum conversions suggested that the effect of reduced shear rate dominated the effect of increased residence time at low screw speeds. After the maxima, the screw configuration with the reverse kneading block exhibited better mixing because of its larger fully filled volume. At the low flow rate, the screw

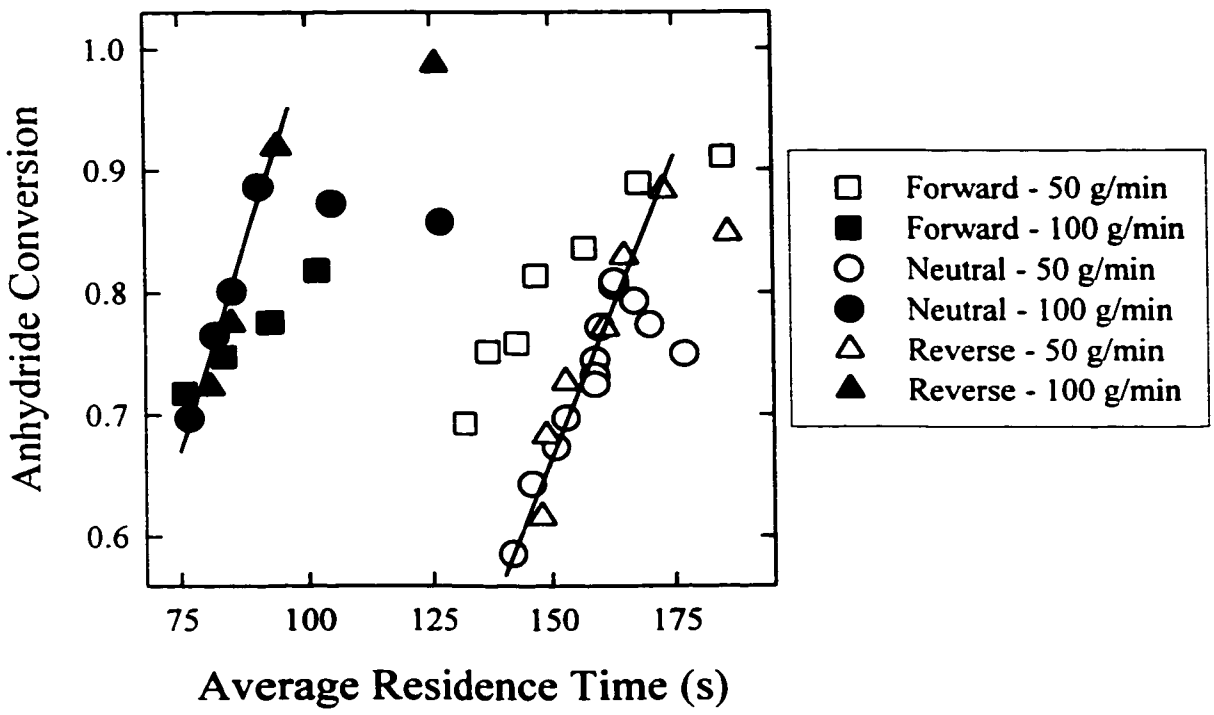

Figure 6.15. Comparison of the Distributive Mixing Results and the Average Residence Times

configuration with the forward kneading block exhibited superior mixing in the same range of average residence times.

The average residence time was not the only significant factor affecting the distributive mixing performance. From Figure 6.15, the flow rate exhibited a significant effect on the mixing process, which was attributed to its effect on the fully filled volume. The fully filled volume is an important variable because it is where the most efficient mixing occurs due to flow recirculation. In addition, significantly higher shear rates are applied to the polymer in fully filled regions as compared to partially filled regions in the extruder. To confirm the dependence of the mixing on the fully filled volume, steady-state macroscopic numerical simulations of the twin screw extruder process were performed using a program developed by Strutt *et al.* (1997; 1998). The program, which is based on the simulation method of Potente *et al.* (1994), yields pressure, filling level, melt temperature, and solid fraction profiles along the extruder for the non-isothermal extrusion of a power-law fluid. Shear viscosity measurements for Petrothene PP and Petrothene with 5wt% Polymer C-SYN were completed using the capillary rheometer (capillary diameter = 0.762 mm, L/D = 40) at 190, 220, and 250 °C. Temperature dependent power-law viscosity models were fitted to the data (linear regression was performed using the linear viscosity model as previously described in Chapter 5, from the linear models: $r^2 = 0.9952$ for Petrothene and $r^2 = 0.9953$ for Petrothene + 5wt% Polymer C-SYN), which are presented in equations 6.1 and 6.2.

Petrothene:

$$\eta = 35985 \exp(-8.52 * 10^{-3} * T)\dot{\gamma}^{(0.439-1)} \quad (6.1)$$

Petrothene + 5wt% Polymer C-SYN:

$$\eta = 29864 \exp(-8.51 * 10^{-3} * T)\dot{\gamma}^{(0.446-1)} \quad (6.2)$$

where: η : apparent shear viscosity (Pa.s)
T : temperature (°C)
$\dot{\gamma}$: apparent shear rate (s^{-1})

The addition of 5wt% low molecular weight polymer to the PP significantly decreased the consistency index. Conversely, the temperature coefficient and the flow index were approximately the same for both materials. Therefore, the tracer decreased the apparent viscosity, but it did not affect the temperature or shear thinning behaviour of the PP. As in the simulations of Strutt (1998), the material properties for a generic PP resin were used for the other required material inputs. Macroscopic simulations were completed for all three screw configurations with the values of the operating conditions used in the experiments. The simulations also required the die pressure at the end of the extruder, and the experimentally measured values were used. A comparison of the predicted average residence times in the melt-melt blending section for the flow of pure Petrothene and Petrothene with 5wt% Polymer C-SYN at 50 g/min is presented in Figure 6.16. The effect of the low molecular weight tracer on the polymer viscosity did not significantly affect the predicted average residences times. A similar trend for the predicted average residence times was observed at 100 g/min. Therefore, all the simulations used in the comparison with the experimental results were completed using the shear viscosity parameters for pure Petrothene PP (equation 6.1).

Compared to the experimentally measured values, the simulations predicted higher pressures, which will result in over estimations of the fully filled volume in the extruder. Even though the predicted pressure values were higher, they followed the same trends as presented in Figure 6.3 for the screw configurations with the neutral and reverse kneading blocks. As well, a comparison of the experimentally measured residence times and the simulation predictions in the melt-melt blending section at 50 g/min is presented in Figure 6.17. The simulations underestimated the experimentally measured average residence times

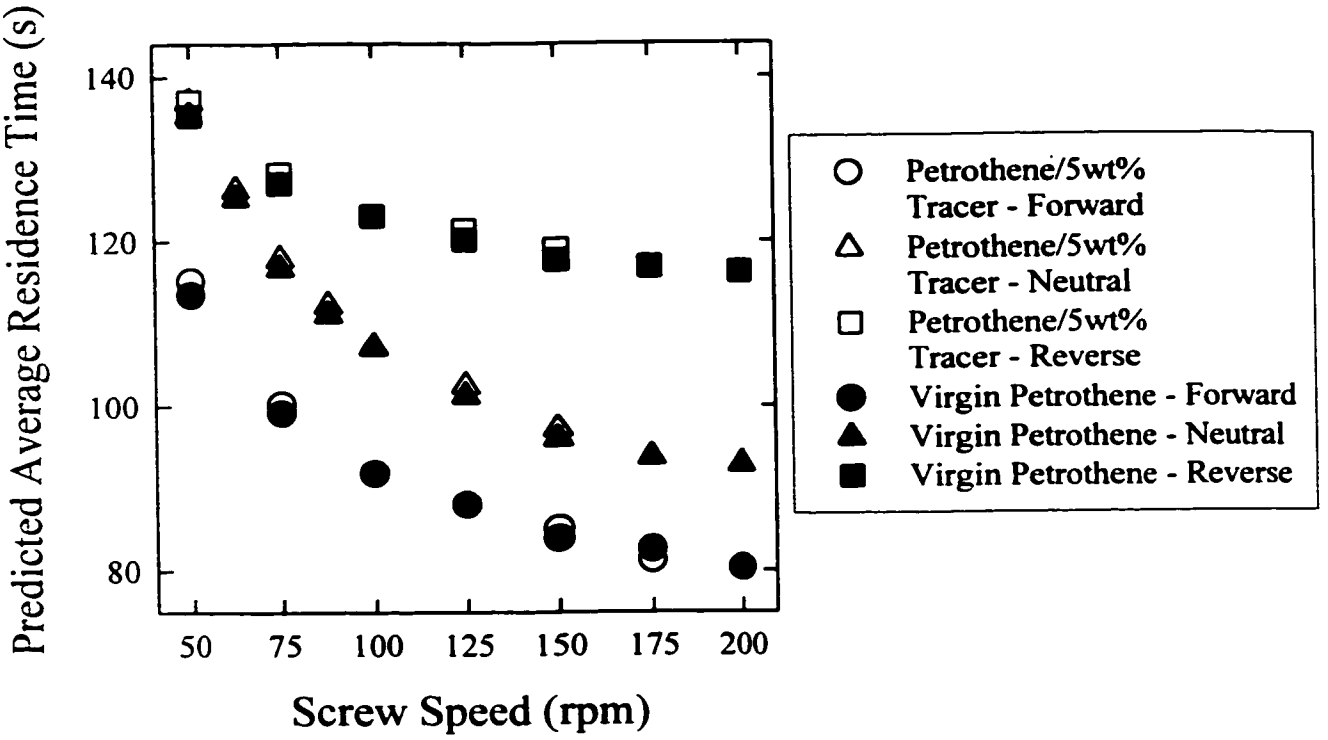

Figure 6.16. Comparison of the Predicted Average Residence Times With and Without Tracer

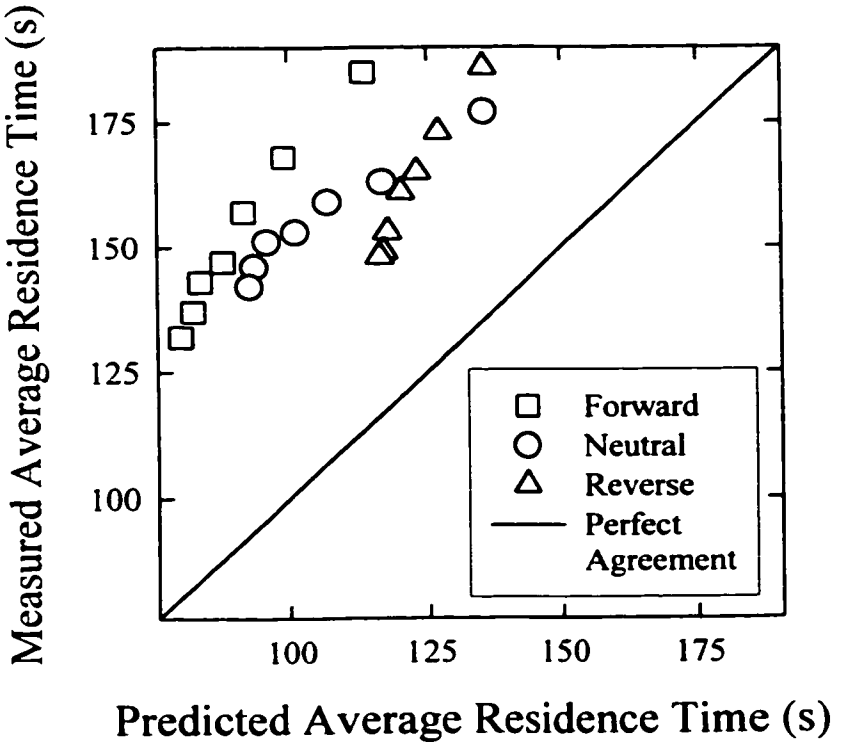

Figure 6.17. Comparison of the Experiment Results and the Simulation Predictions of the Average Residence Time in the Melt-melt Blending Section

by an average of 30%. Regardless of this underestimation, the simulation predictions and the experiment data followed similar trends with respect to the effects of the operating conditions. Therefore, the simulation program was used to predict the fully filled volume in the melt-melt blending section.

The relationship between the experimental anhydride conversion results and the predicted fully filled fraction in the melt-melt blending section is presented in Figure 6.18. The fully filled fraction includes the fully filled kneading block, the fully filled reverse conveying element, and the fully filled conveying elements preceding the kneading block and the slit die. The first two sources were fully filled in all the simulations. As expected, the fully filled volume in the melt-melt blending section followed the trend of (respect to the kneading block design): reverse > neutral > forward. For all three screw configurations, the entire extruder was predicted to be fully filled at 100 g/min and 50 rpm. These data points are not included in Figure 6.18 because the extruder was starved as indicated by pressure measurements at P4 and the melt feeding location in the experiments. The results from the two flow rates for the screw configurations with the neutral and reverse kneading blocks nearly overlapped, which confirmed that the flow rate affected the mixing performances through the fully filled volume. For these two screw configurations, the increase in the fully filled volume dominated the decrease in average residence time at the higher flow rate. The decrease in average residence time exhibited a small effect on the mixing process as indicated by the non-perfect overlapping of the experimental results from the two flow rates. Slightly improved mixing was observed for the screw configuration with the reverse kneading block, which was attributed to its corresponding larger fully filled volume. Once

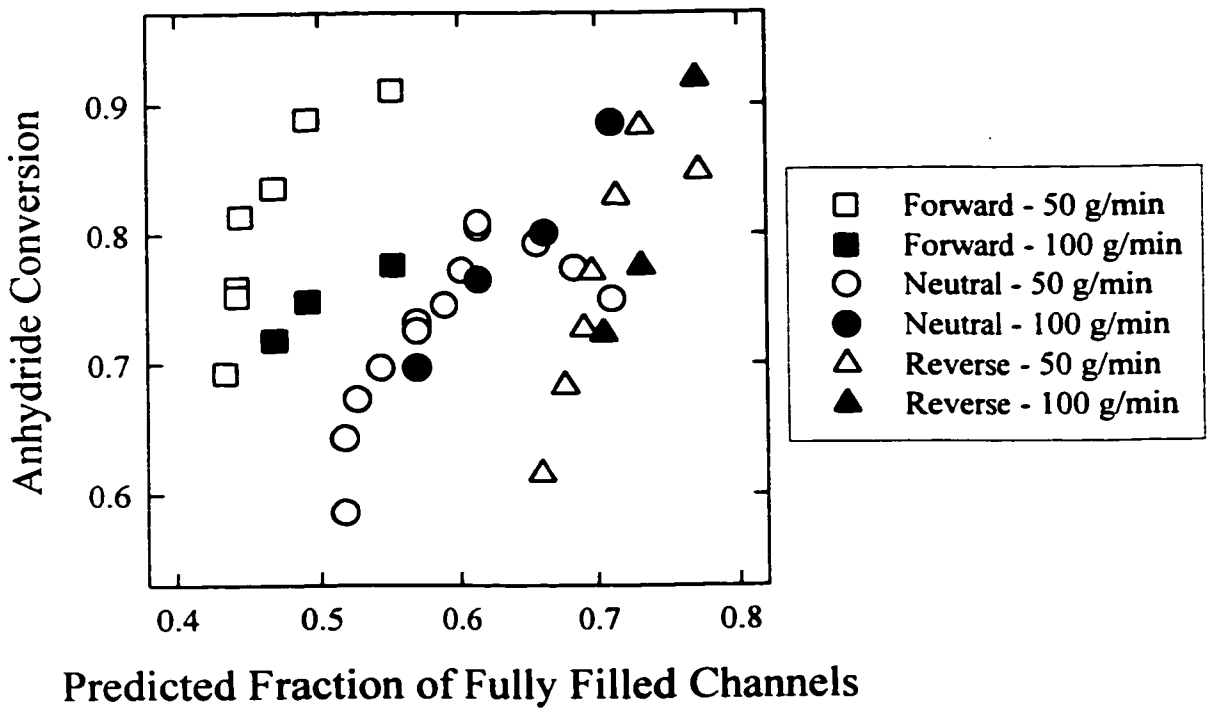

Figure 6.18. Comparison of the Distributive Mixing Results and the Predicted Fully Filled Fraction in the Melt-Melt Blending Section

again, the results for the screw configuration with the forward kneading block did not follow a similar trend.

The screw configuration with the forward kneading block exhibited surprisingly good distributive mixing at the low flow rate. The fully filled volume prior to the forward kneading block was significantly less than that prior to the pressure consuming kneading blocks. Regardless of this difference, the average residence times for the screw configuration with the forward kneading block were similar to the values for the screw configurations with the neutral and reverse kneading blocks. The overall residence time consisted of the following three contributions: the time spent in the conveying elements prior to the kneading block, the time spent in the kneading block, and the time spent in the pumping section prior to the die. The residence time spent in the pumping section prior to the die was independent of the kneading block design. A higher fully filled volume prior to the neutral and reverse kneading blocks corresponded to a larger fraction of the overall residence time spent in that section. Therefore, the local residence time in the forward kneading block may have been longer than the local residence times in the neutral and reverse kneading blocks. The most efficient mixing is expected to occur in the kneading block, which may explain the superior mixing performance of the screw configuration with the forward kneading block at the low flow rate. This possible longer local residence time in the forward kneading block is discussed in detail in Chapter 7.

Using numerical simulations, Lawal and Kalyon (1995a) predicted the possibility of stagnant flow regions in forward kneading blocks with small stagger angles. The stagger angle of 30° used in the experiments is a small stagger angle, which was selected for its large forward pumping capacity. The average values of the RTD spread and relative axial

dispersion (Table 6.3) suggested that the RTD was broader for the screw configuration with the forward kneading block at the low flow rate, although this difference was not observed in the dimensionless washout distributions. The improved mixing may be related to a small amount of material which remained in the forward kneading block for significantly longer times (relative stagnancy), which may be difficult to detect using the cumulative washout distributions. At the higher flow rate, the inferior mixing performance of the screw configuration with the forward kneading block (at screw speeds of 50 and 100 rpm) was attributed to its lower fully filled volume and shorter average residence time as compared with the other two screw configurations. As well, the averages of the RTD spread and relative axial dispersion of all three screw configurations were approximately equal at the higher flow rate, which suggested that the possible stagnant flow regions in the forward kneading block existed only at the lower flow rate.

6.4. Concluding Remarks

The mixing limited interfacial reaction between the reactive polymer tracers was used as a microscopic probe to gain direct evidence on the effects of kneading block design, screw speed, and flow rate on the distributive mixing performance of a twin screw extruder. To obtain good distributive mixing, the selection of the screw configuration and the operating conditions cannot be made independently. Experimental results indicated significant differences in the distributive mixing performances of pressure generating and pressure consuming kneading block designs. In particular, the effects of screw speed and flow rate depended on the kneading block design.

Using a washout of the anhydride reactive polymer, the RTD in the melt-melt blending section was determined. The degree of macromixing, as indicated by visual inspection of the dimensionless distributions, was not significantly affected by the experimental factors. No general relationship existed between the distributive mixing and the degree of macromixing. The only RTD parameter that was significantly affected by all the experimental factors was the average residence time. The average residence time and the fully filled volume were controlling factors for the distributive mixing with neutral and reverse kneading blocks prior to maximum conversions at each flow rate. Average residence time affects the mixing process directly through the applied strain, and the fully filled volume is the region where the highest shear rates are applied to the polymer. After the maxima, reductions in shear rate dominated the effects of increased average residence time and fully filled volume. The superior mixing of the screw configuration with the forward kneading block at the low flow rate was attributed to a longer local residence time in the kneading block and the possibility stagnant flow regions.

CHAPTER 7
GENERATION OF INTERFACIAL AREA ALONG THE LENGTH OF A TWIN SCREW EXTRUDER AND ITS RELATIONSHIP WITH LOCAL RESIDENCE TIME

The previously discussed mixing experiments focused on the analysis of the overall distributive mixing performance of the melt-melt blending section of the twin screw extruder. This chapter is concerned with the analysis of the distributive mixing profile along the length of this section. Using specially designed sampling plates, the polymer melt was sampled upstream and downstream of the kneading block during continuous operation of the twin screw extruder. In particular, the local mixing in the conveying section prior to the kneading block and the local mixing in the kneading block were investigated over a wide range of operating conditions. Using carbon black as a tracer and an IR temperature probe, the local residence times in the conveying section (upstream of the kneading block) and the kneading block were determined. Finally, the local distributive mixing and residence time measurements were compared to investigate their possible relationships.

7.1. Distributive Mixing Profile Measurements

The screw configuration, feeding arrangement, and positions of the sampling plates are presented in Figure 4.8. As depicted in Figure 4.7, each sampling plate contained a pressure transducer mounting and a sampling port controlled by a retractable threaded bolt. This design allowed for the sampling of the polymer melt in the fully filled (pressurized) sections of the twin screw extruder. Only sampling plates S2 and S3, which were located immediately upstream and downstream of the kneading block (sampling port of S2 was 15 mm upstream of the first kneading disc and sampling port of S3 was 15 mm after the last

kneading disc, in the middle of the reverse conveying element) were used to take samples of the polymer melt. Similar to the previous melt-melt blending experiments, the melt feeding location of the twin screw extruder was partially filled, the kneading block consisted of 16 adjacent bilobal kneading discs, and the pressure downstream of the reverse conveying element was zero. The investigated experimental factors were: the kneading block design (stagger angles of 30°, forward; 90°, neutral; -30°, reverse), the screw speed of the twin screw extruder (50 – 100 rpm), and the total flow rate (50, 100 g/min). All the experiments were completed with barrel temperatures of 220 °C in the melt-melt blending section and equal mass flow rates in the two melt streams of Petrothene PP with 5wt% reactive polymer tracer.

For valid analysis of the mixing profile, the sample obtained from the sampling port must be representative of the polymer melt in the entire channel cross section at the sampling position. Therefore, the anhydride conversion in the sample is the bulk conversion, or the average across the entire flow cross section at the sampling plate position. Pure Petrothene PP and Petrothene PP containing 5wt% anhydride reactive polymer were melt-melt blended using the screw configuration with the neutral kneading block to investigate the concentration of the anhydride polymer tracer in the polymer melt obtained from the sampling ports. This blend was required to determine the anhydride relative peak height at zero conversion. Instead of using the film preparation technique described in section 4.3.3.2, the polymer strands from the sampling ports were quickly pressed into thin films between two TEFLON plates (thickness = 3 mm). From FT-IR analysis of these films and the film obtained directly from the slit die at the end of the twin screw extruder, the anhydride relative peak heights at zero conversion were: 2.351 at the die, 2.154 at S2 (prior to the kneading block), and 2.090 at S3 (after the kneading block). The significant differences in the relative

peak heights along the length of the extruder were very surprising, and it suggested that the sampling ports were not obtaining a bulk, or average sample of the polymer melt from the entire channel cross section.

Crystallinity significantly affects the FT-IR spectrum of PP (Zbinden, 1964). FT-IR analysis is based on the vibrational energy levels of characteristic groups, which are significantly different in crystalline and amorphous regions of the polymer. A comparison of the FT-IR spectra of a water quenched film of Petrothene PP and the same film after it was annealed for 14 hours at 140 °C is presented in Figure 7.1. The annealing process did not significantly affect the thickness of the polymer film. The polymer backbone peaks were significantly sharper in the spectrum of the annealed PP due to its higher degree of crystallinity (the peak at 528.5 cm^{-1} in Figure 7.1 is the internal reference used in the calculation of the anhydride conversion). Therefore, precise control of the crystallinity is required for quantitative FT-IR analysis of the peak heights of PP. The film from the slit die was immediately quenched in the water bath, while it took approximately 10 to 15 seconds to collect and press a film of the polymer melt at each sampling port between the TEFLON sheets. In addition, slower cooling of the polymer film between the TEFLON sheets will result in higher crystallinity, which may have contributed to the lower anhydride relative peak heights measured at the sampling ports.

The melt-melt blending experiment with pure Petrothene PP and Petrothene PP with 5wt% anhydride polymer tracer was repeated using the dual strand die in place of the slit die at the end of the twin screw extruder. The same sampling procedure was used to collect polymer strands from the die and the sampling ports. All the collected strands were quickly compression molded into thin films and then water quenched according to the procedure

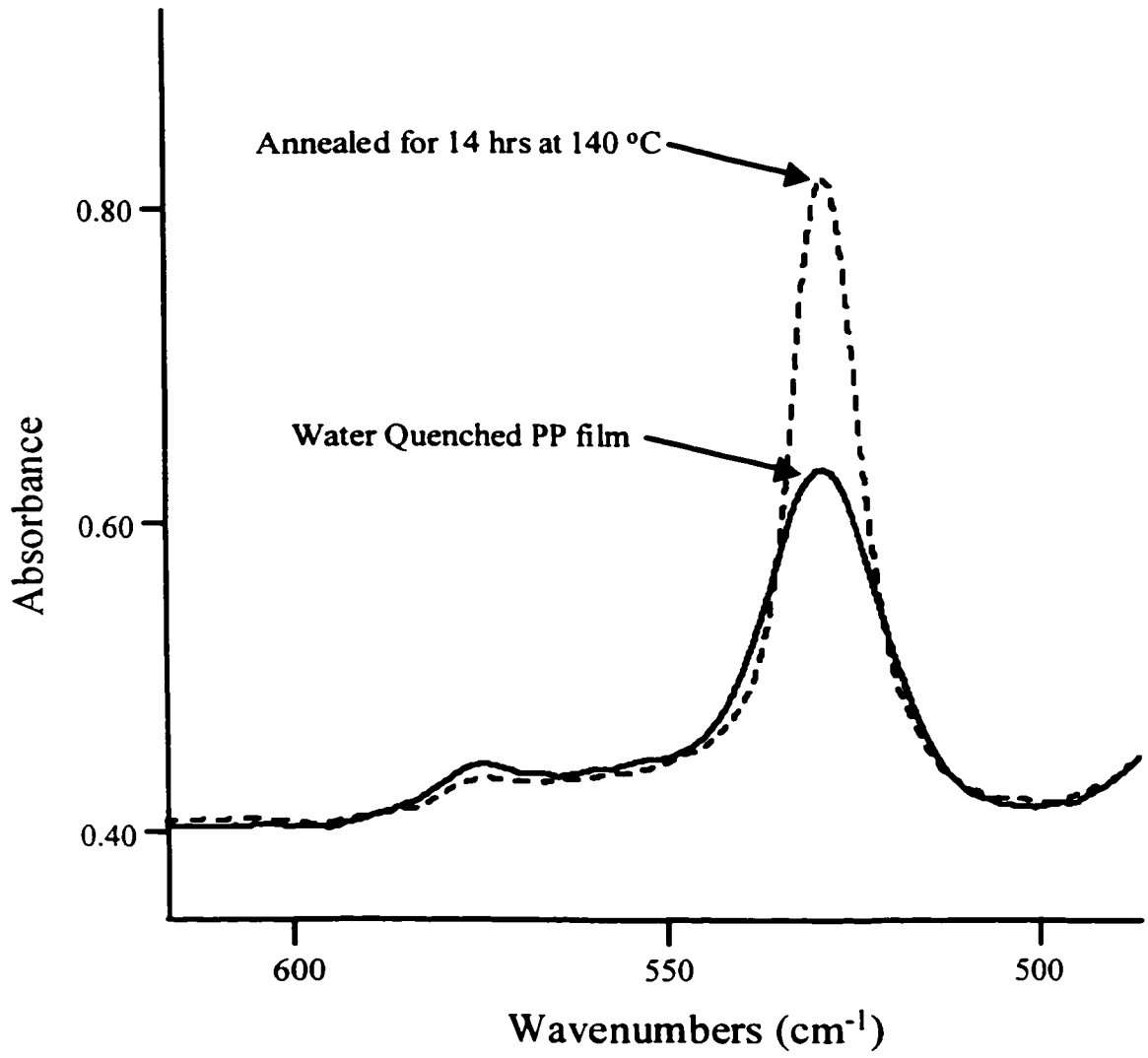

Figure 7.1. The Effect of the Degree of Crystallinity on the FT-IR Spectrum of Petrothene PP

described in section 4.3.3.2. Therefore, all the polymer films for FT-IR analysis contained approximately the same degree of crystallinity. The experimental results of the anhydride relative peak height for zero conversion from the screw configuration with the neutral kneading block are presented in Table 7.1.

Table 7.1. A Comparison of the Anhydride Relative Peak Heights for Zero Conversion Obtained at the Dual Strand Die and Sampling Ports

Total Flow Rate (g/min)	Screw Speed (rpm)	Anhydride Relative Peak Height		
		From Dual Strand Die	From S2	From S3
50	50	2.424	2.424	2.413
50	100	2.417	2.414	2.412
100	50	2.422	2.435	2.434
100	100	2.422	2.415	2.428

The anhydride relative peak height did not depend on the sampling position or the operating conditions when the degree of crystallinity was equal in all the analyzed polymer films. Therefore, the sampling ports effectively removed a bulk, or average sample of the polymer melt from the twin screw extruder. Averaged over the operating conditions, the anhydride relative peak height at zero conversion was (presented as ninety-five percent confidence intervals): 2.421 ± 0.005 at the die, 2.422 ± 0.016 at S2, and 2.422 ± 0.017 at S3. The same procedure was repeated for the screw configuration containing the reverse kneading block, and the average anhydride relative peaks were: 2.419 at the die, 2.426 at S2, and 2.427 at S3. As expected, the kneading block design did not significantly affect the results.

Pressure is required to force the polymer melt through the sampling port. There was a sufficient pressure at the reverse conveying element to allow for polymer melt sampling at S3 in all the experiments. In the case of the screw configurations with the restrictive neutral and

reverse kneading blocks, the pressure at position S2 was adequate for obtaining samples of the polymer melt. Conversely, the pressure upstream of the forward kneading block was insufficient to force the polymer melt through sampling port S2. To obtain a sample of the polymer prior to the forward kneading block, the screws from the twin screw extruder were extracted after establishing steady-state conditions. A small sample of the polymer melt was directly taken from the screw position located at sampling port S2. The small sample was water quenched and then pressed into a thin film using the previously described compression molding procedure. A sample was also taken from the extracted screws at the position of sampling port S3, which allowed for a comparison of the results from the two sampling procedures. Screw extraction and sampling of the polymer melt took approximately 2 min to complete.

Calculation of the anhydride conversion using equation 4.1 required the anhydride relative peak height at full conversion. The reaction was driven to its completion by heating 25 randomly selected films from the experiments with the neutral kneading block in a vacuum oven at 120 to 140 °C for three days. Before FT-IR analysis, the films were compression molded and rapidly quenched in the water bath to control the degree of crystallinity. The average anhydride relative peak heights at full conversion were (presented as ninety-five percent confidence intervals): 1.534 ± 0.028 at the die, 1.538 ± 0.033 at S2, and 1.529 ± 0.010 at S3. Similar to the zero conversion results, the sampling position did not affect the FT-IR analysis when the degree of crystallinity in all the polymer films was equal. In addition, the final conversion was obtained by blending equal masses of the Petrothene PP / reactive polymer blends in the batch mixer at 220 °C for 45 min. FT-IR analysis of the fully reacted product was completed, and the anhydride relative peak height was 1.528. Further

annealing at 140 °C did not change this value. As previously mentioned in Chapter 4, the final anhydride relative peak was accurately determined by both methods.

The distributive mixing profiles along the three screw configurations are presented in Figure 7.2. The screw tips were 540 mm downstream of the melt feeding location, and the length of the die zone was 105 mm. In the case of the screw configuration with the forward kneading block, the experimental results from the two different sampling methods at the position of sampling port S3 are compared in Table 7.2. Screw extraction followed by sampling resulted in an anhydride conversion that was 2.4% (average relative difference) higher than the conversion measured in the sample obtained directly from S3. Therefore, a small amount of reaction occurred by diffusion during the screw extraction procedure. The polymer tracers diffused slowly in molten PP, and therefore, this reaction was limited to the polymer tracers located in the vicinity of the interfaces. Three replicated experiments were completed using the screw configuration with the forward kneading block at 100 g/min and 50 rpm. The relative errors in the anhydride conversions obtained from the die and sampling port S3 were 1.7% and 2.1%, respectively. Considering the experimental reproducibility, the differences between the two sampling methods were not significant.

Table 7.2. Comparison of the Results for the Screw Configuration with the Forward Kneading Block at Position S3

Total Flow Rate (g/min)	Screw Speed (rpm)	Anhydride Conversion From Sampling Port S3	Anhydride Conversion From Extracted Screws
50	50	0.480	0.492
50	75	0.462	0.459
50	100	0.387	0.397
100	50	0.371	0.386
100	100	0.346	0.358

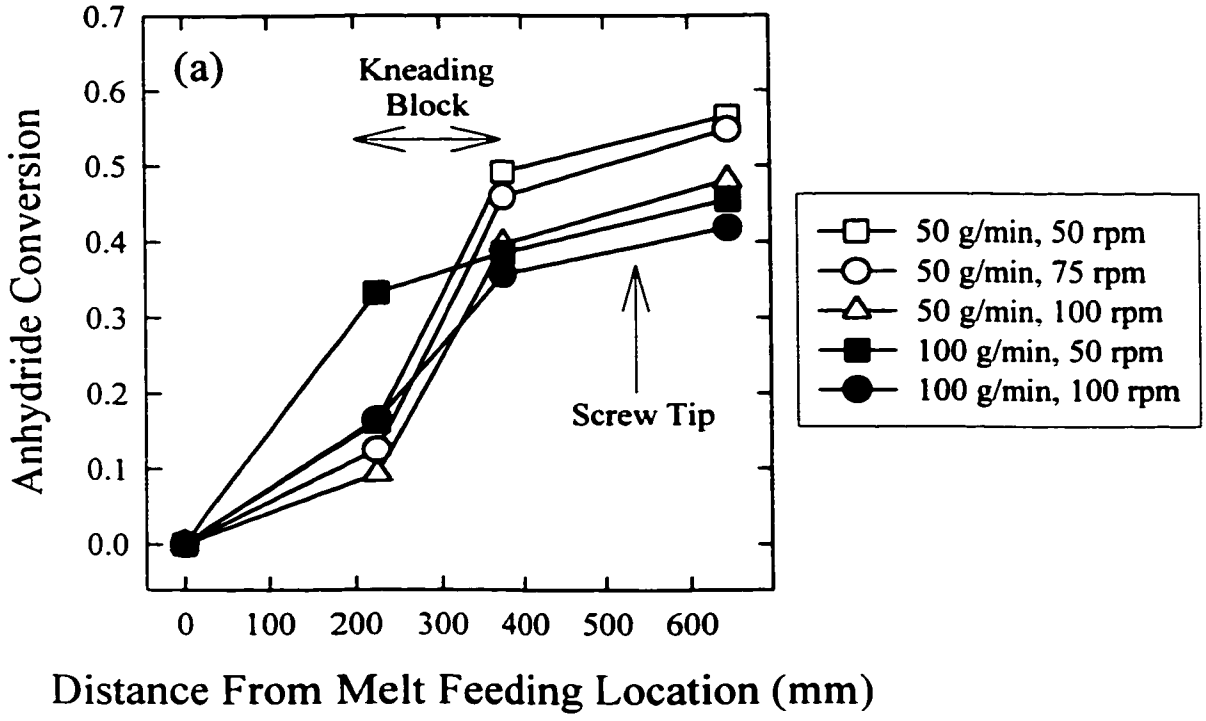
(a)
Kneading Block
Screw Tip
Anhydride Conversion
0.0
0.1
0.2
0.3
0.4
0.5
0.6
0.7
0
100
200
300
400
500
600
Distance From Melt Feeding Location (mm)
50 g/min, 50 rpm
50 g/min, 75 rpm
50 g/min, 100 rpm
100 g/min, 50 rpm
100 g/min, 100 rpm

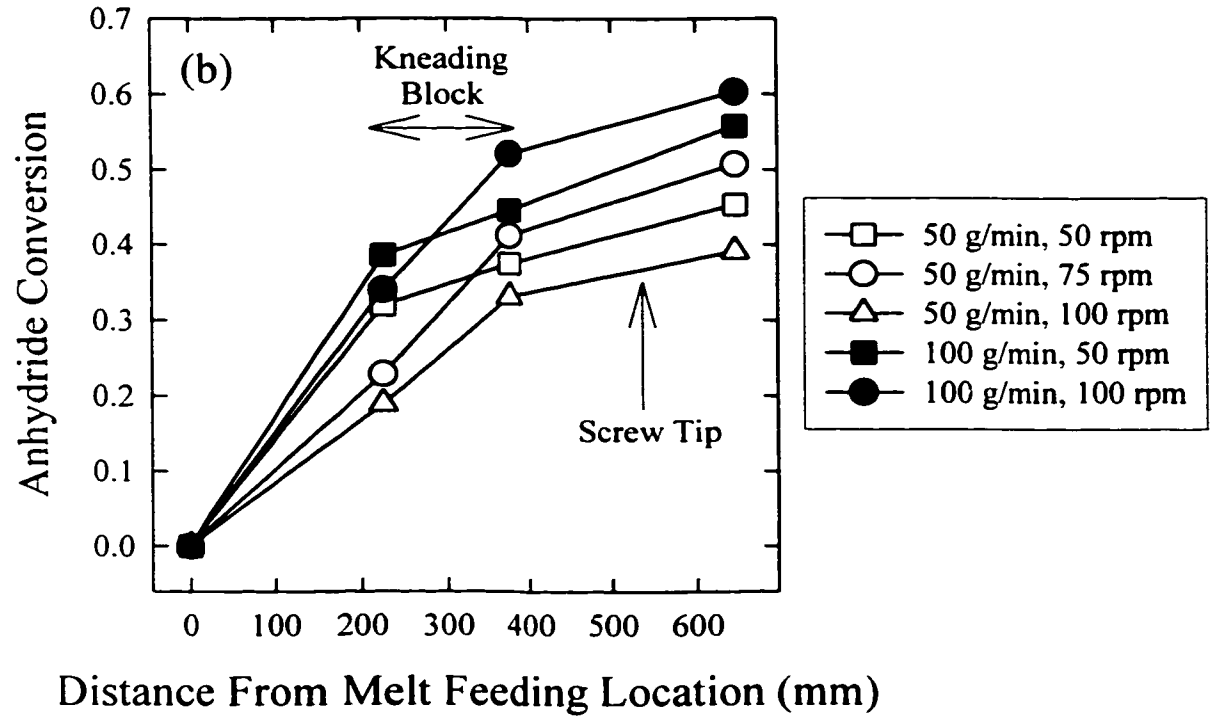
(b)
Kneading Block
Screw Tip
Anhydride Conversion
0.0
0.1
0.2
0.3
0.4
0.5
0.6
0.7
0
100
200
300
400
500
600
Distance From Melt Feeding Location (mm)
50 g/min, 50 rpm
50 g/min, 75 rpm
50 g/min, 100 rpm
100 g/min, 50 rpm
100 g/min, 100 rpm

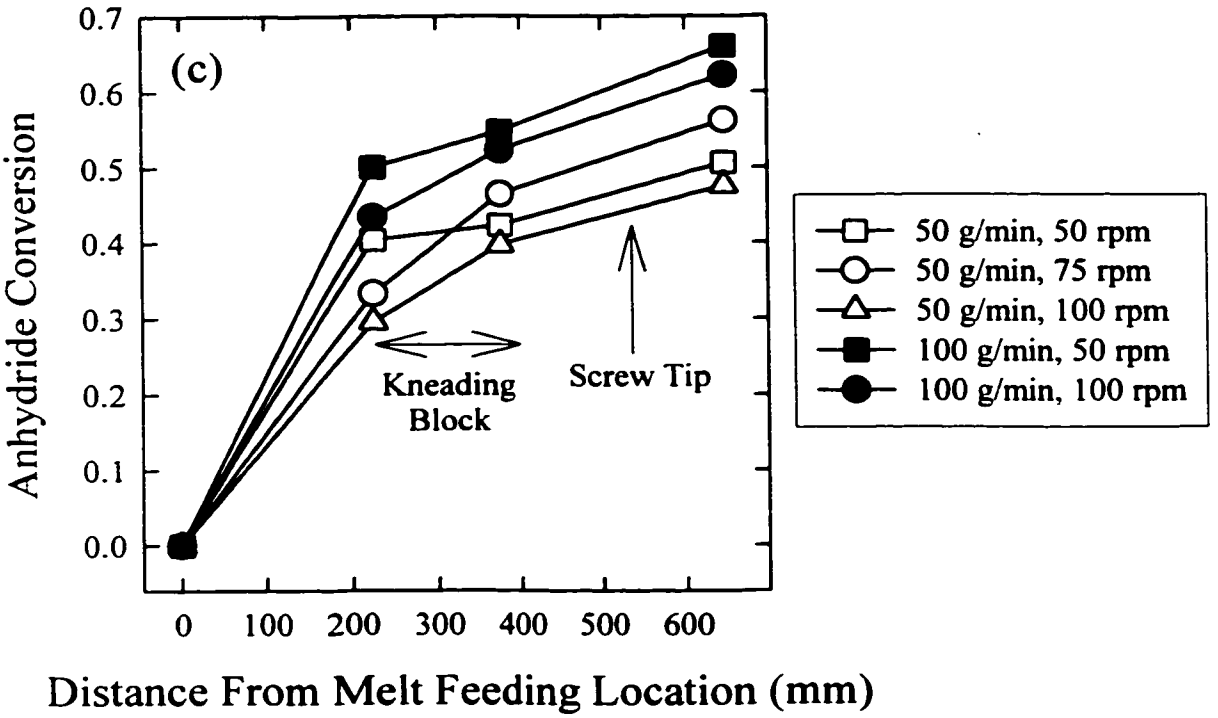

Figure 7.2. Distributive Mixing Profile Along the Length of the Melt-melt Blending Section of the Twin Screw Extruder
a) Screw Configuration with the Forward Kneading Block
b) Screw Configuration with the Neutral Kneading Block
c) Screw Configuration with the Reverse Kneading Block

The mixing profiles depict the evolution, or the development, of the interfacial area as the polymer travels down the melt-melt blending section of the twin screw extruder. Flow rate, screw speed, and kneading block design significantly affected the distributive mixing profiles. The lines included in Figure 7.2 connect the experimental data at each set of operating conditions, and they are not meant to depict the actual mixing profile between the experimental data points. The slope of the line connecting two adjacent sampling positions indicates the average rate of mixing in that local section of the extruder. Surprisingly, the mixing rate was not necessarily greater in the kneading block as compared to the mixing rate in the conveying section prior to the kneading block.

The mixing profiles for the screw configurations with the neutral and reverse kneading blocks were very similar. For example, both screw configurations showed improved overall mixing at the higher flow rate. Conversely, the screw configuration with the forward kneading block showed the opposite trend with respect to the flow rate. The mixing profiles of the three screw configurations are compared in Figure 7.3. The comparison was completed for a screw speed of 50 rpm, but similar trends were observed at all the investigated screw speeds. At 50 g/min (Figure 7.3 a), a significantly larger increase in the mixing was observed across the forward kneading block. This unique behavior of the forward kneading block is further discussed in section 7.1.2. At 100 g/min (Figure 7.3 b), the shapes of the mixing profiles of all three screw configurations were similar. In particular, the largest increase in the mixing occurred in the conveying section prior to each kneading block.

The overall anhydride conversions obtained with the strand die were approximately 35% lower than the results from the previously completed experiments with the slit die (Chapter 6) at the same experimental conditions. The die pressures (averaged over the

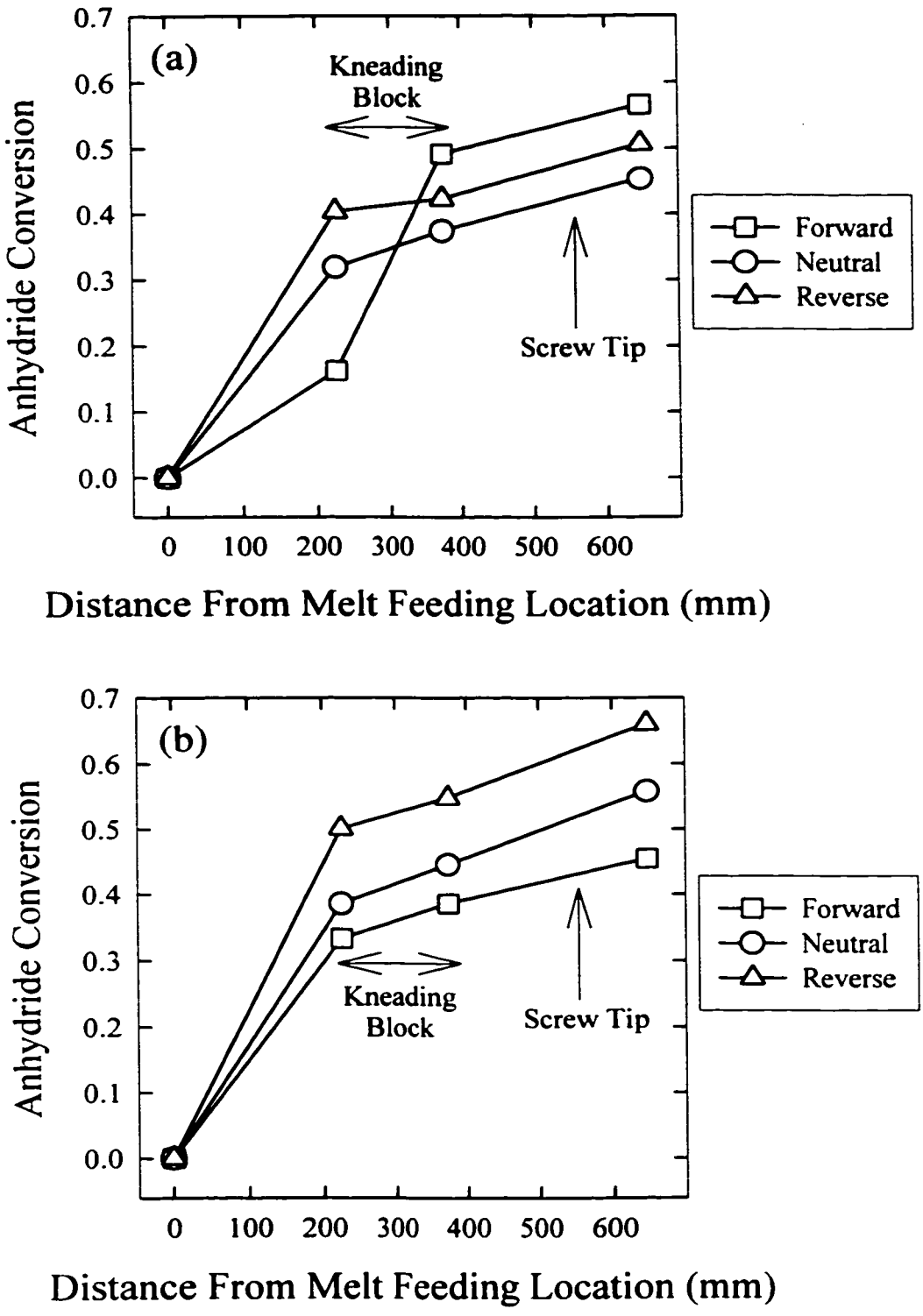

Figure 7.3. Comparison of the Mixing Profiles of the Three Screw Configurations at 50 rpm and (a) 50 g/min, (b) 100 g/min

investigated screw speeds) were: 1.93 MPa for the slit die at 50 g/min, 0.34 MPa for the strand die at 50 g/min, 2.90 MPa for the slit die at 100 g/min, and 0.53 MPa for the strand die at 100 g/min. The pressure prior to the slit die was approximately five times the value prior to the strand die, and therefore, the fully filled volume prior to the slit die was significantly greater. Owing to the higher shear rates applied to the polymer in this fully filled region, the more restrictive slit die caused greater mixing, and a corresponding higher anhydride conversion. At the end of the twin screw extruder the flow of the polymer melt converged into the die from a circular adapter with a diameter of 2.5 cm. Comparing the geometries of the dual strand die and slit die, the latter is expected to result in stronger converging flow (diameter of each strand = 4 mm, gap height in slit die = 0.75 mm). During this converging flow, the polymer melt undergoes elongational deformation, which results in very efficient interfacial area generation because the flow is irrotational (Meijer and Janssen, 1994). Therefore, the strong converging flow caused by the slit die may also have contributed to its higher anhydride conversions.

Regardless of the difference in the overall anhydride conversion, the experimental trends obtained with the dual strand die were identical to the trends discussed in Chapter 6 for the slit die. For example, the overall mixing performances at the strand die and the slit die followed the trends of (with respect to the kneading block design): forward > reverse > neutral at 50 g/min and reverse > neutral > forward at 100 g/min. Once again, the screw configuration containing the forward kneading block exhibited superior mixing at the low flow rate and inferior mixing at the high flow rate. Similar to the results from Chapter 6, screw speed exhibited a non-linear effect on the overall mixing performances of the screw configurations with the neutral and reverse kneading blocks at 50 g/min. Conversely, only a

negative linear screw speed effect on the overall mixing performance of the screw configuration with the forward kneading block was observed.

The mixing performances at the strand die and sampling port S3 are compared in Figure 7.4. Identical trends with respect to the operating conditions and kneading block design were observed at these sampling positions. The conveying section and die located at the end of the extruder increased the overall conversion, as indicated by the shifting of all the data points to higher conversions at the die in Figure 7.4 (both plots have identical scales). The increase is also apparent in the mixing profiles (Figure 7.2) for each screw configuration. Regardless of the experimental factors (kneading block design and operating conditions), the relative increase in the conversion was 17 % between S3 and the die. The die did not affect the mixing trends in the extruder because the screw channel was partially filled immediately after the reverse conveying element. Therefore, the backup length prior to the die did not extend into the kneading block. The pressures and flow patterns in the kneading block were independent of the die restriction. Conversely, if the kneading block is located immediately prior to the die, the pressure profile in the kneading block will depend on the die pressure. In this situation, the die would affect the flow patterns and mixing in the kneading block. The same mixing performance would not be achieved if the die geometry was changed or if the kneading block was moved upstream of the die.

7.1.1. Local Distributive Mixing in the Conveying Section

The mixing achieved by the conveying section prior to the kneading block (from the melt feeding location to sampling port S2) is presented in Figure 7.5. The results were plotted with respect to the specific throughput because it was shown to be a key factor for

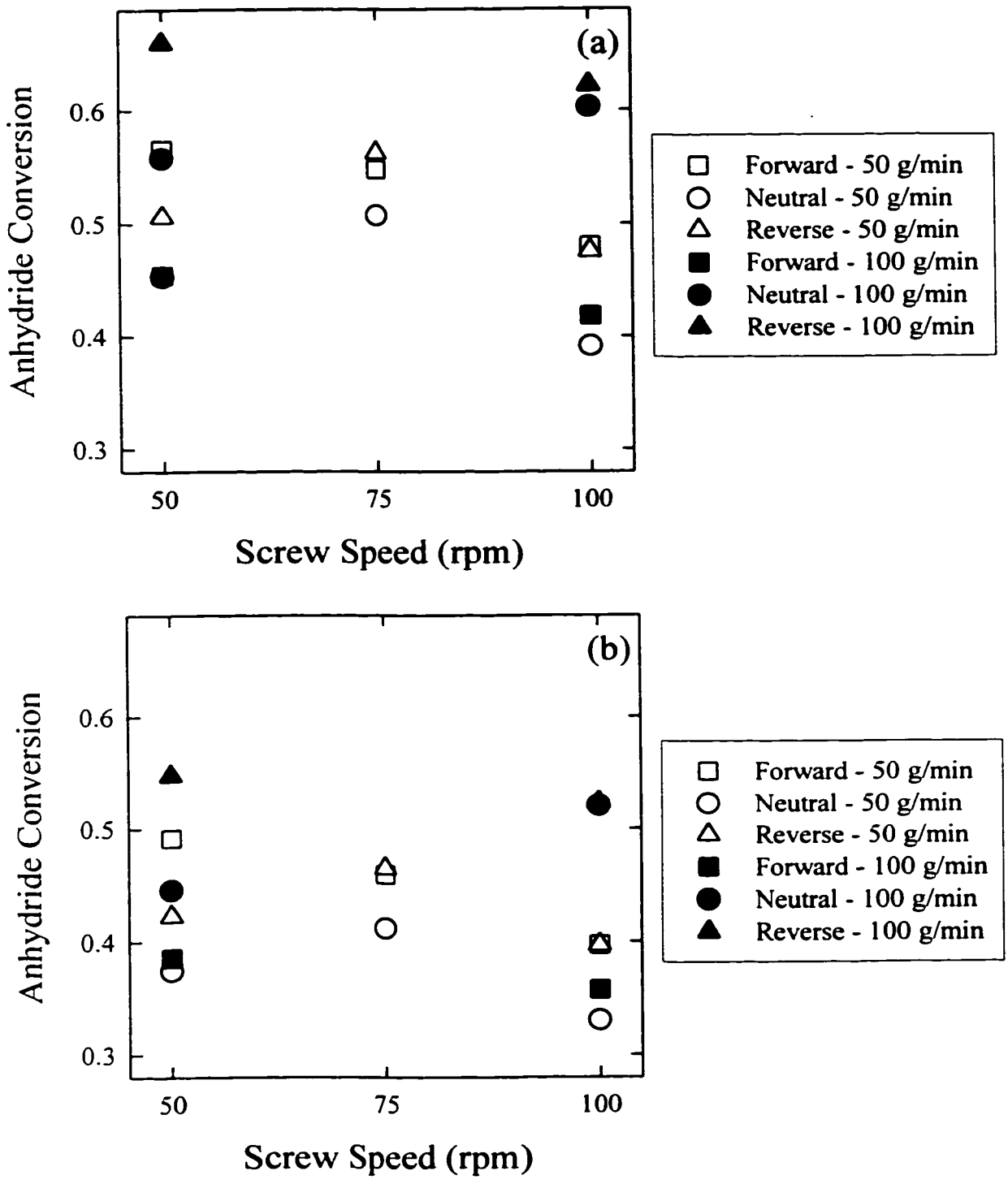

Figure 7.4. Mixing Performances at (a) the Strand Die and (b) Sampling Port S3

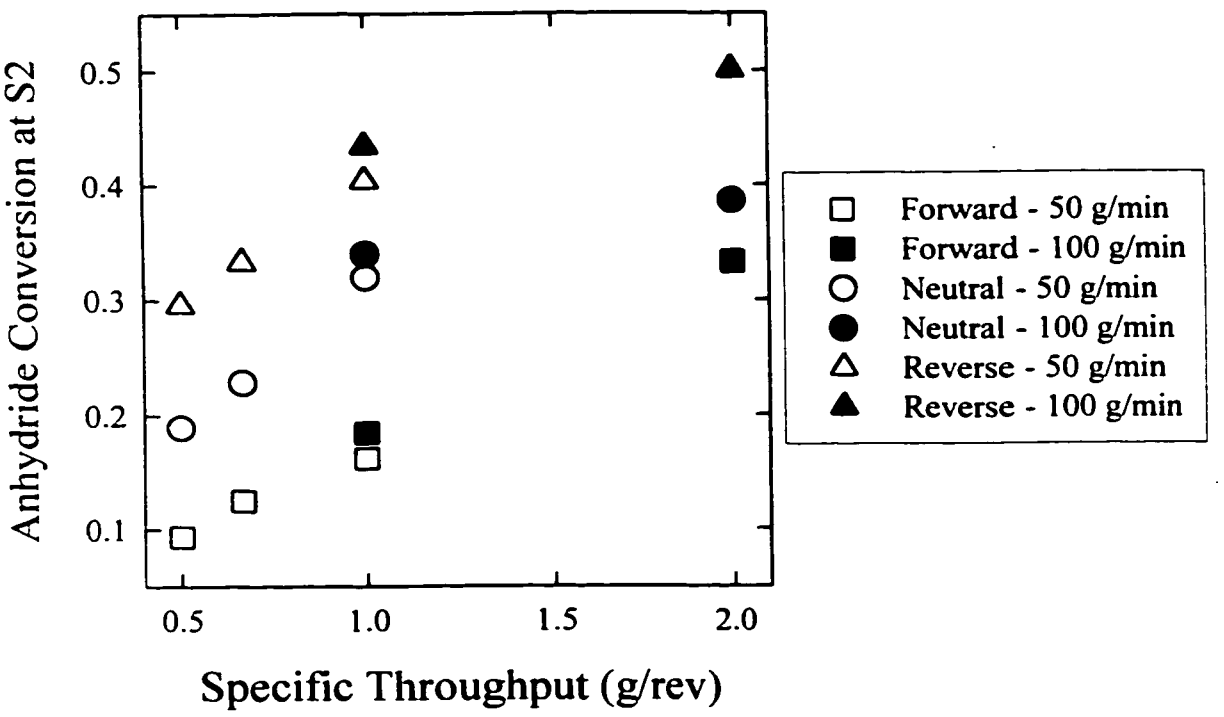

Figure 7.5. Mixing Performance of the Conveying Section Preceding the Kneading Block

distributive mixing in partially filled conveying elements of twin screw extruders (Bigio *et al.*, 1994). In the melt-melt blending experiments, the conveying section between the melt feeding location and the sampling port S2 consisted of a region of partially filled conveying elements followed by a region of fully filled conveying elements. The conveying elements immediately upstream of the neutral and reverse kneading blocks were fully filled to generate the required pressure to force the polymer melt through the flow restriction. As previous discussed in Chapter 5 and 6, a small region of fully filled channels was observed prior to the forward kneading block even though it generated pressure. From Figure 7.5, distributive mixing during polymer melt blending increased with the specific throughput, which is an indication of the degree of channel fill. A specific throughput of one was achieved in the experiments completed at 50 g/min and 50 rpm and 100 g/min and 100 rpm. The latter combination of operating conditions resulted in an anhydride conversion that was 7% higher for each screw configuration. This difference was significantly larger than the average experimental error of 2%, which indicated that the operating conditions may exhibit other effects on the mixing process. Although specific throughput was a key factor for distributive mixing in the conveying section, it did not account for the effect of the upstream kneading block geometry. The kneading block geometry determined the pressure at the end of the conveying section, which affected the mixing process through the fully filed length. As indicated in Figure 6.3, the average pressure at S2, which is an indication of the fully filled length preceding the kneading block, followed the trend of: reverse > neutral > forward for all the operating conditions. This trend is identical to the mixing performance trend in the conveying section with respect to the upstream kneading block design at a given specific throughput.

The screws from the twin screw extruder were extracted after establishing steady-state flow of pure Petrothene PP to determine the fully filled length prior to the kneading block. Using a simple 2^2 factorial design, the fill distribution was investigated at screw speeds of 50 and 100 rpm and flow rates of 50 and 100 g/min. To improve the contrast between the polymer melt and the screws, 0.5wt% TiO_2 was added to the Petrothene PP. The additive increased the measured pressures in the extruder, but it did not affect the fully filled length prior to the kneading block. Photographs of the fill distribution in the conveying section and kneading block are presented in Figures 7.6 to 7.9 (the average pressures 15 mm upstream of the kneading block are also included). From the photographs, all three kneading blocks appeared to be fully filled. The fully filled length in the conveying section prior to the kneading block depended on the operating conditions as well as the kneading block geometry. At a given set of operating conditions, the highest pressures and longest fully filled lengths were measured prior to the reverse kneading block. Once again, the conveying elements immediately preceding the forward kneading block were fully filled even though the pressure at S2 was zero (except at 100 g/min and 50 rpm). For all three screw configurations, the fully filled region was located in the 180 mm length of 20 mm pitch conveying elements preceding the kneading block.

Anhydride conversion in the conveying section prior to the three kneading blocks is related to the fully filled fraction (the ratio of the axial fully filled length and the total length of the conveying section prior to S2, 225 mm) prior to sampling port S2 in Figure 7.10. Linear regression was performed to quantify the relationship between the mixing performance and the axial fully filled fraction, and the best representation of the experimental results is presented in equation 7.1. The correlation coefficient (r^2) was 0.9623, which

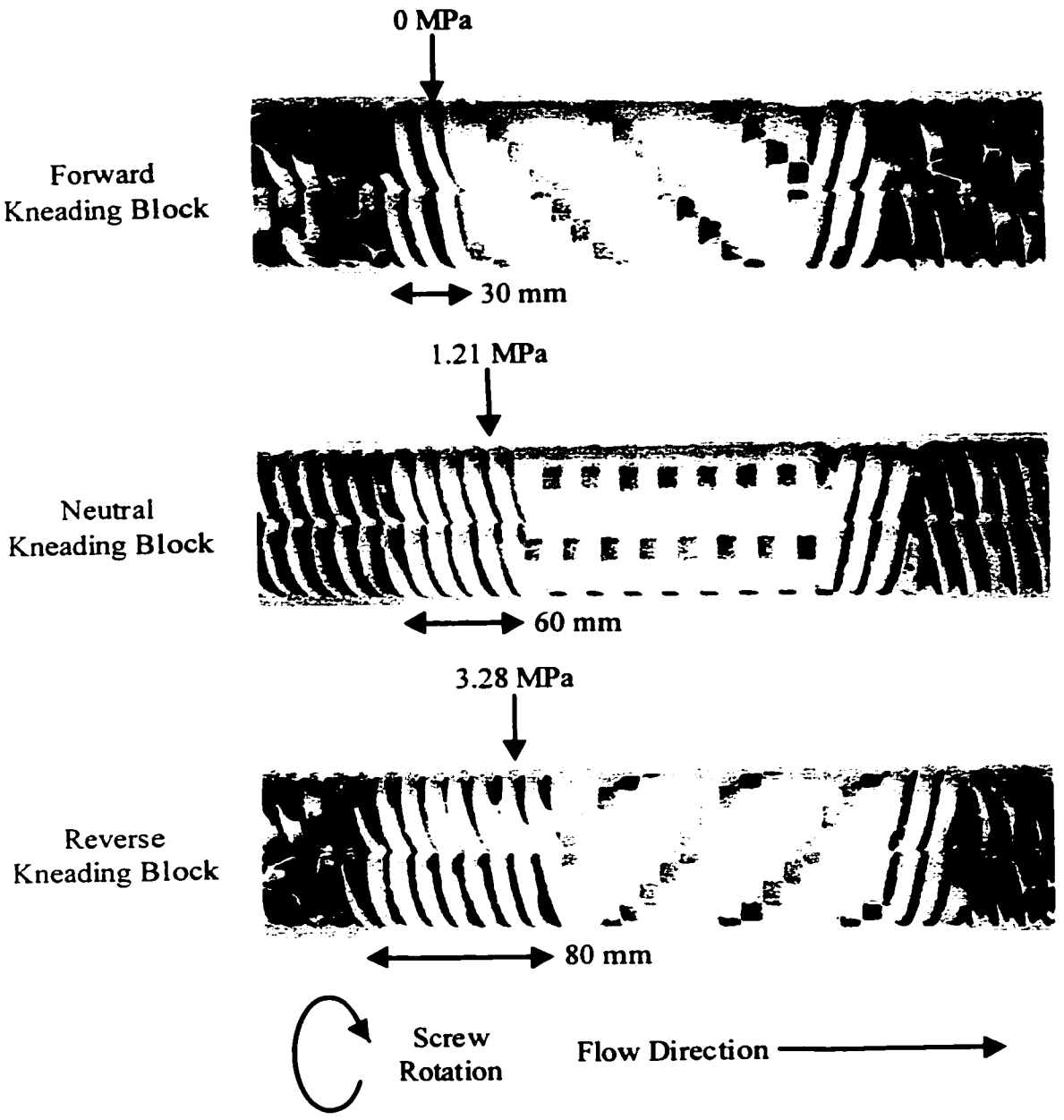

Figure 7.6. Fill Distribution in the Conveying Section and the Kneading Block at 50 g/min and 50 rpm

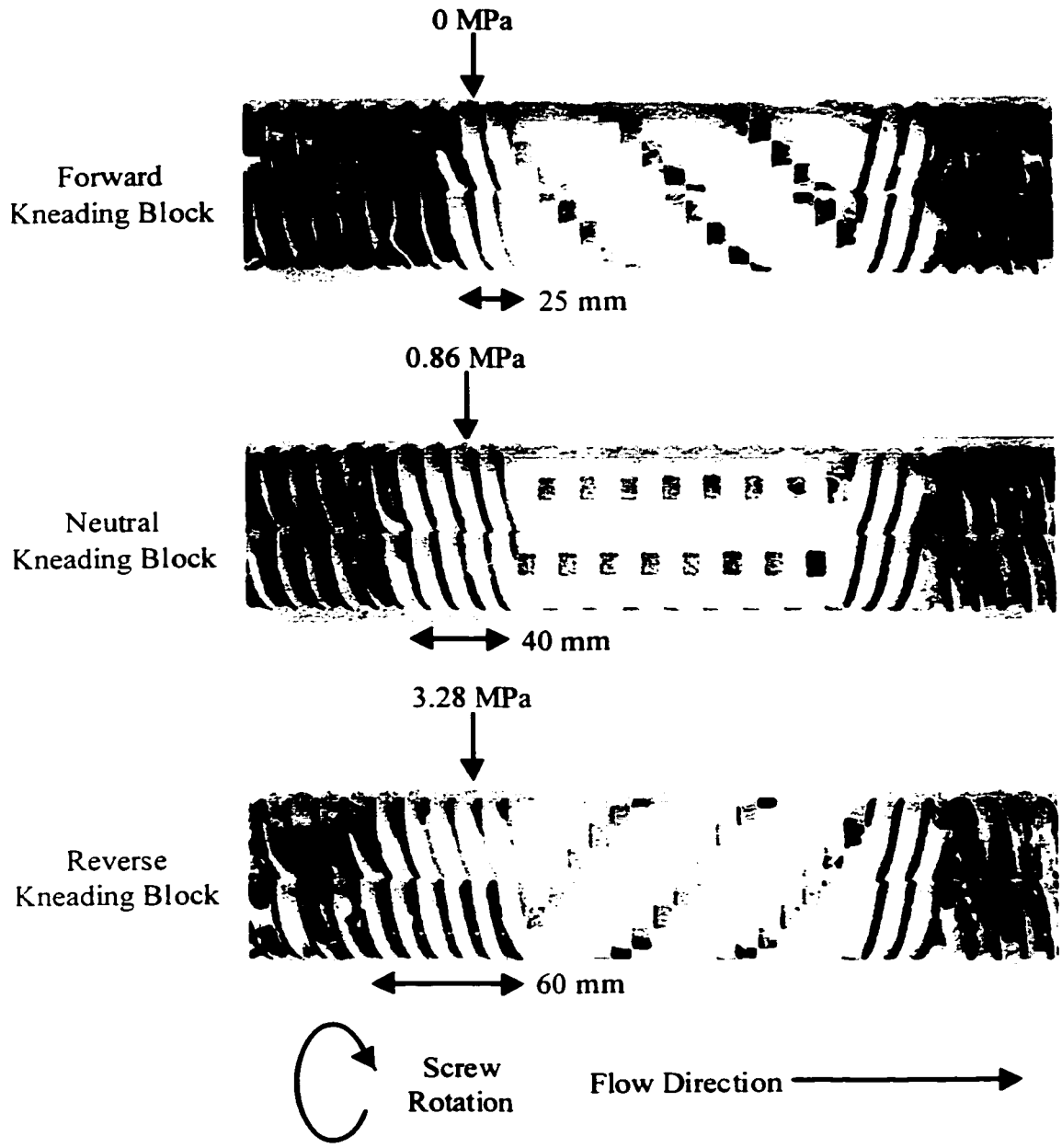

Figure 7.7. Fill Distribution in the Conveying Section and the Kneading Block at 50 g/min and 100 rpm

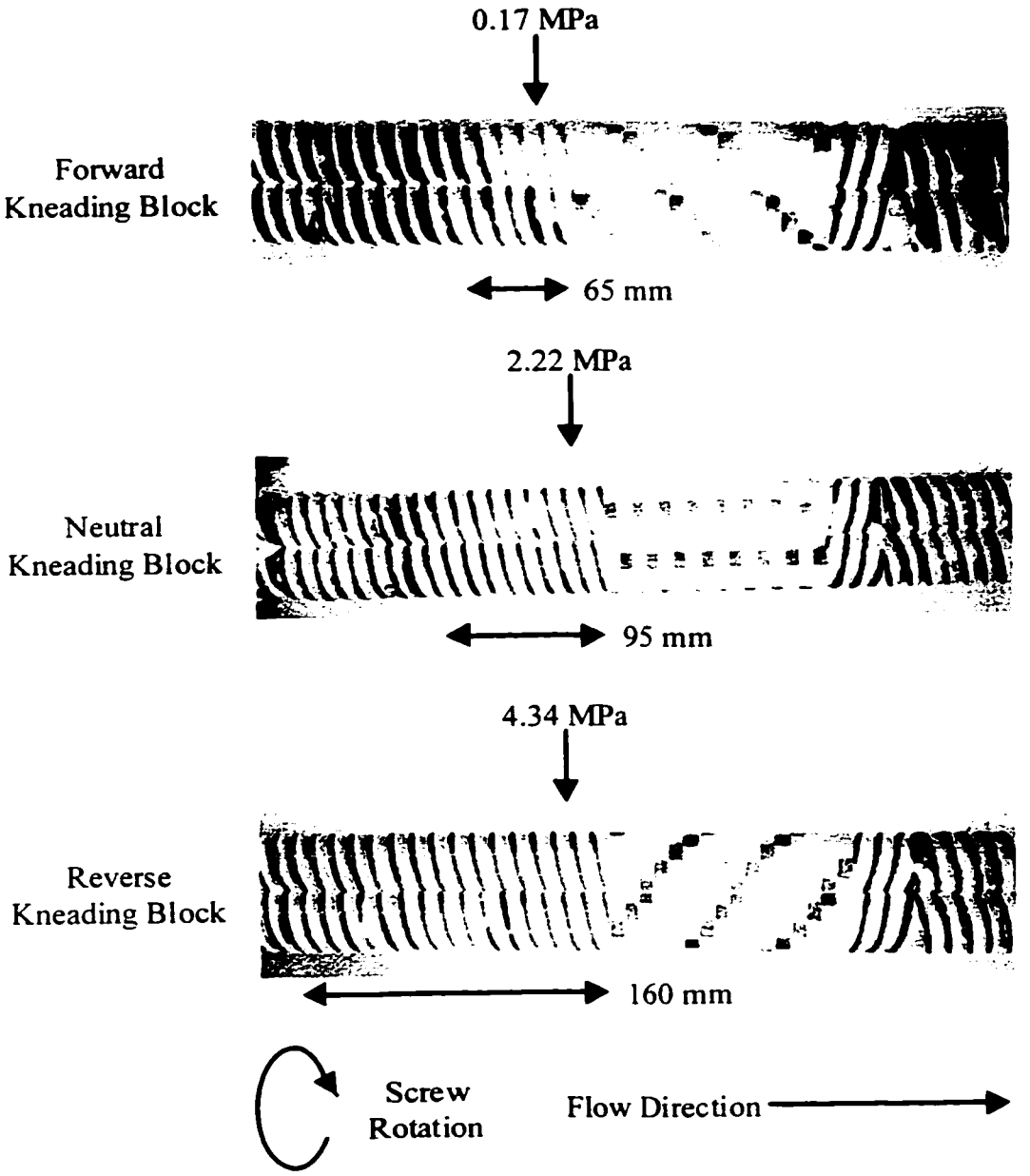

Figure 7.8. Fill Distribution in the Conveying Section and the Kneading Block at 100 g/min and 50 rpm

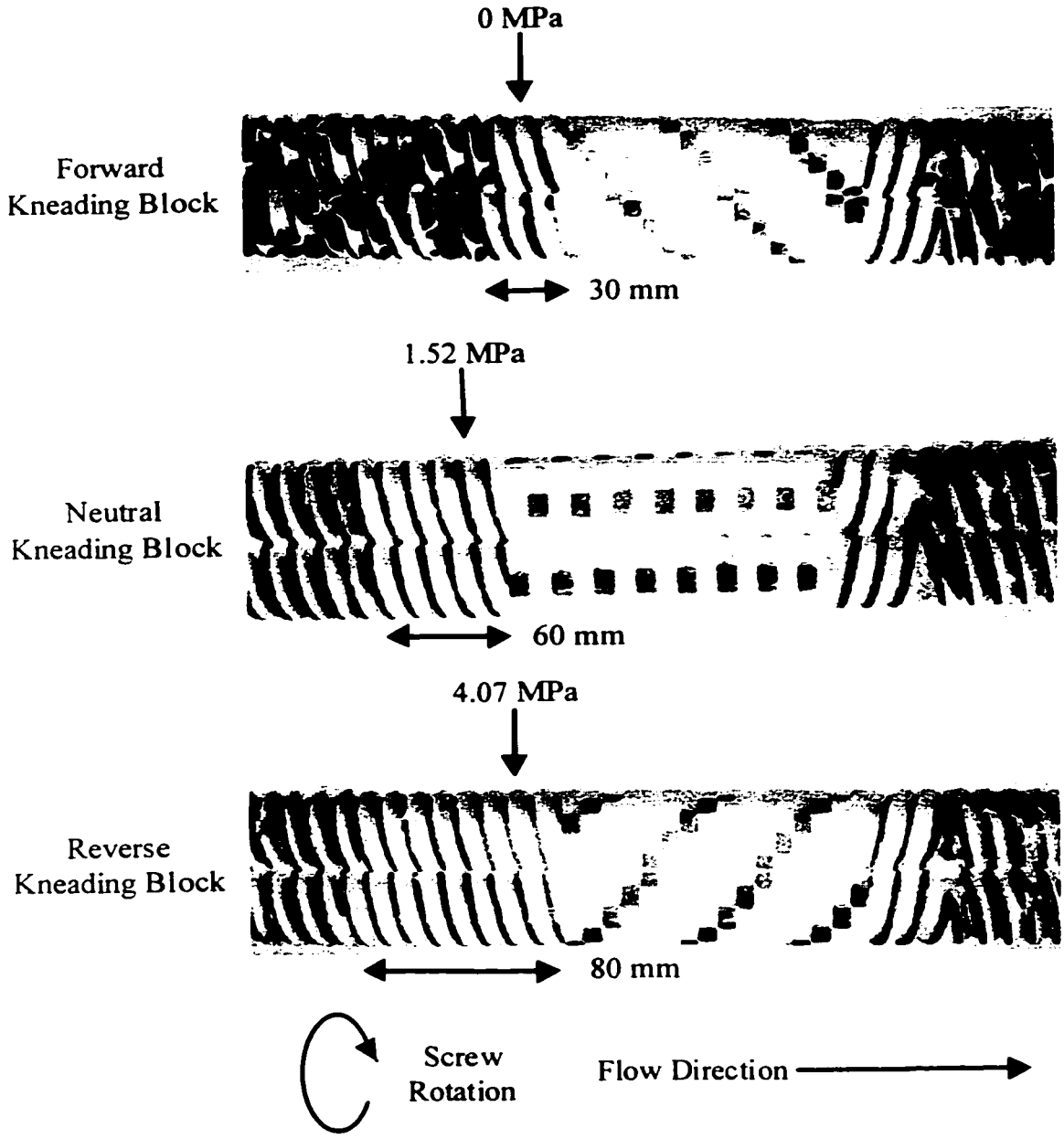

Figure 7.9. Fill Distribution in the Conveying Section and the Kneading Block at 100 g/min and 100 rpm

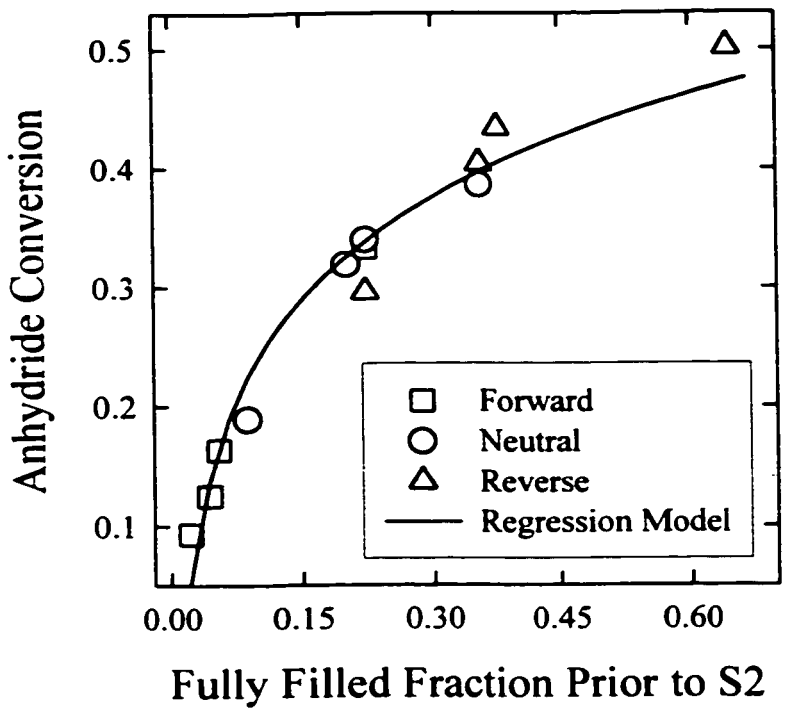

Figure 7.10. Relationship Between Distributive Mixing and Fully Filled Fraction in the Conveying Elements Preceding the Kneading Block

indicated that the regression model satisfactorily represented the experimental results.

$$\text{Anhydride Conversion} = 0.53 + 0.29 * \log(\text{Fully Filled Fraction}) \qquad (7.1)$$

The generation of interfacial area, or distributive mixing, in the conveying section prior to the kneading block was directly related to the fully filled fraction. In contrast to the specific throughput, the results from all three screw configurations followed the same trend with respect to the fully filled fraction, which confirmed its importance in the distributive mixing process. The fully filled fraction was a controlling factor for distributive mixing in the conveying section because it accounted for the effects of the operating conditions and the pressure at the end of the conveying section.

Using linear extrapolation of the first three data points in Figure 7.10, an anhydride conversion of 0.044 was estimated for a zero fully filled fraction (entire section is partially filled) in the conveying section. According to Figure 7.10, the anhydride conversion is 0.3 for a fully filled fraction of approximately 0.2. Assuming an anhydride conversion of approximately 0.044 was achieved in the partially filled region, over 85% of the total mixing in the conveying section occurred in this short fully filled region prior to the kneading block. In the partially filled region of the conveying section, the polymer melt was conveyed forward without significant deformation. Therefore, the material was only subjected to high shear rates in the fully filled region prior to the kneading block. As well, backflow or flow recirculation in the fully filled region may contribute to its superior distributive mixing capability.

The linear-log relationship between the generation of interfacial area and the fully filled fraction (Figure 7.10) suggested that the mixing efficiency decreased along the fully filled region of the conveying section. If the mixing efficiency remained constant along this

section, a linear relationship between the distributive mixing and the fully filled fraction is expected. As reviewed by Agassant and Poitou (1994), mixing efficiency decreases with time in shear flows because the fluid orients with the streamlines. In the twin screw extruder, a longer fully filled length corresponds to a longer time that the polymer melt will be subjected to high shear rates. Mixing efficiency in shear flows is greatly improved by occasional reorientation of the material (Meijer and Janssen, 1994). Therefore, the linear-log relationship in the conveying section suggested that the interfaces were not effectively reoriented in the intermeshing region of the twin screw extruder. Bigio and Erwin (1985) and Bigio *et al.* (1992) observed no reorientation of the material in the nip region (intermeshing zone between the screws) during the mixing of model materials in the conveying elements of a co-rotating twin screw extruder. Incomplete reorientation of a thermoplastic elastomer in the nip region was also observed by Kalyon and Sangani (1989). In the work of Bigio and Erwin (1985) and Bigio *et al.* (1992), the distributive mixing, in terms of the number of striations in the former and the amount of line stretching in the latter, was linearly related to the applied strain. In their analyses, the strain was assumed to be linearly related to the flow length in the twin screw extruder. From Figure 7.10, distributive mixing was not linearly related to the flow length in the fully filled region, which was attributed to poor reorientation of the interfaces. A similar leveling off of the mixing versus the flow length was observed by Bigio and Stry (1990) in a co-rotating twin screw extruder, which was attributed to poor reorientation of the interfaces and possible unmixed regions in the flow.

7.1.2. Local Distributive Mixing in the Kneading Block

The mixing achieved in the kneading block (between S2 and S3) is presented in Figure 7.11 in terms of the absolute anhydride conversion completed in the kneading block (conversion at S3 minus conversion at S2), the fraction of the overall conversion completed in the kneading block (the absolute conversion divided by the conversion at the strand die), and the ratio of the conversion at the end of the kneading block and the conversion entering the kneading block (conversion at S3 divided by the conversion at S2). The lines in Figure 7.11 connect the experimental results for each screw configuration at a given flow rate, and they highlight the effect of screw speed on the mixing performance. All three representations of the mixing achieved in the kneading block showed similar trends with respect to the operating conditions and the kneading block design.

The conversion ratio across the kneading block (Figure 7.11 c) is equivalent to the relative increase in the interfacial area as the material travels through the kneading block. A ratio of one indicates that the material traveled through the kneading block without mixing. Except for the forward kneading block at 50 g/min, there was very little mixing in the kneading blocks at 50 rpm due to the low shear rates applied to the polymer. In general, higher screw speeds and lower flow rates increased the mixing in the kneading blocks due to their corresponding effects on the applied strain. Surprisingly, the mixing in the neutral and reverse kneading blocks at 50 g/min did not increase as the screw speed was increased from 75 to 100 rpm. The neutral and reverse kneading blocks were fully filled, and therefore, the average residence time is expected to be independent of the screw speed (verified in the local residence time experiments discussed in section 7.2). van der Wal *et al.* (1996) performed numerical 3-D isothermal flow simulations of a Newtonian fluid in kneading blocks, and

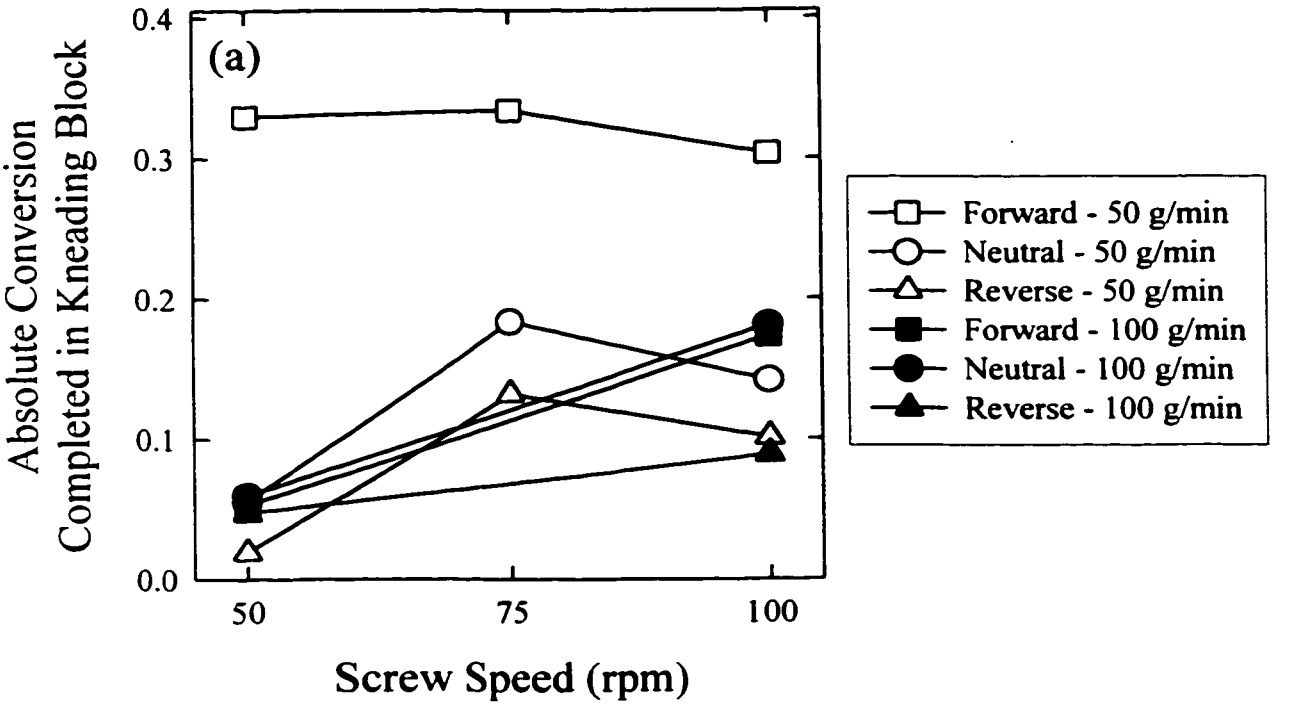
(a)
Absolute Conversion Completed in Kneading Block
0.4
0.3
0.2
0.1
0.0
50
75
100
Screw Speed (rpm)
Forward - 50 g/min
Neutral - 50 g/min
Reverse - 50 g/min
Forward - 100 g/min
Neutral - 100 g/min
Reverse - 100 g/min

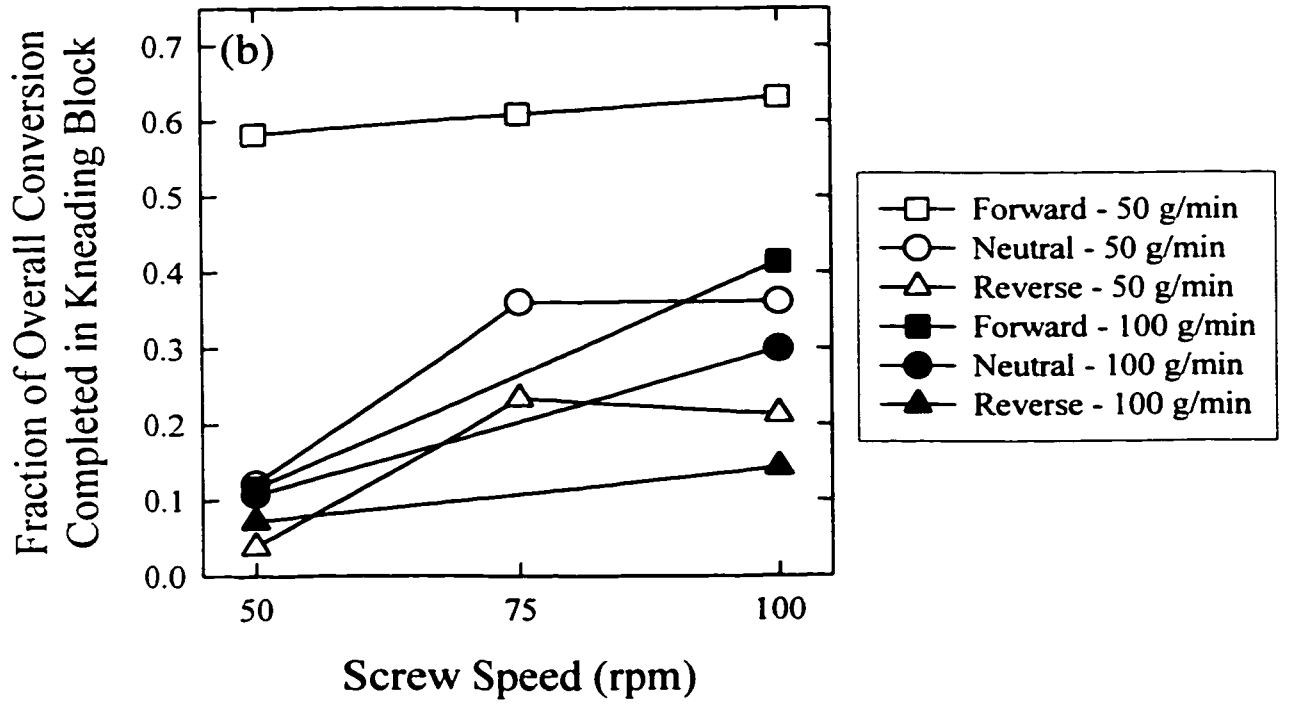
(b)
Fraction of Overall Conversion Completed in Kneading Block
0.7
0.6
0.5
0.4
0.3
0.2
0.1
0.0
50
75
100
Screw Speed (rpm)
Forward - 50 g/min
Neutral - 50 g/min
Reverse - 50 g/min
Forward - 100 g/min
Neutral - 100 g/min
Reverse - 100 g/min

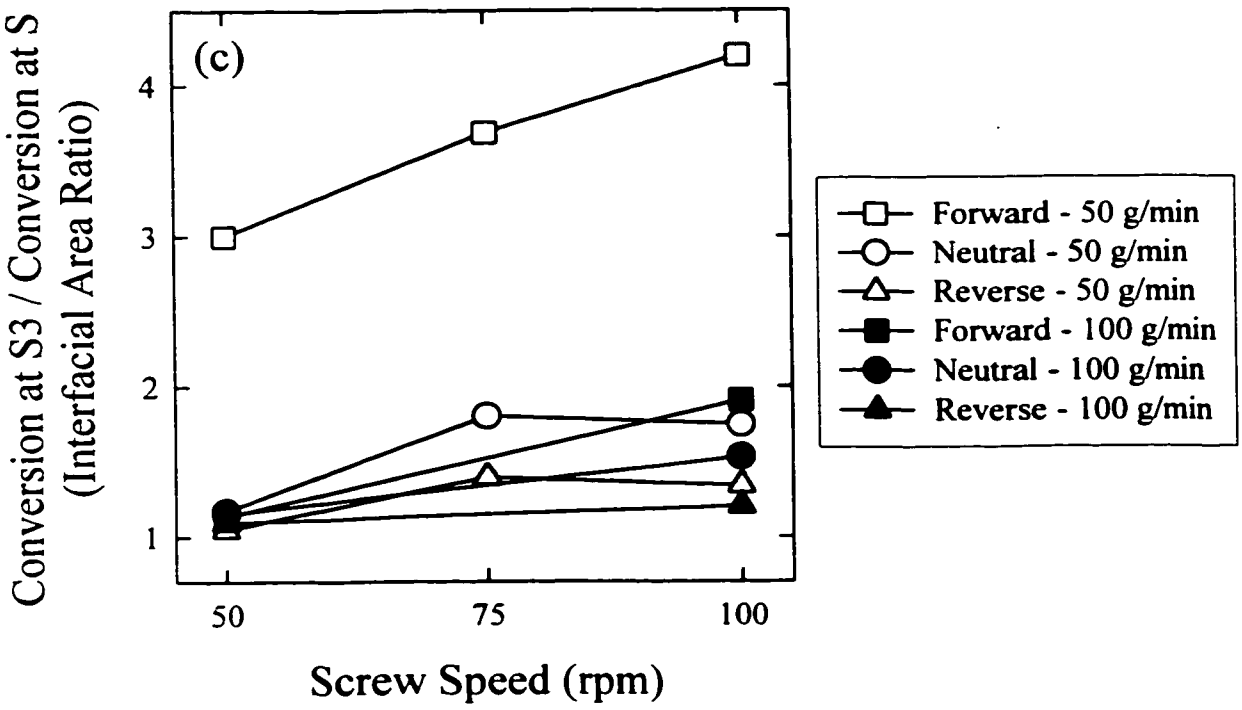

Figure 7.11. Mixing Achieved in the Kneading Block
a) Absolute Anhydride Conversion Between S2 and S3
b) Fraction of Overall Conversion Completed Between S2 and S3
c) Ratio of Conversion at S3 and S2 (Interfacial Area Growth Across Kneading Block)

shear rate was predicted to increase with both screw speed and flow rate. Therefore, a continuous increase in the applied strain with the screw speed is expected. The experimental mixing results suggested that the relationship between the applied strain and screw speed may be more complicated for the non-isothermal flow of shear thinning polymers in kneading blocks.

At both flow rates, the mixing performance in the kneading block followed the trend of: forward > neutral > reverse. This trend was not identical to the overall mixing performance trends (forward > reverse > neutral at 50 g/min and reverse > neutral > forward at 100 g/min). The mixing performance of the forward kneading block at 50 g/min was significantly greater than mixing performances of the restrictive kneading blocks. From Figure 7.11 (c), a 300 to 400% increase in the interfacial area was achieved as the material traveled through the forward kneading block at the lower flow rate. In contrast, the maximum increases in the interfacial area across the neutral and reverse kneading blocks were 80% and 40%, respectively (Figure 7.11 c). Therefore, the kneading block geometry significantly affected the local distributive mixing. The geometry affects the pressure profile and flow patterns in the kneading block, which determine its capability to distribute the material to the high shear rate regions and reorient the interfaces to improve the mixing efficiency. The combination of positive drag flow and negative pressure flow in the forward kneading block geometry yielded the most effective local distributive mixing. Stagnant flow regions in the forward kneading block at the low flow rate may also contribute to its superior mixing performance. Local residence time measurements were completed to investigate this possible flow phenomena, and the results are presented in section 7.2.

Using numerical analysis of the flow of HDPE, the average shear rate in kneading discs was predicted to be independent of the stagger angle (Cheng and Manas-Zloczower, 1997). In addition, flow simulations of a Newtonian material in kneading blocks predicted that the average shear rates in forward and neutral kneading blocks were similar, while the average shear rate was approximately 25% higher in a reverse kneading block (van der Wal *et al.*, 1996). These numerical predictions suggested that the geometry of the kneading block does not significantly affect the average shear rate applied to the polymer. From Figure 7.11, the kneading block geometry clearly affected its mixing performance, and therefore, distributive mixing was not related to the average shear rate. Using numerical analysis of the flow in kneading blocks, Bravo (1998) predicted that the polymer melt experiences a broad distribution of shear rates. In particular, the flow of the polymer through the high shear rate regions in the kneading block may play an important role in the distributive mixing process.

The contribution of the local mixing in the kneading block to the overall mixing of the melt-melt blending section is presented in Figure 7.11 (b). The forward kneading block at 50 g/min caused the greatest contribution of approximately 60% to the overall distributive mixing. Although the screw configuration with the reverse kneading block exhibited good overall mixing (the best at the higher flow rate of the three screw configurations), the contribution of the local mixing in the reverse kneading block was less than 20%. Approximately 70% of the overall mixing occurred in the conveying section prior to the reverse kneading block. Due to its restrictive nature, the reverse kneading block caused the largest fully filled fraction in the conveying section at a given set of operating conditions. The experimental results indicated that the material entering the reverse kneading was not effectively distributed to the high shear rate regions in the kneading block or reoriented to

improve the mixing efficiency. Jaffer *et al.* (1999) presented 3-D numerical simulations of the flow in kneading blocks. A very interesting observation from their research was that the kneading block does not drastically change the ordered helical motion of the polymer entering the kneading block from conveying elements. For effective mixing, the kneading block must disturb the flow patterns to reorient the interfaces that are aligned with the streamlines. An inability to disturb the flow entering the reverse kneading block may have contributed to its poor local distributive mixing.

Similar to the analysis of the mixing in the conveying section (Figure 7.5), the mixing performance in the kneading block is presented in Figure 7.12 as a function of the specific throughput. Clearly, specific throughput was not a key parameter for distributive mixing in the kneading block. The distributive mixing in the conveying section was controlled by the fully filled fraction, which accounts for both the specific throughput and the pressure at the end of the conveying section. The neutral and reverse kneading blocks were always fully filled, and therefore, specific throughput does not have a physical meaning in the kneading block.

7.1.3. The Effect of the Melt Feeding Location on the Distributive Mixing in the Kneading Block

Using the same screw configuration as the mixing profile experiments (Figure 4.8), a series of preliminary experiments were completed to investigate the effect of the melt feeding location on the mixing. In the previous experiments, the melt fed stream was introduced above a partially filled conveying section, which exhibits poor mixing due to the low shear rates applied to the polymer. In contrast, Petrothene PP with 5wt% anhydride polymer tracer was melt feed directly into the intermeshing region of the kneading block 40 mm

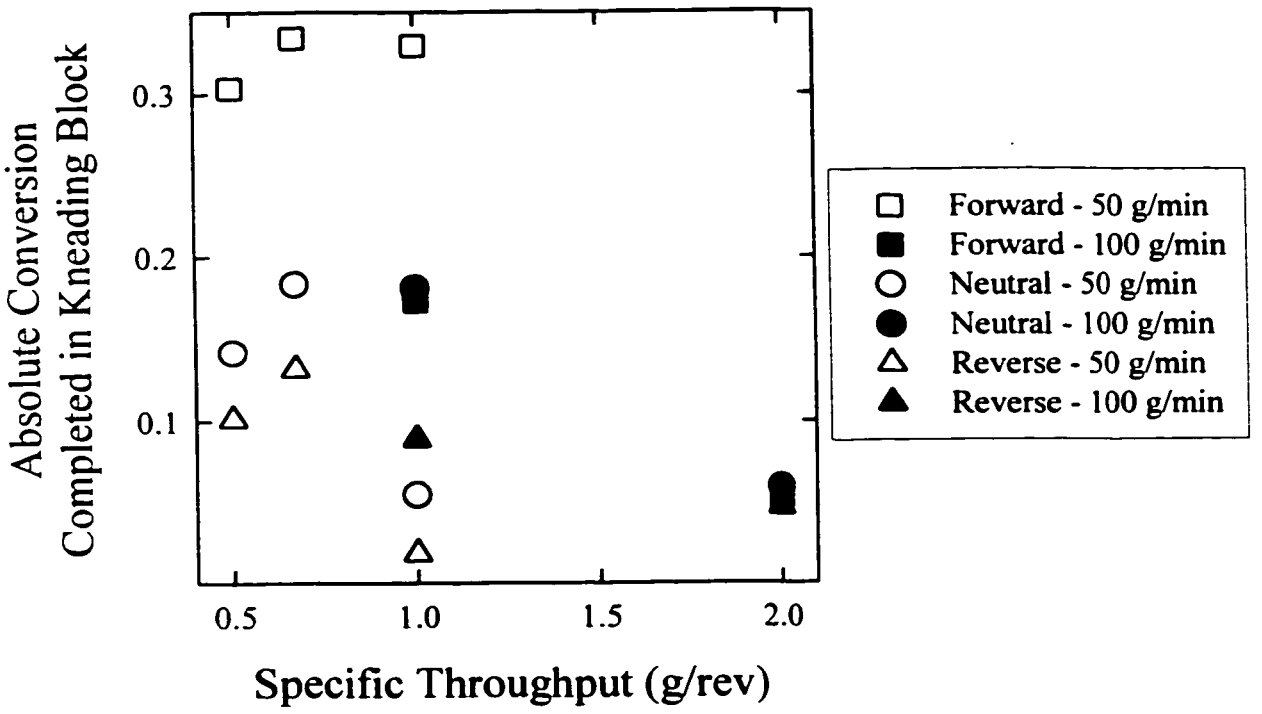

Figure 7.12. The Effect of Specific Throughput on the Kneading Block Mixing Performance

downstream of the first kneading disc in the new experiments. These experiments were completed at 50 g/min and 50 rpm for kneading disc stagger angles of 30°, 60°, 90°, and –30°. The mixing in the kneading block was measured by analyzing the sample obtained from sampling port S3 (total mixing length = 95 mm, 80 mm of kneading discs and 15 mm of the reverse conveying element). In the previous experiments, the orientations of the interfaces entering the kneading block may have depended on the fully filled fraction in the conveying section. A longer fully filled fraction prior to the reverse kneading block may have caused a greater amount of interfacial alignment with the streamlines in the conveying section. This alignment will affect the local mixing in the kneading block. Melt feeding directly into the kneading blocks guaranteed that the mixing performances were evaluated on a common basis (not biased by the amount of interfacial alignment). The new anhydride conversion results in the kneading blocks are compared with the anhydride conversion differences across the kneading blocks from the mixing profile experiments (conversion at S3 minus the conversion at S2, total mixing length = 150 mm, 15 mm of conveying element, 120 mm of kneading discs, and 15 mm of the reverse conveying element) in Table 7.3.

Table 7.3. Comparison of the Mixing Results in the Kneading Block: Effect of Melt Feeding Location

Kneading Block (Stagger Angle)	Anhydride Conversion Difference Across Kneading Block (S3 – S2) from Mixing Profile Experiments	Anhydride Conversion at S3 with Melt Feeding into Kneading Block
Forward (30°)	0.324	0.414
Forward (60°)	Not Investigated	0.252
Neutral (90°)	0.055	0.128
Reverse (-30°)	0.019	0.274

Melt feeding directly into the high shear rate region at the top of the kneading discs improved the local mixing in the kneading block even though the total mixing length was

shorter. In particular, a 14.4 fold increase in the local mixing performance of the reverse kneading block was observed. As previously mentioned, the poor local mixing in the reverse kneading block during the mixing profile experiments may have been caused by its inability to disturb the flow entering from the conveying elements. Therefore, the interfaces were not effectively reoriented or distributed to the high shear rate regions in the reverse kneading block. Melt feeding directly into the reverse kneading block forced the material into the high shear rate region between the disc tip and the barrel wall, which greatly improved the local mixing. From Table 7.3, the best local mixing was achieved by the forward kneading block geometry in both sets of experiments.

Two different forward stagger angles are possible in the kneading blocks of the Leistritz LSM 30.34 twin screw extruder. As compared with the stagger angle of 30° that was used in all the mixing experiments presented in Chapters 5 to 7, a stagger angle of 60° increases the backflow gap (identified in Figure 7.13) between adjacent kneading discs, which may affect the distributive mixing capability of the kneading block. Using numerical simulations, Szydlowski *et al.* (1987) predicted a maximum backward flux for a forward stagger angle of 60°. Conversely, the fraction of the flow that passes over the kneading disc tip, which is a high shear rate region, was predicted to be maximum for small stagger angles (for example 30°). In addition, a larger stagger angle decreases the forwarding capability of the kneading block, which will affect its flow patterns and pressure profile. From the melt-melt blending experiments in the kneading block presented in Table 7.3, a forward stagger angle of 30° resulted in superior distributive mixing. This result suggested that the flow over the kneading disc tip was more important than the flow through the backflow gap for distributive mixing. Pressure transducers were positioned 15 mm upstream and downstream

of the kneading block to investigate the pressure profile. The average pressures and fill distributions of the two kneading blocks are compared in Figure 7.13. For a stagger angle of 30° the average pressure increased from 0 to 1.0 MPa, but for a stagger angle of 60° the average pressure remained constant at 1.0 MPa. As indicated by the pressure measurements, the flow patterns in the two forward kneading blocks were significantly different. The negative pressure flow component in the kneading block with a stagger angle of 30° may have contributed to its superior distributive mixing capability. The preliminary melt-melt blending experiments in the forward kneading blocks indicated that larger backflow gaps do not improve the distributive mixing.

7.2. Local Residence Time Measurements

The method used to perform the local residence time measurements employing a carbon black tracer and the IR temperature probe is discussed in section 4.3.4.2. The screw configuration and probe positions are presented in Figure 4.10. The objective was to determine the local residence time in the conveying section and the kneading block. All the experiments were completed using Petrothene PP and the same barrel temperatures used in the mixing profile experiments. Replicated experiments were completed at all three probe positions for the screw configuration containing the neutral kneading block. The calculated average residence times and variances (using equations 4.9 and 4.10, respectively) are presented as ninety-five percent confidence intervals in Table 7.4. The average relative error (the ratio of the confidence interval and the average value) in the average residence times and variances were 0.015 and 0.23, respectively. Although the reproducibility of the average residence times was adequate, the variance exhibited significant experimental error. As

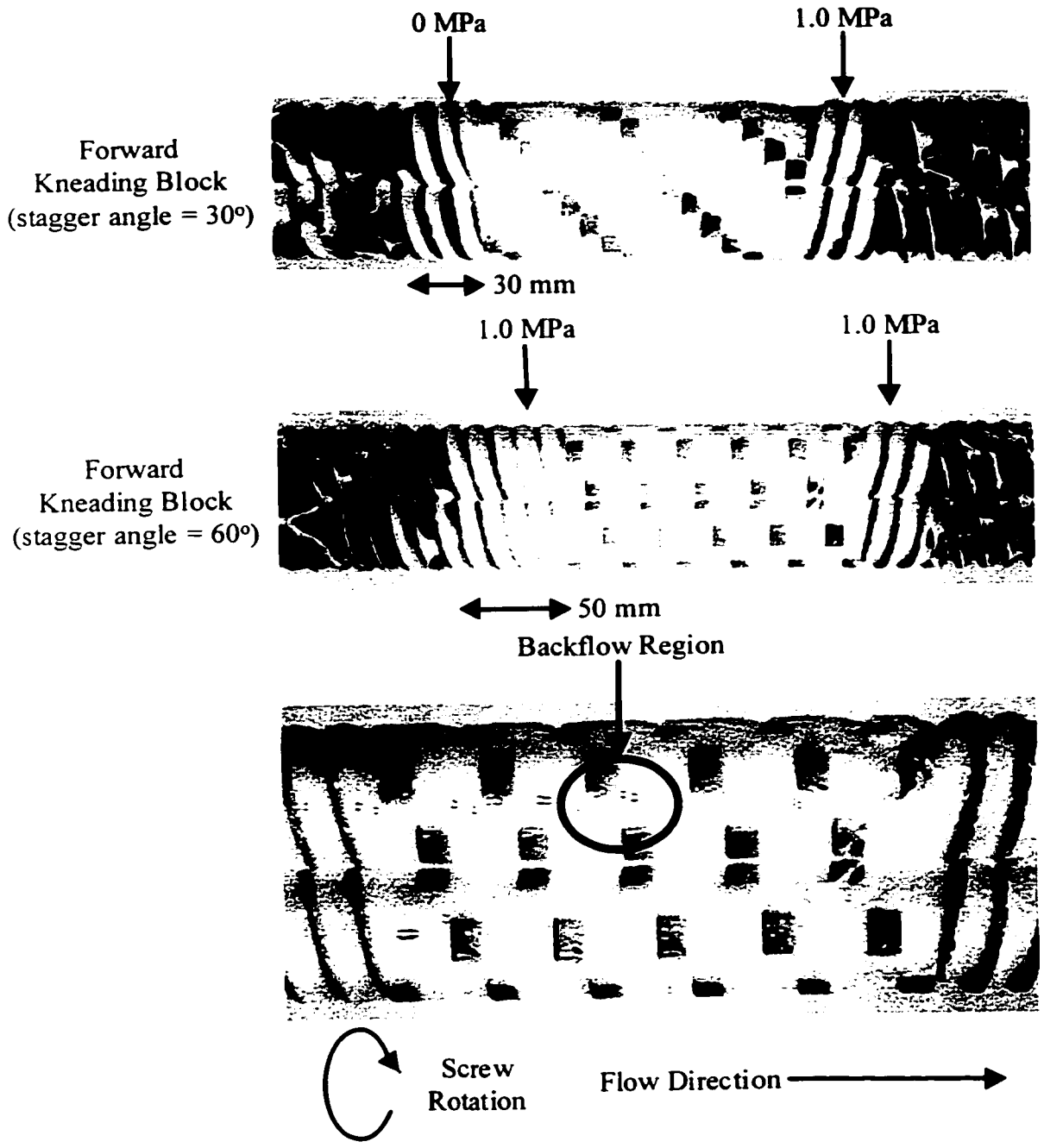

Figure 7.13. Comparison of the Average Pressures and the Fill Distributions for Forward Kneading Blocks with Staggering Angles of 30° and 60°

described in section 4.4.4., the raw temperature data from the IR probe contained significant noise. The values presented in Table 7.4 were calculated using average steady-state temperature baselines. Without this baseline correction, the experimental reproducibility of the variance was even worse. In some situations, negative variances were calculated using the raw temperature data. The baseline correction did not significantly improve the reproducibility of the calculated average residence times.

Table 7.4. Calculated Average Residence Times and Variances from the Local Residence Time Experiments with the Screw Configuration Containing the Neutral Kneading Block

Probe Position	Operating Conditions Screw Speed (rpm) / Flow Rate (g/min)	Average Residence Time (s)	Variance (s^2)
1 (Barrel 5)	50 / 50	69.22 ± 0.35	408.0 ± 126.2
1 (Barrel 5)	200 / 50	33.73 ± 1.00	114.0 ± 31.5
2 (Upstream of Kneading Block)	50 / 50	133.3 ± 0.52	744.0 ± 78.8
2 (Upstream of Kneading Block)	200 / 50	78.16 ± 2.82	219.6 ± 92.4
3 (Downstream of Kneading Block)	50 / 50	181.7 ± 1.17	423.5 ± 68.7
3 (Downstream of Kneading Block)	200 / 50	132.9 ± 0.95	565.4 ± 54.9

Prior to presenting the local residence time results, the validity of the experimental method is discussed. A fundamental assumption in RTD experiments is that the tracer concentration is measured across the entire flow at its detection point. Commonly a mixing cup average of the tracer concentration in the material collected over a time interval is used. Conventional off-line RTD analysis of extruders involves the determination of the tracer concentration in the extrudate. Conversely, local RTD measurements employ a special probe to detect the tracer directly inside the system. In this case, an IR temperature probe was used

to detect the changing surface emissivity, which is directly related to the carbon black concentration according to Nietsch *et al.* (1997). For valid RTD measurements, the probe must measure the carbon black tracer concentration across the entire flow at the probe position (across the entire screw channel cross section from the barrel to the screw surface). The surface of the IR temperature probe is flush with the barrel wall. As the carbon black tracer passes the probe position the polymer melt changes from transparent to a black body and then back to a transparent melt. Initially, there is a certain penetration depth in the transparent polymer melt from which the probe receives thermal radiation. Maier (1996) reported that the penetration depth for the thermal radiation received by the probe can be as great as 1 cm. The carbon black increases the surface emissivity, which correspondingly decreases the penetration depth. When the polymer melt becomes a black body (the penetration depth is nearly zero) the probe receives radiation only from the polymer surface resulting in its lower temperature reading (Nietsch *et al.*, 1997). The penetration depth increases as the carbon black concentration decreases, and radiation is once again received from within the polymer melt (resulting in an increase in the temperature reading). During this entire process, the IR probe does not detect the carbon black tracer across the entire channel depth. The probe temperature reading may be more sensitive to the surface concentration rather than the bulk concentration of the carbon black across the entire channel depth. Therefore, the IR temperature probe measurement of the RTD may be affected by the local flow of the carbon black tracer at the probe position. In particular, the radial flow of the carbon black to and away from the polymer melt surface may significantly affect the RTD measurements using the IR probe method.

To test the potential probe detection problem, a series of experiments were completed in the twin screw extruder to determine if the screw element at the probe position affected the RTD results. The experiments were completed at 50 g/min and 50 rpm with two different screw configurations. The only difference between the two screw configurations (depicted in Figure 7.14) was the stagger angle (90° or –30°) of the four kneading discs surrounding the probe position in the kneading block. This stagger angle will affect the local flow field (pressure profiles, drag flow capability) at the probe position in the kneading block. For each screw configuration, separate experiments were completed with the probe positioned in the kneading block and the reverse conveying element (30 mm separates the two positions). All the experiments were completed using a pulse of 0.2 g PP / carbon black added to barrel 1 of the twin screw extruder. The calculated average residence times and variances at the kneading block and the reverse conveying element are presented in Table 7.5 (presented as ninety-five percent confidence intervals).

Table 7.5. Average Residence Times and Variances at the Kneading Block and the Reverse Conveying Element to Test the IR Temperature Probe RTD Method

Probe Position	Average Residence Time (s)	Variance (s^2)
Kneading Block (reverse stagger)	165.7 ± 3.09	534.1 ± 19.9
Kneading Block (neutral stagger)	163.1 ± 2.00	486.4 ± 37.6
Reverse Element After Reverse Stagger Kneading Block	185.4 ± 3.14	393.2 ± 16.2
Reverse Element After Neutral Stagger Kneading Block	184.3 ± 1.99	414.4 ± 24.7

As expected, it took a longer time for the carbon black tracer to reach the probe position at the reverse conveying element. Surprisingly, the variance at the reverse conveying element was significantly smaller than the variance at the kneading block position.

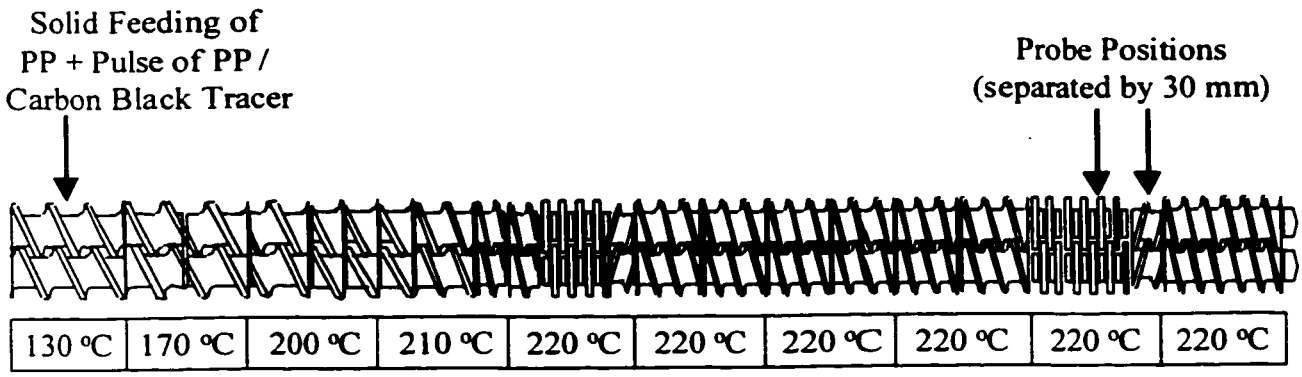

Figure 7.14. Screw Configuration for the Validating Experiments on the Local RTD Method

This decrease in the variance of the RTD as the material traveled down the extruder between the two probe positions is not physically possible. The results verified the fundamental detection problem of the IR temperature probe, and it was attributed to differences in the local flow of the carbon black tracer at the two probe positions. The smaller variance at the reverse conveying element suggested that there was faster radial flow of the carbon black to and away from the polymer melt surface at this probe position. The calculated average residence time at the kneading block probe position was not affected by the stagger angle, which indicated that it was not sensitive to the local flow field. Therefore, the IR temperature probe method is valid for determining the local average residence time in the extruder, but the distribution of residence times depends on the screw element at the probe position.

Chen (1992) and Nietsch *et al.* (1997) observed fluctuating temperature readings when the IR probe was positioned in a partially filled region of the extruder. A zero pressure was measured at probe position 2 (Figure 4.10) prior to the forward kneading block except at 100 g/min - 50 rpm and 75 g/min - 50 rpm. From Figures 7.6 to 7.9, the conveying elements prior to the forward kneading block appeared to be fully filled, regardless of the pressure at S2. The high degree of fill at probe position 2 resulted in adequate contact between the probe surface and the polymer melt for accurate temperature measurement during the experiments (no significant fluctuations). In contrast, the temperature decrease caused by the carbon black tracer during the RTD experiments was detected only when the probe position was pressurized. In order to measure the local residence time in the forward kneading block a new experimental method was required.

Separate experiments were completed by injecting a pulse of 0.05 g PP / carbon black immediately prior to the forward kneading block through an open vertical pressure transducer mounting (identified in Figure 4.10). The carbon black tracer was detected by the IR temperature probe at position 3. In these experiments a solid tracer was added to the flowing polymer melt to measure the average residence time. Hu and Kadri (1999) proposed that the tracer must have an identical geometric shape to the material being investigated for valid RTD results. Within 2 to 3 s after the addition of a pulse of the solid tracer to the screw channel containing the molten PP, the screws were dead stopped and extracted to inspect the state of the tracer. The tracer was visible as a black streak in the screw channel that was approximately 1 figure-8 turn of the screws in length (axial length = 30 mm). The experiment was repeated using PP with 0.5wt% TiO_2 to increase the contrast between the tracer and the polymer melt, and a photograph of the tracer in the extracted screws in presented in Figure 7.15. The long streaks of the tracer indicated that it rapidly melted in the screw channel. If the tracer melted slowly, it would be apparent as a distinct pellet in the screw channel. Even if the pellet melted during the extraction procedure, which takes approximately 2 min, the tracer would remain as a distinct blob. Therefore, the addition of the solid tracer to the polymer melt was considered valid for the residence time experiments because of its rapid melting.

At 100 g/min and 50 rpm (one of the operating conditions that resulted in a pressurized screw channel at probe position 2 prior to the forward kneading block), the average residence times were measured at probe positions 2 and 3 using a pulse of PP / carbon black tracer added to barrel 1 of the extruder. The difference in the average residence times at probe positions 3 and 2 (across the kneading block) was 34.56 ± 1.39 s. Using the

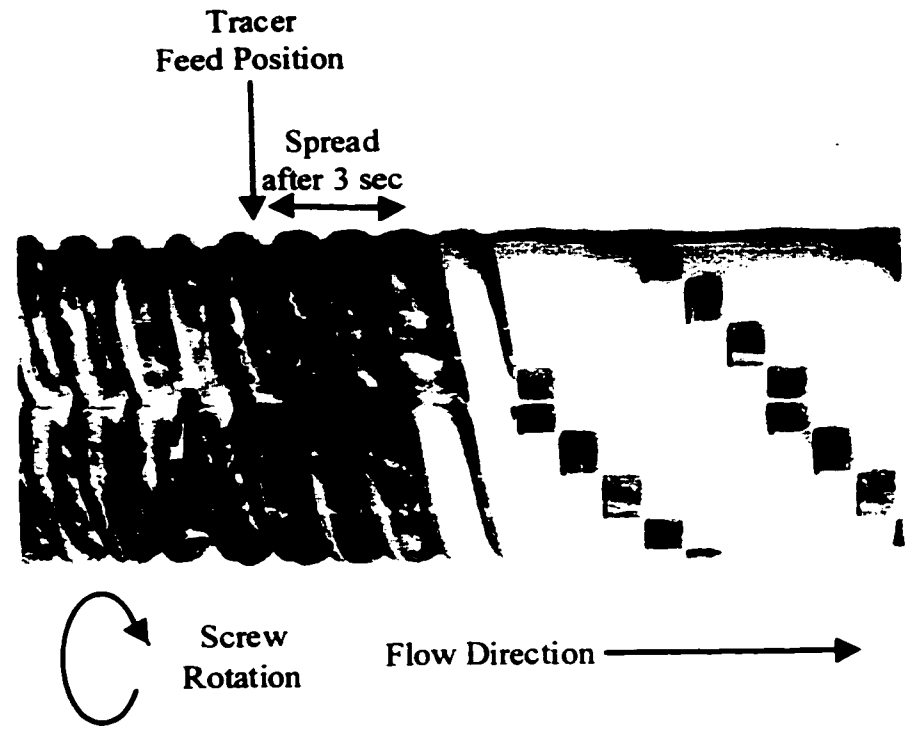

Figure 7.15. Photograph of the Pulse of the Carbon Black Tracer Shortly After its Addition to the Twin Screw Extruder (0.5wt% TiO_2 Added to the PP to Increase the Contrast)

direct residence time measurement procedure (addition of solid tracer immediately prior to the kneading block), the average residence time was 35.61 ± 0.35 s in the forward kneading block. Comparison of these two results indicated that the average residence times in the different sections of the twin screw extruder were additive, or statistically independent. In other words, the residence time in the kneading block did not depend on the residence time in the upstream section of the extruder. This result confirmed the assumption of Huneault *et al.* (1996) and Wetzel *et al.* (1997) that was required for their numerical deconvolution of the overall distributions to yield the local RTD in different sections of the twin screw extruder.

Based on the additivity of residence times, the average residence time in the kneading block is the difference between the average residence times at probe positions 3 and 2. Similarly, the average residence time in the conveying section prior to the kneading block is the difference between the average residence times at probe positions 2 and 1. Finally, the average residence time in the combination of the conveying section and kneading block is the difference between the average residence times at probe positions 3 and 1. The average residence times in the conveying sections, the kneading blocks, and the combination of these two sections are presented in Figures 7.16 to 7.18. Linear regression was used to quantify the factor and interaction effects, and the best representations of the experimental results are compared in Table 7.6 (all coefficients are significant at the 95% confidence level).

The local residence times in the conveying sections (Figure 7.16) followed similar trends with respect to the screw speed and flow rate, and as expected, it decreased with increases in either variable. With respect to the upstream kneading block geometry, the local average residence time in the conveying section followed the trend of: reverse > neutral > forward. The kneading block geometry determined the pressure at the end of the conveying

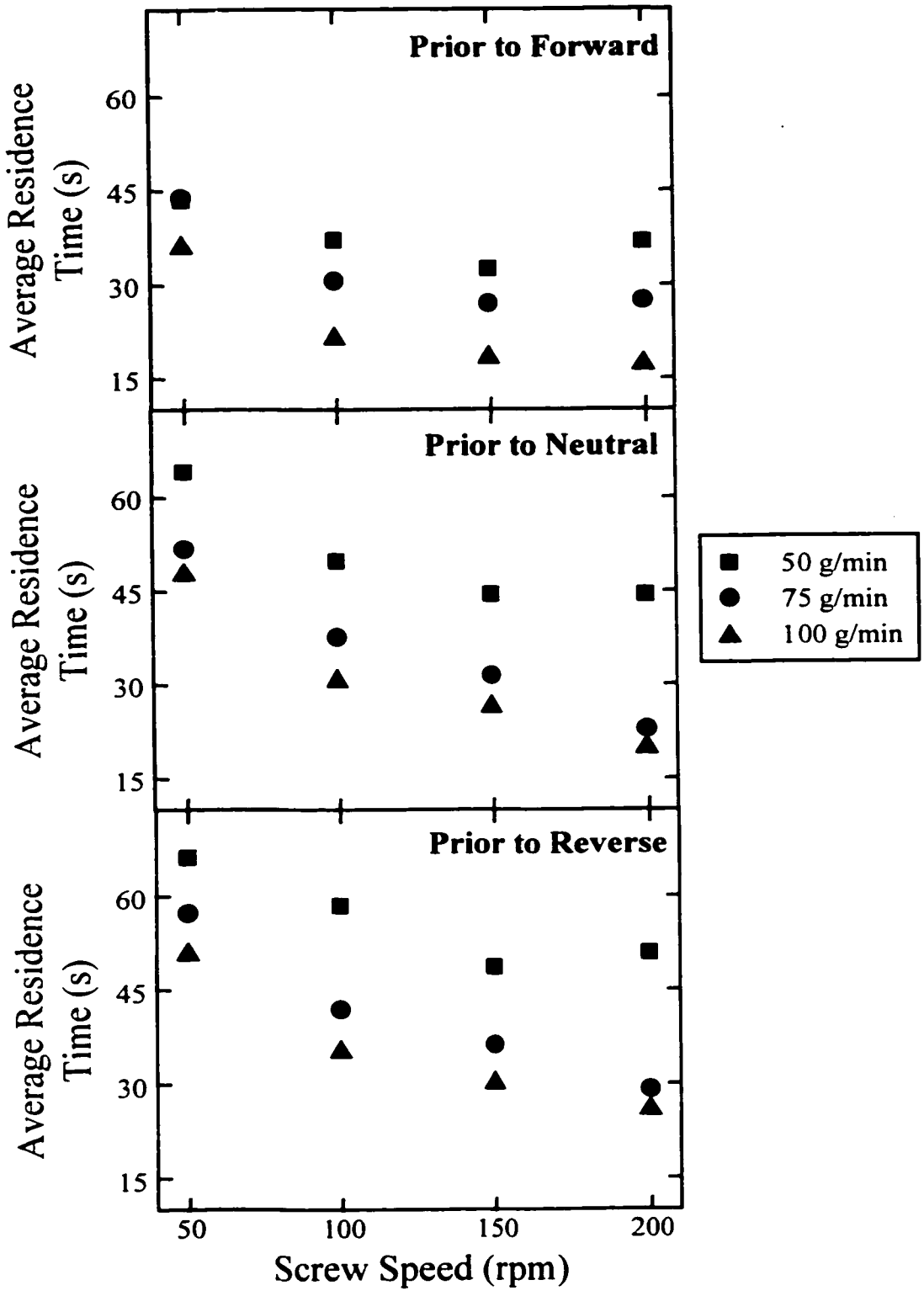

Figure 7.16. Local Residence Time In the Conveying Section Prior to the Kneading Block

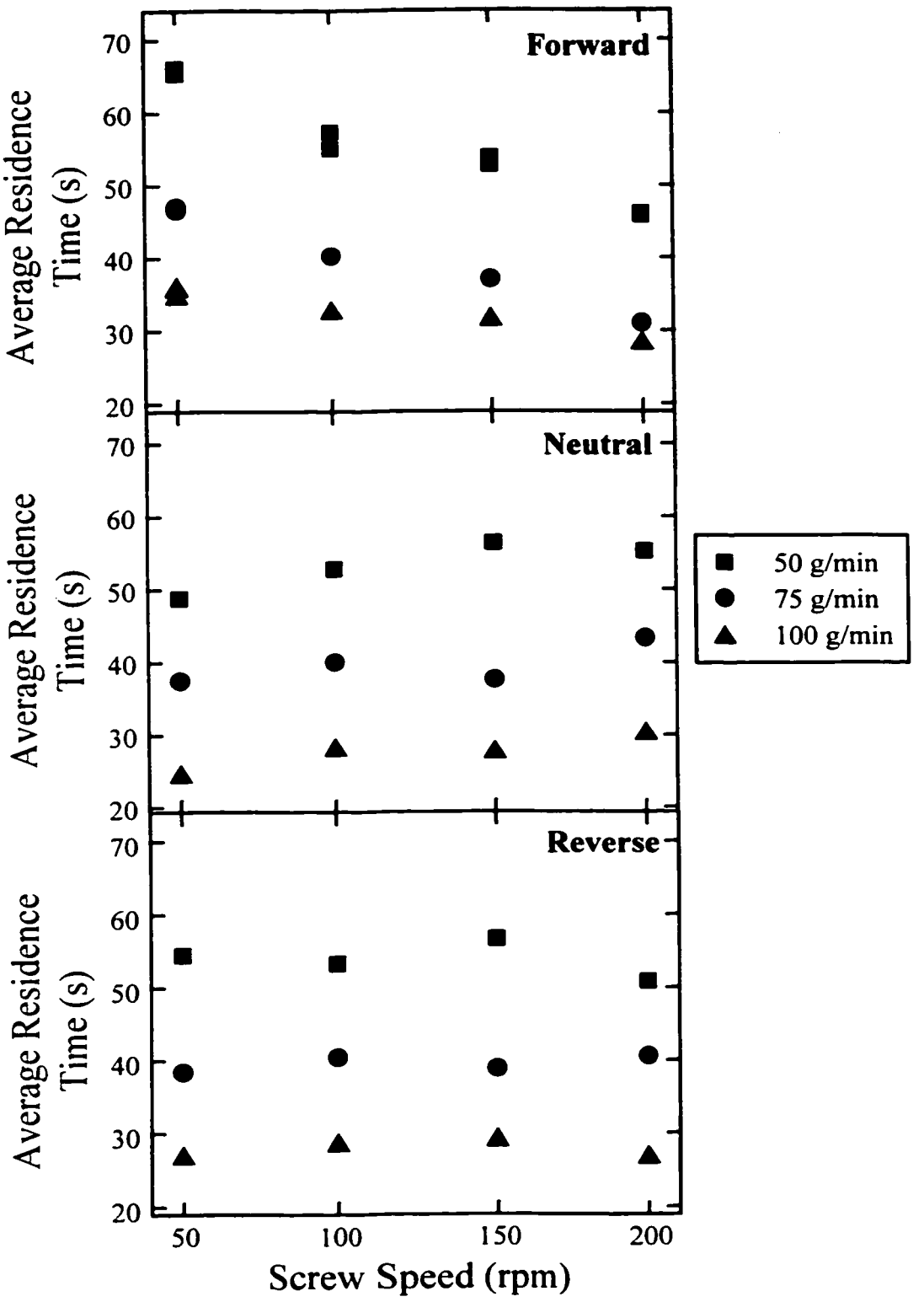

Figure 7.17. Local Residence Time in the Kneading Block

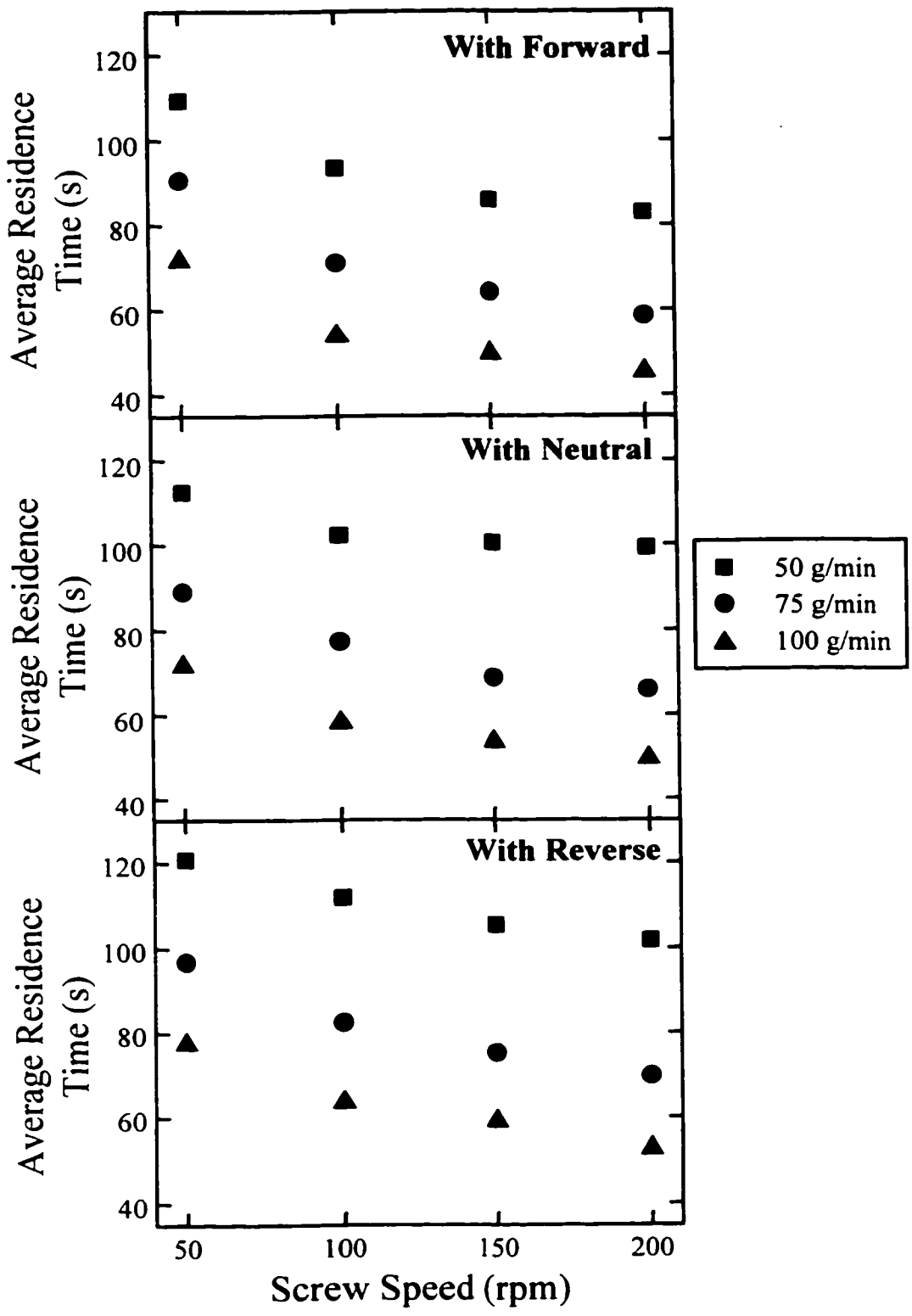

Figure 7.18. Local Residence Time In the Combination of the Conveying Section and the Kneading Block

section, and as expected, the average residence time was longest in the conveying section prior to the reverse kneading block.

Table 7.6. Linear Regression Models of the Local Residence Time Results

Section	Linear Regression Equation	r^2
Conveying Prior to Forward KB	$\bar{t} = 52.8 - 0.37Q + 538\frac{Q}{N^2}$	0.9697
Conveying Prior to Neutral KB	$\bar{t} = \frac{1508}{N} + \frac{1659}{Q}$	0.9564
Conveying Prior to Reverse KB	$\bar{t} = \frac{1469}{N} + \frac{2009}{Q}$	0.9637
Forward Kneading Block	$\bar{t} = 103.5 - 0.20N - 0.66Q + 1.43 * 10^{-3}(N * Q)$	0.9660
Neutral Kneading Block	$\bar{t} = 73.8 + 0.037N - 0.52Q$	0.9826
Reverse Kneading Block	$\bar{t} = 79.6 - 0.52Q$	0.9795
Conveying + Forward KB	$\bar{t} = \frac{1851}{N} + \frac{3718}{Q}$	0.9891
Conveying + Neutral KB	$\bar{t} = \frac{1294}{N} + \frac{4532}{Q}$	0.9893
Conveying + Reverse KB	$\bar{t} = \frac{1536}{N} + \frac{4744}{Q}$	0.9881

Units: Screw speed N [=] rpm, Flow rate Q [=] g/min, Average residence time $\bar{t}$ [=] s

The local average residence times in the neutral and reverse kneading blocks (Figure 7.17) were very similar. Due to their restrictive natures, the neutral and reverse kneading blocks were always fully filled, and the average residence time was simply the ratio of the fully filled volume and the volumetric flow rate. Thus, the average residence times in the neutral and reverse kneading blocks were not significantly affected by the screw speed. The average residence time in the forward kneading block decreased as the screw speed was increased. This observation indicated that the forward kneading block was not fully filled even though it appeared fully filled in the photographs of the extracted screws (Figures 7.6 to 7.9). At low screw speeds, the average residence time in the forward kneading block was significantly greater than the average residence time in the neutral and reverse kneading blocks (approximately 30% longer at 50 rpm). The longer average residence time in the forward kneading block suggested the possibility of stagnant flow regions, which was predicted to occur in forward kneading blocks with small stagger angles (Lawal and Kalyon, 1995). Unfortunately, the IR temperature probe method was not able to accurately determine the local RTD in the forward kneading block due to its fundamental tracer detection problem. Even though the forward kneading block was partially filled as indicated by the local residence time measurements, a portion of the upstream conveying elements were fully filled (Figures 7.6 to 7.9). This polymer backup prior to the partially filled forward kneading block also suggested that the flow contained stagnant regions. As mentioned in Chapter 6 and the mixing profile experiments, these stagnant flow regions may have contributed to the superior distributive mixing performance of the forward kneading block at the low flow rate. Flow stagnation increases the probability of the fluid to travel through the high shear rate regions in the forward kneading block (for example, over the kneading disc tip). Although the

forward kneading block was partially filled, there was no distinct break point between the partially filled and fully filled regions in the kneading block. Therefore, the superior mixing of the forward kneading block was probably not caused by its break point position.

From Figure 7.18 and Table 7.6, the overall average residence times in the combination of the conveying section and kneading block of all three screw configurations followed similar trends. Differences in the local average residence times in the conveying section and kneading block tended to cancel when these two sections were combined. Without analyzing the average residence times in the conveying section and kneading block separately, the residence time results do not show significant differences between the three screw configurations. With respect to the kneading block design, the overall average residence time followed the trend of: reverse > neutral > forward. In addition, the differences between the three screw configurations decreased at higher flow rates. For example, the maximum difference in the average residence time (between the screw configuration with the reverse kneading block and the screw configuration with the forward kneading block) decreased from 18.8 s at 50 g/min and 50 rpm to 7.2 s at 100 g/min and 50 rpm. A similar observation was mentioned in Chapter 6 concerning the overall average residence time in the melt-melt blending of the twin screw extruder. Both measurements indicated that the screw configuration exhibited a less significant effect on the average residence time at higher flow rates.

7.3. Comparison of Local Distributive Mixing and Average Residence Time Results

The local distributive mixing results in the conveying sections and kneading blocks are related to the local average residence times in Figure 7.19. There was no relationship

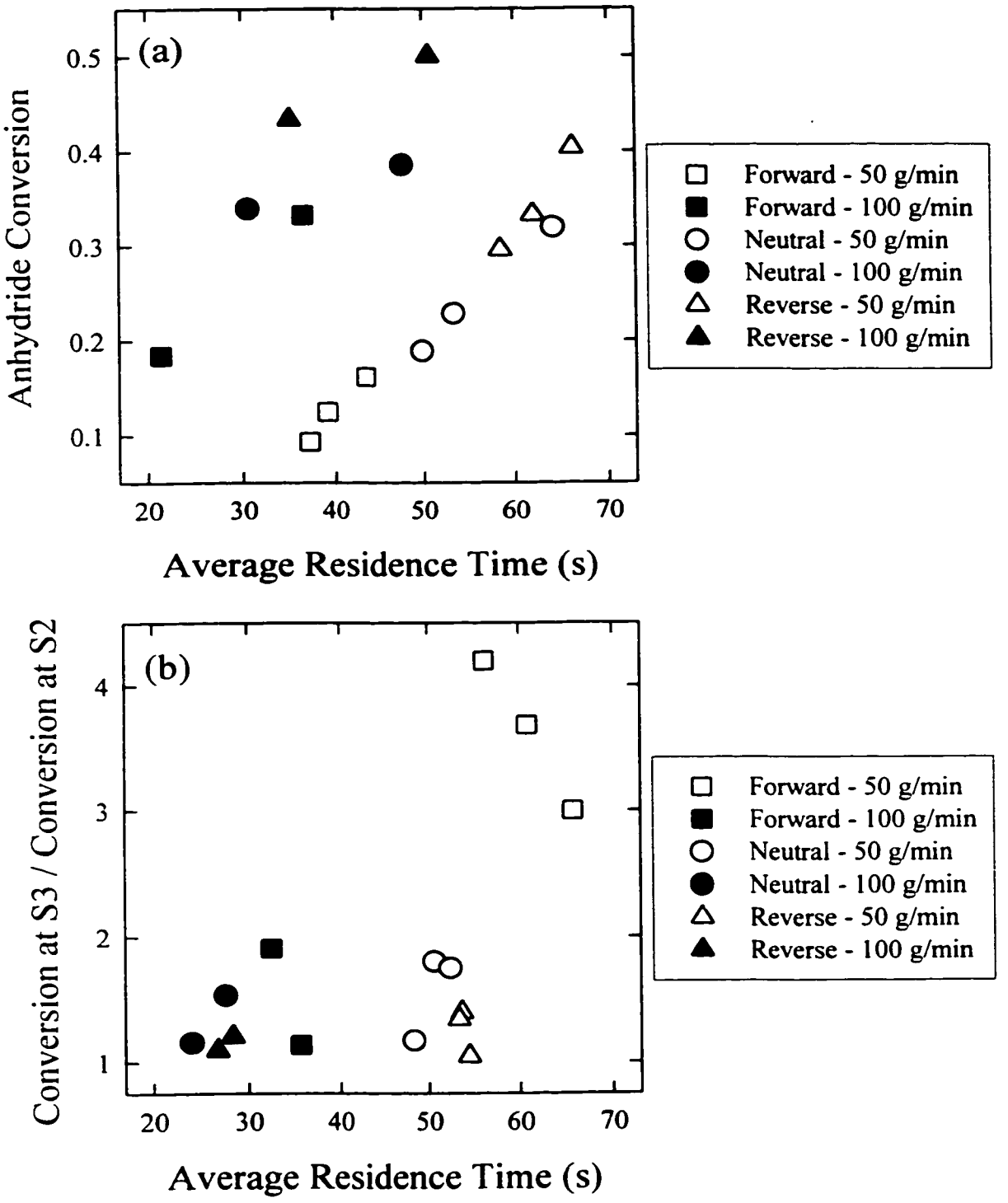

Figure 7.19. Relationship Between the Local Distributive Mixing and the Average Residence Time
(a) Conveying Section
(b) Kneading Block

between the average residence time and the mixing in the kneading block. For the conveying section, the mixing at each flow rate increased with the average residence time. At equal average residence times in the conveying section, the mixing was significantly higher at 100 g/min. This observation indicated the importance of the fill in the conveying section on the mixing process. It was previously shown that the fully filled fraction was a controlling factor for the distributive mixing in the conveying section (Figure 7.10). The mixing in the kneading block is related to the product of the average residence time and screw speed, which is the average number of screw revolutions the material experiences in the kneading block, in Figure 7.20. For each kneading block geometry and flow rate, the distributive mixing improved with the number of screw revolutions the material experienced. A higher number of screw revolutions corresponds to a greater probability that the material will travel through the high shear rate regions in the kneading block. The number of screw revolutions does not account for the differences in the mixing capabilities of the three kneading block geometries. At an equal number of screw revolutions, the forward kneading block yielded the highest amount of interfacial area generation. Bravo (1998) predicted that the highest shear rates are applied to the polymer in the disc – disc gaps and the disc tip – barrel gap. The superior mixing capability of the forward kneading block geometry suggested that a larger fraction of the flow is forced through these high shear rate regions. Szydlowski *et al.* (1987) predicted that the fraction of the flow that passes over the kneading disc tip is maximum for small and large stagger angles (for example 30° and –30°). In contrast to the forward kneading block, the extremely poor distributive mixing capability of the reverse kneading block indicated that the material was not forced through these high shear rate regions.

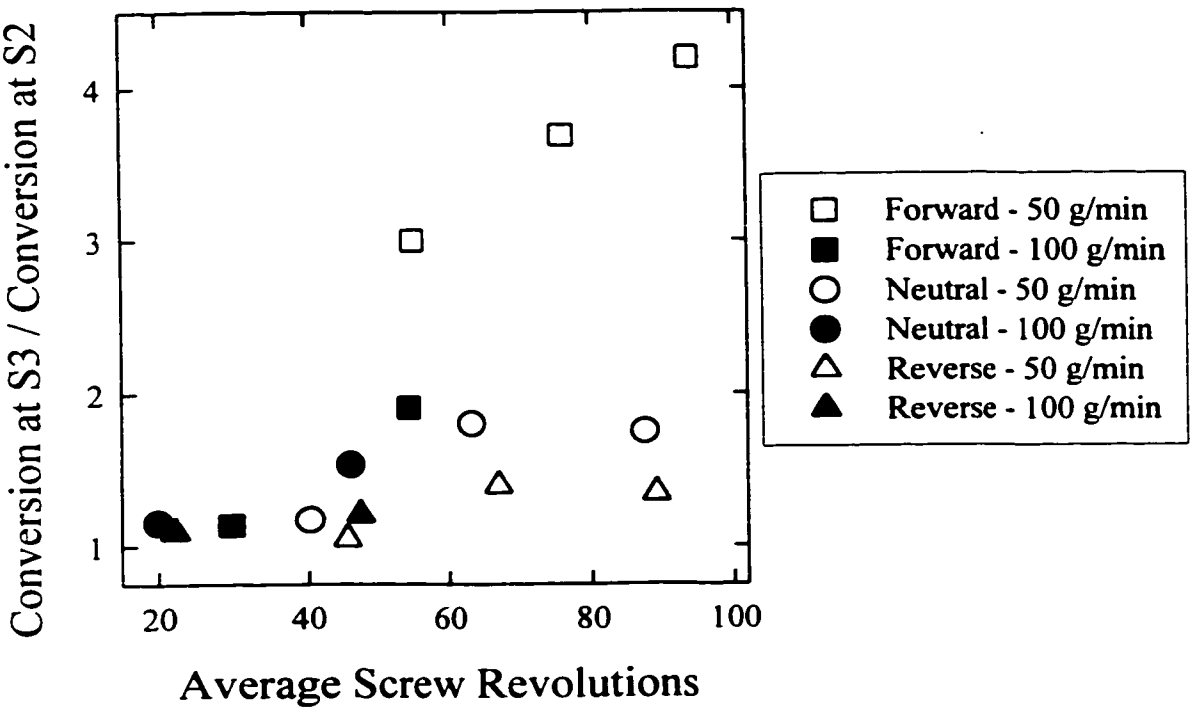

Figure 7.20. Relationship Between the Local Distributive Mixing in the Kneading Block and the Average Number of Screw Revolutions (Average Residence Time * Screw Speed)

7.4. Temperature Rise Across the Kneading Block and its Relationship with Mixing

The temperature rise across the kneading blocks were measured for the flow of pure Petrothene PP using the IR temperature probe at positions S2 and S3. Air cooling of the probe was used to eliminate the contributions of the probe and barrel temperatures to the temperature reading. The temperature rises for the three investigated kneading block geometries are compared in Figure 7.21. Similar to the observations of Maier (1996), the melt temperature measured by the IR temperature probe was most significantly affected by the screw speed. Maier (1996) reported that conveying elements and forward kneading blocks caused similar amounts of shear heating in the extruder, and only reverse elements caused significantly higher melt temperatures. Conversely, the largest temperature rise was measured across the forward kneading block (each kneading block was followed by a reverse conveying element). Compared to the restrictive neutral and reverse kneading blocks, the forward kneading block resulted in average temperatures rises that were: 7.7 °C higher at 50 rpm, 14.3 °C higher at 100 rpm, 14.9 °C higher at 150 rpm, and 18.0 °C higher at 200 rpm. The temperature rise is an indication of the amount of energy inputted to the polymer as it traveled through the kneading block. Larger viscous dissipation and higher melt temperatures occur when the material is forced through high shear rate regions in the kneading block. As expected, the highest temperature rise for the forward kneading block also corresponded with the best distributive mixing performance. The temperature rise measurements confirmed that significantly more material traveled through the high shear rate regions in the forward kneading block.

The higher temperature rise across the forward kneading block may also cause a larger amount of polymer degradation. Polymer samples were collected at various screw

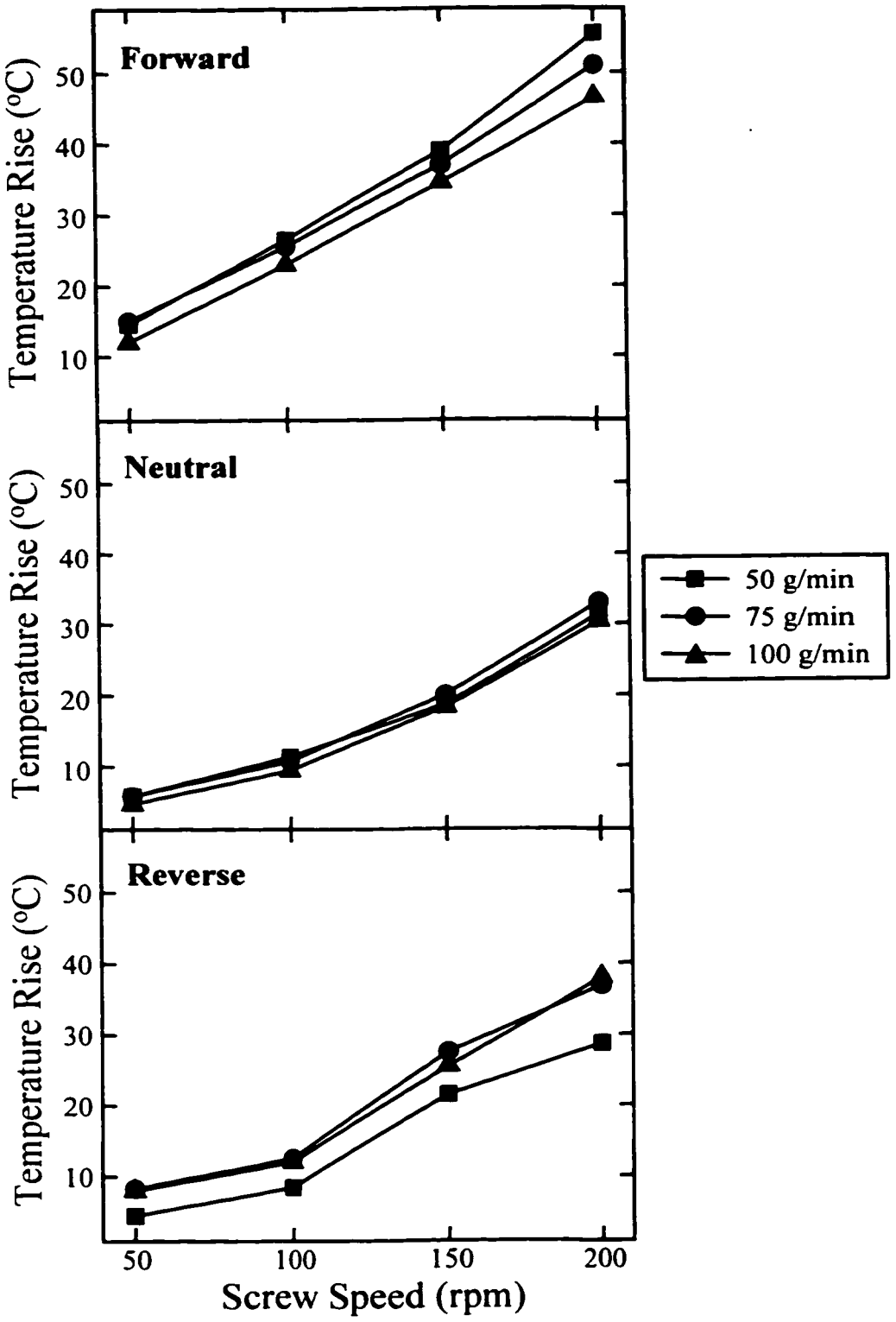

Figure 7.21. Temperature Rise Across the Kneading Blocks

speeds from all three screw configurations at 50 g/min during the distributive mixing experiments. Their apparent shear viscosities at 220 °C were measured and compared with the original 5wt% blend of the polymer tracer in pure PP. The apparent shear viscosities of all the collected samples were not significantly different. In general, the viscosities of the collected samples were 15% lower than the original PP / polymer tracer blend. Therefore, processing in the twin screw extruder degraded the polymer, but the screw configuration and operating conditions did not significantly affect the degree of degradation.

In separate experiments, the melt temperature at the die of the extruder (either the slit or strand die) was measured. Although melt temperatures as high as 280 to 300 °C were measured at the end of the kneading blocks at 200 rpm (depending on the geometry), the melt temperature at the die was between 240 to 250 °C. Maier (1996) showed that the IR temperature probe reading is most affected by the maximum temperature in its acceptance cone. Mixing in the conveying section prior to the die homogenized the polymer melt temperature, which reduced the maximum temperature value detected by the IR probe.

7.5. Concluding Remarks

Using specially designed sampling ports, the distributive mixing profile along the length of the melt-melt blending section of the twin screw extruder was investigated using the mixing limited reaction between the polymer tracers. Surprisingly, the mixing rate in the investigated kneading blocks was not necessarily greater than the mixing rate in the conveying sections. Owing to the higher shear rates applied to the polymer melt and flow recirculation, distributive mixing in conveying sections predominately occurred in the fully filled region. The controlling factor for mixing in conveying sections was the fully filled

fraction, which accounted for the effects of both the operating conditions and the pressure at the end of the conveying section. Mixing did not increase linearly with the fully filled fraction, which suggested that the interfaces were not effectively reoriented in the conveying section. Distributive mixing in kneading blocks is very complicated and depends on the screw speed, flow rate, and kneading block geometry. The local mixing was significantly higher in the forward kneading block at a low flow rate. Conversely, the reverse kneading block did not effectively mix the polymer melt, which was attributed to its inability to disturb the flow entering the kneading block from the conveying elements. To perform distributive mixing, the kneading block must disturb the flow to reorient the interfaces that align with the flow streamlines in the upstream conveying elements.

Local residence time measurements were completed to investigate the flow in the conveying sections and kneading blocks using the IR temperature probe method of Nietsch *et al.* (1997). This method is based on the detection of the changing surface emissivity caused by a pulse of a carbon black tracer. The calculated distribution of residence times depended on the screw element at the probe position. It was proposed that the probe temperature readings are affected by the local radial flow of the carbon black tracer to and away from the polymer melt surface. Conversely, the calculated average residence times were not significantly affected by the local flow field. The local average residence times in the conveying sections prior to the kneading block depended on the operating conditions as well as the pressure at the end of the conveying section. Due to their fully filled nature, the average residence times in neutral and reverse kneading blocks were not significantly affected by the screw speed. In contrast, the local average residence time in the forward kneading block decreased with screw speed, which indicated that the forward kneading block

was not fully filled. The combination of a longer local average residence time and a backup of the polymer in the conveying section preceding the partially filled forward kneading block suggested that there were stagnant flow regions in the forward kneading block.

The mixing in the conveying section was related to the average residence time and the fill. For each kneading block, the mixing was related to the average number of screw revolutions the material experienced. At an equal number of screw revolutions, the distributive mixing was superior in the forward kneading block. As well, a significantly larger melt temperature rise was measured across the forward kneading block. Therefore, a larger fraction of the material traveled through the high shear rate regions in the forward kneading block.

CHAPTER 8
CONCLUSIONS AND RECOMMENDATIONS

8.1. Conclusions

A novel experimental method for directly measuring distributive mixing during polymer blending in twin screw extruders using reactive polymer tracers was presented in this thesis. A common technique used to investigate micromixing in conventional chemical reactors was applied to the analysis of mixing of polymer melts in an extruder. The use of terminally functionalized low molecular weight polymers to study mixing is unique to this research. In contrast to low molecular weight polar compounds, these polymer tracers were compatible with hydrophobic polyolefins, such as PP. The anhydride - primary amine reaction between the polymer tracers was irreversible and mixing limited in the extruder. The conversion of the anhydride functional groups was linearly related to the interfacial area available for the reaction. In addition, no imide was formed during the processing in the extruder, which may have influenced the mixing process due to the evolution of water. Therefore, the coupling reaction was applied to the analysis of distributive mixing during melt-melt blending of segregated PP streams in a co-rotating twin screw extruder. The conversion of the mixing limited interfacial reaction was a direct measurement of the distributive mixing as well as the micromixing because the reaction is a molecular event.

The unique contributions of this research to the field of polymer mixing are: the dependence of distributive mixing on polymer properties, the experimental comparison of the mixing capabilities of different kneading block geometries, the profiles of distributive mixing along the extruder, and the relationships between distributive mixing and RTD measurements.

Lower viscosity polymers were easier to homogenize during melt-melt blending in the extruder. Therefore, both applied strain and material properties affected the distributive mixing process. This unique experimental result confirmed the trends predicted by Nichetti and Manas-Zloczower (1999) using numerical simulations of the length stretch distributions. In the range of the investigated factors, there was no interaction between the effects of the polymer properties and kneading block design on distributive mixing. Conversely, to obtain good distributive mixing, the operating conditions and screw configuration cannot be selected independently.

Screw configurations containing neutral and reverse kneading blocks exhibited similar overall mixing performance trends as well as similar mixing profiles along the melt-melt blending section. Increasing the flow rate simultaneously improved the productivity and product uniformity for these two screw configurations, which indicated that increased fill dominated reduced residence time. In addition, an optimum screw speed at each flow rate existed due to the competing contributions of shear rate, fill, and residence time on the mixing process. Finally, the majority of the distributive mixing occurred in the fully filled conveying elements prior to the restrictive neutral and reverse kneading blocks. Poor reorientation of the interfaces in the conveying elements and intermeshing region caused the distributive mixing efficiency to decrease along the length of the fully filled region prior to the kneading block. Further mixing in the neutral and reverse kneading blocks was limited by their inability to reorient these interfaces that were aligned with the streamlines in the upstream conveying elements. In contrast, melt feeding directly into these kneading block geometries significantly improved their distributive mixing performances because the interfaces were forced into the high shear regions.

The screw configuration containing the forward kneading block exhibited superior mixing at 50 g/min and inferior mixing at 100 g/min as compared to the screw configurations containing the restrictive neutral and reverse kneading blocks. The combination of a longer local average residence time and a polymer backup prior to the partially filled forward kneading block strongly suggested that there were stagnant regions in the flow. This stagnation resulted in greater opportunity for the polymer to travel through the high shear rate regions, which was supported by the significantly larger melt temperature rise measured across the forward kneading block. Preliminary experiments showed that distributive mixing was not improved by increasing the backflow gap in the forward kneading block. Therefore, the flow in the high shear rate gaps, such as between the kneading disc tip and the barrel wall, dominated the distributive mixing in the kneading block.

Distributive mixing increased with the average residence time, but it was not dependent on the macromixing. This observation was similar to the results of Bigg (1975) for the mixing in single screw extruders, which suggested that distributive mixing is dominated by the transverse flow in the extruder channels. In addition, the results indicated that the macromixing does not influence the micromixing in the twin screw extruder. The local RTD method of Niestch *et al.* (1997) was valid for the determination of the local average residence time, but the distribution of residence times was affected by the local flow of the carbon black tracer at the probe position. The average residence times in the conveying sections and kneading blocks were additive, which indicated that the residence times in different sections of the twin screw extruder were statistically independent. This unique experimental observation for co-rotating twin screw extruders confirmed the assumption of Huneault *et al.* (1996) and Wetzel *et al.* (1997) that was required for their

numerical deconvolution of the overall distributions into the local distributions in the extruder.

8.2. Recommendations

In Chapter 3, an alternative method for the preparation of the reactive polymers based on hydrosilylation was proposed. In particular, this method would eliminate the large quantities of solvent that are required to prepare the amine functionalized polymer via hydroboration followed by amination. The remainder of the recommendations concern the mixing experiments in the twin screw extruder.

Over the range of the investigated variables, higher productivity and improved product quality was achieved simultaneously by an increase in the flow rate for the screw configurations containing the neutral and reverse kneading blocks. It is recommended to investigate the dependence of distributive mixing on fill and residence time at higher flow rates for these two screw configurations. An optimum flow rate for distributive mixing may exist, after which, the effect of reduced residence time limits further mixing.

In Chapter 7, a preliminary comparison of the mixing performances of forward kneading blocks with stagger angles of 30° and 60° was presented for one set of operating conditions. It is recommended to extend this comparison over a wide range of operating conditions to confirm the preliminary conclusion concerning the effects of the flow through the backflow gap and the flow over the kneading disc tip on the distributive mixing process. In addition, an experimental investigation of the effect of the kneading disc thickness on the mixing process would be very valuable. Andersen (1994) proposed that thinner kneading discs promote distributive mixing through greater stream splitting and recombination. In

contrast, the experimental results of this research suggested that distributive mixing predominately occurred in the high shear rate regions of the kneading block. A wider kneading disc promotes greater flow over the disc tip, which may improve the distributive mixing.

The mixing experiments were completed using simple kneading blocks with constant stagger angles. Often composite kneading blocks containing sections with different stagger angles or disc thickness are used in twin screw extruders. Based on the experimental mixing results, it is recommended to investigate the mixing performances of the following two composite designs: i) a section of forward staggered kneading discs followed by a section of reverse staggered kneading discs and ii) a section of reverse staggered kneading discs followed by a section of forward staggered kneading discs. The second design may offer the most interesting results because it combines the distributive mixing in the fully filled conveying elements prior to the reverse kneading block followed by the superior local mixing in the forward kneading block.

Finally, the experimental results presented in this thesis could be used to validate numerical simulations of distributive mixing and RTD in twin screw extruders. In particular, the experimental results presented in Chapter 7 concerning the local mixing and residence time in the kneading blocks can be compared with 3-D FEM simulations. In addition, the experimentally measured values of the pressure and temperature can be used as boundary conditions in these simulations.

CHAPTER 9
REFERENCES

Agarwal, S. and G. A. Campbell, "Micromixing in Filled Reaction Injection Molded Composites", *SPE ANTEC Tech. Papers*, 839-842 (1995)

Agassant, J. F. and A. Poitou, "A Kinematic Approach to Distributive Mixing" in *Mixing and Compounding of Polymers: Theory and Practice*, Ch. 2, I. Manas-Zloczower and Z. Tadmor (eds.), Hanser Publishers, Munich (1994)

Andersen, P. G., "Mixing Practices in Corotating Twin-screw Extruders" in *Mixing and Compounding of Polymers: Theory and Practice*, Ch. 20, I. Manas-Zloczower and Z. Tadmor (eds.), Hanser Publishers, Munich (1994)

Angst, W., J. R. Bourne, and P. Dell'ava, "Mixing and Fast Chemical Reaction-IX Comparison Between Models and Experiments", *Chem. Eng. Sci.*, **39**, 335-342 (1984)

Angst, W., J. R. Bourne, and R. N. Sharma, "Mixing and Fast Chemical Reaction-IV The Dimensions of the Reaction Zone", *Chem. Eng. Sci.*, **37**, 585-590 (1982a)

Angst, W., J. R. Bourne, and R. N. Sharma, "Mixing and Fast Chemical Reaction-V Influence of Diffusion within the Reaction Zone on Selectivity", *Chem. Eng. Sci.*, **37**, 1259-1264 (1982b)

Baim, W. and D. Bigio, "The Effect of Viscosity Ratio and Volume Fraction on the Distributive Mixing of Two Miscible Fluids in the NITSE", *SPE ANTEC Tech. Papers*, 266-269 (1994)

Baldyga, J. and J. R. Bourne, "Mixing and Fast Chemical Reaction-VIII Initial Deformation of Material Elements in Isotropic, Homogeneous Turbulence", *Chem. Eng. Sci.*, **39**, 329-334 (1984)

Baldyga, J. and J. R. Bourne, "The Effect of Micromixing on Parallel Reactions", *Chem. Eng. Sci.*, **45**, 907-916 (1990)

Baldyga, J., J. R. Bourne, and R. V. Gholap, "The Influence of Viscosity on Mixing in Jet Reactors" *Chem. Eng. Sci.*, **50**, 1877-1880 (1995)

Baldyga, J., J. R. Bourne, and B. Zimmermann, "Investigation of Mixing in Jet Reactors Using Fast, Competitive-Consecutive Reactions", *Chem. Eng. Sci.*, **49**, 1937-1946 (1994)

Baldyga, J. and S. Rohani, "Determination of the Micromixing Level in a CSTR: Transient Step Response of Reactive Tracers", *Chem. Eng. Sci.*, **42**, 575-580 (1987)

Barresi, A. A., M. Pipino, and G. Raldi, "A Three-Stage Micromixing Model for Very Fast Reactions in Tubular Reactors", *Chem. Eng. Sci.*, **47**, 2831-2836 (1992)

Bawiskar, S. and J. L. White, "A Composite Model for Solid Conveying, Melting, Pressure and Fill Factor Profiles in Modular Co-rotating Twin Screw Extruders", *Intern. Polym. Proc.*, **12**, 331-340 (1997)

Belevi, H., J. R. Bourne, and P. Rys, "Mixing and Fast Chemical Reaction-II Diffusion-Reaction Model for the CSTR", *Chem. Eng. Sci.*, **36**, 1649-1654 (1981)

Bellamy, L. J., *The Infra-red Spectra of Complex Molecules*, Methuen and Company, London (1958)

Benn, F. R., J. Dwyer, and I. Chappell, "The Ene Reaction of Maleic Anhydride with Alkenes", *J. Chem. Soc. Perkin II*, 533-535 (1977)

Bennington, C. P. J. and V. K. Thangavel, "The Use of a Mixing-Sensitive Chemical Reaction for the Study of Pulp Fibre Suspension Mixing", *Can. J. Chem. Eng.*, **71**, 667-675 (1993)

Bigg, D. M., "On Mixing in Polymer Flow Systems", *Polym. Eng. Sci.*, **15**, 684-689 (1975)

Bigio, D., W. Baim, and K. Wang, "Specific Throughput as an Operating Parameter for Mixing", *SPE ANTEC Tech. Papers*, 256-260 (1994)

Bigio, D., W. Baim, and M. Wigginton, "Mixing in Non-intermeshing Twin Screw Extruders", *Intern. Polym. Proc.*, **6**, 172-176 (1991)

Bigio, D., K. Cassidy, M. Dellapa, and W. Baim, "Starve-fed Flow in Co-rotating Twin Screw Extruders", *Intern. Polym. Proc.*, **7**, 111-115 (1992)

Bigio, D. and L. Erwin, "Mixing Studies in Co-rotating Twin Screw Extruders", *SPE ANTEC Tech. Papers*, 45-48 (1985)

Bigio, D. and L. Erwin, "Effect of Screw Stagger on Mixing in a Tangential Counter-rotating Twin Screw Extruder", *Intern. Polym. Proc.*, **4**, 242-246 (1989)

Bigio, D. and L. Erwin, "The Effect of Axial Pressure Gradient on Extruder Mixing Characteristics", *Polym. Eng. Sci.*, **32**, 760-765 (1992)

Bigio, D. and W. Stry, "Measures of Mixing in Laminar Flow", *Polym. Eng. Sci.*, **30**, 153-161 (1990)

Bigio, D. I., J. D. Boyd, L. Erwin, and D. W. Gailus, "Mixing Studies in the Single Screw Extruder", *Polym. Eng. Sci.*, **25**, 305-310 (1985)

Bigio, D. I. and J. H. Conner, "Principal Directions as a Basis for the Evaluation of Mixing", *Polym. Eng. Sci.*, **35**, 1527-1534 (1995)

Bolzern, O. and J. R. Bourne, "Mixing and Fast Chemical Reaction-VI Extension of the Reaction Zone", *Chem. Eng. Sci.*, **38**, 999-1003 (1983)

Borsig, E., A. Fiedlerová, and L. Hrčková, "Influence of Maleic Anhydride on the Molecular Weight of Atactic Polypropylene at the Functionalization Reaction", *J. Macromol. Sci. –Pure Appl. Chem.*, **A32**, 2017-2024 (1995)

Bourne, J. R., "Mixing on the Molecular Scale (Micromixing)", *Chem. Eng. Sci.*, **38**, 5-8 (1983)

Bourne, J. R., F. Kozicki, and P. Rys, "Mixing and Fast Chemical Reaction-I Test Reactions to Determine Segregation", *Chem. Eng. Sci.*, **36**, 1643-1648 (1981a)

Bourne, J. R., F. Kozicki, U. Moergeli, and P. Rys, "Mixing and Fast Chemical Reaction-III Model-Experiment Comparison", *Chem. Eng. Sci.*, **36**, 1655-1663 (1981b)

Bourne, J. R. and S. Rohani, "Mixing and Fast Chemical Reaction-VII Deforming Reaction Zone Model for the CSTR", *Chem. Eng. Sci.*, **38**, 911-916 (1983)

Bourry, D. and B. D. Favis, "Morphology Development in a Polyethylene / Polystyrene Binary Blend During Twin-screw Extrusion", *Polymer*, **39**, 1851-1856 (1998)

Box, G. E. P., W. G. Hunter, and J. S. Hunter, *Statistics for Experimenters: An Introduction to Design, Data Analysis, and Model Building*, John Wiley and Sons, New York (1978)

Bravo, V., "Finite Element Simulation of Flow in Twin Screw Extruders Mixing Elements", PhD dissertation, McMaster University, Hamilton, Ontario, Canada (1998)

Brouwer, T., D. B. Todd, and L. P. B. M. Janssen, "Flow Patterns in Special Twin Screw Mixing Elements", *SPE ANTEC Tech. Papers*, 206-210 (1999)

Brown, H. C., *Hydroboration*, W. A. Benjamin, New York (1962)

Brown, H. C., W. R. Heydkamp, E. Breuer, and W. S. Murphy, "The Reaction of Organoboranes with Chloramine and with Hydroxylamine-O-sulfonic Acid. A Convenient Synthesis of Amines from Olefins *via* Hydroboration", *J. Am. Chem. Soc.*, **86**, 3565-3566 (1964)

Brown, H. C., K. Kim, M. Srebnik, and B. Singaram, "Organoboranes for Synthesis. 7. An Improved General Synthesis of Primary Amines for Alkenes *via* Hydroboration-Organoborane Chemistry", *Tetrahedron*, **43**, 4071-4078 (1987)

Bruce, D., M. Wilson, and S. Generalis, "Flow Field Analysis of Both the Trilobal Element and Mixing Disc Zones within a Closely Intermeshing, Co-rotating Twin-screw Extruder", *Intern. Polym. Proc.*, **12**, 323-330 (1997)

Brydson, J. A., *Flow Properties of Polymer Melts*, 2nd edition, George Godwin, London (1981)

Bur, A. J. and F. Mitchell Gallant, "Fluorescence Monitoring of Twin Screw Extrusion", *Polym. Eng. Sci.*, **31**, 1365-1371 (1991)

Burbank, F., F. Brauer, and P. Andersen, "Experimental Study of Distributive Mixing in a Co-rotating Twin Screw Extruder", *SPE ANTEC Tech. Papers*, 149-152 (1991)

Cartier, H. and G. Hu, "Morphology Development of *in situ* Compatibilized Semicrystalline Polymer Blends in a Co-rotating Twin-screw Extruder", *Polym. Eng. Sci.*, **39**, 996-1013 (1999)

Cassagnau, P., C. Mijangos, and A. Michel, "An Ultraviolet Method for the Determination of the Residence Time Distribution in a Twin Screw Extruder", *Polym. Eng. Sci.*, **31**, 772-778 (1991)

Chella, R. and J. M. Ottino, "Mixing, Diffusion, and Chemical Reaction in a Single Screw Extruder", *ACS Symp. Ser.*, **196** (Chem. React. Eng.-Boston), 567-578 (1982)

Chella, R. and J. M. Ottino, "Conversion and Selectivity Modifications due to Mixing in Unpremixed Reactors", *Chem. Eng. Sci.*, **39**, 551-567 (1984)

Chen, C. C., "Melt Temperature Measurement in a Twin-screw Extruder with Infrared Fiber Optic Probes", *SPE ANTEC Tech. Papers*, 931-936 (1992)

Chen, L., G. H. Hu, and J. T. Lindt, "Residence Time Distribution in Non-intermeshing Counter-rotating Twin-screw Extruders", *Polym. Eng. Sci.*, **35**, 598-603 (1995)

Cheng, H. and I. Manas-Zloczower, "Study of Mixing Efficiency in Kneading Discs of Co-rotating Twin-screw Extruders", *Polym. Eng. Sci.*, **37**, 1082-1090 (1997)

Cho, J. W. and J. L. White, "A Study of the Blending Process in a JSW Modular Co-rotating / Counter-rotating Twin Screw Extruder at Different Barrel Temperatures", *SPE ANTEC Tech. Papers*, 321-327 (1995)

Christiano, J. P. and M. Lindenfelzer, "Investigation of Mixing Patterns in Corotating Fully Intermeshing Twin Screw Extruders Mixing Elements Using Dynamic Pressure Distributions", *SPE ANTEC Tech. Papers*, 78-83 (1997)

Chung, T. C., "Functionalized Polyolefins Prepared by the Combination of Borane Monomers and Transition Metal Catalysts", *Macromol. Symp.*, **89**, 151-162 (1995)

Chung, T. C., H. L. Lu, and C. L. Li, "Synthesis and Functionalization of Unsaturated Polyethylene: Poly(ethylene-*co*-1,4-hexadiene)", *Macromolecules*, **27**, 7533-7537 (1994)

Chung, T. C., H. L. Lu, and C. L. Li, "Functionalization of Polyethylene Using Borane Reagents and Metallocene Catalysts", *Polym. Intern.*, **37**, 197-205 (1995)

Chung, T. C. and D. Rhubright, "Functionalization of Polypropylene by Hydroboration", *J. Polym. Sci.: Part A: Polym. Chem.*, **31**, 2759-2763 (1993)

Curry, J., "Reactive Extrusion of Blends with Interfacial Reactions", *SPE ANTEC Tech. Papers*, 1838-1842 (1995)

Curry, J. and P. Andersen, "Controlling the Crosslink Density of Co-reactive Polymers in an Extruder Reactor", *SPE ANTEC Tech. Papers*, 1938-1943 (1990)

Curry, J. and P. Andersen, "Controlling Crosslink Density of Coreactive Polymers in an Extruder Reactor", *Adv. Polym. Technol.*, **11**, 3-10 (1991/1992)

Dagli, S. S., M. Xanthos, and J. A. Biesenberger, "Kinetic Studies and Process Analysis of the Reactive Compatibilization of Nylon 6 / Polypropylene Blends", *Polym. Eng. Sci.*, **34**, 1720-1730 (1994)

Danckwerts, P. V., "The Definition and Measurement of Some Characteristics of Mixtures", *Appl. Sci. Research*, **A3**, 279-296 (1952)

Danckwerts, P. V., "Theory of Mixtures and Mixing", *Research*, **6**, 355-361 (1953a)

Danckwerts, P. V., "Continuous Flow Systems. Distribution of Residence Times", *Chem. Eng. Sci.*, **2**, 1-13 (1953b)

Danckwerts, P. V., "The Effect of Incomplete Mixing on Homogeneous Reactions", *Chem. Eng. Sci.*, **8**, 93-102 (1958)

David, B. and Z. Tadmor, "Laminar Mixing in Corotating Disk Processors", *Intern. Polym. Proc.*, **3**, 38-47 (1988)

De Roover, B., M. Sclavons, V. Carlier, J. Devaux, R. Legras, and A. Momtaz, "Molecular Characterization of Maleic Anhydride-Functionalized Polypropylene", *J. Polym. Sci.: Part A: Polym. Chem.*, **33**, 829-842 (1995)

De Roover, B., J. Devaux, and R. Legras, "Maleic Anhydride Homopolymerization During Melt Functionalization of Isotactic Polypropylene", *J. Polym. Sci.: Part A: Polym. Chem.*, **34**, 1195-1202 (1996)

Dharmarajan, N., S. Datta, G. Ver Strate, and L. Ban, "Compatibilized Polymer Blends of Isotactic Polypropylene and Styrene-Maleic Anhydride Copolymer", *Polymer*, **36**, 3849-3861 (1995)

Donoian, G. S. and J. P. Christiano, "Effect of Kneading Block Tip Clearance on Performance of Co-rotating Twin-screw Extruders", *SPE ANTEC Tech. Papers*, 220-224 (1999)

Erwin, L., "Principles of Laminar Fluid/Fluid Mixing" in *Mixing in Polymer Processing*, Ch. 1, C. Rauwendaal (ed.), Marcel Dekker, Inc., New York (1991)

Erwin, L., "Theory of Laminar Mixing", *Polym. Eng. Sci.*, **18**, 1044-1048 (1978)

Erwin, L. and F. Mokhtarian, "Analysis of Mixing in Modified Single Screw Extruders", *Polym. Eng. Sci.*, **23**, 49-60 (1983)

Esseghir, M., C. G. Gogos, D. Yu, D. B. Todd, and B. David, "A Comparative Study on the Performance of Three Single-screw Elements in Melt-melt Mixing of Immiscible Blends", *Adv. Polym. Technol.*, **17**, 1-17 (1998)

Favis, B. D. and B. Therrien, "Factors Influencing Structure Formation and Phase Size in an Immiscible Polymer Blend of Polycarbonate and Polypropylene Prepared by Twin-screw Extrusion", *Polymer*, **32**, 1474-1481 (1991)

Ferrari, D. F. and W. E. Baker, "Aminolysis Kinetics of Model and Polymer-bound Anhydride Moieties in Low- and High-Viscosity Media", *J. Polym. Sci.: Part A: Polym. Chem.*, **36**, 1573-1582 (1998)

Fournier, M.-C., L. Falk, and J. Villermaux, "A New Parallel Competing Reaction System for Assessing Micromixing Efficiency – Experimental Approach", *Chem. Eng. Sci.*, **51**, 5053-5064 (1996)

Franzheim, O. and M. Stephan, "Morphology Development of a Polypropylene / Polyamide 6 Blend in the Mixing Zone of a Twin Screw Extruder", *SPE ANTEC Tech. Papers*, 2591-2596 (1997a)

Franzheim, O., M. Stephan, T. Rische, P. Heidemeyer, U. Burkhardt, and A. Kiani, "Analysis of Morphology Development of Immiscible Blends in a Twin Screw Extruder", *Adv. Polym. Technol.*, **16**, 1-10 (1997b)

Frey, J. H. and C. D. Denson, "Imidization Reaction Parameters in Inert Molten Polymers for Micromixing Tracer Studies", *Chem. Eng. Sci.*, **43**, 1967-1973 (1988)

Gale, M., "Compounding with Single-screw Extruders", *Adv. Polym. Technol.*, **16**, 251-262 (1997)

Ganzeveld, K. J. and L. P. B. M. Janssen, "Scale-up of Counter-rotating Closely Intermeshing Twin Screw Extruders Without and With Reactions", *Polym. Eng. Sci.*, **30**, 1529-1536 (1990)

Ganzeveld, K. J. and L. P. B. M. Janssen, "A Mixing Model for Multicomponent Reactions in Twin Screw Extruders Applied to the Polymerization of Urethanes", *Polym. Eng. Sci.*, **32**, 457-466 (1992a)

Ganzeveld, K. J. and L. P. B. M. Janssen, "The Grafting of Maleic Anhydride on High Density Polyethylene in an Extruder", *Polym. Eng. Sci.*, **32**, 467-474 (1992b)

Ganzeveld, K. J. and L. P. B. M. Janssen, "Role of Mixing and Rheology in Reactive Extrusion", *Ind. Eng. Chem. Res.*, **33**, 2398-2403 (1994)

Gasner, G., D. Bigio, C. Kiehl, and F. Magnus, "Mixing Characteristics of Rubber in a Twin Screw Extruder Based on Drag Flow", *SPE ANTEC Tech. Papers*, 324-328 (1996)

Gasner, G. E., D. Bigio, C. Marks, F. Magnus, and C. Kiehl, "A New Approach to Analyzing Residence Time and Mixing in a Co-rotating Twin Screw Extruder", *Polym. Eng. Sci.*, **39**, 286-298 (1999)

Gaylord, N. G., "Compatibilizing Agents: Structure and Function in Polyblends", *J. Macromol. Sci.-Chem.*, **A26**, 1211-1229 (1989)

Gaylord, N. G., R. Mehta, D. R. Mohan, and V. Kumar, "Maleation of Linear Low-density Polyethylene by Reactive Processing", *J. Appl. Polym. Sci.*, **44**, 1941-1949 (1992)

Gaylord, N. G. and M. K. Mishra, "Nondegradative Reaction of Maleic Anhydride and Molten Polypropylene in the Presence of Peroxide", *J. Polym. Sci.: Polym. Lett. Ed.*, **21**, 23-30 (1983)

Gendron, R., L. E. Daigneault, J. Tatibouët, and M. M. Dumoulin, "Residence Time Distribution in Extruders Determined by In-line Ultrasonic Measurements", *Adv. Polym. Technol.*, **15**, 111-125 (1996)

Goffart, D., D. J. van der Wal, E. M. Klomp, H. W. Hoogstraten, L. P. B. M. Janssen, L. Breysse, and Y. Trolez, "Three-dimensional Flow Modeling of a Self-wiping Corotating Twin-screw Extruder. Part I: The Transporting Section", *Polym. Eng. Sci.*, **36**, 901-911 (1996)

Gogos, C. G., M. Esseghir, D. B. Todd, and D. W. Yu, "Dispersive Mixing in Immiscible Polymer Blends", *Macromol. Symp.*, **101**, 185-198 (1996)

Gogos, C. G., M. Esseghir, D. W. Yu, D. B. Todd, and J. E. Curry, "The Twin-screw Mixing Element Evaluator: On-line Performance Evaluation of Modular Twin-screw Mixing Elements", *SPE ANTEC Tech. Papers*, 270-276 (1994)

Greco, P., P. Laurienzo, G. Maglio, M. Malinconico, and E. Martuscelli, "Acid and Base Functionalization of Ethylene-Propylene Rubbers, 2[a]: Influence of Type and Content of Functional Groups on the Mechanical and Thermal Behavior of Elastomeric Network", *Makromol. Chem.*, **188**, 961-969 (1987)

Guichardon, P., L. Falk, and J. Villermaux, "Extension of the Range of the Iodate-Iodide Reaction to Characterize Micromixing Efficiency", in proceedings of *1996 First Joint Topical Conference on Processing, Structure and Properties of Polymeric Materials*, 89-91 (Chicago, Illinois, 1996)

Hazziza-Laskar, J., G. Hélary, and G. Sauvet, "Grafting of Amino Groups on Polybutadiene by Hydrosilylation", *Makromol. Chem., Macromol. Symp.*, **47**, 383-391 (1991)

Heinen, W., C. H. Rosenmöller, C. B. Wenzel, H. J. M. de Groot, J. Lugtenburg, and M. van Duin, "^{13}C NMR Study of the Grafting of Maleic Anhydride onto Polyethylene, Polypropylene, and Ethylene-Propene Copolymers", *Macromolecules*, **29**, 1151-1157 (1996)

Hinze, J. O., *Turbulence*, 2nd edition, McGraw-Hill, New York (1975)

Ho, R. M., A. C. Su, C. H. Wu, and S. I. Chen, "Functionalization of Polypropylene via Melt Mixing", *Polymer*, **34**, 3264-3269 (1993)

Hoffmann, H. M. R., "The Ene Reaction", *Angew. Chem. Internat. Edit.*, **8**, 556-577 (1969)

Hojabr, S., W. E. Baker, K. E. Russell, P. J. McLellan, and M. A. Huneault, "Melt Grafting of Glycidyl Methacrylate onto Polyethylene", *Intern. Polym. Proc.*, **13**, 118-128 (1998)

Hold, P., "Mixing of Polymers – an Overview Part 1", *Adv. Polym. Technol.*, **2**, 141-151 (1982)

Hu, G.-H. and H. Cartier, "Free Radical Grafting of Glycidyl Methacrylate onto PP in a Co-rotating Twin Screw Extruder", *Intern. Polym. Proc.*, **13**, 111-117 (1998)

Hu, G. and I. Kadri, "Preparation of Macromolecular Tracers and Their Use for Studying the Residence Time Distribution of Polymeric Systems", *Polym. Eng. Sci.*, **39**, 299-311 (1999)

Hu, G. H. and J. T. Lindt, "Amidification of Poly(styrene-*co*-maleic anhydride) with Amines in Tetrahydrofuran Solution: A Kinetic Study", *Polym. Bull.*, **29**, 357-363 (1992)

Huneault, M. A., "Morphology Development in High Viscosity Ratio Polymer Blends", in the proceedings of *Compounding '98* (Boston, Aug 24-25, 1998)

Huneault, M. A., M. F. Champagne, and A. Luciani, "Polymer Blend Mixing and Dispersion in the Kneading Section of a Twin-screw Extruder", *Polym. Eng. Sci.*, **36**, 1694-1706 (1996a)

Huneault, M. A., R. Gendron, and L. Daigneault, "Residence Time Distribution in Twin Screw Extruders: Contribution of the Different Screw Functions", *SPE ANTEC Tech. Papers*, 329-333 (1996b)

Ide, F. and A. Hasegawa, "Studies on Polymer Blend of Nylon 6 and Polypropylene or Nylon 6 and Polystyrene Using the Reaction of Polymer", *J. Appl. Polym. Sci.*, **18**, 963-974 (1974)

Immirzi, B., N. Lanzetta, P. Laurienzo, G. Maglio, M. Malinconico, E. Martuscelli, and R. Palumbo, "Acid and Base Functionalization of Ethylene-Propylene Rubbers, 1: Grafting of Tertiary Amino Groups and "Interpolymer" Network Formation", *Makromol. Chem.*, **188**, 951-960 (1987)

Jaffer, S. A., V. L. Bravo, P. E. Wood, A. N. Hrymak, and J. D. Wright, "Experimental Validation of Numerical Simulations of the Kneading Disc Section in a Twin Screw Extruder", accepted in *Polym. Eng. Sci.* (1999)

Janssen, L. P. B. M., "Mixing in Counterrotating Twin-screw Extruders" in *Mixing in Polymer Processing*, Ch. 6, C. Rauwendaal (ed.), Marcel Dekker, Inc., New York (1991)

Janssen, L. P. B. M., *Twin Screw Extrusion*, Elsevier Scientific Publishing Company, Amsterdam (1978)

Janssen, L. P. B. M., R. W. Hollander, M. W. Spoor, and J. M. Smith, "Residence Time Distributions in a Plasticating Twin Screw Extruder", *AIChE J.*, **25**, 345-351 (1979)

Kalyon, D. M. and H. N. Sangani, "An Experimental Study of Distributive Mixing in Fully Intermeshing, Co-rotating Twin Screw Extruders", *Polym. Eng. Sci.*, **29**, 1018-1308 (1989)

Kao, S. V. and G. R. Allison, "Residence Time Distribution in a Twin Screw Extruder", *Polym. Eng. Sci.*, **24**, 645-651 (1984)

Karam, H. J. and J. C. Bellinger, "Deformation and Breakup of Liquid Droplets in a Simple Shear Field", *Ind. Eng. Chem. Fund.*, **7**, 576-581 (1968)

Kim, B. and J. L. White, "Simulation of Thermal Degradation, Peroxide Induced Degradation, and Maleation of Polypropylene in a Modular Co-rotating Twin Screw Extruder", *Polym. Eng. Sci.*, **37**, 576-589 (1997)

Klinger, K. A., M. D. Wolkowicz, and A. A. Adewole, "DSC Picture of a Polymer Blend Carcass: Rate of Mixing", *SPE ANTEC Tech. Papers*, 187-195 (1997)

Koning, C., W. Bruls, F. Op Den Buijsch, and L. v.d. Vondervoort, "Reactive Compatibilization of Impact Modified Poly(styrene-*co*-maleic anhydride) / Poly(phenylene oxide) Blends by Primary Amine Terminated Polystyrene", *SPE ANTEC Tech. Papers*, 2572-2576 (1997)

Lawal, A. and D. M. Kalyon, "Mechanisms of Mixing in Single and Co-rotating Twin Screw Extruders", *Polym. Eng. Sci.*, **35**, 1325-1338 (1995a)

Lawal, A. and D. M. Kalyon, "Simulation of Intensity of Segregation Distributions Using Three-dimensional FEM Analysis: Application to Corotating Twin Screw Extrusion Processing", *J. Appl. Polym. Sci.*, **58**, 1501-1507 (1995b)

Lee, M., "Extrusion of Polymers and Polymer Blends with Supercritical Carbon Dioxide", PhD dissertation, University of Waterloo, Waterloo, Ontario, Canada (1999)

Lee, S.-H. and J. L. White, "Continuous Mixing of Low Viscosity and High Viscosity Polymer Melts in a Modular Co-rotating Twin Screw Extruder", *Intern. Polym. Proc.*, **12**, 316-322 (1997)

Lewis, L. N., R. J. Uriarte, and N. Lewis, "The Effect of Metal Colloid Morphology on Catalytic Activity: Further Proof of the Intermediacy of Colloids in the Rhodium-catalyzed Hydrosilylation Reaction", *J. Mole. Catal.*, **66**, 105-113 (1991)

Li, T. and I. Manas-Zloczower, "Evaluation of Distributive Mixing Efficiency in Mixing Equipment", *Chem. Eng. Comm.*, **139**, 223-231 (1995)

Liang, C. Y. and F. G. Pearson, "Infrared Spectra of Crystalline and Stereoregular Polymers Part I. Polypropylene", *J. Mol. Spectroscopy*, **5**, 290-306 (1960)

Lin-Vien, D., N. B. Colthup, W. G. Fateley, and J. G. Grasselli, *The Handbook of Infrared and Raman Characteristic Frequencies of Organic Molecules*, Academic Press, Boston (1991)

Liu, N. C. and W. E. Baker, "Reactive Polymers for Blend Compatibilization", *Adv. Polym. Technol.*, **11**, 249-262 (1992)

Liu N. C. and W. E. Baker, "Basic Functionalization of Polypropylene and the Role of Interfacial Chemical Bonding in its Toughening", *Polymer*, **35**, 988-994 (1994)

Liu, N. C., W. E. Baker, and K. E. Russell, "Functionalization of Polyethylenes and Their Use in Reactive Blending", *J. Appl. Polym. Sci.*, **41**, 2285-2300 (1990)

Liu, N. C., H. Q. Xie, and W. E. Baker, "Comparison of the Effectiveness of Different Basic Functional Groups for the Reactive Compatibilization of Polymer Blends", *Polymer*, **34**, 4680-4687 (1993)

Luciani, A. and L. A. Utracki, "The Extensional Flow Mixer, EFM", *Intern. Polym. Proc.*, **11**, 299-309 (1996)

Maier, C., "Infrared Temperature Measurement of Polymers", *Polym. Eng. Sci.*, **36**, 1502-1512 (1996)

Maier, C., M. Lambla, and D. Bigio, "Non-homogeneous Mixing Rates and Conversion", *SPE ANTEC Tech. Papers*, 123-126 (1994)

Malz, H. and C. Tzoganakis, "Hydrosilylation of Terminal Double Bonds in Polypropylene Through Reactive Processing", *Polym. Eng. Sci.*, **38**, 1976-1984 (1998)

Maréchal, P., G. Coppens, R. Legras, and J. Dekoninck, "Amine / Anhydride Reaction versus Amide / Anhydride Reaction in Polyamide / Anhydride Carriers", *J. Polym. Sci.: Part A: Polym. Chem.*, **33**, 757-766 (1995)

Maric, M. and C. W. Macosko, "Coupling Reactions at Poly(styrene) / Poly(dimethylsiloxane) Interfaces with Application to Melt Blending", in proceedings of *Polyblends '99* (Boucherville, Quebec, Canada, Oct. 13-15, 1999)

Meijer, H. E. H. and J. M. H. Janssen, "Mixing of Immiscible Liquids" in *Mixing and Compounding of Polymers: Theory and Practice*, Ch. 4, I. Manas-Zloczower and Z. Tadmor (eds.), Hanser Publishers, Munich (1994)

Mirone, P. and P. Chiorboli, "Infrared and Raman Spectra and Vibrational Assignment of Maleic Anhydride", *Spectrochimica Acta.*, **18**, 1425-1432 (1962)

Mohr, W. D., R. L. Saxton, and C. H. Jepson, "Mixing in Laminar-flow Systems", *Ind. Eng. Chem.*, **49**, 1855-1856 (1957)

Mülhaupt, R., T. Duschek, and B. Rieger, "Functional Polypropylene Blend Compatibilizers", *Makromol. Chem., Macromol. Symp.*, **48/49**, 317-332 (1991)

Nachtigall, S. M. B., R. Baumhardt Neto, and R. S. Mauler, "A Factorial Design Applied to Polypropylene Functionalization with Maleic Anhydride", *Polym. Eng. Sci.*, **39**, 630-637 (1999)

Nauman, E. B. and B. A. Buffham, *Mixing in Continuous Flow Systems*, John Wiley and Sons, New York (1983)

Nemes, S., J. Borbély, J. Borba, G. Deák, and T. Kelen, "Reactive Propylene Oligomers: Propylene Oligomers with Primary-OH, Tertiary-OH, and α,β-di-OH End Groups", *Polym. Bull.*, **29**, 135-138 (1992)

Nichetti, D. and I. Manas-Zloczower, "Modeling Extrusion Processability for Materials with Various Molecular Parameters", *SPE ANTEC Tech. Papers*, 250-254 (1999)

Nietsch, T., P. Cassagnau, and A. Michel, "Melt Temperatures and Residence Times in an Extruder by Infrared Spectroscopy", *Intern. Polym. Proc.*, **12**, 307-315 (1997)

Nishio, T., Y. Suzuki, K. Kojima, and M. Kakugo, "Morphology of Maleic Anhydride Grafted Polypropylene and Polyamide Alloy Produced by Reactive Processing", *J. Polym. Eng.*, **10**, 123-149 (1991)

Oberlehner, J., P. Cassagnau, and A. Michel, "Local Residence Time Distribution in a Twin Screw Extruder", *Chem. Eng. Sci.*, **49**, 3897-3907 (1994)

Oostenbrink, A. J. and R. J. Gaymans, "Maleic Anhydride Grafting on EPDM Rubber in the Melt", *Polymer*, **33**, 3086-3088 (1992)

Ottino, J. M., "Lamellar Mixing Models for Structured Chemical Reactions and Their Relationship to Statistical Models: Macro- and Micromixing and the Problem of Averages", *Chem. Eng. Sci.*, **35**, 1377-1391 (1980)

Ottino, J. M., "Efficiency of Mixing from Data on Fast Reactions in Multi-jet Reactors and Stirred Tanks", *AIChE J.*, **27**, 184-192 (1981)

Ottino, J. M. and R. Chella, "Laminar Mixing of Polymeric Liquids; A Brief Review and Recent Theoretical Developments", *Polym. Eng. Sci.*, **23**, 357-379 (1983)

Ou, J. and W. E. Ranz, "Mixing and Chemical Reactions; A Contrast Between Fast and Slow Reactions", *Chem. Eng. Sci.*, **38**, 1005-1013 (1983a)

Ou, J. and W. E. Ranz, "Mixing and Chemical Reactions; Chemical Selectivities", *Chem. Eng. Sci.*, **38**, 1015-1019 (1983b)

Painter, P. C., M. M. Coleman, and J. L. Koenig, *The Theory of Vibrational Spectroscopy and its Application to Polymeric Materials*, John Wiley and Sons, New York (1982)

Pardos, F., "Forecast for the World Plastics Industry to 2020", *Plastics Engineering*, **55**, 53-57 (1999)

Pelter, A., K. Smith, and H. C. Brown, *Borane Reagents*, Academic Press, London (1988)

Phan, T. T. M., A. J. DeNicola, Jr., and L. S. Schadler, "The Effect of Addition of Polyoxypropylenediamine on the Morphology and Mechanical Properties of Maleated Polypropylene / Maleated Rubber Blends", *SPE ANTEC Tech. Papers*, 2557-2561 (1997)

Polance, R. and K. Jayaraman, "Mixing in Reactive Extrusion of Low-Density Polyethylene Melts: Linear vs. Branched", *Polym. Eng. Sci.*, **35**, 1535-1545 (1995)

Potente, H., J. Ansahl, and B. Klarholz, "Design of Tightly Intermeshing Co-rotating Twin Screw Extruders", *Intern. Polym. Proc.*, **9**, 11-25 (1994)

Potente, H., M. Bastian, M. Stephan, and P. Pötschke, "Morphology Development of Polymer Blends in Twin Screw Extruders", in the proceedings of *PPS-15* ('s Hertogenbosch, The Netherlands, May 31 – June 4, 1999)

Rabek, J. F., *Experimental Methods in Polymer Chemistry: Physical Principles and Applications*, John Wiley and Sons, Chichester (1980)

Ramakrishnan, S., "Well-defined Ethylene-Vinyl Alcohol Copolymers via Hydroboration: Control of Composition and Distribution of the Hydroxyl Groups on the Polymer Backbone", *Macromolecules*, **24**, 3753-3759 (1991)

Rauwendaal, C., "Analysis and Experimental Evaluation of Twin Screw Extruders", *Polym. Eng. Sci.*, **21**, 1092-1100 (1981)

Rauwendaal, C., "Mixing in Single-screw Extruders" in *Mixing and Compounding of Polymers: Theory and Practice*, Ch. 9, I. Manas-Zloczower and Z. Tadmor (eds.), Hanser Publishers, Munich (1994)

Rios, A. C., P. J. Gramann, and T. A. Osswald, "Comparative Study of Mixing in Corotating Twin Screw Extruders Using Computer Simulation", *Adv. Polym. Technol.*, **17**, 107-113 (1998)

Rios, A. C. and T. A. Osswald, "Novel BEM Simulation of Mixing in Polymer Flows Including Non-linear Effects", *SPE ANTEC Tech. Papers*, 245-249 (1999)

Rodriguez-Veloz, O. and M. R. Kamal, "The Development of Laminar Morphology in a Co-rotating Twin Screw Extruder", *Adv. Polym. Technol.*, **18**, 89-108 (1999)

Rösch, J. and R. Mülhaupt, "Comparison of Maleic Anhydride-Grafted Poly(propylene) with Maleic Anhydride-grafted Polystyrene-*block*-poly(ethene-*co*-but-1-ene)-*block*-polystyrene as Blend Compatibilizers of Poly(propylene) / Polyamide-6 Blends", *Makromol. Chem., Rapid Commun.*, **14**, 503-509 (1993)

Rosen, S. L., *Fundamental Principles of Polymeric Materials*, 2nd edition, John Wiley and Sons, New York (1993)

Sakai, T., "Intermeshing Twin-screw Extruders" in *Mixing and Compounding of Polymers: Theory and Practice*, Ch. 21, I. Manas-Zloczower and Z. Tadmor (eds.), Hanser Publishers, Munich (1994)

Sakai, T., "The Development of On-line Techniques and Novel Processing Systems for the Monitoring and Handling of the Evolution of Microstructure in Nonreactive and Reactive Polymer Systems", *Adv. Polym. Technol.*, **14**, 277-290 (1995)

Sanchez, R., D. I. Bigio, and S. Karnik, "Mixing of a Low Molecular Weight Additive in a Co-rotating Twin Screw Extruder: Visualization of the Flow Path", *SPE ANTEC Tech. Papers*, 3724-3729 (1997)

Scott, C. and C. Macosko, "Model Experiments for the Interfacial Reaction Between Polymers During Reactive Polymer Blending", *J. Polym. Sci.: Part B: Polym. Phys.*, **32**, 205-213 (1994a)

Scott, C. E. and C. W. Macosko, "Morphology Development During Reactive and Non-reactive Blending of an Ethylene-Propylene Rubber with Two Thermoplastic Matrices", *Polymer*, **35**, 5422-5433 (1994b)

Shearer, C. J., "Mixing of Highly Viscous Liquids: Flow Geometries for Streamline Subdivision and Redistribution", *Chem. Eng. Sci.*, **28**, 1091-1098 (1973)

Shearer, G. and C. Tzoganakis, "Free Radical Hydrosilylation of Polypropylene", *J. Appl. Polym. Sci.*, **65**, 439-447 (1997)

Shenoy, U. V. and H. L. Toor, "Unifying Indicator and Instantaneous Reaction Methods of Measuring Micromixing", *AIChE J.*, **36**, 227-232 (1990)

Shida, M., R. N. Shroff, and L. V. Cancio, "Correlation of Low Density Polyethylene Rheological Measurements with Optical and Processing Properties", *Polym. Eng. Sci.*, **17**, 769-774 (1977)

Shih, C., "Fundamental Understandings of Compounding Processes – Review from an Industrial Prospective", presented at *Polyblends '99* (Boucherville, Quebec, Canada, Oct. 13-15, 1999)

Shiono, T., H. Kurosawa, O. Ishida, and K. Soga, "Synthesis of Polypropylenes Functionalized with Secondary Amino Groups at the Chain Ends", *Macromolecules*, **26**, 2085-2089 (1993)

Simmons, A. and W. E. Baker, "Basic Functionalization of Polyethylene in the Melt", *Polym. Eng. Sci.*, **29**, 1117-1123 (1989)

Song, Z. and W. E. Baker, "Basic Functionalization of Molten Linear Low-density Polyethylene with 2-(Dimethylamino)ethyl Methacrylate in an Intermeshing Corotating Twin-screw Extruder", *J. Appl. Polym. Sci.*, **41**, 1299-1313 (1990)

Song, Z. and W. E. Baker, "Melt Grafting of t-Butylaminoethyl Methacrylate onto Polyethylene", *Polymer*, **33**, 3266-3273 (1992a)

Song, Z. and W. E. Baker, "Chemical Reactions and Reactivity of Primary, Secondary, and Tertiary Diamines with Acid Functionalized Polymers", *J. Polym. Sci.: Part A: Polym. Chem.*, **30**, 1589-1600 (1992b)

Spencer, R. S. and R. M. Wiley, "The Mixing of Very Viscous Liquids", *J. Colloid Sci.*, **6**, 133-145 (1951)

Strutt, D. B., "A Study of Reactive Flow of Polypropylene in Single- and Twin-screw Extruders", PhD dissertation, University of Waterloo, Waterloo, Ontario, Canada (1998)

Strutt, D., C. Tzoganakis, and T. A. Duever, "Response Surface Analysis of Average Residence Times in a Co-rotating Twin Screw Extruder", *SPE ANTEC Tech. Papers*, 146-150 (1997)

Sun, Y., G. Hu, M. Lambla, and H. K. Kotlar, "*In situ* Compatibilization of Polypropylene and Poly(butylene terephthalate) Polymer Blends by One-Step Reactive Extrusion", *Polymer*, **37**, 4119-4127 (1996)

Sundararaj, U., Y. Dori, and C. W. Macosko, "Sheet Formation in Immiscible Polymer Blends: Model Experiments on Initial Blend Morphology", *Polymer*, **36**, 1957-1968 (1995)

Szydlowski, W. and J. L. White, "Improved Model of Flow in the Kneading Disc Region of an Intermeshing Co-rotating Twin Screw Extruder", *Intern. Polym. Proc.*, **2**, 142-150 (1988)

Szydlowski, W., R. Brzoskowski, and J. L. White, "Modelling Flow in an Intermeshing Co-rotating Twin Screw Extruder: Flow in Kneading Discs", *Intern. Polym. Proc.*, **1**, 207-214 (1987)

Tessier, M. and E. Marechal, "Study of the Synthesis of Poly(isobutylene-b-Amide-11) by Polycondensation of α,ω-Dianhydride Oligoisobutylene with α,ω-Diamino Oligoamide-11. I. Study of Amine – Anhydride and Amide – Anhydride Reactions on Low Molecular Weight Models and on Oligomers and Polymers", *J. Polym. Sci.: Part A: Polym. Chem.*, **26**, 2785-2810 (1988)

Thompson, M. R., "Maleation of Polypropylene and EPDM Through Reactive Extrusion Using the Alder Ene Reaction", PhD dissertation, University of Waterloo, Waterloo, Ontario, Canada (1998)

Thompson, M., J. P. Puaux, A. N. Hrymak, and A. E. Hamielec, "Modeling the Residence Time Distribution of a Non-intermeshing Twin Screw Extruder", *Intern. Polym. Proc.*, **10**, 111-119 (1995)

Thompson, M., C. Tzoganakis, and G. L. Rempel, "Terminal Functionalization of Polypropylene via the Alder Ene Reaction", *Polymer*, **39**, 327-334 (1998a)

Thompson, M. R., C. Tzoganakis, and G. L. Rempel, "Evaluation of Vinylidene Content in Controlled-rheology Polypropylene", *J. Polym. Sci.: Part A: Polym. Chem.*, **35**, 3083-3086 (1997)

Thompson, M. R., C. Tzoganakis, and G. L. Rempel, "A Parametric Study of the Terminal Maleation of Polypropylene Through an Alder Ene Reaction", *J. Polym. Sci.: Part A: Polym. Chem.*, **36**, 2371-2380 (1998b)

Thompson, M. R., C. Tzoganakis, and G. L. Rempel, "Maleation of EPDM Through Reactive Extrusion", *SPE ANTEC Tech. Papers*, 1744-1748 (1998c)

Titier, C., J. Pascault, and M. Taha, "Synthesis of Epoxy-Amine Multiacrylic Prepolymers by Reactive Extrusion", *J. Appl. Polym. Sci.*, **59**, 415-423 (1996)

Tzoganakis, C. and H. Malz, "*Hydrosilylation of Polypropylene*", International Patent Application PCT/CA97/00412, July 12, 1997, pursuant to U.S. Provisional 60/019,678

Tzoganakis, C., Y. Tang, J. Vlachopoulos, and A. E. Hamielec, "Measurements of Residence Time Distribution for the Peroxide Degradation of Polypropylene in a Single-screw Plasticating Extruder", *J. Appl. Polym. Sci.*, **37**, 681-693 (1989)

Vainio, T., G. Hu, M. Lambla, and J. V. Seppälä, "Functionalized Polypropylene Prepared by Melt Free Radical Grafting of Low Volatile Oxazoline and its Potential in Compatibilization of PP / PBT Blends", *J. Appl. Polym. Sci.*, **61**, 843-852 (1996)

Vainio, T., G. Hu, M. Lambla, and J. V. Seppälä, "Functionalization of Polypropylene with Oxazoline and Reactive Blending of PP with PBT in a Corotating Twin-screw Extruder", *J. Appl. Polym. Sci.*, **63**, 883-894 (1997)

van der Wal, D. J., D. Goffart, E. M. Klomp, H. W. Hoogstraten, and L. P. B. M. Janssen, "Three-dimensional Flow Modeling of a Self-Wiping Corotating Twin–screw Extruder. Part II: The Kneading Section", *Polym. Eng. Sci.*, **36**, 912-924 (1996)

Vergnes, B., G. Della Valle, and L. Delamare, "A Global Computer Software for Polymer Flows in Corotating Twin Screw Extruders", *Polym. Eng. Sci.*, **38**, 1781-1792 (1998)

Vermeesch, I. And G. Groeninckx, "Chemical Modification of Poly(styrene-*co*-maleic anhydride) with Primary *N*-alkylamines by Reactive Extrusion", *J. Appl. Polym. Sci.*, **53**, 1365-1373 (1994)

Vermeesch, I. M., G. Groeninckx, and M. M. Coleman, "Poly(styrene-*co*-*N*-maleimide) Copolymers: Preparation by Reactive Extrusion, Molecular Characterization by FTIR, and Use in Blends", *Macromolecules*, **26**, 6643-6649 (1993)

Villermaux, J. and L. Falk, "A Generalized Mixing Model for Initial Contacting of Reactive Fluids", *Chem. Eng. Sci.*, **49**, 5127-5140 (1994)

Wang, X. C., C. Tzoganakis, and G. L. Rempel, "Reactive Extrusion of Acrylic Acid Grafted Polypropylene with Hexadecylamine", *Polym. Eng. Sci.*, **34**, 1750-1757 (1994)

Weiss, R. A. and H. Stamato, "Development of an Ionomer Tracer for Extruder Residence Time Distribution Experiments", *Polym. Eng. Sci.*, **29**, 134-139 (1989)

Wetzel, M. D., C. Shih, and U. Sundararaj, "Determination of Residence Time Distribution During Twin Screw Extrusion of Model Fluids", *SPE ANTEC Tech. Papers*, 3707-3712 (1997)

White, J. L., *Twin Screw Extrusion: Technology and Principles*, Hanser Publishers, Munich (1990)

White, J. L. and Z. Chen, "Simulation of Non-isothermal Flow in Modular Co-rotating Twin Screw Extrusion", *Polym. Eng. Sci.*, **34**, 229-237 (1994)

White, J. L. and W. Szydlowski, "Composite Models of Modular Intermeshing Corotating and Tangential Counterrotating Twin Screw Extruder", *Adv. Polym. Technol.*, **7**, 419-426 (1987)

Wolf, D., N. Holin, and D. H. White, "Residence Time Distribution in a Commercial Twin-screw Extruder", *Polym. Eng. Sci.*, **26**, 640-646 (1986)

Wu, J., "Micromixing of a Polymer Melt in Twin-screw Extruders with Kneading Discs", PhD dissertation, University of Delaware, Delaware, USA (1994)

Wu, C. H. and A. C. Su, "Functionalization of Ethylene-Propylene Rubber via Melt Mixing", *Polym. Eng. Sci.*, **31**, 1629-1636 (1991)

Wu, C. H. and A. C. Su, "Suppression of Side Reactions During Melt Functionalization of Ethylene-Propylene Rubber", *Polymer*, **33**, 1987-1992 (1992)

Xie, Y., D. Tomayko, D. I. Bigio, and G. Batch, "Experimental and Statistic Analysis of Residence Time Distribution in Corotating Twin Screw Extruder", *SPE ANTEC Tech. Papers*, 89-93 (1997)

Yao, W. G., K. Takahashi, and Y. Abe, "Analytical Study on Flow and Distributive Mixing of a New Type Pin Mixing Section for Screw Extruder", *Intern. Polym. Proc.*, **11**, 222-227 (1995)

Zbinden, R., *Infrared Spectroscopy of High Polymers*, Academic Press, New York (1964)

APPENDIX I
COMMENTS ON THE REGRESSION ANALYSIS OF RTD DATA

Linear regression is a powerful tool that can be used to quantify a relationship between a collection of experimental data and the investigated factors as well as their interactions. In this work, linear regression was performed to quantify the dependence of the distributive mixing and RTD results on the operating conditions of the twin screw extruder. Statistical analysis was used to test the significance of these coefficients, and it was attempted to use only terms that had physical meaning in the extrusion process. For example, the terms used in the average residence time models were the flow rate and the specific throughput, which is an indication of the degree of channel fill.

In a recent publication, Gasner *et al.* (1999) proposed "A New Approach to Analyzing Residence Time and Mixing in a Co-Rotating Twin Screw Extruder." The objective was to use regression analysis to quantify statistical models of the average residence time data, which then can be used to predict the average residence time over a wide range of operating conditions. Gasner *et al.* (1999) proposed to perform linear regression of the experimental data using the regression model presented in equation 1.

$$\bar{t} * N = \beta_0 + \beta_1 \frac{N}{Q} \tag{1}$$

where: $\bar{t}$: average residence time (seconds)
N : screw speed (revolutions/second)
Q : flow rate (g/second)
β_0, β_1 : regression coefficients

Instead of using the average residence time as the dependent variable in the regression model, Gasner *et al.* (1999) proposed to use the product of the average residence time and the screw speed. This product was referred to as the Tmean screw revolutions, or the average number of screw revolutions required to extrude the tracer out of the system.

The problem with this new method is that the screw speed is incorporated into both the dependent and independent variables of the model presented in equation 1. There is automatically a relationship between the independent and dependent variables in equation 1, or in other words, this method had forced a relationship on the dependent variable. If the regression model is a good fit to the experimental data (i.e. a high correlation coefficient is obtained), there is no way to determine if the "goodness" of the fit is due to the forced relationship or a true relationship between the independent and dependent variables.

After performing regression analysis in the form of equation 1, it was proposed to rearrange the regression model to obtain the dependence of the average residence time on the operating conditions (Gasner *et al.*, 1999). The rearranged model is depicted in equation 2.

$$\bar{t} = \frac{\beta_0}{N} + \frac{\beta_1}{Q} \tag{2}$$

A regression equation is an empirical model, which attempts to represent the experimental data over the range of the given independent variables. It is not a theoretical equation that can be manipulated or rearranged. The coefficients (β_0, β_1) that were determined using the model presented in equation 1 are specifically related to the form of equation 1. As well, a certain error structure in the dependent variable is assumed when performing linear regression. Rearranging a linear regression model disregards these assumptions. The combination of these two fundamental errors invalidates the proposed approach of Gasner *et al.* (1999).

Linear regression can be used to directly fit the average residence time data to the expression presented in equation 2 (dependent variable = average residence time; independent variables = reciprocal of screw speed and flow rate; specify zero intercept). Most software packages have the option of specifying a zero intercept for the regression

analysis. The direct regression method results in the same final form of the regression model without performing the two fundamental errors in the method proposed by Gasner *et al.* (1999). A few examples of the regression analysis are presented to highlight the problems in the proposed analysis method of Gasner *et al.* (1999).

First is a comparison of the regression models obtained using the new approach proposed by Gasner *et al.* (1999) and direct linear regression of the average residence time data. The experimental set of average residence times used in this example was taken from the work of Kao and Allison (1984), which was used as an example by Gasner *et al.* (1999) for their new approach. The data were obtained over a range of screw speeds and flow rates in a co-rotating twin screw extruder. The linear regression models determined using the proposed method (after rearranging) of Gasner *et al.* (1999) and the direct regression method are presented in equations 3 and 4, respectively (units: average residence time = seconds, flow rate = mL/seconds, screw speed = revolutions/second).

$$\bar{t} = \frac{11.58}{Q} + \frac{53.9}{N} \tag{3}$$

$$\bar{t} = \frac{12.57}{Q} + \frac{51.8}{N} \tag{4}$$

The coefficients are not equal in these two equations, which confirmed the problems of the proposed method of Gasner *et al.* (1999). As well, the correlation coefficient (r^2) for the regression of $\bar{t} * N$ versus N/Q (Tmean screw revolution versus screw speed divided by flow rate) was 0.9900 as compared to the r^2 value of 0.9983 for the direct regression model. Even though the method of Gasner *et al.* (1999) forced a relationship on the dependent variable, the direct regression method resulted in a better fit to the experimental data.

The second example is a worst case scenario that confirms that the regression method of Gasner *et al.* (1999) forces a relationship on the dependent variable. Consider the residence time measurements collected from a co-rotating twin screw extruder, which is operated at a flow rate of 50 g/min over a range of screw speeds from 50 to 200 rpm. From Chapter 6, the average residence times were in the range of 100 to 200 seconds for these operating conditions during the melt-melt blending experiments. To ensure that there was no relationship between the average residence times and the operating conditions, the values of the average residence time were random numbers between 100 and 200 seconds (completed using the rand() function in Microsoft Excel). Regression analysis of the random average residence time data set was performed using the method of Gasner *et al.* (1999) and the direct regression method.

The relationship between a set of random average residence times and the screw speed divided by the flow rate (N/Q) is presented in Figure 1. As expected, the random average residence times did not depend on the operating conditions. Using the direct regression method, the following regression model was calculated:

$$\bar{t} = \frac{-947}{Q} + \frac{7868}{N}, r^2 = 0.0227 \qquad (5)$$

The direct regression method confirmed that there was no relationship between the random average residence times and the experimental factors.

The relationship between the product of the random average residence time and the screw speed (Tmean screw revolutions) and N/Q is presented in Figure 2. The linear regression model developed using the approach of Gasner *et al.* (1999) is included in Figure 2, and the calculated regression model is presented in equation 6.

$$\bar{t} = \frac{121.7}{Q} + \frac{6.05}{N} \quad , r^2 = 0.8194 \tag{6}$$

Considering that the average residence times were random values, the high correlation coefficient (r^2) confirmed that the regression method of Gasner *et al.* (1999) forced a relationship on the dependent variable. The two regression methods were compared using many sets of random average residence times, and the method of Gasner *et al.* (1999) always predicted a relationship with a correlation coefficient (r^2) between 0.65 and 0.85. The comparison was also completed over many different ranges of the random average residence times and similar results were observed. The only requirement was that a large amount of random average residence times (around 25 to 30 values) was required to observe the forced relationship.

In summary, regression analysis can be effectively used to quantify the relationship between the experimental results and the independent variables. Automatically correlating the dependent and independent variables forced a relationship on the dependent variable even when no relationship existed. Care must be exercised when performing regression analysis and an understanding of the assumptions is required to obtain valid results.

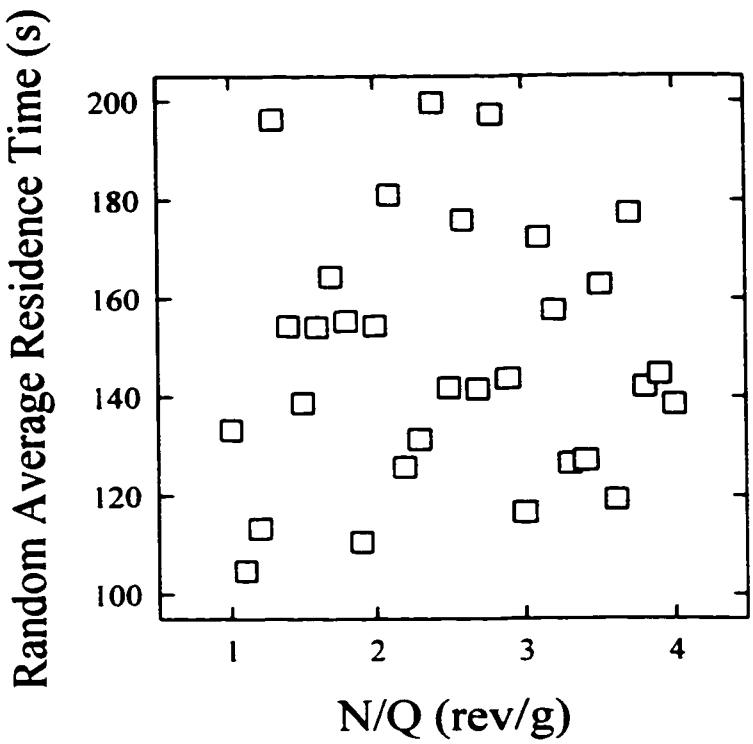

Figure 1. Random Average Residence Times

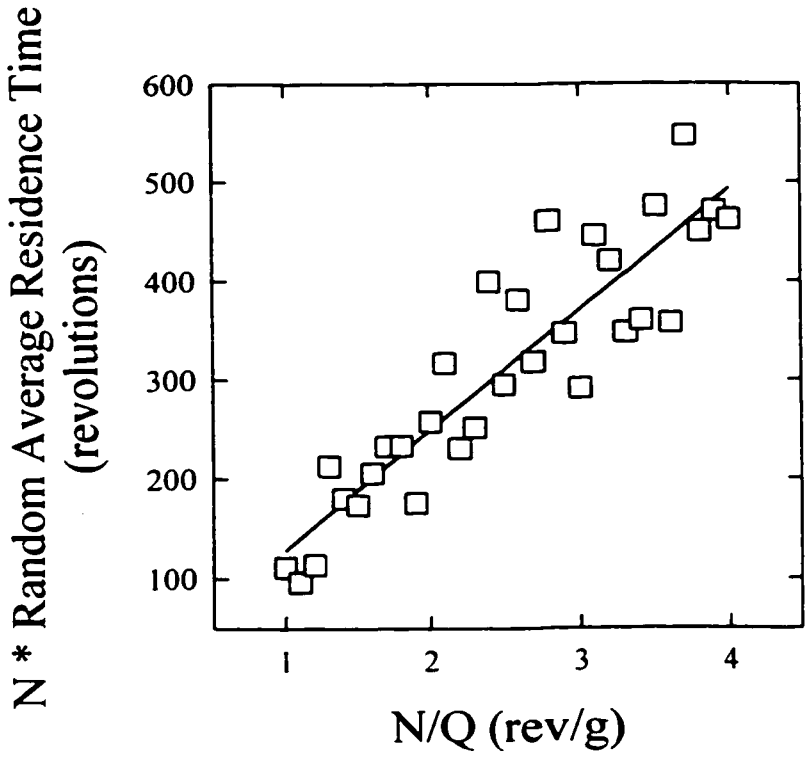

Figure 2. Forced Relationship Caused by Regression Method of Gasner *et al.* (1999)